



HAL
open science

Inclusion complexes of amylose : morphogenesis, crystal structure and release of bioactive molecules

Cong Anh Khanh Le

► **To cite this version:**

Cong Anh Khanh Le. Inclusion complexes of amylose : morphogenesis, crystal structure and release of bioactive molecules. Analytical chemistry. Université Grenoble Alpes, 2018. English. NNT : 2018GREAV033 . tel-02018878

HAL Id: tel-02018878

<https://theses.hal.science/tel-02018878>

Submitted on 14 Feb 2019

HAL is a multi-disciplinary open access archive for the deposit and dissemination of scientific research documents, whether they are published or not. The documents may come from teaching and research institutions in France or abroad, or from public or private research centers.

L'archive ouverte pluridisciplinaire **HAL**, est destinée au dépôt et à la diffusion de documents scientifiques de niveau recherche, publiés ou non, émanant des établissements d'enseignement et de recherche français ou étrangers, des laboratoires publics ou privés.

THÈSE

Pour obtenir le grade de

DOCTEUR DE LA COMMUNAUTE UNIVERSITE GRENOBLE ALPES

Spécialité : **Sciences des Polymères**

Arrêté ministériel : 25 mai 2016

Présentée par

Cong Anh Khanh LE

Thèse dirigée par **Jean-Luc PUTAUX**, Directeur de Recherche, CNRS
et codirigée par **Denis WOUESSIDJEW**, Professeur, UGA

préparée au sein du **Centre de Recherches sur les
Macromolécules Végétales (CERMAV)**, UPR 5301 CNRS
dans l'**École Doctorale Chimie et Sciences du Vivant**

Inclusion complexes of amylose: morphogenesis, crystal structure and release of bioactive molecules

Thèse soutenue publiquement le **3 Décembre 2018**
devant le jury composé de :

Madame Nathalie CAYOT

Professeur, AgroSup, Dijon (Rapporteur)

Madame Patricia LE BAIL

Chargée de Recherche, INRA, Nantes (Rapporteur)

Monsieur Martin BRINKMANN

Directeur de Recherche, Institut Charles Sadron, Strasbourg (Examinateur)

Monsieur William HELBERT

Directeur de Recherche, CERMAV, Grenoble (Président)

Monsieur Jacques PECAUT

Ingénieur de Recherche, CEA-INAC, Grenoble (Examinateur)

Monsieur Jean-Luc PUTAUX

Directeur de Recherche, CERMAV, Grenoble (Directeur de thèse)

Monsieur Denis WOUESSIDJEW

Professeur, DPM, Grenoble (Co-directeur de thèse, invité)

Monsieur Luc CHOISNARD

Maître de Conférences, DPM, Grenoble (Co-encadrant, invité)



*This thesis is dedicated, with love and gratitude, to my parents and teachers.
Most of them would never read it so, unless someone tells them, they will never know.*

Acknowledgements

First, I would like to thank my supervisors Dr. Jean-Luc Putaux, Prof. Denis Wouessidjewe and Dr. Luc Choisnard who offered me the chance to work on this project. I am grateful for all the time they spent to teach me, for their help and support throughout my PhD.

Thanks to Yu Ogawa for conducting modeling and solid-state NMR experiments.

Thanks to Frédéric Dubreuil for conducting AFM experiments.

Thanks to Yoshi Nishiyama and Karim Mazeau for teaching me modeling, for their encouragement and scientific support.

Thanks to Annabelle Gèze for supervising the in vitro release experiments conducted at Département de Pharmacochimie Moléculaire (DPM) and to Véronique Blanc-Marquis for her technical support.

Thanks to Florent Grimaud and Gabrielle Véronèse for the reception at Laboratoire d'Ingénierie des Systèmes Biologiques et des Procédés (LISPB, Toulouse) and for teaching me how to biosynthesize amylose in vitro.

Thanks to Noriyuki Isobe for the determination of degree of polymerization of native amylose.

Thanks to Daisuke Sawada for teaching the use of the SHELX program.

Thanks to Nathalie Cayot, Patricia Le Bail and Martin Brinkmann for participating to my defense jury and for accepting to review this manuscript.

Thanks to William Helbert and Jacques Pécaut for being the members of my thesis committee and my defense jury, and for illuminating discussions.

Thanks to Christine Lancelon-Pin, Marie-France Métral, and Pierre Sailer for sample preparation and technical support.

Thanks to Henri Chanzy and Laurent Heux for illuminating discussions.

Thanks to my friend Kim Anh Nguyen who forwarded me the information of the application of this thesis. I would not know about this PhD project without her help.

Also, there are so many other people that I would like to thank, but I won't mention them all by name, because someone would be forgotten. Huge thanks to all of the past and present members of Centre de Recherches sur les Macromolécules Végétales (CERMAV), more particularly the Glycomaterials group for the last few brilliant years! I've had great time and a lot of memories.

I have to say an extra special thanks to my family, especially my wife, Mai, who have always followed and supported me.

Finally, I would like to thank LabEx Arcane for funding my PhD. Without this, it would not have been possible to carry out this work. Also, thank you to the Société Française des Microscopies, the Glyco@Alps program and the Polysolvat-12 meeting for offering me scholarships to participating to national and international conferences.

Table of contents

Résumé	11
Summary	13
Résumé des travaux de thèse	15
Introduction	23
Chapter I. Bibliography	
I.1. Amylose	27
I.1.1. Chemical structure	27
I.1.2. Sources of amylose	29
I.1.2.1. Native amylose	29
I.1.2.2. <i>In vitro</i> biosynthesis of amylose	30
I.1.3. Solvents and conformation of amylose in solution	31
I.1.3.1. Solvents	31
I.1.3.2. Conformation of amylose in solution	32
I.1.4. Crystalline structure of recrystallized amylose: A- and B-amylose	34
I.2. Crystalline inclusion complexes of amylose: V-amylose	38
I.2.1. Definition	38
I.2.2. Preparation methods	38
I.2.2.1. Crystallization of amylose in aqueous solution in the presence of a complexing agent	38
I.2.2.2. Crystallization of amylose in the dry state (sealed-heating method)	39
I.2.2.3. Crystallization of amylose by solvent removal	40
I.2.2.4. Vine-twinning enzymatic polymerization	40
I.2.2.5. Insertion of a complexing agent in preformed V-amylose	40
I.2.3. V-amylose polymorphism	41
I.2.3.1. Compact-helix V-amylose	42
I.2.3.1.1. V _{6I}	43
I.2.3.1.2. V _{6II}	44
I.2.3.1.3. V _{6III}	45
I.2.3.1.4. V ₇	46
I.2.3.1.5. V ₈	48
I.2.3.2. Extended-helix V-amylose	49
I.2.3.2.1. V _{KOH} and isomorphous structures	50
I.2.3.2.2. V _{KBr} and isomorphous structures	50
I.2.3.3. Other unresolved structures and towards new structures of V-amylose	50
I.2.4. Origin of polymorphism	51
I.2.4.1. Complexing agent	52
I.2.4.2. Degree of polymerization of amylose	53
I.2.4.3. Concentration of amylose	53
I.2.4.4. Concentration of complexing agent	53
I.2.4.5. Temperature of crystallization	54
I.2.4.6. Solvent	54
I.2.5. Properties and potential applications of V-amylose	55
I.2.5.1. Identification, quantification and fractionation of amylose from native starch	55
I.2.5.2. Modulation of starch digestibility and glucose response	55
I.2.5.3. Effect on the functional properties of starch	56
I.2.5.4. Encapsulation of flavors and bioactive molecules	57
I.2.5.5. Other potential applications	57
I.3. Objectives of the thesis	58

Chapter II. Materials and methods

II.1. Materials	61
II.1.1. Native amylose	61
II.1.2. Synthetic amylose	61
II.1.2.1. Amylose synthesized <i>in vitro</i> using amylosucrase	61
II.1.2.2. Amylose synthesized <i>in vitro</i> by phosphorylase	62
II.1.3. Complexing agents	62
II.2. Preparation of the inclusion complexes	70
II.2.1. Crystallization protocol	70
II.2.2. Treatments of the complexes	71
II.2.2.1. Hydrated / wet samples	71
II.2.2.2. Dry samples	71
II.2.2.3. Treatment with solvents	71
II.3. Characterization techniques	71
II.3.1. Differential interference contrast (DIC) optical microscopy	71
II.3.2. Atomic force microscopy	71
II.3.3. X-ray diffraction (XRD)	72
II.3.3.1. Diffraction by crystals	72
II.3.3.2. Experimental procedure	73
II.3.4. Transmission electron microscopy (TEM)	73
II.3.4.1. Principle	73
II.3.4.2. Experimental procedure	74
II.3.5. Solid-state ¹³ C nuclear magnetic resonance (NMR) spectroscopy	75
II.3.5.1. Principle	75
II.3.5.2. Experimental procedure	77
II.3.6. Fourier-transform infrared (FT-IR) spectroscopy	77
II.3.6.1. Principle	77
II.3.6.2. Experimental procedure	79
II.3.7. Density measurement	79
II.3.8. Molecular modeling	79
II.3.8.1. V _{1-butanol}	79
II.3.8.1.1. Building the rigid symmetrical amylose helices	79
II.3.8.1.2. Packing energy calculation and geometry optimization	79
II.3.8.1.3. Model refinement	79
II.3.8.2. Molecular dynamics of V _{ibuprofen}	80
II.3.9. Dissolution tests of V-ibuprofen complexes	81
II.3.9.1. Ibuprofen quantification assays	81
II.3.9.2. Determination of ibuprofen content in the complex	81
II.3.9.3. Determination of the solubility of ibuprofen in the dissolution media	81
II.3.9.4. <i>In vitro</i> dissolution studies	82

Chapter III. Crystal and molecular structure of V_{1-butanol}

III.1. Introduction	85
III.2. Results and discussion	86
III.2.1. Crystal morphology and the unit cell	86
III.2.2. ¹³ C CP/MAS NMR spectroscopy	87
III.2.3. Molecular modeling and crystal structure determination	88
III.2.3.1. Strategy	88
III.2.3.2. Selection of helical conformation and exhaustive search of helix position	89
III.2.3.3. Addition of the C6 hydroxyl group, 1-butanol and water	91
III.2.3.4. Structure refinement	91
III.3. Conclusions	98

Chapter IV. Morphology and crystal structure of different forms of V-amylose

IV.1. Introduction	101
IV.2. V _{6I} complexes.....	102
IV.2.1. Complexing agents	102
IV.2.2. Morphology and crystal structure.....	102
IV.2.3. Effect of drying and rewetting on the crystal structure.....	103
IV.3. V _{6II} complexes	104
IV.3.1. Complexing agents	104
IV.3.2. Morphology and crystal structure.....	105
IV.3.3. Effect of drying on the crystal structure	107
IV.4. V _{6III} complexes with glycerol.....	109
IV.4.1. Formation of complexes	109
IV.4.2. Morphology and crystal structure.....	110
IV.5. V ₇ complexes	111
IV.5.1. Complexing agents	111
IV.5.2. Morphology and crystal structure.....	111
IV.5.3. Effect of drying on the crystal structure	113
IV.6. V ₈ complexes	115
IV.6.1. Complexing agents	115
IV.6.2. Morphology and crystal structure.....	115
IV.6.3. Effect of drying on the crystal structure	117
IV.7. A new V-amylose allomorph obtained with 4-hydroxybenzoic acid.....	117
IV.7.1. Formation of complexes	118
IV.7.2. Morphology and crystal structure.....	118
IV.7.3. Effect of drying on the crystal structure	120
IV.8. A new V-amylose allomorph obtained with (-)-borneol, R-(+)-camphor, <i>cis</i> -decahydro-1-naphthol, decahydro-2-naphthol, and 1,3-butanediol.....	121
IV.8.1. Morphology and crystal structure.....	121
IV.8.2. Effect of drying on the crystal structure	123
IV.9. A new V-amylose allomorph obtained with 1-naphthol.....	125
IV.9.1. Morphology and crystal structure.....	126
IV.9.2. Effect of drying on the crystal structure	126
IV.10. A new V-amylose allomorph obtained with quinoline.....	126
IV.10.1. Morphology and crystal structure.....	127
IV.10.2. Effect of drying on the crystal structure	129
IV.11. A new V-amylose allomorph obtained with salicylic acid	129
IV.11.1. Morphology and crystal structure.....	129
IV.11.2. Effect of drying on the crystal structure	131
IV.12. Study of the complexes by FT-IR spectroscopy	132
IV.13. Study of the helical conformation by ¹³ C CP/MAS NMR spectroscopy	136
IV.14. Classification of complexes – proposition of a nomenclature	140
IV.15. Conclusions.....	143

Chapter V. Factors affecting the crystallization and crystal structure of V-amylose

V.1. Introduction.....	147
V.2. Complexes with <i>n</i> -alcohols, <i>n</i> -diols, <i>n</i> -amines, dicarboxylic acids, octanal, stearamide	148
V.3. Complexes with straight-chain saturated fatty acids	150
V.4. Complexes with 1,3-butanediol.....	160
V.5. Complexes with esters	161
V.6. Complexes with some bicyclic compounds	162
V.7. Complexes with 1-naphthol	166
V.8. Complexes with quinoline	168

V.9. Complexes with salicylic acid.....	169
V.10. General conclusions.....	171
Chapter VI. Molecular structure and release properties of V_{ibuprofen}	
VI.1. Introduction	179
VI.2. Morphology and crystallization behavior of V _{ibuprofen} complexes	179
VI.2.1. V _{IBU} crystals from dilute solutions	180
VI.2.2. V _{IBU} crystals from concentrated solutions	180
VI.3. Molecular modeling	189
VI.4. <i>In vitro</i> release properties of ibuprofen from the complexes	190
VI.4.1. Ibuprofen content in the complexes	190
VI.4.2. <i>In vitro</i> dissolution studies	192
VI.5. Conclusions	195
Conclusions and perspectives	199
References	207
Annexes	
Annex 1. Supplementary material of Chapter III.....	229
Annex 2. Supplementary material of Chapter IV	237
Annex 3. Supplementary material of Chapter V.....	247
Annex 4. Supplementary material of Chapter VI	261

Résumé

L'amylose est un homopolymère quasi-linéaire d'unités glucosyles liées en $\alpha(1,4)$ qui, extrait de l'amidon natif, possède la propriété remarquable de former des complexes cristallins avec une grande variété de petites molécules organiques. Ces complexes sont regroupés sous le terme générique d'amylose V. Nous avons testé la capacité de 121 composés à induire la cristallisation de l'amylose à partir de solutions aqueuses diluées. La morphologie et la structure des cristaux lamellaires formés ont été caractérisées par microscopie électronique en transmission ainsi que par diffraction des électrons et des rayons X. Les données révèlent que les structures de ces complexes peuvent être classées en 10 familles dont 5 sont décrites pour la première fois. Des spectres de résonance magnétique nucléaire du solide du ^{13}C montrent clairement que l'hélicité de l'amylose V est corrélée à la résonance du carbone C1 qui se déplace vers les champs faibles lorsque le nombre d'unités glucosyles par tour augmente. Des modèles géométriques préliminaires ont été proposés pour tous les allomorphes, la structure de cristaux de V_{1-butanol} ayant été analysée en détail en combinant des calculs de conformation et d'énergie d'empilement avec un affinement de structure de polymère cristallin classique. Tous les allomorphes contiennent des simples hélices d'amylose d'ordre 6, 7 ou 8 et les molécules invitées peuvent être localisées dans ces hélices, entre elles ou les deux. Chaque type d'allomorphe peut être obtenu avec différents complexants et la conformation de l'hélice d'amylose dépend de la taille du complexant. De plus, un ligand donné est susceptible d'induire la formation de plusieurs allomorphes. Le polymorphisme cristallin de l'amylose serait donc une caractéristique plus générale que ce qui avait été rapporté auparavant. La propension au polymorphisme dépend non seulement de la nature du complexant mais aussi des conditions de cristallisation. Le degré de polymérisation de l'amylose, sa concentration et celle du complexant, la température de mélange ou de cristallisation et la composition du solvant ont un impact significatif sur la formation de cristaux et la structure de l'amylose V. Par ailleurs, nous avons utilisé les complexes avec l'ibuprofène comme modèle afin d'évaluer le potentiel de l'amylose V comme système de délivrance de principes actifs. Différentes fractions d'ibuprofène, probablement corrélées aux positions possibles de la molécule dans le cristal, sont sélectivement relarguées en variant le pH du milieu de dissolution. Puisque le relargage intervient principalement à pH élevé, ces complexes d'inclusion sont donc potentiellement intéressants pour cibler une libération intestinale et pourraient donc améliorer l'effet thérapeutique de l'ibuprofène en évitant les dommages à l'estomac.

Mots-clés: biopolymère, amylose, cristal, complexe d'inclusion, analyse structurale, relargage

Summary

Amylose, a mostly linear homopolymer of $\alpha(1,4)$ -linked glucosyl units extracted from native starch, has the remarkable property to form "V-amylose" crystalline complexes with a variety of small organic molecules. We have tested the ability of 121 compounds to induce the crystallization of amylose from dilute aqueous solutions. The morphology and structure of the resulting lamellar crystals were characterized by transmission electron microscopy as well as electron and X-ray diffraction. The data revealed that the structures of the complexes could be classified into 10 families, 5 of which were described for the first time. In addition, ^{13}C solid-state nuclear magnetic resonance spectra clearly showed that the helicity of V-amylose was correlated with the resonance of carbon C1 that was shifted downfield with increasing number of glucosyl units per turn. Tentative geometrical models were proposed for all allomorphs and the structure of V_{1-butanol} was analyzed in more details by combining conformational and packing energy calculations with classical crystalline polymer structure refinement. All allomorphs contained 6-, 7- or 8-fold amylose single helices and the guest molecules could be located inside these helices, in-between, or both. Each allomorph could be obtained with different complexing agents and the helical conformation was found to depend on the size of the complexing agent. In addition, a given ligand could induce the formation of several allomorphs, suggesting that the polymorphism of V-amylose crystals is a more general characteristic than what was previously reported. The propensity for polymorphism does not only depend on the nature of the complexing agent but also on the crystallization conditions. The degree of polymerization of amylose, its concentration and that of the complexing agent, the temperature of mixing and crystallization, and the solvent composition have a significant impact on the formation and crystal structure of V-amylose. In addition, crystalline complexes prepared with ibuprofen were used as a model to evaluate the potential of V-amylose as a delivery system of bioactive molecules. Distinct fractions of ibuprofen, likely correlated with the different locations of the guest in the crystal, were selectively released by varying the pH of the dissolution medium. Since the release mainly occurred at high pH, these inclusion complexes appear to be potentially interesting for intestinal targeting and would thus improve the therapeutic effect of ibuprofen while avoiding stomach damage.

Keywords: biopolymer, amylose, crystal, inclusion complex, structural analysis, release

Résumé des travaux de thèse

L'amylose est un homopolymère quasi-linéaire d'unités α -D-glucosyles reliées par des liaisons glucosidiques $\alpha(1\rightarrow4)$. Ce polysaccharide est l'un des principaux constituants des grains d'amidon natifs (environ 20-30% de sa masse). Il peut être aussi synthétisé *in vitro* par différentes enzymes. L'amylose possède la propriété remarquable de former des complexes d'inclusion lorsqu'il est recristallisé *in vitro* en présence d'une grande variété de petites molécules organiques. Dans cette forme, appelée "V-amylose", le polymère adopte une conformation en hélice simple et les molécules invitées peuvent être localisées dans ces hélices, entre elles ou les deux.

Les complexes d'inclusion présentent plusieurs propriétés intéressantes et applications potentielles, par exemple dans l'industrie alimentaire et pharmaceutique. Des agents complexants tels que le 1-butanol, le thymol ou la menthone ont également été utilisés pour fractionner l'amidon natif en ses principaux constituants (amylopectine et amylose). De plus, l'amylose présentant des propriétés de complexation très similaires à celles des cyclodextrines, il a été exploité pour encapsuler des arômes et des molécules bioactives.

L'amylose V peut être préparée sous différentes formes (fibres, monocristaux lamellaires, sphérolites) selon les conditions de cristallisation. La diffraction des rayons X et celle des électrons ont permis d'identifier différents allomorphes. Des modèles moléculaires basés sur des simples hélices gauches ont été proposés, mais seul un petit nombre d'entre eux ont été validés par des méthodes cristallographiques. En particulier, plusieurs informations structurales restent à déterminer, telles que la conformation hélicoïdale ou la localisation des molécules invitées. De plus, le phénomène de complexation et les paramètres qui influent sur la formation d'une structure cristalline spécifique doivent être étudiés en détail.

Cette thèse visait à étudier la cristallisation de l'amylose V en présence de divers complexants organiques afin de mieux comprendre l'interaction de l'amylose avec les molécules invitées et, si possible, prédire la structure qui résulterait de la cristallisation en présence d'un ligand donné. Comme c'est généralement le cas avec les polymères, il n'a pas été possible de faire croître des monocristaux d'amylose V d'une taille suffisante pour permettre leur analyse par cristallographie aux rayons X. Notre approche générale a donc consisté à préparer des cristaux lamellaires à partir de solutions aqueuses diluées. Nous avons caractérisé leur morphologie et leur structure en combinant microscopie électronique en transmission (MET) et diffraction électronique (DE) de ces monocristaux, avec des données de diffraction des rayons X de poudres hydratées. Le protocole général de cristallisation consistait à solubiliser l'amylose

dans l'eau ou dans un mélange eau / DMSO à haute température, à y ajouter un agent complexant puis à maintenir la solution à une température prédéterminée pour induire la cristallisation.

La première partie de ce travail a donc été consacrée à l'optimisation des protocoles de cristallisation en étudiant l'impact de plusieurs paramètres (degré de polymérisation (DP) et concentration en amylose, nature du solvant, température et temps de cristallisation) sur la morphologie et la structure des cristaux. L'étude des complexes préparés avec une série d'acides gras linéaires saturés (de C3 à C20) a apporté un résultat nouveau et inattendu: un acide gras donné pouvait induire la formation d'allomorphes différents contenant des hélices d'ordre 6 ou 7, jusqu'à 3 allomorphes dans certains cas. Cette observation nous a incités à tester davantage de séries de molécules de structure chimique différente (diols, esters, amines, cétones, composés aromatiques, etc.).

Dans un second temps, nous avons caractérisé les nombreux cristaux préparés dans diverses conditions et analysé la quantité importante de données collectées à l'aide des différentes techniques d'imagerie, de diffraction et de spectroscopie. Plusieurs conclusions ont pu être tirées. Dans la gamme de conditions de cristallisation sélectionnées, sur les 121 agents testés, 28 n'ont conduit à aucune cristallisation et 43 ont induit la formation de 2 à 4 allomorphes.

Dix familles d'allomorphes de cristaux lamellaires de V-amylose contenant des hélices d'ordre 6, 7 ou 8 ont été identifiées, parmi lesquelles 5 correspondent à des structures précédemment publiées et 5 sont de nouveaux allomorphes décrits pour la première fois. Afin de distinguer ces structures, nous avons élargi la précédente nomenclature des formes d'amylose V. Les 10 allomorphes ont été nommés en fonction de la conformation de l'amylose et de la taille relative de la maille cristalline: V6_I, V6_{II}, V6_{III}, V6_{IV}, V7_I, V7_{II}, V7_{III}, V7_{IV}, V8_I et V8_{II}. Des analyses spectroscopiques ont complété les données de cristallographie. Les spectres infrarouge montrent une augmentation de l'intensité de bandes vibrationnelles spécifiques par rapport à l'amylose amorphe ou aux amyloses cristallines de type A ou B. En outre, la bande proche de 1022 cm⁻¹ pourrait être utilisée comme empreinte de l'amylose V. En nous appuyant sur des résultats de la littérature, nous avons observé une corrélation significative entre l'hélicité de l'amylose V et la résonance du carbone C1 dans les spectres de résonance magnétique nucléaire à l'état solide du ¹³C. La résonance est décalée vers les plus faibles champs lorsque le nombre d'unités glucosyles par tour d'hélice augmente. Trois déplacements chimiques du C1 ont été identifiés, correspondant probablement aux hélices d'ordre 6, 7 et 8.

Bien que nous ayons proposé des modèles géométriques pour chaque allomorphe, nous avons mené une étude plus détaillée des cristaux de V_{1-butanol}. D'une part, ce complexe revêt une importance historique puisque le 1-butanol a été l'un des premiers complexants utilisés dans les

années 1940 pour fractionner l'amidon natif par cristallisation sélective avec l'amylose. D'autre part, parmi les 5 formes cristallines connues auparavant, c'était la seule pour laquelle l'organisation des hélices était encore hypothétique. De plus, 43 de nos agents complexants testés ont donné l'allomorphe V6_{II} obtenu avec le 1-butanol. Notre approche a reposé sur des analyses d'énergie de conformation et d'empilement, combinées à l'affinement classique de la structure des polymères cristallins. Le modèle avec le facteur d'accord le plus faible est décrit par un réseau orthorhombique $P2_12_12_1$ de simples hélices gauches d'ordre 6 antiparallèles dans lesquelles les groupements hydroxyméthyles présentent un désordre conformationnel. La maille contient 4 molécules de 1-butanol et 16 molécules d'eau réparties dans 4 poches interstitielles allongées et 1 molécule de 1-butanol à l'intérieur de chaque hélice. Ce résultat confirme le modèle proposé par Helbert et Chanzy (1994). Cependant, notre structure n'a été affinée qu'avec les données de DE du plan de base des cristaux. Par conséquent, les positions atomiques le long de l'axe c ne sont pas connues avec précision. Afin de déterminer la structure 3D, des clichés de DE doivent être enregistrés sur des cristaux inclinés autour des axes principaux de l'espace réciproque et l'intensité des tâches de diffraction analysée quantitativement.

En raison du temps limité et du grand nombre de ligands testés, nous n'avons pas pu effectuer le même type d'analyse pour les 5 nouveaux allomorphes, mais nous avons proposé des modèles géométriques basés sur les données cristallographiques et spectroscopiques. L'empilement des hélices dans les structures V6_I, V7_I, V7_{III}, V7_{IV} et V8_I est plutôt compact et les agents complexants ne seraient situés que dans les hélices. En revanche, il y a plus d'espace interstitiel dans V6_{II}, V6_{III}, V6_{IV}, V7_{II} et V8_{II} pour accueillir les molécules invitées. De plus, les agents complexants peuvent éventuellement être situés à l'intérieur des hélices, à l'exception de V6_{IV}. Puisque V6_{IV} a été obtenu avec de l'acide 4-hydroxybenzoïque, dont la taille semble être incompatible avec la cavité d'une hélice d'ordre 6, le ligand cyclique ne devrait être localisé que dans les espaces interstitiels. Tous les modèles géométriques proposés doivent encore être validés par une analyse structurale détaillée associant données expérimentales et modélisation.

Nos résultats montrent que chaque allomorphe peut être obtenu avec différents agents complexants. Cependant, V6_I, V6_{II} et V7_{II} sont les formes les plus répandues. De plus, la conformation hélicoïdale dépend de la taille du ligand. Des complexes de type V6 ont été obtenus avec des molécules à chaînes carbonées linéaires, tandis que les molécules à chaîne ramifiée ou cycliques ont tendance à induire des hélices d'ordre 7. Des complexes de type V8 ont été obtenus avec du 1-naphthol, de la quinoléine et de l'acide salicylique. Cependant, il reste toujours difficile de prédire la structure cristalline en fonction de la nature du ligand car un agent complexant est susceptible d'induire différentes structures cristallines.

Le polymorphisme de l'amylose V ayant été observé avec un grand nombre d'agents complexants, c'est donc une caractéristique plus générale que ce qui avait été précédemment rapporté dans la littérature. La propension d'un complexe au polymorphisme est non seulement liée à la nature de l'agent complexant, mais également aux conditions de cristallisation. Les ligands à chaîne linéaire sont plus susceptibles d'induire un polymorphisme que les composés à chaîne ramifiée ou cyclique. En outre, les molécules à chaîne linéaire, les alcools, les acides gras, les aldéhydes, les amides et les amines induiront probablement la formation d'allomorphes différents que les esters et les cétones.

Différents paramètres, notamment le DP de l'amylose, sa concentration et celle du ligand, la température de mélange et de cristallisation, et la composition du solvant ont un impact important sur la cristallisation et la structure de l'amylose V. Diverses conditions de cristallisation ont dû être explorées afin d'explorer le polymorphisme. Cependant, le mécanisme qui contrôle la structure finale n'est pas encore totalement éclairci.

Nous avons montré que l'eau jouait un rôle crucial sur la stabilité et la cristallinité des complexes. Lors du séchage, V6_I, V6_{II}, V6_{IV}, V7_I, V7_{II} et V7_{IV} ont été transformés en structures hexagonales plus compactes. Pour V7_{III}, V8_I et V8_{II}, une perte significative de cristallinité a été observée, mais la structure cristalline est restée la même. V6_{III} est la seule structure qui s'est montrée stable au séchage. De manière surprenante, dans de nombreux cas, après un séchage sous vide entraînant une perte de cristallinité, la structure d'origine a été restaurée de manière réversible par réhydratation en atmosphère humide. Dans de nombreuses études précédentes, l'accent était mis sur le piégeage et la libération de l'agent complexant, mais au vu de nos résultats, le rôle de l'eau doit être étudié de manière plus approfondie.

Nos résultats suggèrent également que d'autres allomorphes d'amylose V restent à découvrir. De nouveaux agents complexants doivent donc être testés. L'influence de facteurs tels que la composition du solvant et les additifs doit aussi être étudiée de manière plus approfondie. Dans notre étude, seul le DMSO a été utilisé en tant qu'additif. De plus, différentes techniques de préparation pourraient être testées comme par exemple l'insertion d'un ligand dans des hélices préformées ou le chauffage en ampoule scellée.

Pour évaluer le potentiel de l'amylose en tant que système de vectorisation de principes actifs, nous avons étudié des complexes modèles préparés en présence d'ibuprofène racémique. Des fractions très cristallines de cristaux lamellaires ont été préparées par cristallisation en solution aqueuse ou un mélange eau / DMSO (0,1 à 1% en masse d'amylose). Le diagramme de diffraction électronique du plan de base des cristaux, le profil de DRX de poudre et les spectres de spectroscopie IR et de RMN du solide du ¹³C ont montré que le complexe présentait un type

allomorphique V7_{II}. Des modèles moléculaires numériques avec ou sans ibuprofène interstitiel ont été construits et optimisés par dynamique moléculaire en se basant sur la maille isomorphe du complexe V_{2-propanol} précédemment publiée. Le résultat suggère que la stabilité des complexes ne dépendrait pas de la présence d'ibuprofène dans les espaces interstitiels. Toutefois, l'adéquation entre le diagramme de DE expérimental et ceux calculés à partir des modèles proposés n'est pas encore suffisamment satisfaisant. Il faudra donc poursuivre l'étude de simulation pour améliorer le modèle à l'aide d'une analyse de l'énergie d'empilement.

Notre étude de dissolution *in vitro* a révélé que les complexes de V_{ibuprofène} présentaient différents profils de libération. En particulier, différentes fractions d'ibuprofène sont libérées sélectivement en fonction du pH du milieu. Ce résultat suggère que l'ibuprofène serait localisé à différents endroits dans la maille et aurait différentes interactions avec l'amylose. Par exemple, les molécules d'ibuprofène situées à l'intérieur de l'hélice seraient plus étroitement liées et joueraient un rôle plus important sur la stabilité des complexes que celles situées dans l'espace inter-hélice. La libération intervient principalement à pH élevé, les complexes d'inclusion semblent être un système de délivrance d'ibuprofène potentiellement intéressant pour le ciblage intestinal et permettraient donc d'améliorer son effet thérapeutique et d'éviter les dommages à l'estomac.

Introduction

Amylose is an almost linear homopolymer of α -D-glucosyl units bound through $\alpha(1\rightarrow4)$ glucosidic linkages. This polysaccharide is one of main components of native starch granules, accounting for about 20-30% of its weight. In addition, it can be synthesized *in vitro* by using different enzymes. The linear nature of the chain and the type of glucosidic bond have a significant influence on the behavior of amylose in solution. An important property of amylose is its versatility to form inclusion complexes when it is crystallized in the presence of a large variety of inorganic and organic guests. In this so-called *V-amylose* form, the polymer adopts a single helical conformation.

The inclusion complexes present a number of interesting properties and potential applications, *i.e.* in food and pharmaceutical industry. For instance, the complexation of amylose with lipids modulates the rheological and hydrolysis properties of amylose/starch and they are used in the baking industry to delay the staling of bread. Organic complexing agents like 1-butanol, thymol or menthone, have also been used for the fractionation of native starch into its amylopectin and amylose constituents. In addition, amylose present complexation properties very similar to those of cyclodextrins. Therefore, it has been exploited to encapsulate flavors and bioactive molecules.

V-amylose can be prepared in different crystalline forms (fibers, lamellar single crystals, spherulites) depending on the crystallization conditions. X-ray and electron diffraction have allowed identifying different allomorphs. Molecular models based on left-handed single helices have been proposed but only a small number of them have been validated by crystallographic approaches. In particular, several structural details remain unresolved, like the helical conformation, packing arrangement and location of the guest molecules. Moreover, the complexation phenomenon and crystallization parameters affecting the crystal structure still remain to be investigated in details

This thesis aimed at further elucidating the formation and crystallization behavior of V-amylose from dilute solutions. The complexation was systematically investigated by varying several crystallization parameters: degree of polymerization of amylose, nature of complexing agent, concentration of amylose and complexing agent, crystallization temperature, and solvent composition. A major part of this study was devoted to the structural characterization of the crystalline complexes in both hydrated and dry states. The collection of crystallographic data from different allomorphs, especially those that we have identified for the first time, allowed proposing

a helical conformation and packing arrangement for each allomorphic family. In addition, in order to evaluate the potential of V-amylose as a delivery system of bioactive molecules, complexes with ibuprofen were prepared as a model to investigate the encapsulation and release properties in relation to the crystal structure.

This manuscript is divided into six chapters. **Chapter I** is a bibliographic review on amylose and its inclusion complexes under the generic name of V-amylose. **Chapter II** presents the materials, the experimental protocols to prepare the complexes and the characterization techniques that were used. In **Chapters III to VI**, we describe and discuss the results of our study. **Chapter III** presents the molecular and crystal structure of V_{1-butanol} which is one of the first molecules that have been used to recrystallize amylose on a large scale but which model was still hypothetical. In **Chapter IV**, we describe the morphology and crystal structure of all allomorphic families determined in this thesis. **Chapter V** describes the effect of different crystallization parameters on the formation and crystal structure of V-amylose complexes prepared with different guest molecules. Finally, **Chapter VI** presents the crystal structure and release properties of the V_{ibuprofen} complex.

Chapter I

Bibliography

I.1. Amylose

Amylose is a polysaccharide that, together with amylopectin, is a main component of native starch granules, accounting for about 20-30% of its weight (Hanashiro, 2015). In addition, amylose can be synthesized *in vitro* by using different enzymes (Ohdan et al., 2006). In contrast to highly branched amylopectin, amylose is generally considered as linear or slightly branched. The linear nature has an important effect on the physicochemical properties of amylose, *i.e.* the conformation in solution and the crystallization properties. In the starch granules, amylose contributes to the amorphous regions in alternation with the semi-crystalline layers of amylopectin. However, in terms of *in vitro* crystallization, amylose is more versatile than amylopectin.

I.1.1. Chemical structure

Amylose is a homopolymer of α -D-glucosyl units. Although the polysaccharide was once considered linear in which the glucose units bound to each other uniquely through $\alpha(1\rightarrow4)$ glucosidic linkages, evidence revealed that the molecule may contain a few very long branches or multiple short branches linked with the main chain through $\alpha(1\rightarrow6)$ linkages (Hanashiro, 2015; Jane, 2009; Takeda et al., 1990; Tester et al., 2004). The chemical structure of a linear amylose is illustrated in **Figure I.1** whereas the proposed structure for the branched amylose is shown in **Figure I.2**. Native amylose would contain less than 1% branching points.

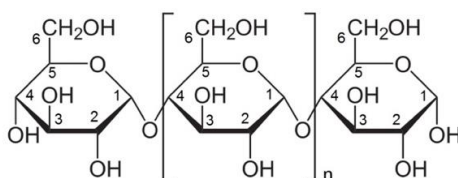


Figure I.1. Chemical structure of linear amylose.

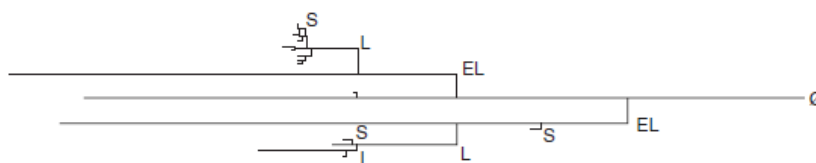


Figure I.2. Proposed structure of the branched amylose. EL, extremely long; L, long; and S, short chains; \emptyset , reducing end (Takeda et al., 1990).

The presence of branches in native amylose was first demonstrated by the incomplete degradation of amylose by β -amylase which is an exo-acting enzyme splitting selectively the $\alpha(1\rightarrow4)$ bonds (Peat et al., 1952; Peat et al., 1949). However, amylose is totally degraded into maltose by the successive action of a β -amylase and a debranching enzyme which specifically hydrolyzes the $\alpha(1\rightarrow6)$ bonds (Banks & Greenwood, 1966; Kjølberg & Manners, 1963). Several other evidences for the existence of $\alpha(1\rightarrow6)$ linkages were then reported from the differences in size distribution of amyloses with and without debranching by an isoamylase (Colonna & Mercier, 1984; Würsch & Hood, 1981) or the differences in molecular size determined by osmotic pressure measurement and determination of the non-reducing terminal residues by periodate oxidation (Potter & Hassid, 1948a, 1948b). Recently, the advancement in atomic force microscopy has enabled imaging branched amylose, revealing the presence of single-branched molecules with a long side-chain and multiple-branched molecules with shorter side-chains (Gunning et al., 2003).

Similarly to other native polysaccharides, amylose is polydisperse in molecular size (Hanashiro, 2015). The size of the polymer is defined by its molecular weight (M) or more frequently its degree of polymerization given by $DP = M/M_0$, where M_0 is the molecular weight of the monomer unit. Because of the polydispersity, the M or DP values are generally expressed as average values and can be either weight- or molar-based (denoted by subscript w for weight-average or n for number-average, respectively, as in M_w , DP_w or M_n , DP_n). Different methods are now available to characterize the chain length of amylose. However, each technique often only gives either the number or weight-average value. For example, the osmometry (Potter & Hassid, 1948b; Van Dijk et al., 1976), the determination of the reducing residues such as a modified Park–Johnson method (Hizukuri et al., 1981; Potter & Hassid, 1948a), and a bicinchoninic acid method using a microtiter plate format (Utsumi et al., 2009), give a number-average value, while viscometry (Banks & Greenwood, 1968b) and light scattering measure a weight-average value (Miles et al., 1985). The most common technique for measuring the size of amylose is a variant of high-pressure liquid chromatography (HPLC) in combination with a weight- and/or a molar-based detection method, known as gel-permeation chromatography (GPC) or high-performance size-exclusion chromatography (HPSEC) (Ozcan & Jackson, 2002; Takeda et al., 1984; Van Dijk et al., 1976). These techniques make the characterization of an amylose solution easier and the result can be expressed as a size distribution. There is no specified range for the molecular size of amylose. The DP_n can vary from a few dozens to several thousands (Bertoft, 2004).

I.1.2. Sources of amylose

I.1.2.1. Native amylose

Native amylose designates the molecules retrieved by fractionation of starch. The amylose content depends on the botanical as well as varietal sources of starches. So-called 'standard' starches contain 20-30 wt% amylose. In 'waxy' starches produced by certain mutant plants, the amount of amylose is nearly zero to a few percent, while 'high-amylose' starches can contain up to 80-100% amylose (Bertoft, 2004; Carciofi et al., 2012; Hanashiro, 2015).

Native amylose contains a mixture of linear and branched molecules (Hanashiro, 2015). So far, no effective method for the separation of linear and branched amyloses is known (Buléon et al., 1998). The ratio of linear to branched molecules is usually measured by determining the β -amylase limit dextrin that is labeled at its reducing end prior to β -amylolysis (Hanashiro et al., 2013; Takeda et al., 1992a). On a molar basis, branched molecules are accounted for 15-70% with typical values of 20–50% , depending on the botanical and varietal sources (Hanashiro, 2015; Jane, 2009). The amount of branched amylose also varies between the different molecular weight fractions. For example, the fraction of large molecules (DP 2500) of maize and rice amyloses are mainly branched molecules (66% for maize, 61% for rice) while the fraction of small molecules (DP 400) contains lower amounts of branched chains (29% for maize, 25% for rice) (Hanashiro, 2015; Jane, 2009).

The average chain length of native amylose considerably varies between the different botanical sources with DP_n in the range of $5 \cdot 10^2$ to $6 \cdot 10^3$ (Jane, 2009; Ong et al., 1994). Generally, cereal amyloses are shorter than amyloses from root and tuber starches, and branched amylose molecules are 1.5–3.0-fold larger than linear ones from the same preparation (Hizukuri et al., 1989; Takeda et al., 1992b; Takeda et al., 1989). On a molar basis, long amyloses with $DP > 1000$ are predominant (75–90%) in potato and sweet potato starch, while short amyloses with $DP < 1000$ are predominant (50–75%) in amyloses from maize, wheat, barley, and rice (Hanashiro & Takeda, 1998).

Many experimental methods are described in the literature for the fractionation of amylose from starch. Based on their underlying separation principles, Hanashiro (2015) divides them into four groups: (1) aqueous leaching (hot-water extraction) of amylose (Banks et al., 1959; Greenwood & Thomson, 1962; Higginbotham & Morrison, 1949; Hizukuri, 1991; Meyer et al., 1940a; Meyer et al., 1940b; Mua & Jackson, 1995; Young, 1984), (2) precipitation of an insoluble complex of amylose with complexing agents (Bourne et al., 1948; Kuge & Takeo, 1968; Lansky et al., 1949; Leiser et al., 1967; Marotta & Ryan, 1965; Schoch, 1941),

(3) chromatography (Karve et al., 1981; Kennedy et al., 1992; Ulmann & Richter, 1962; Yamada & Taki, 1976), and (4) separation of soluble amylose from an insoluble complex of amylopectin with a lectin, concanavalin A (Matheson, 1996; Matheson & Welsh, 1988). Other techniques such as selective retrogradation (Etheridge et al., 1962; Hathaway, 1971; Kurimoto & Yoshida, 1973; Young, 1984) or ultracentrifugation (Takeda et al., 1986) have also been reported. Each method has advantages and disadvantages in terms of its requirement of starch amount, yield and purity of amylose, and throughput. Methods 3 and 4 require less samples and are suitable for high-throughput analysis, but they are not suitable for large-scale production due to low yields. With aqueous leaching, the yield and composition of leached materials depend on several factors, *i.e.*, extraction temperature, heating rate, starch concentration, stirring speed, defatting and other treatments of starch granules before leaching. However, the leached product always contains a certain amount of amylopectin. The fractionation by formation of insoluble complexes of amylose (method 2) allows a higher purity of amylose and is usually used to further purify amylose obtained from other methods, *e.g.* aqueous leaching. However, the complexing agents, among which 1-butanol is widely used, should be carefully chosen.

1.1.2.2. *In vitro* biosynthesis of amylose

Amylose can be synthesized *in vitro* using various enzymes, as listed in **Table I.1** (Ohdan et al., 2006). Unlike native amylose, synthetic amylose has a narrower molecular weight distribution and an unbranched, linear structure. In addition, while the fractionated native amylose is usually contaminated by amylopectin, the *in vitro* synthesis of amylose allows obtaining pure fractions. However, the chain length of amylose and yield depend on the enzymes that are used.

Glucan phosphorylase (GP) and its substrate, glucose-1-phosphate (G-1-P), constitute an excellent system to produce amylose since the molecular size of amylose can be controlled precisely with high yield (>60%) (Ohdan et al., 2006; Yanase et al., 2005). However, the problem of this system is that G-1-P is too expensive for industrial purposes. Similarly, starch (glycogen) synthases (Leloir et al., 1961; Recondo & Leloir, 1961; Rongine et al., 1960; Tanaka & Akazawa, 1971) are not suitable for the mass production since their substrates (UDP- and ADP-glucose) are not available on an industrial scale.

Isoamylases (Akai et al., 1971; Harada et al., 1972; Masashi & Kaname, 1975), CGTase (Niemann et al., 1992; Shibuya et al., 1993), D-enzyme (Walker & Whelan, 1959), amylosucrases (De Montalk et al., 2000; Potocki-Veronese et al., 2005; Roblin et al., 2012)

require cheaper substrates and produce amylose with high yields. However, it is not possible to obtain amylose with a desired chain length using these methods since the DP of the products is about 10-100 glucose units.

Recently, the combination of a GP with sucrose phosphorylase and cellobiose phosphorylase allowed the production of synthetic amylose using cheaper substrates (Ohdan et al., 2006, 2007; Waldmann et al., 1986; Yanase et al., 2006). Sucrose phosphorylase and cellobiose phosphorylase catalyze, respectively, the phosphorolysis of sucrose and cellobiose and produce G-1-P which can be used by the GP for amylose synthesis. These methods yield amylose with a desired chain length similar to the amylose production using GP and G-1-P.

Table I.1. Enzymes that synthesize amylose *in vitro* and corresponding substrates (Ohdan et al., 2006).

Enzyme	Substrate
Starch (glycogen) synthase	ADP-glucose (UDP-glucose)
Isoamylase	Starch
CGTase	Cyclodextrin
D-enzyme	Maltodextrin
Amylosucrase	Sucrose
Glucan phosphorylase	G-1-P
Sucrose phosphorylase + glucan phosphorylase	Sucrose
Cellobiose phosphorylase + glucan phosphorylase	Cellobiose

I.1.3. Solvents and conformation of amylose in solution

I.1.3.1. Solvents

The dissolution of amylose is essential for many applications. Amylose can easily be dissolved in several solvents such as DMSO, urea solutions (6-10 M), DMSO/urea mixtures, formamide, aqueous alkaline solutions, acidic conditions and DMAc/LiCl, etc. (Banks & Greenwood, 1971a; Bertoft, 2004; Buléon et al., 1998). The solutions of amylose in these solvents are usually used for separation, purification and characterization of the structure of amylose. However, due to the solvent toxicity, water is better choice, for instance in food or pharmaceutical industries. The solubility of amylose in water is generally lower and depends on different factors. In addition to conventional factors such as temperature, pressure and molecular weight, the crystallinity or the organization of amylose chains strongly affects the solubility of the polymer. Amorphous amylose can be cold-water soluble (Protzman et al., 1967; Sarko et al., 1963) while that occurring in natural starch is easily leached into warm water (70-90 °C) (Green et al., 1975; Mitchell, 1977).

On the other hand, amylose obtained by retrogradation or recrystallization is in an organized stable crystalline state which is no longer soluble in cold or warm water (Green et al., 1975; Mitchell, 1977; Protzman et al., 1967; Sarko et al., 1963). Commercial retrograded amylose is insoluble in water unless heated above 120 °C, preferably 140 to 170 °C (autoclave) to destroy hydrogen bonding (Johannes, 1958; Protzman et al., 1967; Young, 1984). Oxidation and degradation may occur at high temperatures (Protzman et al., 1967), but the problem can be avoided by removing oxygen by nitrogen bubbling or addition of a reducing agent such as bisulfites. Furthermore, an alternative method for preparing aqueous solutions of amylose is to dissolve amylose in a good solvent such as DMSO or alkaline solution and then dilute with water to the desired concentration. The advantage of this method is that the conventional autoclaving procedure is avoided.

It is important to note that a solution of amylose in water is metastable at room temperature. With time, a significant precipitation (or retrogradation) of amylose is observed, the rate of which depends upon amylose concentration, ionic strength, and particularly upon the molecular weight of amylose (Foster & Serman, 1956; Loewus & Briggs, 1957; Whistler & Johnson, 1948). The dependence on molecular weight is particularly striking, as low molecular weight amylose alkaline solution (DP of about 100) shows signs of turbidity within minutes of neutralization while high molecular weight amylose solution (DP of about 1000 and higher) remain stable for days or weeks, under comparable conditions. Pfannemüller et al. (1971) reported that the retrogradation rate of amyloses in water containing 5% of DMSO exhibits a sharp maximum at DP_n of 80. A solution of shorter and longer molecules is more stable.

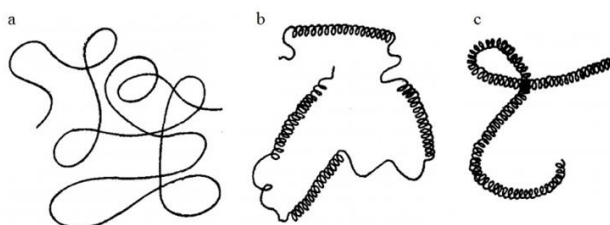


Figure I.3. Conformational models proposed for amylose in solution: a) random coil having no helical character, b) interrupted helix with helical segments connected by short random coils, c) helix with the overall form of a random coil. Adapted from Banks and Greenwood (1971a).

I.1.3.2. Conformation of amylose in solution

The conformation of amylose in solution has been the subject of many studies (Banks & Greenwood, 1971a; Everett & Foster, 1959; Hayashi et al., 1981; Jane et al., 1985;

St.-Jacques et al., 1976). Different techniques (viscometry, optical rotation, fluorescence spectroscopy, depolarization, NMR spectroscopy) have been employed but the results are still controversial. The models vary from a random coil, interrupted helix to a rigid helix, as shown in **Figure I.3** (Banks & Greenwood, 1971a). A random coil (**Figure I.3a**) has no helical character and the arrangement of successive units is random. In both interrupted helix (**Figure I.3b**) and helical models (**Figure I.3c**), the amylose chain organized in the helical portions are thought to be stabilized by intra-molecular hydrogen bonds. However, due to the flexibility of the amylose chain, any of the three structures can adopt the overall shape of a random coil model.

Several studies has shown that amylose exists as a helix in neutral aqueous solution. Foster and Zucker (1952) using streaming dichroism concluded that the uncomplexed amylose has the same conformation in aqueous solution as amylose complexed with iodine. Later studies showed a remarkable difference in optical rotation and the intrinsic viscosity between neutral aqueous solution and the alkaline solution of amylose (Hayashi et al., 1981; Rao & Foster, 1963). The authors suggested that amylose adopts a helical state stabilized by hydrogen bonds in neutral solution. In alkaline solution, the hydrogen bonds collapses and the helix transforms into a negatively charged expanded coil, consistent with a drop in intrinsic viscosity. The helix-coil transition occurs at about pH 12 (Erlander & Purvinas, 1968). Holló and Szejtli (1958) showed that the intrinsic viscosity of an amylose aqueous solution was almost unaltered by the addition of iodine up to the point of equivalence for formation of the complex. A similar behavior was also observed by addition of sodium dodecyl sulfate into an amylose solution (Rao & Foster, 1963).

These results supported the fact that amylose must predominantly contain helical segments in the absence of complexing agent. The drop in viscosity at higher complexing agent concentration probably represents an increase in helix content and in perfection of the helical structure. Szejtli and Augustat (1966) concluded that, in aqueous solution at room temperature, the rotation about the $\alpha(1\rightarrow4)$ glucosidic bonds was hindered by steric factors and only the helix, or the interrupted helix structure, may exist. Erlander and Tobin (1968) suggested that the helical conformation of amylose in DMSO/water solution is stabilized by means of the hydrogen bonds between the hydroxyl group of adjacent glucose (the C2 and C3'). St.-Jacques et al. (1976) also came to the same conclusion after observing the upfield shift of signals attributed to HO(2) and HO(3') hydroxyl protons in the NMR spectra of amylose in DMSO solution.

In contrast, a number of studies have brought evidence which favors the concept that amylose in aqueous solution and in the absence of a complexing agent behaves as a random

coil. The investigation of the viscosity of amylose as a function of M_w in water and neutral aqueous potassium chloride solution gave the relation $\eta = 0.115 M_w^{0.5}$ (Banks & Greenwood, 1963, 1968a; Banks & Greenwood, 1969; Cowie, 1960, 1963; Everett & Foster, 1959). The exponent value of M_w is that expected for a random coil. If amylose possesses a helical, rod-like structure, an exponent of 1.8 would be expected (Young, 1984). Related investigations showed that amylose in "good" solvents such as DMSO, alkaline solution and formamide gave an exponent values of M_w in range of 0.62-0.89, indicating that the random coil was expanded as a result of long-range interactions with the solvents (Banks & Greenwood, 1968b; Banks & Greenwood, 1969; Banks & Greenwood, 1971a; Burchard, 1963; Cowie, 1960; Everett & Foster, 1959; Nakanishi et al., 1993). Banks and Greenwood (1968b) believe that amylose in solution behaves like a random coil and, while there may be some helical character present, it is a very loose in structure.

In contradiction with the previous evidence in favor of a helical conformation of amylose in aqueous solution (Holló & Szejtli, 1958; Rao & Foster, 1963), Banks and Greenwood (1971b) showed that the viscosity decreased upon addition of complexing agents. The authors also pointed out the errors that the previous works suffered from. The ionic strength varied during the experiment, and, more importantly, an incorrect viscosity function was used. This result unambiguously confirmed that amylose existed as random coils in aqueous solution and adopted a helical structure upon the addition of complexing agents. They also suggested that the helicity resulted not only from intramolecular hydrogen bonds but also as a consequence of the geometry of the $\alpha(1\rightarrow4)$ glucosidic linkages. In agreement with this conclusion, Jane et al. (1985) observed the marked downfield shift of the signals of C1 and C4 carbons for amylose complexes formed by addition of DMSO, triiodide, alcohols, etc., into aqueous amyloextrin solutions. The changes in the ^{13}C NMR spectra were shown to be reversed by the chemical destruction of the complexing agent, confirming the role of complexing agent in the helix \rightarrow coil transition. From the review of its behavior in diluted solution, amylose is likely to have the conformations indicated in **Figure I.4** (Banks & Greenwood, 1971a).

I.1.4. Crystalline structure of recrystallized amylose: A- and B-amylose

Native starch granules exhibit two allomorphic types (A- and B-type) that can be readily identified by X-ray diffraction (XRD) and solid-state ^{13}C NMR spectroscopy (**Figure I.5**) (Lourdin et al., 2015). However, starch granules of many different sources exhibit a third XRD pattern referred to as C-type but it has been shown to correspond to a mixture of A- and B-types.

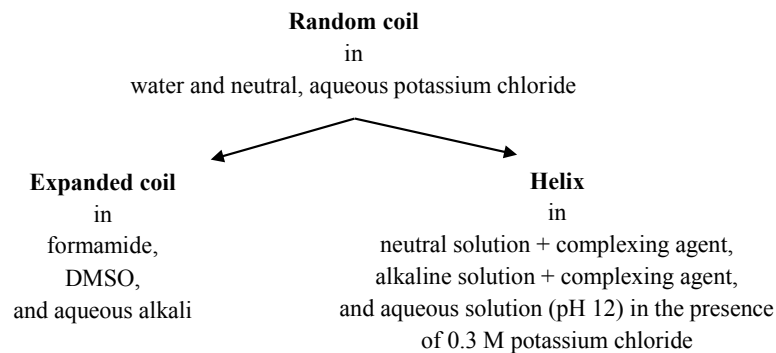


Figure I.4. Conformation of amylose in dilute solution. Adapted from Banks & Greenwood (1971a).

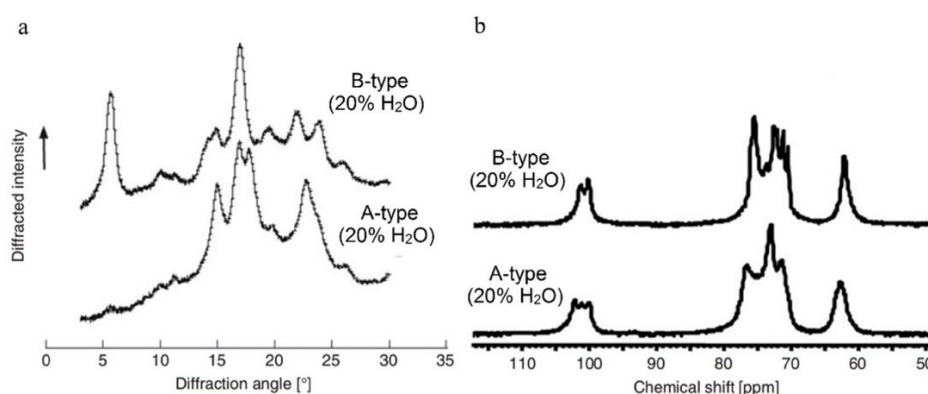


Figure I.5. X-ray diffraction profiles (a) and solid-state ^{13}C CP-MAS NMR spectra (b) of A and B starch recorded at 20% H_2O . Adapted from Buléon et al. (2007).

It is generally accepted that, in starch granules, amylose forms amorphous layers separated by the layers of semicrystalline amylopectin. (Lourdin et al., 2015; Tester et al., 2004). The extraction of amylose from starch granules by leaching in appropriate conditions does not significantly affect the crystallinity or disrupt the granules (Montgomery & Senti, 1958). Recently, amylose-only starch granules were successfully produced with high yield in barley by suppression of amylopectin synthesis via silencing the entire complement of genes encoding starch branching enzymes (Carciofi et al., 2012). The amylose-only starch exhibited a relatively low crystallinity (25%), and contained a mixture of B (55%) and V (45%) allomorphs. The V-type was thought to correspond to the crystalline complexes of amylose with the lipids present in the starch granules (see Section I.2.). A similar composition was also observed for high-amylose starches (Morell et al., 2003).

Various studies have shown that of both A-type and B-type can be prepared *in vitro* in the form of single crystals or spherocrystals, as shown in Figures I.6 and I.7, by recrystallization of amylose, especially short-chain amylose or limit dextrans (Buléon et al., 1984; Creek et al.,

2006; Gidley & Bulpin, 1987; Helbert et al., 1993; Imberty et al., 1987; Montesanti, 2008; Montesanti et al., 2010; Pfannemüller, 1987; Popov et al., 2009; Popov et al., 2006; Putaux et al., 2011a; Ring et al., 1987). The solvent, temperature, concentration of amylose and DP of amylose are the main decisive parameters that control the morphology and the crystal structure (Buléon et al., 2007). A general rule is that long chains and low crystallization temperatures favor B-type, whereas short chains, high temperatures and high concentrations induce A-type (Buléon et al., 2007). In addition, a high concentration of amylose, at least 5 wt%, is required for the formation of spherocrystals while single crystals are prepared at lower concentrations (*ca.* 0.05 wt%) (Buléon et al., 2007; Helbert, 1994; Ring et al., 1987). Precipitants such as ethanol and acetone can be added to promote the crystallization of A-amylose while this is not essential for B-amylose (Buléon et al., 1984; Imberty et al., 1987; Montesanti et al., 2010).

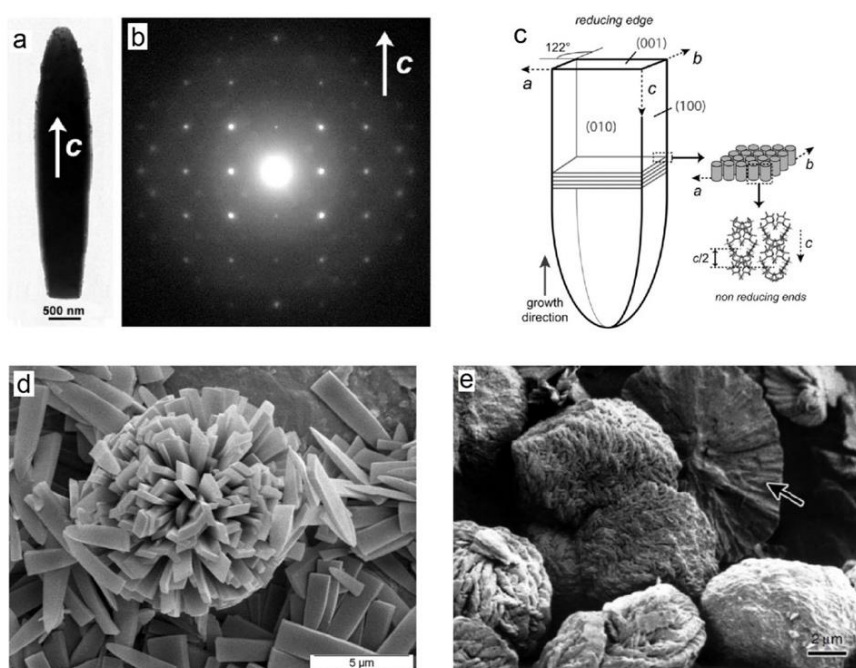


Figure I.6. a) TEM image of a single crystal of A-amylose; b) example of ED pattern properly oriented with respect to the crystal (Montesanti et al., 2010); c) scheme describing the orientation of double helices in the crystal (Putaux et al., 2011b); d) SEM image of A-amylose single crystals radially organized in a spherical aggregate (Montesanti et al., 2010); e) SEM image of A-amylose spherulites. The radial organization is well revealed in the fracture of one of them, as indicated by the arrow (Helbert, 1994).

Micrometer-size single crystals of A-amylose with a faceted morphology, as shown in **Figure I.6**, have been prepared in dilute solutions of short-chain amylose (Montesanti et al., 2010). The electron diffraction (ED) analysis showed that the chain axis was parallel but in an opposite direction to that of the crystal growth (**Figure I.6**). In addition, the crystals exhibited

a suitable size and sufficient perfection to allow the collection of ED as well as XRD datasets up to the resolution of 0.151 nm (Montesanti, 2008; Popov et al., 2009). On the other hand, lamellar B-amylose crystals with a similar size and perfection have never been prepared from dilute solution. The only lamellar B-type crystals reported in the literature, so far, were aggregated (Figure I.7a) but monocrystalline zones could be identified, giving single crystal ED patterns (Figure I.7b) (Buléon et al., 1984).

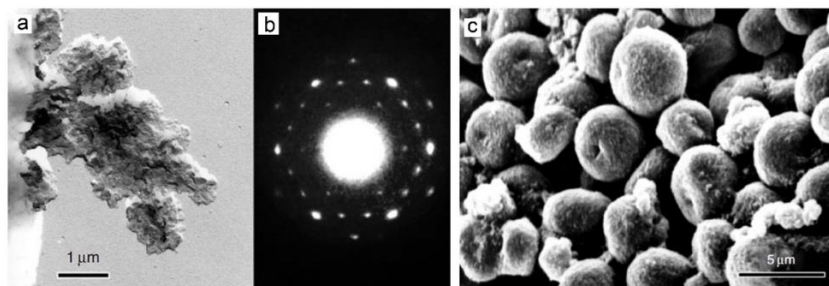


Figure I.7. a) TEM image of B-amylose lamellar crystals prepared by *in vitro* crystallization (Buléon et al., 1984); b) base-plane ED pattern recorded on a single crystal (Buléon et al., 1984); c) SEM image of B-amylose spherocrystals (Helbert, 1994).

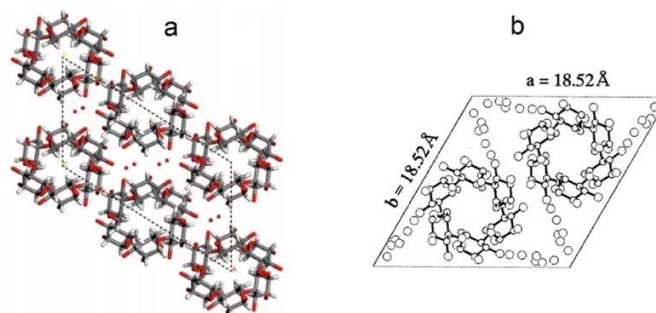


Figure I.8. Projection in the (a,b) plane of the molecular models of A- and B-amylose (Popov et al., 2009; Takahashi et al., 2004).

By comparison to the starch granules, which exhibit a relatively low crystallinity and a complex ultrastructure, model crystals of recrystallized amylose are more suitable for studying the morphology and crystal structure of allomorphs A and B (Imberty et al., 1987; Imberty & Perez, 1988). In the most recent models, based on diffraction data of single crystals and fibers, amylose are organized in parallel-stranded 6-fold left-handed double helices with pitches of 2.12 and 2.11 nm for A and B-type, respectively (Montesanti, 2008; Popov et al., 2009; Takahashi et al., 2004). In the A-type, these double helices are packed with the $B2$ space group in a monoclinic unit cell ($a = 2.083$ nm, $b = 1.145$ nm, $c = 1.058$ nm, $\gamma = 122^\circ$) with 8 water molecules per unit cell (Figure I.8a) (Popov et al., 2009). In the B structure, double helices are

packed with the $P6_1$ space group in a hexagonal unit cell ($a = b = 1.852$ nm, $c = 1.057$ nm, $\gamma = 120^\circ$) with 36 water molecules per unit cell (**Figure I.8b**) (Takahashi et al., 2004). On the basis of the space group, the repeating unit is a maltotriosyl unit in the A-form and a maltosyl unit in the B-form. This is supported by the solid-state ^{13}C NMR data: the C1 peak in the spectra of the A-form is a triplet while it is a doublet in the spectra of the B-form (**Figure I.5b**).

I.2. Crystalline inclusion complexes of amylose: V-amylose

I.2.1. Definition

V-amylose is the generic term to describe crystalline helical inclusion complexes of amylose with small guest molecules (Putseys et al., 2010; Obiro et al., 2012). V-amylose was first reported by Katz (1930) who studied the baking of bread and characterized samples of starch precipitated with alcohols (Katz & Derksen, 1933; Bear, 1942). By studying complexes with iodine, Freudenberg et al. (1939) proposed that V-amylose contained single helices. Later, XRD studies confirmed without ambiguity the helical nature of V-amylose (Rundle et al., 1944; Rundle & Edwards, 1943). The structure was also characterized and supported by NMR spectroscopy (Gidley & Bociek, 1988; Jane et al., 1985; Veregin et al., 1987). The flexibility of the linear chain and the geometry of the $\alpha(1\rightarrow4)$ glucosidic bonds (French, 1979; French & Murphy, 1977b) are thought to promote helical trajectories, generating a central cavity that can host complexing molecules. A large variety of inorganic and organic molecules have the ability to form the complexes with amylose (Tomasik & Schilling, 1998a, 1998b). The most common are iodine, fatty acids, alcohols, ketones, esters as well as many flavor compounds. Recently, the inclusion complexes of amylose with several polymers (Gotanda et al., 2016; Kadokawa et al., 2001; Kadokawa et al., 2002) and carbon nanotubes (Lii et al., 2003; Yang et al., 2008) have also been reported. V-amylose complexes with lipids have been detected in native starch granules (Carciofi et al., 2012; Gernat et al., 1993; Morell et al., 2003; Morrison, 1988). However, the structure of V-amylose has generally been studied from samples prepared by *in vitro* crystallization.

I.2.2. Preparation methods

I.2.2.1. Crystallization of amylose in aqueous solution in the presence of a complexing agent

As previously mentioned, aqueous amylose solutions are metastable with the chains adopting a random coil conformation. In the presence of suitable complexing agents, amylose forms helical inclusion complexes and, at low amylose concentration, crystallizes in the form of lamellar crystals. The procedure generally involves dissolving amylose in an appropriate solvent, adding the complexing agent at an elevated temperature and incubating the mixture at

a suitable temperature or cooling down to allow the crystallization to occur. The most frequently used solvents are water (Helbert, 1994; Nuessli et al., 2003; Takeo & Kuge, 1969), alkaline solution (Karkalas et al., 1995; Takeo et al., 1973), and DMSO/water mixtures (Biliaderis & Galloway, 1989; Godet et al., 1993). In water, high temperatures (120-170 °C) and high pressures (autoclave) are required for a complete solubilization. Prior to heating, oxygen must be removed from the system by nitrogen bubbling in order to avoid degradation and oxidation. In alkaline solution and DMSO, the dissolution of amylose occurs at room temperature in about 24 h but the process can be accelerated by heating to a higher temperature (90-100 °C). Then, the solution is diluted with water to reach the desired concentration. Besides, a neutralization step is required for the complex formation in alkaline medium (Karkalas et al., 1995; Takeo et al., 1973).

Several specific techniques such as homogenization (Lesmes et al., 2008; Meng et al., 2014), extrusion-cooking (Colonna & Mercier, 1983; De Pilli et al., 2008; Mercier et al., 1980; Raphaelides et al., 2010; Raphaelides et al., 2015), steam jet-cooking (Byars et al., 2003; Fanta et al., 1999; Fanta et al., 2002; Fanta et al., 2008) and microwave heating (Felker et al., 2013) have been applied to prepare V-amylose complexes. They are thought to increase the solubility of both amylose and ligand under high-shearing and high-heating temperature conditions, and thus enhance the complexation. In addition, these techniques allow to manipulate high starch / amylose concentrations (10-20 wt%), and are thus suitable for a large-scale production. Besides, the preparation of V-amylose complexes in differential scanning (DSC) calorimetry pans (Cieśla & Eliasson, 2003; Creek et al., 2007; Sievert & Holm, 1993), visco-analyzers and rheometers (D'Silva et al., 2011; Nelles et al., 2000; Obiro et al., 2012) have also been reported. Recently, Rangelov et al. (2017) reported a new method of preparation of V-amylose complexes with lysophosphatidylcholine by mechanical milling of aqueous suspension of starch (10 wt%) in the presence of complexing agent. In addition, Le Bail et al. (2013) reported the formation of V-amylose complexes under high pressure treatment. The advantage of the use of high pressure and mechanical milling is that they allow producing a large amount of compound in a mild condition (low temperature, *i.e.* 40 °C).

I.2.2.2. Crystallization of amylose in the dry state (sealed-heating method)

The procedure consists in sealing the physical mixture of amylose and complexing agent in a glass container and then heating at 100-150 °C to allow the formation of complexes (Oguchi et al., 1998; Tozuka et al., 2006; Uchino et al., 2001, 2002). The predissolution of amylose in a solvent is not necessary. Despite being prepared in the dry state, the resulting V-amylose appears to be significantly crystalline, as indicated by rather well defined powder XRD patterns.

I.2.2.3. Crystallization of amylose by solvent removal

This method has been used to prepare the complexes of amylose in the presence of solvent molecules such as DMSO and ethylenediamine (French & Zobel, 1967; Simpson, 1970; Zobel et al., 1967). First, concentrated amylose solutions (20-25 wt%) in the solvent are prepared, then casted in the form of a film on a glass plate. After evaporation of the excess solvent, the crystalline films are uniaxially stretched so that fiber XRD patterns of the resulting V-amylose can be recorded.

I.2.2.4. Vine-twinning enzymatic polymerization

This method uses glucan phosphorylase (GP) and glucose-1-phosphate (G-1-P) to enzymatically construct an amylose helix around appropriate hydrophobic ligands such as lipids, single-wall carbon nanotubes, ibuprofens and many polymers (Gelders et al., 2005b; Kadokawa, 2012; Yang et al., 2008; Yang et al., 2013). In particular, for amylose-polymer inclusion complexes, the method has been referred as 'vine-twinning polymerization'.

This biotechnology approach shows several advantages over other preparation methods of V-amylose. First, it allows preparing inclusion complexes with polymers or carbon nanotubes which are hardly obtained by other methods. Second, the DP of amylose can be controlled by varying the amount of reacted G-1-P (Gelders et al., 2005b; Kaneko et al., 2009; Kaneko et al., 2008b; Putseys et al., 2009). Thirdly, it allows selective inclusions: i) of one from a mixture of two resembling guest polymers (Kaneko et al., 2007; Kaneko et al., 2008a); ii) of one from a mixture of two stereoisomers (Gotanda et al., 2016); and iii) of a specific range of molecular weights of guest polymers (Kaneko et al., 2009). On the other hand, the disadvantages of this method are the use of expensive substrate (G-1-P) and extended reaction times for preparing small amounts of amylose complexes.

I.2.2.5. Insertion of a complexing agent in preformed V-amylose

This method uses a preformed V-amylose to produce inclusion complexes of a desired complexing agent. One of the approaches is to exchange the complexing agent present in the preformed V-amylose by the new one. This can be done by dispersing or successive washing the preformed V-amylose crystals with the new complexing agents (solvents) or with hydroalcoholic solutions of the new complexing agents (Helbert & Chanzy, 1994; Hinkle & Zobel, 1968; Senti & Witnauer, 1952; Takeo & Kuge, 1969; Zobel et al., 1967). It is interesting to note that the exchange of complexing agents can result in a change in crystal structure and helical conformation but the initial morphology of the crystal is maintained.

Recently, Kong and Ziegler (2014) proposed another approach for preparing amylose complexes in which the guest molecules were inserted into preformed "empty" V-amylose helices. The "empty" V-amylose was prepared by thoroughly drying V-amylose complexed with highly volatile ethanol. The preformed "empty" V-amylose and the guest molecules were then mixed together in an acetone/ethanol/water mixture to induce the formation of complexes. The acetone/ethanol/water mixture was used to increase the diffusibility of the guest molecules.

The advantage of the above techniques is that the insertion of the desired complexing agent can be conducted at room temperature and without solubilizing amylose. However, the results would depend on the affinity of the complexing agents with the preformed V-amylose.

I.2.3. V-amylose polymorphism

In the literature, V-amylose complexed with more than 150 different complexing agents have been prepared in the form of crystalline fibers or lamellar crystals (Helbert, 1994). They have been grouped into 8 allomorphic families based on XRD or ED patterns, as listed in **Table I.2**. The origin of the polymorphism has been accounted for by the flexibility of the linear amylose chains that adapt their arrangements and helical conformation to adjust to the molecular shape and chemical nature of the complexing agents (Biais, 2006; French, 1979; Helbert, 1994).

Although the knowledge of the molecular structure is important to understand the interaction between amylose and complexing agents, the conformation and packing of amylose are difficult to determine, with a limited number of ED or XRD reflections recorded from fiber and lamellar crystals. Therefore, only a small number of structures have been resolved and several models are still hypothetical (Putaux et al., 2011b).

It is interesting to note that all the models proposed for V-amylose are based on left-handed single helices with different conformations (**Figure I.9**). In the following, the V-amylose allomorphic families will be presented in two groups of amylose helical conformations: compact-helix and extended-helix.

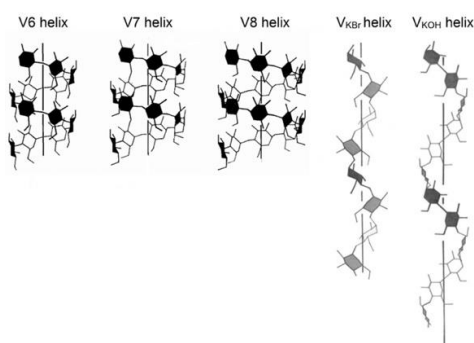


Figure I.9. Known V-amylose single helices. Adapted from French (1979).

Table I.2. Known V-amylose allomorphs.

Allomorph	Crystal system	Cell parameters (nm)			Helicity			References
		<i>a</i>	<i>b</i>	<i>c</i>	<i>n</i>	<i>p</i> (nm)	<i>h</i> (nm)	
V _{6I} (V _h)	hexagonal	1.37	1.37	0.81	6	0.81	0.13	(1)
	orthorhombic	1.37	2.37	0.81	6	0.81	0.13	(2)
V _{6II} (V _{1-butanol})	orthorhombic	2.65	2.74	0.80	6	0.80	0.13	(3)
V _{6III} (V _{DMSO})	orthorhombic	1.92	1.92	2.44/0.81	6	0.81	0.14	(4,5)
V ₇ (V _{2-propanol})	orthorhombic	2.83	2.95	0.80	7	0.80	0.11	(6)
V ₈ (V _{1-naphthol})	tetragonal	2.32	2.32	0.79	8	0.79	0.10	(7)
V _{KBr}	tetragonal	1.07	1.07	1.61	4	1.61	0.40	(8)
V _{KOH}	orthorhombic	0.88	1.23	2.24	6	2.24	0.37	(9)

n: number of monomers per turn; *p*: pitch; *h*: raise per monomer; (1) Brisson et al. (1991); (2) Rappenecker and Zugenmaier (1981); (3) Helbert and Chanzy (1994); (4) French and Zobel (1967); (5) Winter and Sarko (1974a); (6) Nishiyama et al. (2010); (7) Cardoso et al. (2007); (8) Senti and Witnauer (1952); (9) Sarko and Biloski (1980).

I.2.3.1. Compact-helix V-amylose

The majority of examples of V-amylose complexed with iodine and small organic molecules contain compact helices whose cavity can host the complexing agents. Depending on the nature and size of the guest molecule, helices with 6, 7 and 8 glucosyl residues per turn have been reported (Putaux et al., 2011b). All of them have a similar pitch of about 0.8 nm, indicating a compact arrangement of glucosyl residues (Figure I.9). The characterization of compact-helix complexes having different helical conformations by solid-state ¹³C NMR revealed that all the V-amylose single helices give only one signal for each carbons of the glucosyl residues and are thus more symmetric than that of the double-stranded A- and B-type (Gidley & Bociek, 1988; Horii et al., 1987; Veregin et al., 1987). The helices are stabilized by intramolecular hydrogen bonds between O-2 and O-3(2) of each pair of contiguous glucose residues and between atoms O-6(i+7) and O-2(i+1) of each pair of contiguous helix loops (Brisson et al., 1991; Rappenecker & Zugenmaier, 1981; Sarko & Zugenmaier, 1980; Takeo & Kuge, 1969).

Five allomorphic families of compact-helix V-amylose have been reported, in which three contain 6-fold helix, one contains 7-fold helix and one contains 8-fold helix. Helbert (1994) proposed a nomenclature system for the compact-helix V-amylose based on the number of residues per turn and volume of inter-helical space. Consequently, the three 6-fold V-amylose families can be called as V_{6I}, V_{6II} as V_{6III} as a function of the volume of inter-helical space. The 7- and 8-fold V-amylose families can be called V₇ and V₈, respectively.

Some of the compact-helix V-amylose samples have been prepared as fibers yielding well-resolved X-ray fiber diffraction diagram (Bluhm & Zugenmaier, 1981; French & Zobel, 1967; Hinkle & Zobel, 1968; Rappenecker & Zugenmaier, 1981; Simpson, 1970; Winter & Sarko, 1972; Zaslów et al., 1974; Zobel et al., 1967). However, when crystallized from dilute solution, amylose can form micrometer-size lamellar single crystals that can be analyzed by electron diffraction (Buléon et al., 2007; Putaux et al., 2011b). The crystals are about 10 nm-thick and the chain axis is perpendicular to the lamella surface. This implies that when chains are much longer than the lamella thickness, chain folding occurs, favored by the so-called 'flip' between two adjacent glucosyl residues which leads to a reversal of molecular trajectory (Jacob et al., 1998).

I.2.3.1.1. V_{6I}

V_{6I}, also frequently called V_h, is the best documented crystalline V-amylose family in the literature (Buléon et al., 2007). It can be prepared with iodine as well as many organic molecules having a linear aliphatic chain such as fatty acids, alcohols, emulsifiers (Bluhm & Zugenmaier, 1981; Brisson et al., 1991; Helbert, 1994; Takeo et al., 1973; Takeo & Kuge, 1969). In addition, some bulky molecules such as quinoline, (-)-borneol, *trans*-decalin, *p*-aminobenzoic acid and analogues were also reported to yield this structure, although their size are not compatible with the 6-fold helical cavity (Helbert, 1994; Tozuka et al., 2006).

Rappenecker and Zugenmaier (1981) first proposed a model determined from XRD data of crystalline fibers (**Figure I.10d**), which consists of a pseudo-hexagonal orthorhombic unit cell, space group $P2_12_12_1$, with $a = 1.365$ nm, $b = 2.370$ nm, and $c = 0.805$ nm. The unit cell contains two 6-fold left-handed helices and 16 water molecules (eight inside and eight between the helices). Within the model, the helices are packed on a hexagonal network but with a regularly alternating arrangement of up and down chains. Bluhm and Zugenmaier (1981) also proposed a similar model from fibers of V_{6I} obtained with iodine.

On the other hand, lamellar single crystals prepared in dilute solution exhibit a characteristic hexagonal shape and give a sharp ED diagram with a hexagonal symmetry (**Figure I.10a** and **I.10b**) (Brisson et al., 1991; Helbert, 1994). Based on the ED data, Brisson et al. (1991) proposed a another model based on a hexagonal unit cell, space group $P6_522$ with $a = b = 1.365$ nm, and $c = 0.805$ nm (**Figure I.10c**). The unit cell contains one 6-fold left-handed helix and 18 water molecules (6 inside and 12 between the helices). The helices are thus packed on a hexagonal network with statistically random up/down chain disorder.

The two models are essentially similar in terms of helical conformation and hexagonal arrangement of helix. The center-to-center helix distance (helix packing diameter) is equal to the

a -parameter (1.37 nm). In the compact arrangement, the complexing agent can only reside inside the helix since the interstitial space is limited (Bluhm & Zugenmaier, 1981; Godet et al., 1993).

Upon thorough drying, V_{6I} is transformed into the so-called V_a with a smaller unit cell ($a = b = 1.30$ nm and $c = 0.79$ nm for the hexagonal unit cell, and $a = 1.30$ nm, $b = 2.25$ nm and $c = 0.79$ nm for the orthorhombic one) (Mikus et al., 1946; Murphy et al., 1975; Takeo et al., 1973; Takeo & Kuge, 1969; Winter & Sarko, 1974b). The hexagonal arrangement remains the same but the helices get closer, probably due to the elimination of interstitial water molecules. Indeed, Murphy et al. (1975) showed that the dry complex was nearly free of water.

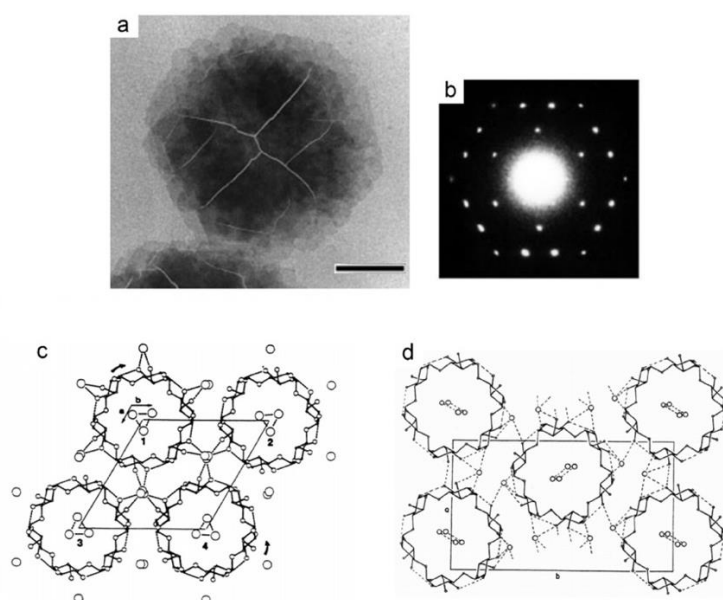


Figure I.10. V_{6I} crystals: a) TEM image (bar: 1 μm) and b) corresponding base-plane ED pattern (Helbert, 1994); c,d) projections on the (a,b) plane of the molecular models based on hexagonal (Brisson et al., 1991) and orthorhombic unit cells (Rappenecker & Zugenmaier, 1981), respectively.

I.2.3.1.2. V_{6II}

V_{6II} complexes, also called V_{*n*-butanol} type, can be obtained by crystallization of amylose in the presence of *n*-butanol as well as other linear aliphatic alcohols, ketones having 6-8 carbons, hexanal, ethyl hexanoate, hexanoic acid and some dicarboxylic acids (Biais, 2006; Conde-Petit et al., 2006; Helbert, 1994; Helbert & Chanzy, 1994; Hinkle & Zobel, 1968; Schoch, 1942; Takeo et al., 1973; Takeo & Kuge, 1971). These crystals are very sensitive to desolvation. Air or vacuum drying the crystals results in a transition from V_{6II} to V_{6I} and finally to V_a.

Lamellar crystals prepared from dilute solution have a rectangular shape (Figure I.11a). Base-plane ED patterns recorded on frozen-hydrated crystals at low temperature exhibit a rectangular pattern (Figure I.11b) that can be indexed on the basis of an orthorhombic unit cell,

space group $P2_12_12_1$, with $a = 2.74$ nm, $b = 2.65$ nm and $c = 0.80$ nm (Helbert & Chanzy, 1994). The same result is obtained from XRD powder data of hydrated crystals (Helbert & Chanzy, 1994; Le Bail et al., 2005). Since $V6_{II}$ can easily be transformed into $V6_I$ upon drying, the crystals have been thought to contain 6-fold left handed-helices. Helbert and Chanzy (1994) proposed that amylose helices were organized in antiparallel pairs with some solvent molecules located between the helices and occupying about 10% of the cell volume (Figure I.11c). Although crystalline fibers of $V6_{II}$ prepared with *n*-butanol have also been studied (Hinkle & Zobel, 1968), there is still no conclusive data regarding the helical conformation and packing arrangement of the amylose chains.

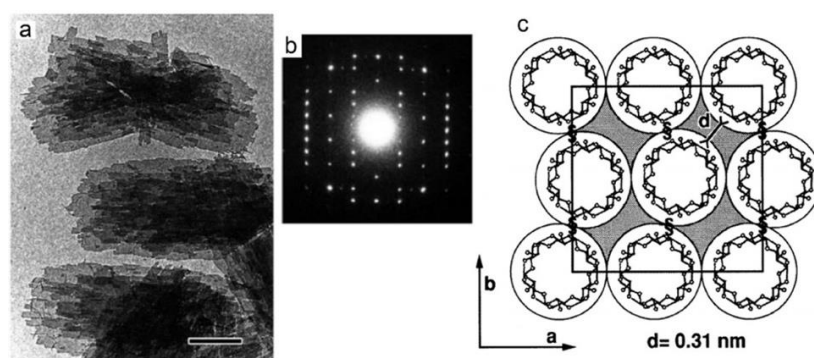


Figure I.11. $V6_{II}$ crystals: a) TEM image (scale bar: 1 μm) of single crystals of $V_{1\text{-butanol}}$ and b) corresponding base-plane ED pattern; c) projection on (a,b) plane of the probable organization of amylose helices within the unit cell. The guest solvent molecules occupy the shaded areas. Adapted from Helbert & Chanzy (1994).

I.2.3.1.3. $V6_{III}$

The term $V6_{III}$ was once used to refer the $V_{2\text{-propanol}}$ crystals and isomorphous complexes (Biais et al., 2006; Conde-Petit et al., 2006; Helbert, 1994). However, the structure of $V_{2\text{-propanol}}$ has recently been solved by refinement against ED data combined with packing analyses, showing that the complexes contain 7-fold helices (Nishiyama et al., 2010) rather than the previously proposed 6-fold helices (Buléon et al., 1990).

The term $V6_{III}$ is now used to name the 6-fold allomorphic family of V_{DMSO} (French & Zobel, 1967) and isomorphous structures (French & Murphy, 1977a; Hulleman et al., 1996; Simpson, 1970). The crystals have been prepared in the form of fibers and characterized by XRD. Lamellar single crystals were also prepared from dilute solutions in the presence of glycerol (Hulleman et al., 1996). They have a square shape with lateral dimensions of several micrometers and give sharp base-plane ED patterns that exhibit a square symmetry (Figure I.12a and I.12b).

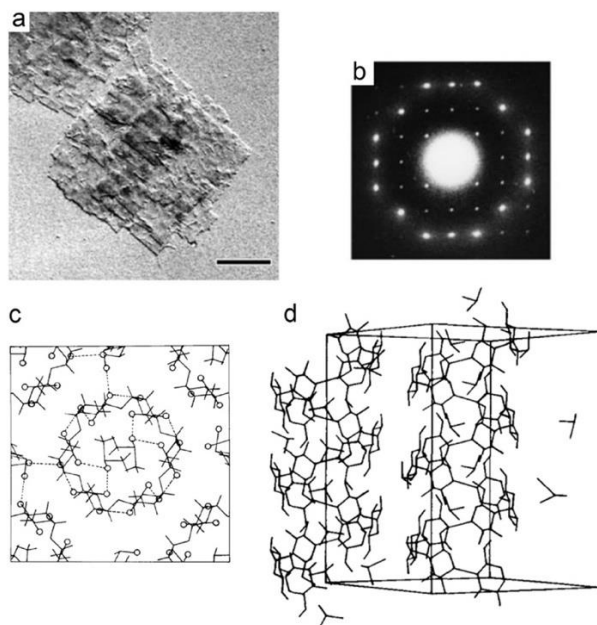


Figure I.12. V_{6III} structure: a) TEM image (scale bar, 1 μm) of single crystals of V_{glycerol} and b) corresponding base-plane ED pattern (Hulleman et al., 1996); c) projection in the (a,b) plane and d) 3D view of the V_{DMSO} structure (Winter & Sarko, 1974a).

Winter and Sarko (1974a) proposed a molecular model for V_{DMSO} based on fiber XRD data (Figure I.12c,d). The unit cell is pseudo-tetragonal orthorhombic with space group $P2_12_12_1$ with $a = b = 1.917$ nm and $c = 2.439$ nm. It contains two antiparallel 6-fold left-handed helices with three turns per crystallographic repeat. DMSO is located both inside and between the helix along with some water molecules. The interstitial DMSO is thought to be the source for additional layer lines and the higher crystallographic repeat which is three times of the 0.81-nm helix repeat distance. Similar lattices constants have been found for V_{glycerol} (French & Murphy, 1977a) and $V_{\text{ethylenediamine}}$ (Simpson, 1970) by XRD but the c -parameter was reported to be equal to the helix repeat. On the other hand, Hulleman et al. (1996) found a pseudo-tetragonal unit cell with a slightly different from b , based on ED data ($a = 1.93$ nm, $b = 1.86$ nm and $c = 0.83$ nm).

Unlike other V_6 complexes, the V_{6III} is stable under vacuum, suggesting that water and complexing agents are bound very tightly. The removal of the complexing agent and water from V_{6III} complexes requires drastic conditions such as washing with alcoholic solutions. This results in a transition into V_{6I} (French & Zobel, 1967; Hulleman et al., 1996).

I.2.3.1.4. V7

This 7-fold allomorphic family includes $V_{2\text{-propanol}}$ and isomorphous complexes prepared with DMSO, branched alcohols, ketones with 3-5 carbons, short-chain fatty acids and many cyclic compounds (Brisson et al., 1991; Helbert, 1994; Le Bail et al., 2005; Nishiyama et al.,

2010; Nuessli et al., 2003; Putaux et al., 2008; Shogren et al., 2006; Simpson et al., 1972; Takeo et al., 1973; Takeo & Kuge, 1969, 1971; Yamashita & Hirai, 1966; Zaslow, 1963). The crystals prepared from dilute solution are rectangular lamellae, radiating from the same nucleation site, forming characteristic flower-like aggregates (**Figure I.13a**) (Buléon et al., 1990; Nuessli et al., 2003; Putaux et al., 2008; Yamashita et al., 1973; Yamashita & Hirai, 1966). They yield a sharp base-plane ED pattern exhibiting an orthorhombic symmetry (**Figure I.13b**).

The existence of a 7-fold helical conformation was first proposed by Zaslow (1963) for complexes with *tert*-butanol and was then supported by Yamashita and Hirai (1966). However, Brisson et al. (1991) observed that the isomorphous complexes prepared with 2-propanol or acetone could be transformed into V6_I after washing with alcohols and drying without changing the crystal morphology. The authors thus proposed an alternate model based on 6-fold helices and the "V6_{III}" denomination was then given for this allomorphic type by Helbert (1994). Recently, the crystallographic study by Nishiyama et al. (2010) has demonstrated that the constituting helices were more likely 7-fold. Consequently, we will use the notation "V7" to name this allomorphic family.

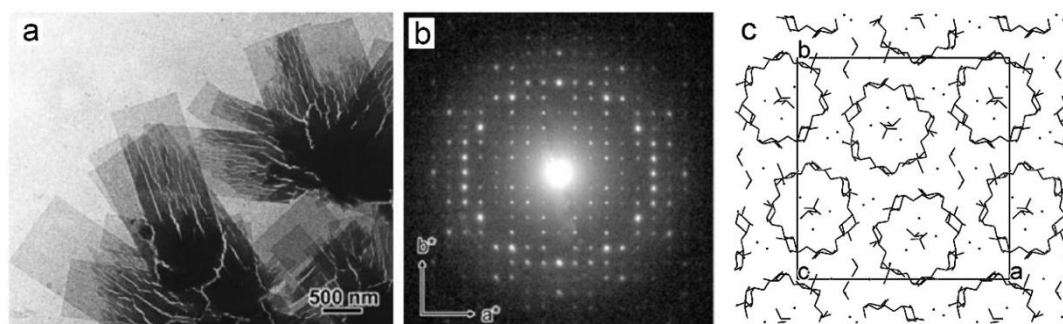


Figure I.13. V7 structure: (a) TEM image of single crystals of V₂-propanol and (b) corresponding ED pattern recorded at low temperature (Putaux et al., 2008); (c) projection on the (a, b) plane of the molecular structure (Nishiyama et al., 2010).

The model proposed for V7 prepared with 2-propanol (Nishiyama et al., 2010) is based on an orthorhombic unit cell with space group $P2_12_12_1$, and $a = 2.826$ nm, $b = 2.950$ nm and $c = 0.801$ nm (**Figure I.13c**). The 7-fold left-handed helices are organized along alternating motifs of four helices in a close-packed hexagonal arrangement together with four others in a nearly square organization surrounding a central column of water and 2-propanol.

Upon thorough drying, V7 complexes are transformed into a new structure with pseudo-hexagonal unit cell with $a = b = 1.47$ nm (Yamashita & Hirai, 1966; Zaslow, 1963). The 7-fold helical conformation remains unchanged, but the packing arrangement is reverted from

orthorhombic to hexagonal, probably due the removal of interstitial waters and complexing agent. This behavior is similar to that of V6_{II} complexes. At present, there is still no name proposed for this structure. Since it is an anhydrous form of V7, we will refer it as V7_a. Similarly, the V_a-type obtained by drying V6_I and V6_{II} can be called V6_a. In addition, the extraction of complexing agents from V7 complexes using *n*-aliphatic alcohols miscible with water (methanol, ethanol and *n*-propanol) or their aqueous solution results in a transition from 7- to 6-fold helices (Biais et al., 2006; Buléon et al., 1990; Helbert, 1994; Takeo & Kuge, 1969).

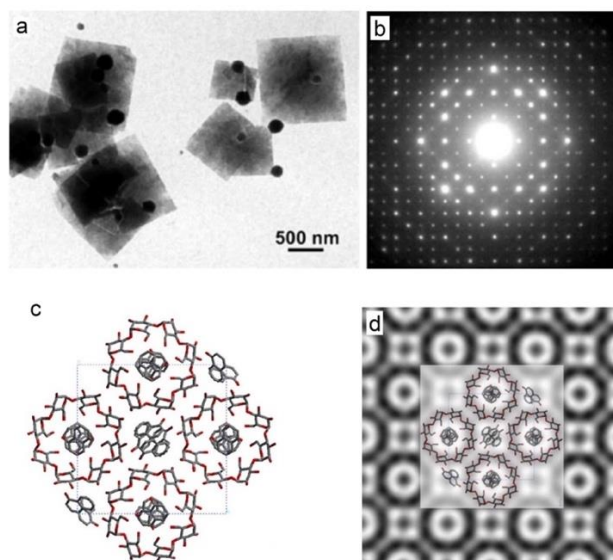


Figure I.14. V8 structure: (a) TEM image of single crystals of V_{1-naphthol}; (b) corresponding base-plane ED pattern recorded at low temperature; (c) projection of the (*a*,*b*) plane of the molecular model; (d) averaged high-resolution lattice image recorded along the helical axis with the inset of molecular model (Cardoso et al., 2007).

I.2.3.1.5. V8

The V8 family includes V_{1-naphthol} and the isomorphous V_{quinoline} (Helbert, 1994; Putaux et al., 2008; Yamashita & Monobe, 1971). So far, no third complex with a similar structure has been identified. Lamellar single crystals of V_{1-naphthol} prepared in dilute solution have a squarish shape and yield a base-plane ED pattern with a square symmetry (Figure I.14a and I.14b) (Cardoso, 2007). The most recent molecular model proposed by Cardoso (2007) contains antiparallel 8-fold left-handed helices packed in a tetragonal unit cell (space group $P4_32_12$) with $a = b = 2.32$ nm and $c = 0.79$ nm. 2.25 1-naphthol molecules are located inside the helix while two other molecules are located in-between. No water molecule was included in the model. The proposed model superimposed well onto high-resolution TEM lattice images, which is considered to be the strongest evidence for the 8-fold helical model (Figure I.14c,d) (Cardoso et al., 2007).

Lamellar crystals of $V_{\text{quinoline}}$ exhibit a morphology similar to that of $V_{1\text{-naphthol}}$ (Helbert, 1994; Putaux et al., 2008). Helbert (1994) reported that the a and b parameters (4.66 nm) was twice larger than those of $V_{1\text{-naphthol}}$. However, a recent study by Putaux et al. (2008) found similar unit cell parameters for the two complexes. The V_8 complexes were found to be stable upon drying. In addition, the transformation from 8-fold helix into 6-fold helix has not been reported by solvent exchange (Cardoso, 2007).

I.2.3.2. Extended-helix V-amylose

Unlike compact amylose helices, the extended helices exhibit a much longer pitch which varies depending on the number of glucosyl residues per turn (Table I.2). In addition, the intramolecular hydrogen bonds, which are responsible for the conformation of compact helices, are not possible in these extended conformation (Sarko & Biloski, 1980; Sarko & Zugenmaier, 1980). The helices assume much more extended shapes, losing the inner cavity found in the compact helix (Figure I.9). Therefore, the amylose chains have been called linear and the extended-helix amylose complexes are not considered as V-amylose by some authors (French & Murphy, 1977a; Sarko & Zugenmaier, 1980). However, these forms are still mathematically helices and may be described with the same parameters. Therefore, the extended-helix amylose complexes generally meet all the criteria of V-amylose. They have been induced when complexing amylose with several alkali and inorganic salts (Miller & Brannon, 1980; Sarko & Biloski, 1980; Senti & Witnauer, 1948; Senti & Witnauer, 1946; Senti & Witnauer, 1952). The complexes can be classified into several allomorphic families based on their fiber XRD pattern. However, there is still no nomenclature system for them, so far.

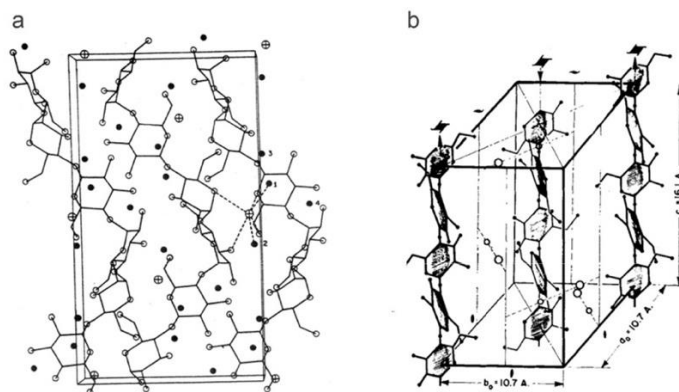


Figure I.15. a) Molecular structure of V_{KOH} ; potassium ions are designated by \oplus (Sarko & Biloski, 1980). b) Molecular structure of V_{KBr} ; bromide and potassium ions are designated by large and small open circle, respectively (Senti & Witnauer, 1952).

I.2.3.2.1. V_{KOH} and isomorphous structures

V-amylose complexed with a series of alkali including lithium (LiOH), sodium (NaOH), potassium (KOH), ammonium (NH₄OH), cesium (CsOH), guanidinium hydroxides can be obtained during the solid-state deacetylation of amylose triacetate by alkali solutions in 75% ethanol, as first reported by Senti and Witnauer (1948). All of the alkali-amylose complexes are isomorphous, exhibiting similar fiber XRD patterns and unit cell parameters.

The detailed structure of V_{KOH} has been determined by Sarko and Biloski (1980) based on fiber XRD data (Figure I.15a). The unit cell is orthorhombic with space group $P2_12_12_1$, with $a = 0.884$ nm, $b = 1.231$ nm, and c (fiber repeat) = 2.241 nm. The unit cell contains two 6-fold left-handed helices, four KOH and 12 water molecules. Intramolecular hydrogen bonds are absent but the structure is extensively hydrogen-bonded, largely through water molecules. Upon extracting alkali with methanol, the fiber pattern disappears and is not restored by rehydration. In contrast, extraction with 75% MeOH or EtOH results in the characteristic compact-helix V structure. Soaking in 75% alcohol containing 2% alkali restores the original pattern.

I.2.3.2.2. V_{KBr} and isomorphous structures

A series of isomorphous V-amylose complexes with salts such as iodide, bromide, acetate, formate and bicarbonate of potassium can be obtained from V_{KOH} fibers by exchange the salts with alkali in a hydroalcoholic solution (Senti & Witnauer, 1952). The molecular and crystal structure of V_{KBr} , shown in Figure I.15b, has been determined based on fiber XRD data (Miller & Brannon, 1980; Senti & Witnauer, 1952). In this structure, two left-handed 4-fold helix, together with four KBr molecules are packed into a tetragonal unit cell, space group $P4_32_12$, with $a = b = 1.07$ nm, and c (fiber axis) = 1.61 nm. The adjacent amylose are bonded alternately through primary hydroxyl groups and potassium ions while bonding through anions contacts is less important. Water was not included in the model although the water content was measured to be about 10.6%. Drying the complex led to a smaller unit cell, with $a = b = 1.02$ nm, and c (fiber axis) = 1.64 nm.

I.2.3.3. Other unresolved structures and towards new structures of V-amylose

Several other complexes have been reported to exhibit powder or fiber XRD patterns that are distinct from those of the previously described allomorphic families. However, their crystal structures still remain unknown. First are the complexes of amylose with salicylic acid and some analogues prepared by sealed-heating method (Oguchi et al., 1998; Uchino et al., 2002). These complexes gave similar powder XRD patterns, and thus appeared to be

isomorphous. In addition, there are some similarities in their powder XRD patterns with that of polyisobutylene- γ -cyclodextrin (CD) complex. Therefore, the authors claimed that the complexes contained 8-fold helices similar to that of V8 obtained with 1-naphthol (Oguchi et al., 1998; Uchino et al., 2002). However, there is no confirming data for this suggestion and the unit cell parameters as well as space group are still unknown.

Second, Helbert and Chanzy (1994) obtained orthorhombic unit cells by swelling $V_{n\text{-butanol}}$ crystals in different solvents or mixtures of solvents. Although the molecular structure of $V_{n\text{-butanol}}$ (V6II) and the swollen crystals have not been resolved, the authors believed that they had a similar organization of 6-fold left-handed helices, with the exception that the inter-helical space and shape varied depending on the swelling agents.

The $V_{K\text{ acetate}}$ and $V_{K\text{ propionate}}$ complexes can be obtained from V_{KOH} fiber by exchange method, similar to the previous method used to prepare V_{KBr} (Senti & Witnauer, 1952). They are orthorhombic structures and appear to be isomorphous, with the unit cell having $a=1.10$ nm, $b=1.81$ nm, c (fiber axis) = 1.79 nm for $V_{K\text{ acetate}}$ and $a=1.14$ nm, $b=1.80$ nm, $c=1.76$ nm for $V_{K\text{ propionate}}$ (Senti & Witnauer, 1952). The molecular structure of these complexes is still unknown. However, since K acetate also yields an isomorphous tetragonal structure to that of V_{KBr} and the c -parameter is similar between the orthorhombic and tetragonal structures, the orthorhombic structure is expected to have an extended helical conformation.

Finally, Senti and Witnauer (1952) reported that the amylose complexes with ammonium fluoride had an orthorhombic unit cell with $c = 1.89$ nm without any further information about the crystal structure. French and Murphy (1977a) noted that the c -parameter of 1.89 nm is similar with the 5-fold left-handed extended helix of the so-called intermediate amylose.

From the above examples, it is likely that other forms of V-amylose remain to be discovered. In addition, modeling works suggest allowed and disallowed helical conformations from an n - h map, in which n is the number of monomers per turn and h is the raise per monomer (French et al., 1978). The allowed values of n range from 2-10 and h ranges from 0.08-0.44 nm. This indicated that many V-amylose structures may possibly exist in addition to the wide variety of already observed forms. New complexing agents as well as suitable preparation methods with a variation of conditions would be required to allow these new forms to appear.

1.2.4. Origin of polymorphism

The formation of V-amylose results from the interaction between amylose and complexing agents in solution or in solid state. However, the structure, yield and crystallinity of complexes with a given agent may vary with the conditions of crystallization. Different

parameters have been shown to have significant effects on the formation of V-amylose, such as the nature of complexing agent, degree of polymerization of amylose, nature and composition of the solvent, concentration of complexing agent, concentration of amylose and temperature.

I.2.4.1. Complexing agent

The complexing agents of amylose were once described as molecules having a polar group in addition to a dominant nonpolar portion (Bear, 1944). However, several hydrophobic compounds such as hydrocarbons or halogenated hydrocarbons are also effective complexing agents while some of them are not (French & Whelan, 1963; Kuge & Takeo, 1968). In addition, molecules such as 1-naphthol and quinoline form complexes with amylose while their analogues like 8-quinolinol do not. Therefore, no clear rule is now available for predicting the possibility for a molecule to form a complex with amylose.

In addition, the nature of the complexing agent does not allow predicting the crystal structures of the resulting complexes. Indeed, an allomorphic type such as V7 can be obtained with a variety of molecules having very different chemical natures (propanoic acid, 2-propanol, acetone, thymol, etc.). In addition, a few complexing agents such as hexanoic acid, some dicarboxylic acids and *n*-alcohols can produce crystals with both V6_I and V6_{II} structures depending on the crystallization condition (Biais et al., 2006; Helbert, 1994; Takeo et al., 1973).

On the other hand, several studies suggested that the dimension of the complexing agent was closely related to the induced helical conformation of amylose (Rutschmann & Solms, 1990; Takeo & Kuge, 1969; Yamashita et al., 1973; Yamashita & Hirai, 1966; Zaslów, 1963). More particularly, linear molecules such as aliphatic fatty acids and *n*-alcohols whose diameter in cross-section is about 0.3 nm yield 6-fold helical complexes while those having branched chain or ring structures with a diameter in cross-section of 0.45-0.65 nm induce V7. V8 can be obtained with bulkier molecules such as 1-naphthol and quinoline. While most of the known complexing agents followed the above rule, some exceptions have been reported. For example, molecules such as DMSO (Simpson et al., 1972), propionic and butyric acids (Helbert, 1994; Takeo et al., 1973), 2-propanol, acetone and quinoline (Helbert, 1994), and salicylic acid (Oguchi et al., 1998) are capable to induce two different helical conformations. Quinoline, (-)-borneol, *trans*-decalin were reported to form V6_I complexes although their size is not compatible with either the helix cavity or inter-helix space (Helbert, 1994). The above results suggest that the mechanism of complex formation is complicated and it seems impossible to predict the allomorphic structure of the complexes using a simple rule.

I.2.4.2. Degree of polymerization of amylose

The flexibility of amylose and the geometry of the $\alpha(1\rightarrow4)$ glucosidic bonds allow the folding of polymer chain and the formation of the lamellar crystals of V-amylose with a wide range of DP. However, there exists a minimum DP of amylose essential for the formation of stable helical complexes (Dvonch et al., 1950; Gelders et al., 2004; Godet et al., 1995). Shorter chain lengths favor the formation of A- and B-amylose (Buléon et al., 1984). The minimum DP depends on the complexing agents. Godet et al. (1995) reported that the complexation required a minimum DP of around 30-40 for palmitic (hexadecanoic) acid, and DP 20-30 for lauric (dodecanoic) and caprylic (octanoic) acids. With this DP, the helix can accommodate two fatty acids per chain. Similar results were reported for glycerol monostearate (GMS) and docosanoic acid (C22). A minimum DP of 35 and 40 is required for GMS and C22, respectively, corresponding to the length needed to include two ligand molecules (Gelders et al., 2004). In addition, Godet et al. (1995) noted that the yield of complexes increased with increasing DP, which could be explained by the lower solubility of amylose and its ability to form complexes that can precipitate. Furthermore, the DP of amylose can have a significant effect on the morphology and perfection of the crystals. Cardoso et al. (2007) suggested that DP 100 amylose formed crystals of V_{1-naphthol} with an optimum perfection due to the absence of chain-folding.

I.2.4.3. Concentration of amylose

The concentration of amylose has a significant impact on the morphology and crystallinity of the complexes. The crystallization from dilute solution (0.05-0.1 wt%) usually produces lamellar single crystals whereas high amylose concentrations (> 0.5 wt%) results in spherulites or polycrystalline aggregates (Conde-Petit et al., 2007; Fanta et al., 2008; Helbert, 1994; Nuessli et al., 2003). In addition, when the concentration of amylose is higher than a certain value, the retrogradation of amylose is more favored over the complexation with the complexing agent, resulting in the formation of semicrystalline B-amylose (Nuessli et al., 2003).

I.2.4.4. Concentration of complexing agent

According to Helbert (1994), there exists a critical concentration of each complexing agent necessary for the formation of the complexes. For poorly water-soluble complexing agents such as long-chain fatty acids, the critical concentration is very low. The complexing agents are usually added at saturation to ensure the complete complexation. For water-miscible complexing agents such as acetic and propionic acids, a concentration of complexing agent up to 40-50 vol% is required (Helbert, 1994; Takeo et al., 1973).

In addition, some complexing agents such as *n*-propanol, as well as propionic and butyric acids induce more than one type of allomorph, depending on their concentration (Helbert, 1994; Takeo et al., 1973). At critical concentration, the complexes adopt an orthorhombic structure (V6_{II} or V7) with a large inter-helix space for the complexing agents to reside. In contrast, at high concentration, the crystals adopt a compact V6_I structure. This variation in crystal structure can be attributed to the change of hydration state of amylose as a function of the complexing agent concentration. According to Helbert (1994), when the complexing agent is added at a low critical concentration, it is totally solvated and forms orthorhombic complexes with amylose. On the other hand, at high concentration, it may capture all solvent molecules leading to the desolvation of amylose. Consequently, the association between the complexing agent and amylose mediated by water is no longer possible and the crystallization simply results from a desolvation of the polymer (Helbert, 1994).

I.2.4.5. Temperature of crystallization

Previous studies have shown that the crystallinity of V-amylose complexed with lipids was controlled by the temperature of crystallization (Biliaderis & Galloway, 1989; Gelders et al., 2004; Karkalas et al., 1995). In particular, an incubation at ≤ 60 °C yields amorphous complexes due to a high nucleation rate whereas the crystallinity significantly increases when crystallization is carried out at ≥ 90 °C due to a slow nucleation. Moreover, the crystallization temperature varies for different complexing agents. For example, complexes with 1-naphthol crystallize at room temperature (Yamashita & Monobe, 1971) whereas those with fatty acids can be formed within a wide range of temperatures (30-90 °C) (Zabar et al., 2009). This difference in crystallization behavior could be attributed to a difference in solubility. Complexes with a higher solubility would crystallize at higher supercooling (Yamashita & Monobe, 1971).

I.2.4.6. Solvent

V-amylose has frequently been prepared by crystallization from aqueous solutions, neutralized alkali solutions or DMSO/water mixtures. This does not generally have an influence on the nature of the complexes, but rather on the quality of the crystals. However, Helbert (1994) reported that the crystal structure of amylose complexes with some molecules varied in the presence of DMSO. The complexation with quinoline resulted in a V8 structure only in the presence of 15% DMSO, while without DMSO, V6_I crystals were obtained. For *n*-butanol and *n*-pentanol, the complexation in water yielded V6_{II} but in DMSO/water mixture, V6_I crystals were formed instead. The origin of the effect of DMSO on the formation of V-amylose complexes

is still unclear but previous studies have shown that DMSO affected the conformation of amylose in solution (Erlander & Tobin, 1968; Jane et al., 1985; St.-Jacques et al., 1976). DMSO also affects the solubility of amylose, complexing agent and probably V-amylose.

I.2.5. Properties and potential applications of V-amylose

I.2.5.1. Identification, quantification and fractionation of amylose from native starch

The formation of complexes with iodine has commonly been used to identify amylose in starchy products and to measure the amylose content by differential scanning calorimetry (Creek et al., 2007; Sievert & Holm, 1993). Moreover, the formation of V-amylose has been applied for selective fractionation of amylose from starch (Banks & Greenwood, 1967; Bourne et al., 1948; Cantor et al., 1957; French & Whelan, 1963; Kuge & Takeo, 1968; Schoch, 1942, 1944; Whistler & Hilbert, 1945). Upon addition of complexing agents into the starch solution, amylose forms inclusion complexes and precipitates, whereas amylopectin remains in solution. Amylose can then be separated and the process can be repeated on the recovered amylose to increase its purity.

I.2.5.2. Modulation of starch digestibility and glucose response

The formation of V-amylose with fatty acids have been shown to reduce the digestibility of starch and increase the resistance to enzymatic hydrolysis (Biais et al., 2006; Cui & Oates, 1999; Eliasson & Krog, 1985; Gelders et al., 2005a; Godet et al., 1996; Guraya et al., 1997; Holm et al., 1983; Sievert & Wursch, 1993). The resistance to enzymatic hydrolysis increases with increasing crystallinity of V-amylose (Seneviratne & Biliaderis, 1991). During hydrolysis the amorphous regions are degraded first, followed by the more crystalline regions (Biais et al., 2006). Therefore, there is an increase in crystallinity with hydrolysis to an optimum, beyond which it decreases due to degradation of crystalline regions (Biais et al., 2006; Godet et al., 1996). In lamellar crystals of V-amylose, the amorphous component is made of the folded section of the chains. As a consequence, if amylose with appropriate DP is used, chain-folding would not occur and the resulting complexes would exhibit a higher crystallinity and stability.

Starch with induced or added V-amylose would modulate the glycemic response due to an increased resistance to hydrolysis resulting in a slower digestion (Obiro et al., 2012). Recent studies in humans reported that the consumption of bread containing amylose-lipids complexes resulted in lower postprandial plasma glucose and insulin levels compared to regular bread (Hasjim et al., 2010; Lau et al., 2016). Therefore, V_{lipids} complexes would help improve glycemic regulation and may help in the prevention and management of insulin resistance and metabolic syndrome including diabetes and obesity (Hasjim et al., 2010; Lau et al., 2016).

I.2.5.3. Effect on the functional properties of starch

The functional properties of starch such as pasting behavior, viscosity, retrogradation, water and oil adsorption and swelling power are modulated in the presence of lipids. The effects are attributed to the formation of amylose-lipids complexes, as reviewed by Putseys et al. (2010), Obiro et al. (2012) and Panyoo and Emmambux (2017).

The formation of amylose-lipids complexes decreases solubility, leaching of amylose, swelling capacity and granule disruption of starch (Bhatnagar & Hanna, 1994; Galloway et al., 1989; Krog, 1973; Mira et al., 2007; Navarro et al., 1996; Raphaelides & Georgiadis, 2007). This results in a decrease or absence in the first pasting peak viscosity (D'Silva et al., 2011; Singh et al., 2002). On the other hand, after a prolonged pasting time (30–120 min) beyond the initial peak viscosity, the second pasting peak viscosity increases again due to the formation of complexes of leached amylose with the added or native lipids (D'Silva et al., 2011; Nelles et al., 2000; Nelles et al., 2003). It was shown that during this second increase in paste viscosity, the starch granules are completely disintegrated (Nelles et al., 2003) and no micron-scale structures could be observed (Obiro et al., 2012).

The formation of amylose complexes also competes and reduces the retrogradation of starch. As a consequence, at high starch concentrations, the addition of ligands results in a weaker starch gels or a no or reduced gel formation (D'Silva et al., 2011; Raphaelides, 1993; Richardson et al., 2003). This behavior can provide possible means for improving the mouth feel of starch-containing foods (D'Silva et al., 2011). In addition, the formation of amylose complexes has an anti-staling effect and increases the shelf-life of gluten-free bread formulations due to the unavailability of amylose for retrogradation (Nunes et al., 2009; Purhagen et al., 2012). On the other hand, at low starch concentration, the complexation of amylose with flavor compounds induces the gelation (Conde-Petit & Escher, 1992; Conde-Petit & Escher, 1995; Nuessli et al., 1995). This is attributed to the intergranular networks composed of the inclusion complexes which provide the physical cross-links between granules.

Pastes of V-amylose complexes are very spreadable at high concentration. Their flow properties are very similar to commercial shortening (Byars et al., 2009). In addition, the gelation by amylose complexes with sodium palmitate is pH-dependent and thermally reversible (Byars et al., 2012). The gelling properties of these materials suggest practical applications as thickeners and as dispersants for lipids in foods, lotions and water-based lubricants (Byars et al., 2012).

I.2.5.4. Encapsulation of flavors and bioactive molecules

The capacity of formation inclusion complexes of amylose has been exploited for the encapsulation of a wide range of compounds that serve as flavor components, nutraceutical, pharmaceutical, or bioactive substances (Conde-Petit et al., 2006; Obiro et al., 2012; Panyoo & Emmambux, 2017; Putseys et al., 2010). Among these are fatty acids (Bhosale & Ziegler, 2010; Lesmes et al., 2009; Yang et al., 2009), esters of vitamins (Kong & Ziegler, 2014; Ma et al., 2011), ibuprofen (Yang et al., 2013; Zhang et al., 2016), genistein (Cohen et al., 2008; Cohen et al., 2011), salicylic acid (Oguchi et al., 1998), and many flavors such as linalool, citronellol, limonene, β -pinene, geraniol, menthol and menthone, camphor, thymol, etc. (Ades et al., 2012; Conde-Petit et al., 2006; Heinemann et al., 2005; Kuge & Takeo, 1968; Nuessli et al., 2003; Tapanapunnitikul et al., 2007; Wulff et al., 2005; Yeo et al., 2016) (Itthisoponkul et al., 2007; Putaux et al., 2008). The inclusion complexes with some drugs such as rifampicin (Ribeiro et al., 2017), nimesulide and praziquantel (Carbinatto et al., 2016) were also reported, although the size of the complexing agents seems to be incompatible with the regular helical cavity.

The use of V-amylose as an encapsulation and delivery system presents many advantages. First, amylose is readily available at relatively low cost. The polymer is considered nontoxic and biodegradable (Obiro et al., 2012). Second, the formation of V-amylose complexes has been demonstrated to increase thermal and oxidative stability of the ligands (Cohen et al., 2008; Cohen et al., 2011; Lalush et al., 2005; Szejtli & Bánky-Elöd, 1975; Yang et al., 2009). The increased stability would be useful for protecting the thermal- or oxygen-sensitive molecules such as unsaturated fatty acid, vitamins, etc. during storage and processing. Third, the formation of complexes increases the retention time of volatile ligands, *i.e.* flavors (Arvisenet et al., 2002; Jouquand et al., 2006; Wulff et al., 2005). Fourth, the complexes are stable in gastric conditions and slowly release the ligand in the intestine. It can thus be used as intestinally targeted and controlled release delivery system (Cohen et al., 2008; Cohen et al., 2011; Lalush et al., 2005; Yang et al., 2013; Yang et al., 2009; Zhang et al., 2016). Finally, Cohen et al. (2011) reported that amylose-genistein complexes increased the bioavailability of the ligand and suggested that starch can affect the bioavailability of additional food components.

I.2.5.5. Other potential applications

V-amylose have been shown to have potential applications to produce aerogels (Kenar et al., 2014), water-resistant paper (Fanta et al., 2017), films with increased surface hydrophobicity and high elongation (Fanta et al., 2016) and fat replacers (Singh & Byars, 2009;

Singh et al., 2014; Singh & Kim, 2009). In addition, amylose-lipids complexes were shown to potentially inhibit azoxymethane-induced preneoplastic lesions (precursors of colon cancer) (Zhao et al., 2014; Zhao et al., 2011).

I.3. Objectives of the thesis

One of the main objectives of this thesis was to systematically study the crystallization of amylose in solution in the presence of a variety of organic molecules in different conditions, in order to understand the effect of the nature of complexing agents and several crystallization parameters (crystallization temperature, concentration of amylose and complexing agent, DP of amylose, presence of DMSO) on the formation of amylose complexes and their crystal structure.

Another important objective was to collect the crystallographic data on the different allomorphic families, especially those that we have identified for the first time during this works, in order to propose a conformation and a packing arrangement of amylose helices for each allomorph. In particular, our study have focused on the determination of the molecular and crystal structure of $V_{1\text{-butanol}}$ whose model was still hypothetical and of historical importance since it is one of the first molecules that have been used to recrystallize amylose on a large scale.

We have also investigated the encapsulation and release properties of a bioactive molecule, namely ibuprofen, by its V -amylose complex, as an example to evaluate the potential of V -amylose as a delivery system for drugs. A crystallographic study was conducted to understand the effect of the crystal structure on the release properties.

Chapter II

Materials and methods

II.1. Materials

II.1.1. Native amylose

Potato amylose was purchased from Sigma-Aldrich and further purified as previously reported (Helbert, 1994). Briefly, 30 g of amylose was dissolved in 1 L of dimethyl sulfoxide (DMSO) by stirring for 12 h at room temperature. The solution was centrifuged (2500 g, 20 min) to remove residual aggregates. Amylose was precipitated by addition of an equal volume of ethanol, kept at 4 °C for 12 h, filtered (glass filter G5) and extensively rinsed with ethanol, acetone and diethyl ether, successively, using a Büchner device hooked to a water suction pump. Amylose was then dried for one week in an exhaust hood at room temperature. The chain length distribution was determined by Noriyuki Isobe (Université de Tokyo) by size exclusion chromatography (SEC) with multi-angle laser light scattering (MALLS) detection after dissolution of amylose in LiCl/1,3-dimethyl-2-imidazolidinone. The weight-average degree of polymerization DP_w was 6474 (Figure II.1 and Table II.1) so this fraction will be referred to as DP6500 in the following. The M_w/M_n ratio of native amylose was 2.58, indicative of a high polydispersity.

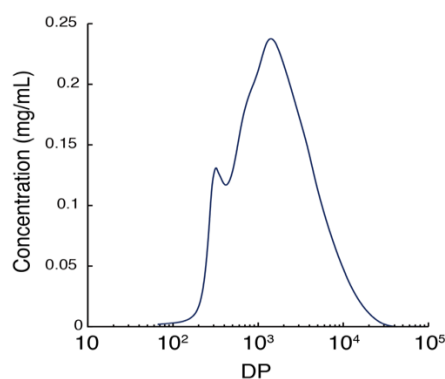


Figure II.1. SEC-MALLS Chromatogram of purified native potato amylose and dissolution in LiCl/DMAc.

II.1.2 Synthetic amylose

II.1.2.1. Amylose synthesized *in vitro* using amylosucrase

Using the method described in details in a previous paper (Potocki-Veronese et al., 2005), a linear amylose-like polymer was enzymatically synthesized *in vitro* from sucrose by the amylosucrase from *Neisseria polysaccharea*, at Laboratoire d'Ingénierie des Systèmes Biologiques et des Procédés in Toulouse. The synthesis reaction was carried out at 30 °C in

phosphate-buffered saline (PBS, pH 7.3) containing 100 mM sucrose and purified amylosucrase (enzyme activity of $0.5 \text{ U}\cdot\text{mL}^{-1}$). Amylose was then precipitated from the reaction medium with 1/4 volume of 2-propanol at $4 \text{ }^\circ\text{C}$ for 12 h, and collected by centrifugation (2500 g, 20 min). The resulting polymer was purified using the protocol previously described for native amylose. The *DP* distribution was determined by high-performance anion-exchange chromatography with pulsed amperometric detection (HPAEC-PAD) after dissolution in 1 N NaOH (Potocki-Veronese et al., 2005). The DP_w of the total fraction was 86 (Figure II.2, Table II.1) so it will be referred to as DP86 in the following. The synthesized amylose has a lower polydispersity compared to the native amylose, indicated a lower M_w/M_n of 1.25. Part of the total DP86 fraction was further fractionated by preparative gel filtration in a P6DG column (Biorad). In particular, we have used three fractions with DP_w of 60, 80 and 130, which will be referred to as DP60, DP80 and DP130, respectively (Table II.1 and Figure II.2). The M_w/M_n of all synthesized amylose fractions was close to 1, indicating a narrow size distribution.

II.1.2.2. Amylose synthesized *in vitro* by phosphorylase

Amylose fractions synthesized *in vitro* by phosphorylase (Ohdan et al., 2006) with $\text{DP}_w = 28, 192$ and 601, referred to as DP28, DP192, and DP600, respectively, were purchased from Shoko Co Ltd (Japan) and used without further purification. The characteristics of all fractions used in this study are summarized in Table II.1.

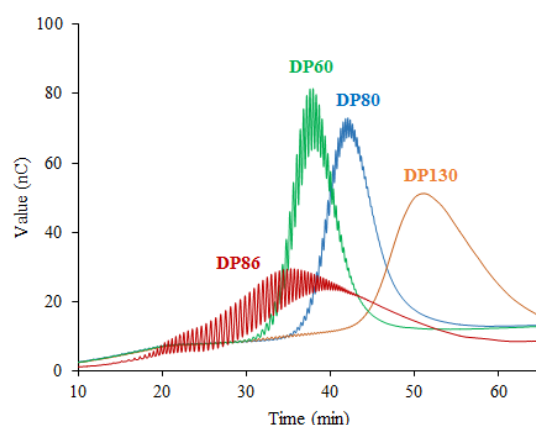


Figure II.2. HPAEC chromatograms of the total amylose fraction (DP86) synthesized *in vitro* by amylosucrase and 3 fractions (DP60, DP80 and DP130) obtained by fractionation of DP86.

II.1.3. Complexing agents

121 organic molecules were tested for their complexing ability, as listed in Table II.2. They have different functional groups such as carboxylic acids, alcohols, amines, ketones,

aldehydes, amides, esters, ethers, etc. They can be saturated or unsaturated with open chain (straight or branched) or ring structure. In addition, molecules with very similar structures such as isomers or those belonging to homologous series were also tested. A number of complexing agents are flavors and bioactive molecules such as: ibuprofen, ketoprofen, salicylic acid, azelaic acid, menthol, linalool, citral, carvacrol, etc.

Table II.1. Molecular characteristics of the fractions used in this study. DP_w is the weight-average degree of polymerization. M_w and M_n are the weight- and number-average molecular weights, respectively.

Fraction	DP50 ^{a,c}	DP80 ^{a,c}	DP86 ^{a,b}	DP130 ^{a,c}	DP28 ^d	DP192 ^d	DP600 ^d	DP6500 ^e
DP_w	60	80	86	130	28	192	601	6474
M_w	9738	12816	13788	21078	4500 ^d	31200 ^d	97500 ^d	1048827
$\frac{M_w}{M_n}$	1.05	1.07	1.25	1.07	1.06 ^f	1.01 ^f	1.04 ^f	2.58

^a synthesized *in vitro* by amylosucrase; ^b total fraction; ^c fractionated from the total fraction.

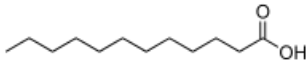
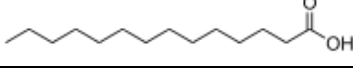
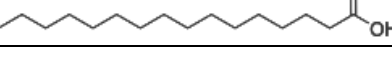
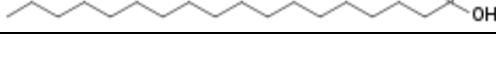
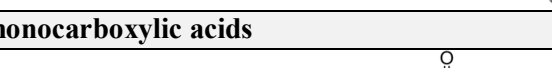
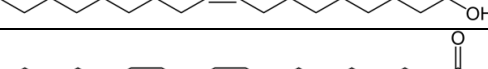
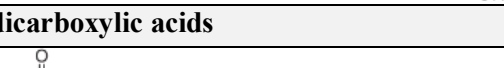
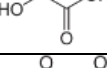
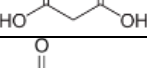
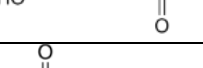

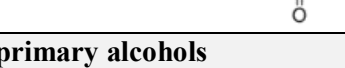
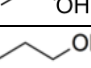
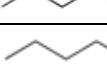
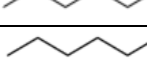
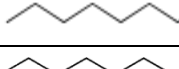
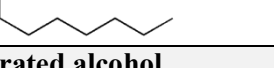
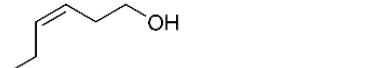
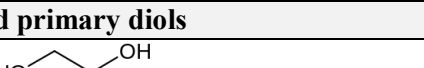
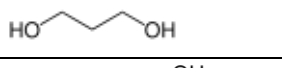



^d synthesized *in vitro* by phosphorylase

^e native amylose from potato (Sigma Aldrich)

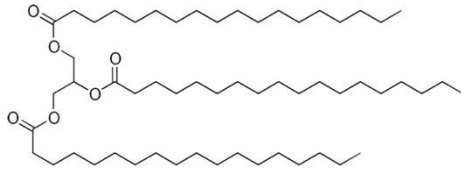
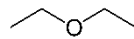
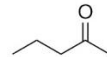


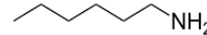

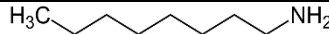

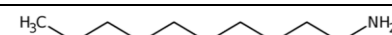

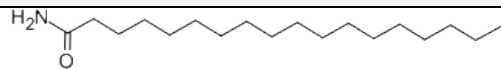
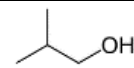
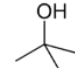
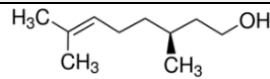
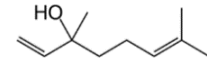
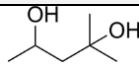
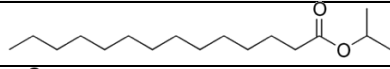
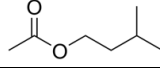
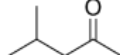
^f values given by the manufacturer

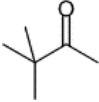
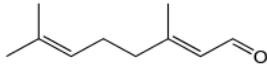
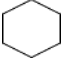
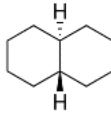
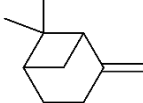
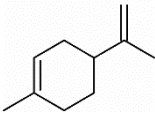
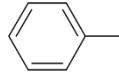
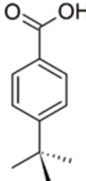
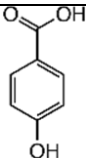
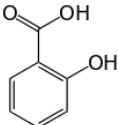
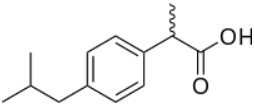
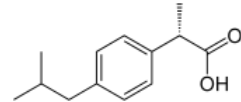
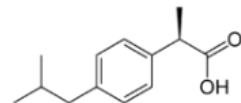
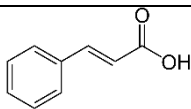
Table II.2. List of complexing agents

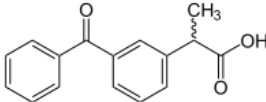
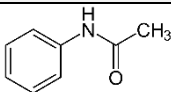

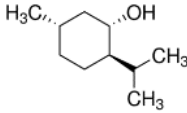
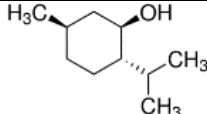
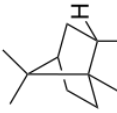
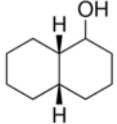
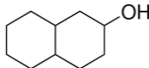
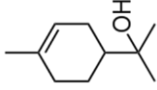
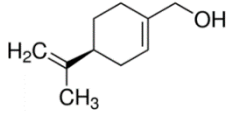
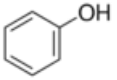
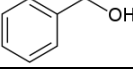
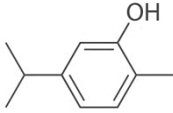
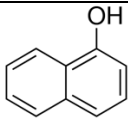
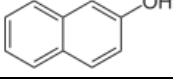
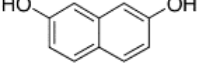
Complexing agent	Abbreviation	Structure
Alkanes		
Hexane	HAN	
Decane	DEAN	
Hexadecane	HEDAN	
Straight-chain saturated monocarboxylic acids		
Propanoic acid (propionic acid)	PA	
Butanoic acid (butyric acid)	BA	
Pentanoic acid (valeric acid)	VA	
Hexanoic acid (caproic acid)	COA	
Octanoic acid (caprylic acid)	OA	
Decanoic acid (capric acid)	CIA	

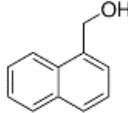
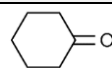
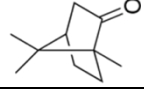
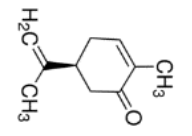
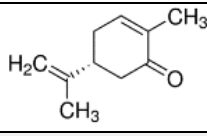
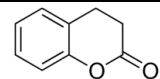
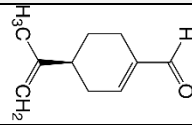
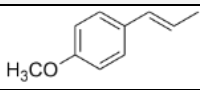
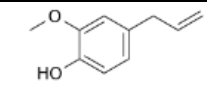
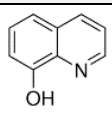
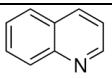
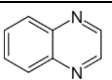
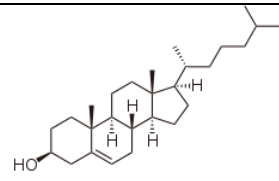
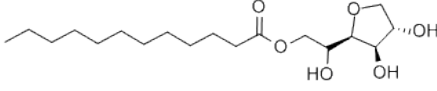
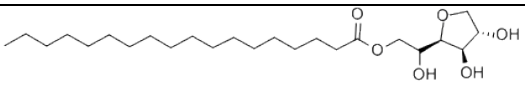
Dodecanoic acid (lauric acid)	LA	
Tetradecanoic acid (myristic acid)	MYA	
Hexadecanoic acid (palmitic acid)	PMA	
Octadecanoic acid (stearic acid)	SA	
Icosanoic acid (arachidic acid)	ARA	
Straight-chain unsaturated monocarboxylic acids		
Oleic acid	OLAN	
Linoleic acid	LINA	
Straight-chain saturated dicarboxylic acids		
Ethanedioic acid (oxalic acid)	OXA	
Propanedioic acid (malonic acid)	MAA	
Hexanedioic acid (adipic acid)	ADA	
Nonanedioic acid (azelaic acid)	AZA	
Dodecanedioic acid	DODA	
Straight-chain saturated primary alcohols		
Ethanol	ET	
1-Propanol (<i>n</i> -propanol)	POL	
1-Butanol (<i>n</i> -butanol)	BU	
1-Pentanol (<i>n</i> -pentanol)	PENO	
1-Octanol (<i>n</i> -octanol)	OCTO	
1-Dodecanol (<i>n</i> -dodecanol)	DODO	
1-Tetradecanol (<i>n</i> -tetradecanol)	TEDO	
1-Hexadecanol (<i>n</i> -hexadecanol)	HEDO	
Straight-chain unsaturated alcohol		
<i>cis</i> -3-Hexen-1-ol	HENOL	
Straight-chain saturated primary diols		
1,2-Ethandiol (ethylene glycol)	EG	
1,3-Propanediol	PDIOL	
1,4-Butanediol	BDIOL	

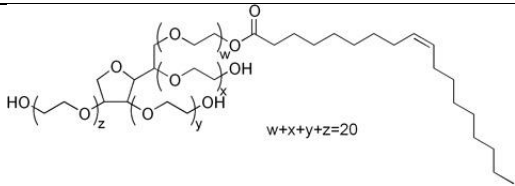
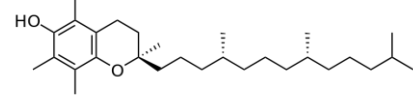
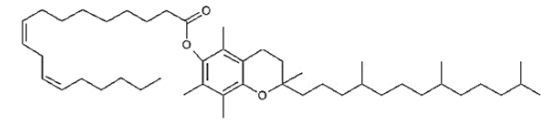
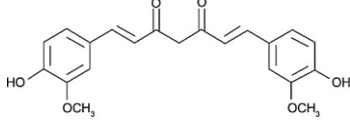
1,5-Pentanediol	PEDIOL	
1,6-Hexanediol	HDIOL	
2-(2-Hydroxyethoxy)ethan-1-ol (diethylene glycol)	DEG	
Straight-chain secondary alcohols		
2-Propanol	IP	
2-Butanol (sec-butanol)	SB	
Straight-chain secondary diols		
1,2-Propanediol (propylene glycol)	PG	
1,3-Butanediol	BBOL	
Triol		
1,2,3-Propanetriol (glycerol)	GOL	
Halogeno-alcohol		
11-bromo-1-undecanol	BUN	
Straight-chain esters		
Ethyl butanoate (ethyl butyrate)	EB	
Ethyl pentanoate (ethyl valerate)	EV	
Ethyl hexanoate (ethyl caproate)	EC	
Propyl acetate	PRAT	
Butyl acetate	BAT	
Pentyl acetate	PAT	
Lysophosphatidylcholine	LYS	
Alkyl sulfate		
Sodium octadecyl sulfate	SODS	
Diester		
Diethyl malonate	DEM	
Triesters		
Triacetin	TAN	

Tristearin	TSA	
Ether		
Diethyl ether	DET	
Ketones		
Pentan-2-one	PON	
Aldehyde		
Octanal	OTAL	
Straight-chain primary amines		
1-Butylamine (<i>n</i> -Butylamine)	BUA	
1-Hexylamine (<i>n</i> -Hexylamine)	HEA	
1-Heptylamine (<i>n</i> -Heptylamine)	HEPA	
1-Octylamine (<i>n</i> -Octylamine)	OCTA	
1-Nonylamine (<i>n</i> -Nonylamine)	NONA	
1-Decylamine (<i>n</i> -Decylamine)	DECA	
1-Dodecylamine (<i>n</i> -Dodecylamine)	DODEA	
Straight-chain amide		
Stearamide	SAD	
Branched-chain saturated alcohol		
2-Methylpropan-1-ol (isobutanol)	IB	
2-Methylpropan-2-ol (<i>tert</i> -butanol)	TB	
Branched-chained unsaturated alcohols		
β -Citronellol	BCIT	
Linalool	LIN	
Branched-chain secondary diol		
2-Methyl-2,4-pentanediol	MPDIOL	
Branched-chain esters		
Isopropyl myristate	IPM	
Isopentyl acetate	IPAT	
Branched-chain ketones		
4-Methylpentan-2-one	MPON	

3,3-Dimethylbutan-2-one	DMBON	
Branched-chain aldehyde		
Citral (<i>cis, trans</i> mixture)	CI	
Cycloalkanes		
Cyclohexane	CHAN	
<i>trans</i> -Decahydronaphthalene (<i>trans</i> -decalin)	TDEC	
β -Pinene	PIN	
Aromatic hydrocarbons		
Limonene	LIMO	
Toluene	TO	
Aromatic carboxylic acids		
4- <i>tert</i> -Butylbenzoic acid	TBBA	
4-Hydroxybenzoic acid	HBA	
Salicylic acid	SAL	
Ibuprofen (isomer mixture)	IBU	
(<i>S</i>)-(+)-Ibuprofen	SIBU	
(<i>R</i>)-(-)-Ibuprofen	RIBU	
Cinnamic acid	CINA	

Ketoprofen	KETO	
Aromatic amide		
Acetanilide	ACA	
Cyclic alcohols		
Cyclohexanol	CHOL	
(1 <i>S</i> ,2 <i>R</i> ,5 <i>S</i>)-(+)-Menthol	MEN+	
(1 <i>R</i> ,2 <i>S</i> ,5 <i>R</i>)-(-)-Menthol	MEN-	
(-)-Borneol	BOR	
<i>cis</i> -Decahydro-1-naphthol	CDNAP	
Decahydro-2-naphthol (isomer mixture)	DNAP	
Terpineol	TER	
(-)-Perillyl alcohol	PAL	
Phenol	PhO	
Benzyl alcohol	BAC	
Carvacrol	CV	
1-Naphthol	INAP	
2-Naphthol	NAP	
2,7-Dihydroxynaphthalene	DHN	

1-Naphthalenemethanol	NM	
Cyclic ketones		
Cyclohexanone	CHON	
(+)-Camphor	CAM	
(S)-(+)-Carvone	CARS	
(R)-(-)-Carvone	CARR	
Lactone		
Dihydrocoumarin	DHC	
Cyclic aldehyde		
(S)-Perillaldehyde	PAD	
Cyclic ethers		
<i>trans</i> -Anethol	AN	
Eugenol	EU	
Heterocyclic aromatic compounds		
8-Hydroxyquinoline	HQ	
Quinoline	QN	
Quinoxaline	QNX	
Cholesterol	CLS	
Span 20	SZO	
Span 60	SCO	

Tween 80	TSO	
D,L- α -tocopherol	TOCO	
α -Tocopheryl linoleate	LINO	
Curcumin	CUR	

II.2. Preparation of the inclusion complexes

II.2.1. Crystallization protocol

V-amylose lamellar crystals were prepared in aqueous solutions of amylose in different conditions (concentration of amylose, complexing agent and DMSO, DP of amylose and crystallization temperature). Amylose solutions (0.1-0.5 wt%) were prepared by two methods: i) dispersing amylose in water, bubbling with nitrogen for 20 min and then autoclaving at 160 °C for 30 min, and ii) dissolving amylose in DMSO at 90 °C for 1 h, then diluting in water (90 °C); the DMSO concentration varied from 2, 5, 10, 15, 20 and 30 vol%.

Most complexing agents were added into amylose solution after the dissolution at 75-90 °C. Fatty acids having 10-20 carbons, dodecanedioic acid, *n*-aliphatic alcohols having 10-16 carbons, (-)-borneol, *R*-(+)-camphor, decahydro-2-naphthol, *cis*-decahydro-1-naphthol and *trans*-decalin were added to amylose suspension before autoclaving since these complexing agents are thermally stable. Most molecules are poorly soluble and were used at saturation for complexation. However, for water-miscible agents such as short-chain fatty acids (propanoic and butanoic acids) and alcohols (ethanol, *n*-propanol and 2-propanol) and diols having 2-6 carbons, the complexation results depended on the concentration of complexing agents. Therefore, they were used at 5-80 vol%. Water-immiscible pentanoic acid was used at 1-5 vol%. The crystallization mixtures were incubated at different temperatures (25, 40, 50, 60, 75, 90, 100 and 115 °C). After 1-2 weeks, the precipitates were recovered by centrifugation and washed with water containing the same amount of complexing agent present in the reaction medium.

Recrystallization. The complexation mixture containing crystals was heated up to about 90 °C to redissolve crystals, then cooled back to the crystallization temperature to allow the complexes to recrystallize. The procedure could be repeated several times. The lamellar crystals obtained were generally more individualized.

II.2.2. Treatments of the complexes

II.2.2.1. Hydrated / wet samples

V-amylose crystals are sensitive to dehydration. Therefore, it is important to characterize the crystals in a hydrated state to maintain the crystal structure. Suspensions of lamellar crystals were centrifuged and the supernatant was removed. The crystals were then deposited on absorbent paper for a few minutes to remove the solvent in excess.

II.2.2.2. Dry samples

Wet samples were dried using two methods: drying in primary vacuum or lyophilization.

II.2.2.3. Treatment with solvents

Wet crystals were dispersed in methanol, 2-propanol or *tert*-butanol. Some crystals were kept in suspension, while others were recovered by centrifugation and dried in vacuum.

II.3. Characterization techniques

II.3.1. Differential interference contrast (DIC) optical microscopy

DIC optical microscopy, also known as Nomarski microscopy, is used to enhance the contrast of unstained and transparent samples. A light polarized at 45° is divided into two rays polarized at 0 and 90° that are then focused to pass through two adjacent points in the sample (around 0.2 μm apart). If the travel regions of the two rays differ in refractive index or thickness, they will experience a different optical path length and thus have different phases. After traveling through the sample, they are recombined into one ray polarized at 135°. This generates an interference, brightening or darkening the image depending on the optical path difference.

A drop of crystal suspension was deposited on a glass slide and covered with a glass slip. The specimens were observed in DIC mode using a Zeiss Axiophot II microscope equipped with polarized light. The images were recorded with an Olympus SC50 digital camera operated by the Olympus Stream software.

II.3.2. Atomic force microscopy

Atomic force microscopy (AFM) is a type of scanning probe microscopy with a high resolution on the order of a few angstroms. AFM uses a cantilever with a sharp tip (probe) at

its end to scan the specimen surface (**Figure II.3**). When the tip is brought in proximity of the sample surface, the local forces between the tip and the sample result in a deflection of the cantilever and thus allows local imaging of the topography of the sample surface by recording the height of the probe that corresponds to a constant probe-sample interaction.

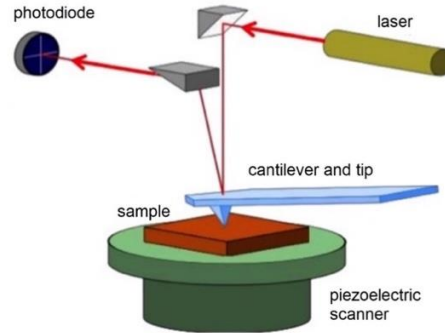


Figure II.3. Typical configuration of an AFM.

AFM imaging was carried out by Frédéric Dubreuil (CERMAV) with a Dimension Icon (Bruker) and a Pico Plus (Molecular Imaging) microscopes equipped with silicon probes having a nominal spring constant of 37 N m^{-1} and a nominal tip radius of 6 nm (ACT AFM probes from AppNano) using a standard procedure for tapping mode in air. The data were treated and analyzed using the Gwyddion software. Topographic variations were determined after baseline correction via height distribution analysis on various areas and different images. For a good statistical distribution, at least 20 measurements were performed for each sample.

The surface roughness was calculated as $Rq = \sqrt{\frac{1}{N} \sum_1^N (Z_i - \bar{Z})^2}$ where \bar{Z} is the average height.

II.3.3. X-ray diffraction (XRD)

II.3.3.1. Diffraction by crystals

A crystal consists of a periodic spatial arrangement of atoms. Mathematically, a crystal can be considered as a three-dimensional arrangement of points called a point lattice. The lattice can be reproduced by repeating a small unit, referred to as *unit cell* which is defined by three vectors \mathbf{a} , \mathbf{b} , and \mathbf{c} and the interaxial angles between them, α , β , and γ . A plane which passes through 3 lattices points which are not aligned is called a lattice plane. In real space, a set of parallel lattice planes is described using $(h \ k \ l)$ Miller indices and the (x, y, z) coordinates of any point in the lattice planes satisfies the equation: $hx + ky + lz = n$, where n is an integer number.

When a radiation with a λ wavelength illuminates a crystalline specimen, part of the beam is deflected in specific directions due to Bragg diffraction (**Figure II.4**). The angle of the

incidence of the parallel planes appearing at intervals d (d -spacing) is θ . The waves reflected by the two planes have an optical path difference of $2d\sin\theta$. They interfere with each other to enhance the intensities when the optical path difference equals an integer multiple (n) of the incident wavelength λ . Therefore, the condition of diffraction for mutual intensity enhancement is given by the equation $2d\sin\theta = n\lambda$, which is called Bragg's law. A diffraction pattern from a single crystal usually contains many distinct peaks, each corresponding to a different d -spacing and a different set of planes ($h k l$) in real space.

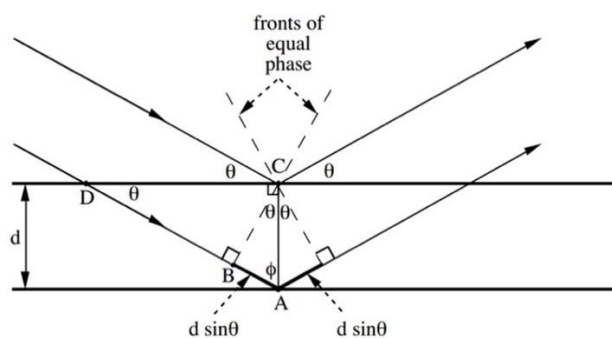


Figure II.4. Geometry for interference of a wave scattered from two crystal planes separated by a spacing d .

II.3.3.2. Experimental procedure

After decantation, the crystals were further centrifuged and the pellets were allowed to settle onto a piece of bolting cloth inside a closed chamber with a 95% relative humidity controlled humidity (95% relative humidity). After a few days of equilibration, strips of the resulting crystal mats were introduced into glass capillaries which were then flame-sealed immediately and X-rayed in a Warhus vacuum chamber using a Philips PW3830 generator operating at 30 kV and 20 mA (Ni-filtered $\text{CuK}\alpha$ radiation, $\lambda = 0.1542$ nm). Two-dimensional diffraction patterns were recorded on Fujifilm imaging plates, read off-line using a Fujifilm BAS 1800-II bioimaging analyzer. The resulting ring patterns were radially averaged to get diffraction profiles. The diffraction data were calibrated using a calcite powder standard and the unit cell parameters refined using the *CelRef* module of the LMGP package (Laugier & Bochu).

II.3.4. Transmission electron microscopy (TEM)

II.3.4.1. Principle

A beam of electrons is transmitted through thin (< 500 nm for a polymer) specimens to form an image of their volume with a resolution of a few angstroms. A beam of electrons is generated by an electron gun and accelerated by an anode (Figure II.4). The illumination

system consists of a number of electromagnetic lenses that modify the trajectory of the incident electrons. The condenser lenses modify the size, position and intensity of the beam. The condenser aperture controls the parallelism and coherency of electron beam that irradiates the specimen. The objective lens forms a first magnified image using the electrons that have passed through the specimen. This image is further magnified by intermediate and projective lenses and visualized on a fluorescent screen, or recorded using a digital camera.

The TEM can be operated in imaging or diffraction mode (**Figure II.5a** and **II.5b**). In imaging mode, the intermediate lens is adjusted so that its object plane is the image plane of the objective lens. The objective aperture is inserted at the back focal plane of the objective lens to increase the contrast by blocking all the electrons scattered at large angles. A so-called bright-field image is formed by the electrons transmitted through the specimen. In diffraction mode, the objective aperture is removed. The selected area aperture is used to select a circular region of the specimen from which the diffraction pattern is recorded. Its diameter is generally 500 nm or 1 μm . The intermediate lens is readjusted so that its object plane is the back focal plane of the objective lens, allowing projecting the diffraction pattern of the specimen on-screen. By comparison with XRD that were used to record powder (ring) patterns on a large number of crystals, selected area electron diffraction (SAED) allowed probing individual crystals and thus record spot patterns. However, polymer crystals are extremely sensitive to radiation damage from the electron beam and are decrystallized in a matter a seconds at room temperature. Therefore, the samples must be observed under low dose conditions. The crystal structure can also be preserved if the specimen is kept at low temperature during the observation.

II.3.4.2. Experimental procedure

Drops of dilute crystal suspensions were deposited onto carbon-coated grids previously glow-discharged in a Pelco easiGlow station, and allowed to dry. The specimens were observed under low dose illumination with a FEI-Philips CM200 'Cryo' microscope operating at 200 kV. For electron diffraction, the TEM grids were mounted on a Gatan 626 specimen holder and fast-frozen into liquid nitrogen just after air-drying and prior to being introduced in the microscope. The holder was then cooled down with liquid nitrogen and the observation was made at -176 °C. Base-plane ED patterns were recorded at a voltage of 200 kV, from selected areas of about 1 μm^2 . Images and diffraction patterns were recorded on a TVIPS TemCam F216 camera. Some ED patterns were also recorded on Fujifilm imaging plates. The diffraction patterns were calibrated using a gold-coated carbon film as standard.

In the specific case of the $V_{1\text{-butanol}}$ complex (see **Chapter III**), the intensity of the reflections in the base-plane ED diagram was measured semi-automatically using a tailor-made program, as described by Nishiyama et al. (2010). First, the 100 and 010 vectors of the base-plane diagram were determined by measuring the position of the 600 and 060 diffraction spots. 16×16 pixels² boxes were extracted around each spot at each point defined by these base vectors. The intensity was calculated by fitting the data with a Gaussian peak function and a linear background. The saturated peaks were interpolated by fitting the non-saturated base of the reflection with a Gaussian function. The intensities of the reflections were averaged according to the symmetry of the pattern and normalized using the strongest value as reference.

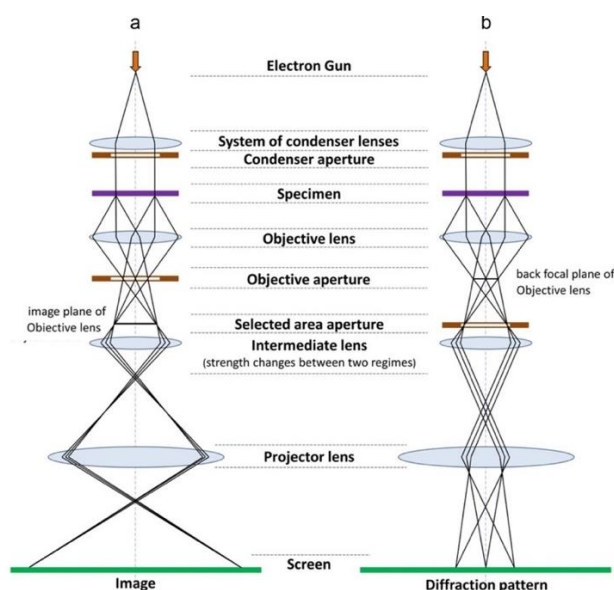


Figure II.5. Schemes illustrating the imaging (a) and diffraction (b) modes to operate a TEM. In each case, the intermediate lens selects either the image plane (a) or the back focal plane (b) of the objective lens as its object.

II.3.5. Solid-state ^{13}C nuclear magnetic resonance (NMR) spectroscopy

II.3.5.1. Principle

All isotopes that contain an odd number of protons and/or neutrons (*e.g.* ^1H and ^{13}C) have a nonzero nuclear spin. A spinning charge generates a magnetic field that results in a magnetic moment proportional to the spin. In the presence of an external magnetic field B_0 , two spin states exist: one up and one down, where one aligns with the magnetic field and the other opposes it. The sample is submitted to an oscillation frequency, usually referred as a radio-frequency pulse, whose energy exactly corresponds to the difference in energy of the two spin states (ΔE), inducing the excitation of this set of nuclei from the low to the high energy state.

Once the radio-frequency pulse is switched off, the nuclei magnetization returns to the initial equilibrium state by precessing about the main field B_0 which is called *free induction decay*. It is the precession of the magnetization that is detected as the signal in the nuclear magnetic resonance (NMR) spectroscopy.

The ΔE or the resonance frequency is proportional to the spin magnetic moment. However, not all nucleus of an isotope with the same magnetic moment yield a resonant signal at the same frequency values. The difference arises from the differing electronic environment of the nucleus of interest, which depends on the local geometry (binding partners, bond length, bond angle, etc.). The variation of the resonance frequencies of the same kind of nucleus, due to the variation in the electron distribution, is called a *chemical shift*. The extent of the chemical shift is given with respect to a reference frequency or reference sample. The chemical shift δ is usually expressed in parts per million (ppm) by frequency, calculated from the expression

$$\delta = \frac{\nu_{sample} - \nu_{ref}}{\nu_{ref}}$$

where ν_{sample} is the absolute resonance frequency of the sample and ν_{ref} is the absolute resonance frequency of a standard reference compound, measured in the same magnetic field B_0 .

The electronic environment around a nucleus is generally anisotropic, so its chemical shift is also anisotropic and depends on the orientation of the molecules with respect to the magnetic field. On the one hand, in liquid-state NMR, such anisotropic information, chemical shift anisotropy (CSA) is averaged out due to a fast and random molecular tumbling and only a single isotropic chemical shift value is observed with a narrow peak width. On the other hand, in solid-state NMR, molecules are immobile and often oriented in random directions with respect to the magnetic field, which gives rise to a broad lineshape for each nucleus in a static condition. Such a lineshape is characteristic to the solid-state structure and dynamics of the molecule, and thus provides important information for structural analysis. However, the peak broadness results in peak overlap and makes interpretation of NMR spectra very challenging. To overcome this problem, the anisotropic NMR interactions are suppressed by macroscopically rotating the sample at the 54.44° magic angle with respect to the magnetic field (Andrew et al., 1958), typically at a frequency of a few to tens of kHz. This technique, namely magic angle spinning (MAS), which is essentially mimicking molecular motion in solution state, makes the lineshapes narrower. Therefore, the resolution improves and a more precise structural analysis of molecular solids is possible.

Cross polarization (CP) is another important technique in solid-state NMR, which allows to efficiently detect a dilute spin such as ^{13}C . This exploits the polarization of abundant spins, such as ^1H , which is dipolar coupled with the rare spin. The natural polarization of abundant spins is transferred to the dilute spin during a so-called contact time, by using a low power pulse on both channels for dilute and abundant spins. The CP provides an enhancement of signals from dilute spins as well as faster repetition rate of the measurement.

The combination of CP and MAS techniques is a powerful analytical tool for structural analysis of solid organic materials (Snape et al., 1989). However, the quantitiveness of CP/MAS NMR is not always valid in specific cases (Smernik & Malcolm Oades, 2000; Smernik & Oades, 1999, 2000). In particular, this is a problem for a solid system where molecules with different dynamics co-exist. The direct excitation of carbon, or "single-pulse" (SP) NMR was suggested as a valid alternative for quantitative analysis for such systems, although the direct excitation of dilute spins requires much longer acquisition times compared to the case of CP.

II.3.5.2. Experimental procedure

Solid-state ^{13}C NMR analyses were performed by Yu Ogawa (CERMAV) on a Bruker Avance III 400 MHz spectrometer (^{13}C frequency of 100.6 MHz) using CP/MAS. The spinning speed was set at 12 kHz, with a sweep width of 29761 Hz, and a recycle delay at 2 s. Each spectrum was averaged over about 6000 scans. The ^{13}C chemical shifts were calibrated with respect to that of the glycine carboxyl group (176.03 ppm). SP/MAS solid-state NMR experiments were carried out as well using a ^{13}C 90° pulse of 4 μs and a delay time of 64 s.

II.3.6. Fourier-transform infrared (FT-IR) spectroscopy

II.3.6.1. Principle

Infrared (IR) spectroscopy is a type of vibrational spectroscopy that studies the interaction of infrared radiation with matter. It covers a range of techniques, mostly based on absorption spectroscopy. The IR portion of the electromagnetic spectrum is usually divided into three regions: near-IR (14000-4000 cm^{-1}), mid-IR (4000-400 cm^{-1}) and far-IR (400-4 cm^{-1}). The mid-IR spectroscopy provides characteristic fundamental vibrations that are employed for the elucidation of molecular structure and was used in this study. The infrared spectrum is a plot of measured infrared light absorbance (or transmittance) versus frequency or wavelength of the light. The typical frequency units used in IR spectroscopy are reciprocal centimeters, also called wavenumbers, with the symbol cm^{-1} . The frequency (ν , sec^{-1}), wavelength (λ , cm), and wavenumber (W) are related to each other via the following equation:

$$W = \frac{\nu}{c} = 1/\lambda$$

where c is the speed of light ($\text{cm}\cdot\text{s}^{-1}$). When a molecule absorbs infrared radiation, its chemical bonds vibrate in various modes. For example, six vibrational modes are involved for the CH_2 portion of a CH_2X_2 group, where X can represent any other atoms: symmetric and antisymmetric stretching, scissoring, rocking, wagging and twisting, as shown in **Figure II.6**.

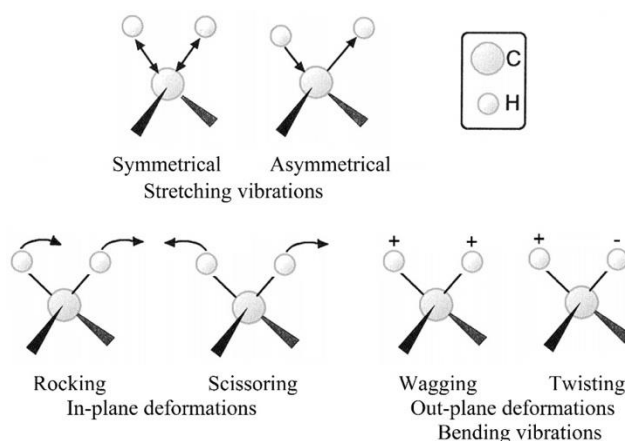


Figure II.6. Vibration modes of a CH_2 portion in a CH_2X_2 where X can be any other atom.

The first necessary condition for a molecule to absorb IR light, or to be IR-active, is that the molecule must have a vibration during which the change in dipole moment with respect to distance is non-zero. The second necessary condition for IR absorbance is that the frequency of the light impinging on a molecule must equal a vibrational frequency within the molecule (resonant frequency). If the frequency of a photon does not meet the criterion, it will be transmitted by the sample. The frequency (ν) of the absorbed light corresponding to the frequency of the vibration modes excited by the light is given in the following equation:

$$\nu = \frac{1}{2\pi} \left(\frac{k}{\mu} \right)^{1/2}$$

where k is the force constant of the bond and μ is reduced mass which refers to $(M_1M_2)/(M_1+M_2)$ where M_1 and M_2 are the masses of the two atoms, respectively. Therefore, different molecules vibrate at different frequencies because their structures are different and thus can be distinguished using infrared spectroscopy.

The attenuated total reflection (ATR) mode allows analyzing samples (powders, pastes, liquids) directly without further preparation. The specimen is deposited onto a diamond crystal through which IR light is passing. The multiple reflections of the beam creates an evanescent wave that penetrates into the specimen and the signal is collected by a detector.

II.3.6.2. Experimental procedure

FT-IR spectra of hydrated complexes (desorbed in a chamber with 95% relative humidity) were recorded with a Perkin-Elmer Spectrum 2 FT-IR spectrophotometer equipped with an ATR accessory. Measurements were done in the 4000-400 cm^{-1} range with a resolution of 2 cm^{-1} and eight repeat scans were averaged for each spectrum.

II.3.7. Density measurement

The measurement was only carried out for $V_{\text{ibuprofen}}$ and $V_{\text{1-butanol}}$ crystals. Fragments of mats of crystals equilibrated at 95% RH were floated in 1,2-dichloroethane ($d = 1250 \text{ g.L}^{-1}$) to which 1,1,2-trichloro-1,2,2-trifluoroethane ($d = 1560 \text{ g.L}^{-1}$) was slowly added. When the film remained in equilibrium in the mixture of liquids, its density was equal to that of the liquid which was measured using a pycnometer.

II.3.8. Molecular modeling

II.3.8.1. $V_{\text{1-butanol}}$

II.3.8.1.1 Building the rigid symmetrical amylose helices

Regular left- and right-handed amylose helices having 6, 7, or 8 glucosyl units per turn and the hydroxymethyl groups in gauche-gauche (*gg*) conformation (Horii et al., 1983) were generated by propagating a α -D-glucosyl residue in ${}^4\text{C}_1$ chair conformation using the parameters n (number of residues per turn) and h (rise per residue) (Nishiyama et al., 2010). The glucosyl residues were taken from the previously reported rigid helices (Nishiyama et al., 2010; Putaux et al., 2011). The energy of the resulting helices was not further optimized.

II.3.8.1.2. Packing energy calculation and geometry optimization

The non-bonded interaction was considered using Buckingham's potential [$E = A \exp(-B \times r) - C/r^6$], where the A , B , C parameters are different for each type of atom pair (Dauchez et al., 1993). This function was applied with a cutoff of 1 nm. The molecule geometry was optimized using the Universal Force Field (Rappé et al., 1992) in the Forcite module of Material Studio (Forcite).

II.3.8.1.3. Model refinement

The structure refinement against experimental electron diffraction data was conducted using the SHELXL program (Sheldrick, 2015). An intensity average was calculated for groups of symmetry-related reflections. The program used the atomic scattering factors for electrons from the International Tables for Crystallography (Cowley et al., 2004). The models were

refined using the conjugate-gradient least-square (CGLS) regression method with an isotropic approach of the thermal parameters. The so-called "1-2" and "1-3" distances are defined as the distances between an atom and its first and second neighbor, respectively. The isotropic U -values of equivalent atoms were restrained to be equal, and 1-2 and 1-3 distances were restrained using the DFIX and DANG instructions. Anti-bumping restraints were applied if the two atoms were closer to each other than the target distance. At the beginning of the refinement, the standard deviation sd for 1-2 and 1-3 distances was set 10 times lower than the default value (0.02 in the first DEFS parameter) to restrain the conformation of amylose. The resolution limit was first set to 0.35 nm, then decreased to 0.3 nm and finally to 0.24 nm. In the final refinement, sd was set to the default value (0.02) to allow the helix to further relax. The reliability factor $R1$ was calculated as:

$$R1 = \frac{\sum ||F_{obs}| - |F_{cal}||}{\sum |F_{obs}|}$$

where F_{obs} and F_{cal} are the observed and calculated structure factors, respectively.

II.3.8.2. Molecular dynamics of $V_{ibuprofen}$

Atomistic molecular dynamics simulations were performed using the Gromacs 5.1 package (Hess et al., 2008) and the Gromos 56A6_{CARBO_R} force field (Plazinski et al., 2016) with a modified Lennard-Jones repulsive parameter for the CH1 atom type. In the simulations, the motion equations were solved by a standard leapfrog algorithm with integration step of 2 fs. The length of covalent bonds was constrained by using the LINCS algorithm. All the equilibration and production runs were achieved in the NPT ensemble (constant number of particles, pressure, and temperature). The velocity-rescaling algorithm was used for temperature control with a coupling time of 0.1 ps. The pressure was regulated to 1 bar using a Berendsen pressure coupling algorithm with a pressure coupling constant of 2.0 ps (Berendsen et al., 1984). The pressure was anisotropically regulated. The long-range interactions were calculated by using the particle-mesh Ewald summation method with a cut-off distance of 0.9 nm and the long-range dispersion force was corrected for both energy and pressure. All analyses was performed using GROMACS tools. Trajectories were visualized with the VMD software (Humphrey et al., 1996) and final models were displayed using PyMOL (DeLano, 2002).

In another procedure, the molecule geometry was optimized by the Forcite module in Materials Studio (Forcite) using the Universal Force Field (Rappé et al., 1992). The non-bonded electrostatic and van der Waals forces were controlled by the Ewald summation method. Water was packed into the cell using the Amorphous Cell module with the Universal Force Field. The

module builds molecules in a cell using a Monte Carlo protocol and minimizes close contacts between atoms, while ensuring a realistic distribution of torsion angle (Akkermans et al., 2013; Chen et al., 2012).

II.3.9. Dissolution tests of V-ibuprofen complexes

II.3.9.1. Ibuprofen quantification assays

The ibuprofen fraction in the complexes, the ibuprofen solubility values and the *in vitro* dissolution characteristics of the complexed drug were determined using a Shimadzu UV-1603 ultraviolet spectrophotometer. In ethanol, the ibuprofen concentration (C_{ibu} , mg.L⁻¹) was calculated from the equation $C_{ibu} = 712.56 * A - 3.0633$ ($R^2 = 0.9998$) by measuring the absorbance (A) at 263.9 nm. At pH 12.69 in a 0.1 M NaOH solution, the ibuprofen concentration was spectrophotometrically assayed at 264.3 nm and calculated from the equation $C_{ibu} = 517.44 * A - 4.4734$ ($R^2 = 0.9998$).

II.3.9.2. Determination of ibuprofen content in the complex

The ibuprofen content was evaluated by two methods. In the first one, 15 mg of the freeze-dried complex was introduced in a 5 mL volumetric flask and completed with ethanol 96%. The mixture was sonicated for 30 min and then filtered (PVDF, 0.22 μm). The ibuprofen concentration in the filtrate was determined spectrophotometrically at 263.9 nm. In the second method, 20 mg of freeze-dried complex was mixed with 10 mL of a 0.1 M NaOH aqueous solution, agitated (500 rpm) for 2 h at 37 °C, filtered (PVDF, 0.22 μm), and assayed at a wavelength of 264.3 nm. In both methods, the ibuprofen weight percentage was calculated according to the following equation:

$$\%ibu = 100 \times \frac{C_{ibu} \times V}{1000 \times m_{complex}}$$

in which V is the volume of solvent in mL (ethanol or 0.1 M NaOH solution), and $m_{complex}$ is the weight of the freeze-dried complex in mg.

II.3.9.3. Determination of the solubility of ibuprofen in the dissolution media

Excess ibuprofen was introduced in 15 mL of each medium in a 25 mL Erlenmeyer flask equilibrated at 37 °C in a water bath. The mixture was stirred at 500 rpm for 2 h to reach equilibrium. Then, 2 mL of the solution was filtered (PVDF, 0.22 μm) and the pH was adjusted to 12.69 by adding a known volume of a 5 M NaOH solution. Ibuprofen concentrations were determined by measuring the absorbance at a wavelength of 264.3 nm after appropriate dilution. The whole test was made in triplicate.

II.3.9.4. *In vitro* dissolution studies

The experiments were performed using a basket apparatus (Sotax AT7, Sotax Switzerland) and the rotating speed of the baskets was set at 50 rpm. Briefly, 190 mL of a dissolution medium (0.1 M HCl or phosphate buffers pH 5.5, 6.8 and 7.2) was placed into the vessel and equilibrated at 37 ± 0.5 °C. A sample of the freeze-dried complex containing 10 mg ibuprofen was placed in the basket and the position of the latter was adjusted so that the sample was fully immersed. At appropriate intervals during 6 h, a 2 mL sample was taken from the release medium, filtered (0.22 μ m PVDF filter), adjusted to pH 12.69 with a 5 M NaOH solution and spectrophotometrically assayed at 264.3 nm for cumulated drug release. A similar experiment was performed in the presence of amylose as reference to control the absence of detectable UV signal due to the presence of the polymer in the considered wavelength region. Also, a dissolution study of pure ibuprofen in each medium was conducted at 37 °C by incubating 10 mg of drug instead of the complex into 190 mL acidic or buffer solutions. It should be noted that all the drug release experiments were performed under conditions that ensure that the maximum concentration corresponding to 100% of ibuprofen release in the vessel did not exceed 70% of the saturating ibuprofen concentration.

In addition, a two-stage dissolution test was carried out with the complex. The procedure was as follows: a first step in acidic medium (pH 1.2) was performed at 37 ± 0.5 °C after introducing 120 mg of the complex in the basket, rotating at 50 rpm, in 170 mL of 0.1 M HCl. Samples were collected at predetermined time intervals and spectrophotometrically assayed as previously described. Then, 20 mL of a solution equilibrated to 37 ± 0.5 °C, containing either 1.293 g ($\text{KH}_2\text{PO}_4 \cdot 2\text{H}_2\text{O}$) and 0.832 g NaOH or 2.493 g $\text{KH}_2\text{PO}_4 \cdot 2\text{H}_2\text{O}$, 0.245 g $\text{Na}_2\text{HPO}_4 \cdot 12\text{H}_2\text{O}$ and 0.680 g NaOH, was added to the acidic medium, in order to adjust the pH to 6.8 and 5.5, respectively. The release study at this stage was performed during 6 h. All the tests were made in triplicate.

Chapter III

Crystal and molecular structure of V₁-butanol

III.1. Introduction

As presented in **Chapter I**, five allomorphic families of V-amylose lamellar crystals containing compact 6-, 7- or 8-fold helices have been reported in the literature, including V_{6I} , V_{6II} , V_{6III} , V_7 and V_8 . The detailed crystal structure of V_{6I} , V_{6III} , V_7 and V_8 has been resolved based on ED or fiber XRD data, in combination with molecular modeling (Brisson et al., 1991; Cardoso, 2007; Nishiyama et al., 2010; Rappenecker & Zugenmaier, 1981; Winter & Sarko, 1974). On the other hand, the crystal structure of V_{6II} is still speculative.

V_{6II} complexes were first prepared with *n*-butanol (Rundle & Edwards, 1943; Schoch, 1942). Several other complexing agents such as ketones (Takeo & Kuge, 1971), fatty acids (Biais, 2006), alcohols (Biais, 2006; Helbert, 1994), esters (Biais, 2006) were then shown to induce the formation of this crystalline structure.

In the V_{6II} family, $V_{1\text{-butanol}}$ has been the most studied complex. Although crystalline fibers (Hinkle & Zobel, 1968) and single crystals (Booy et al., 1979; Helbert & Chanzy, 1994; Manley, 1964; Yamashita, 1965) of $V_{1\text{-butanol}}$ have been prepared and characterized by ED and XRD, no definitive three-dimensional model is available yet. Hypotheses for the helical conformation and the arrangement of amylose helices for V_{6II} have been proposed (Helbert & Chanzy, 1994; Yamashita, 1965). From diffraction data, it was found that the helical repeat was about 0.8 nm, *i.e.* the same as that of 6-fold V_{6I} complexes. In addition, the reversible conversion into the V_{6I} structure without a change in morphology supports the occurrence of the 6-fold helix for these crystals. Helbert and Chanzy (1994) proposed a packing arrangement of amylose in V_{6II} crystals and that *n*-butanol together with some water molecules were located between the helices (**Figure I.11**). The location of the guest molecules inside the helices is still elusive. At present, no crystallographic study has allowed confirming the hypotheses on the crystal structure of V_{6II} , mainly because the ED and XRD data recorded on the lamellar crystals are not resolved enough for refining the structure. The present work was therefore undertaken to solve the molecular and crystal structure of the $V_{1\text{-butanol}}$. For this, lamellar $V_{1\text{-butanol}}$ single crystals were prepared and their ED diagrams used for a structure determination based on conformational and packing energy analyses, combined with classical crystalline polymer structure refinement (Nishiyama et al., 2010).

III.2. Results and discussion.

III.2.1. Crystal morphology and the unit cell

Figure III.1 shows electron micrographs of typical crystals of V_1 -butanol prepared from dilute aqueous amylose solutions. They generally consist of stacks of thin rectangular-shaped lamellae. Each lamella is about 2-5 μm wide and 8-12 μm long. Spiral dislocation growth was not observed but the crystals thickened by epitaxial growth oriented on the neighboring lamellae. In addition, cross-shaped or rosette-shaped twinned crystals consisting of two or three platelets with angles of intersection close to 60 or 90° were usually observed (**Figure III.1b** and **III.1c**). Interestingly, as previously mentioned in other studies (Booy et al., 1979; Helbert & Chanzy, 1994; Manley, 1964; Yamashita, 1965), the crystals frequently showed cracks along the longer dimension of the rectangular lamellae. These cracks, which are likely caused by anisotropic shrinkage during the drying of the crystal in air or in the vacuum of the TEM, are absent when the crystals are observed under frozen-solvated conditions.

Figure III.2a shows a part of a typical base-plane ED pattern of V_1 -butanol recorded on a 1 μm^2 surface of the lamellar crystal in frozen-hydrated state at low temperature. The diffraction spots extend to a resolution of 0.24 nm and distributed symmetrically in a lattice defined by the two orthogonal axes a^* and b^* aligned parallel to the shorter and longer dimensions of the lamella, respectively.

The ED diffraction pattern is identical to those reported by Booy et al. (1979) and Helbert and Chanzy (1994). It can be indexed according to an orthorhombic unit cell (space group $P2_12_12_1$) with lattice constants $a = 2.65 \pm 0.01$ nm, $b = 2.74 \pm 0.01$ nm, in agreement with those calculated from the XRD pattern ($a = 2.655 \pm 0.001$ nm, $b = 2.708 \pm 0.001$ nm, $c = 0.798 \pm 0.001$ nm) (**Figure III.2b**). These results confirm the cell parameters given earlier (Booy et al., 1979; Helbert & Chanzy, 1994). A list of independent intensities for reflections up to a 0.24 nm resolution, averaged from several ED patterns, is presented in **Annex 1, Table S.III.1**.

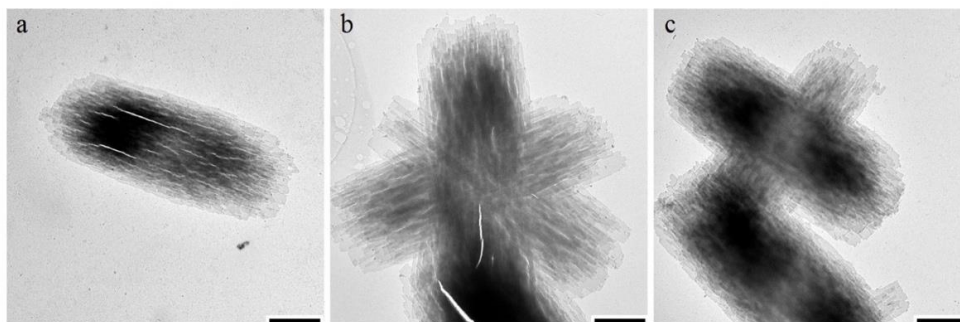


Figure III.1. TEM images of V_1 -butanol crystals: a) rectangular crystal favoring an epitaxial growth; b,c) twinned configurations of crystals at 60 and 90°, respectively. Scale bars: 2 μm .

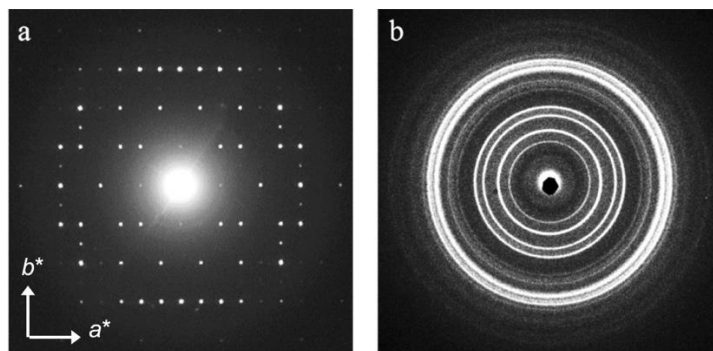


Figure III.2. a) ED pattern recorded on a frozen-hydrated $V_{1\text{-butanol}}$ crystal at low temperature; b) XRD powder pattern recorded on a hydrated film of $V_{1\text{-butanol}}$ crystals.

III.2.2. ^{13}C CP/MAS NMR spectroscopy

Figure III.3 shows a typical ^{13}C CP/MAS NMR spectrum recorded on hydrated crystals of $V_{1\text{-butanol}}$. Only one signal was detected for each carbon site suggesting that the helix was rather symmetrical, in agreement with a previous study (Le Bail et al., 2005). The resolved resonances at 102.4, 81.8, 74.7, 71.7 and 61.0 ppm can be assigned to C1, C4, C3, and C2-C5 and C6 carbon atoms of the glucosyl units, respectively. The broad peak centered at 61.0 ppm is an overlap of the resonance of C6 carbon of the glucosyl units and that of C(OH) carbon of 1-butanol. Besides, the sharp peaks at 35.0, 19.4 and 14.3 ppm correspond to the resonances of other carbon atoms of 1-butanol, suggesting that the molecule is not mobile and would be located in crystallographic positions. In addition a shoulder at 100.4 ppm was also observed, indicating the presence of some B-amylose (Horii et al., 1987; Veregin et al., 1987a).

As noted in previous studies, the chemical shifts of the C1 and C4 atoms depend on the values explored by the torsion angles about the glucosidic linkages and thus reflect the global helical conformation of the chain (Gidley & Bociek, 1988; Horii et al., 1987; Veregin et al., 1987a). Gidley and Bociek (1988) showed that the ^{13}C chemical shifts were indistinguishable between 6- and 7-fold helices but the C1 and C4 signals were shifted upfield by about 1 ppm with respect to the V8 structure. Kawada and Marchessault (2004) also found that the complexes prepared with lauric (dodecanoic) acid which would contain 6-fold helices, presented the same C1 chemical shift at 103 ppm to that of V_{thymol} which is a 7-fold complex (Putaux et al., 2008). In contrast, several studies indicated that there are significant differences in the C1 resonance between the 6-, 7-, and 8-fold complexes. In particular, the C1 signal is located at 102.2-102.7, 103.3-103.4, and 105 ppm for 6, 7-, and 8-fold complexes, respectively (Le Bail et al., 2005; Rondeau-Mouro et al., 2004). However, all the above studies are in agreement regarding the upfield shifts of the resonance in these complexes as opposed to V8

complexes. In the present study, the C1 chemical shift in $V_{1\text{-butanol}}$ was found at 102.4 ppm, which means the complexes would have 6- or 7-fold helices.

Previous works reported that the C6 resonance is correlated with the conformation of the hydroxymethyl group (Horii et al., 1983; Veregin et al., 1987b). For cyclodextrins, the resonances in the range 59.6-61.7 ppm and 62.7-65.9 ppm are related to gauche-gauche (*gg*) and gauche-trans (*gt*) conformations, respectively (Veregin et al., 1987b). Similar correlations have been found for cellulose, showing 60-62.6 ppm for *gg*, 62.5-64.5 ppm for *gt*, and 65.5-66.5 ppm for trans-gauche (*tg*) (Horii et al., 1983). In the case of $V_{1\text{-butanol}}$, because of the overlap between resonances of C6 carbons of amylose with that of carbon atoms of 1-butanol (Figure III.3), it is impossible to unambiguously determine the conformation of the hydroxymethyl group. However, the chemical shift of C6 in $V_{1\text{-butanol}}$ is rather broad, in agreement with previous studies (Le Bail et al., 2005; Veregin et al., 1987a). This suggests a broad distribution of hydroxymethyl conformation, and all *gg*, *gt*, and *tg* conformations would be present in $V_{1\text{-butanol}}$.

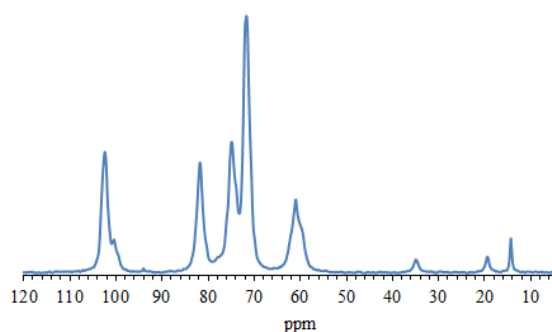


Figure III.3. ^{13}C CP/MAS NMR spectrum recorded on hydrated crystals of $V_{1\text{-butanol}}$.

III.2.3. Molecular modeling and crystal structure determination

III.2.3.1. Strategy

The few reflections observed in ED or powder XRD patterns are not sufficient for a crystal structure determination by conventional direct refinement methods. Therefore, the dataset has been complemented by additional data of various origins. Since $V_{6\text{II}}$ complexes with similar diffraction patterns can be obtained with many guest molecules having a molecular geometry different from that of 1-butanol, it seems reasonable to assume that amylose is in an arrangement of minimum packing energy, which might be further stabilized by the complexing agent and the water molecules. As a consequence, a packing analysis would allow selecting the possible amylose helical conformations and helix packing arrangements that can be used as a starting models for the structure refinement. The approach used in the present study is similar to that described by Nishiyama et al. (2010) with some modifications.

III.2.3.2. Selection of helical conformation and exhaustive search of helix position

Six regular left- and right-handed amylose helices, having 6, 7, or 8 glucosyl residues per turn and a pitch of 0.8 nm were built as described previously (Nishiyama et al., 2010). These helices will be referred to as L6, L7, L8, R6, R7, and R8, respectively. As shown by the ^{13}C NMR data, all *gg*, *gt*, and *tg* conformations would be present in $V_{1\text{-butanol}}$. Therefore, to simplify the procedure of packing analysis, the hydroxyl group on the C6 atom was initially removed rather than being fixed in a unique orientation. Another advantage of the removal of the C6 hydroxyl group is that the calculations were three times faster than testing separately the three conformations (*gg*, *gt*, and *tg*) (Nishiyama et al., 2010). Examples of the constructed helices with removed C6 hydroxyl groups are presented in **Figure III.4**.

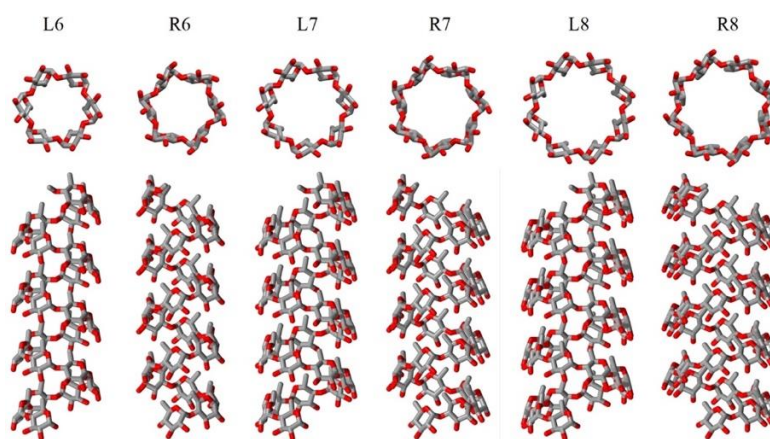


Figure III.4. Axial and longitudinal view of 6-, 7- and 8-fold left- and right-handed helices with C6 hydroxyl groups removed. Hydrogens were omitted for clarity.

Each constructed helix was introduced in the unit cell (space group $P2_12_12_1$) with parameters $a = 2.65$ nm, $b = 2.74$ nm, and $c = 0.80$ nm. The search of best helix positions was performed by translating the helix along a and b axes every 0.01 increment (fractional coordinates), corresponding to about 0.02 nm, within $1/8^{\text{th}}$ of the (a,b) projection of the unit cell. This was sufficient to cover all the possibilities regarding the symmetry of the unit cell. At each position, the helix was rotated around its helical axis by 1° steps between 0 and 360° and translated along c -axis from 0 to 0.12 nm with an interval of 0.03 nm. Only the non-bonded interaction was considered using Buckingham's potential with a cutoff of 1 nm. At each translational position in the (a,b) plane, the minimum packing energy and the corresponding rotation angle and translation along c were saved. A contour map of these grid-searches was then drawn, as exemplified for L6 and R6 helices (**Figure III.5**). From this data, the lowest packing energy of each helix was determined and tabulated in **Table III.1**. As noted, the 6-fold

helices are the most energetically favored while the energy of structures based on 7- or 8-fold helices would be too high. **Figure III.6** illustrates examples of the lowest energy packing for L6, L7, and L8 helices, projected on the (a,b) plane of the unit cell. Whereas the 6-fold structure seems acceptable, a significant overlap was observed in the models for 7- and 8-fold helices. This is not surprising since the theoretical helix diameter (1.37 nm) calculated from the unit cell parameters is equal to the outer diameter of 6-fold helices. On the other hand, 7- and 8-fold helices which outer helix diameters are 1.50 nm and 1.62 nm respectively, would be too large for the unit cell size, leading to the observed collision.

In the 6-fold family, L6 and R6 helices have similar packing energy profiles (**Figure III.5**). Each of them presents three local energy minima with the helix centered at the fractional coordinates $(0.00,0.00)$, $(0.08,0.17)$ and $(0.08,0.33)$ in the (a,b) plane. All the structures corresponding to these local minima were retained for further analysis. It is important to note that the energy calculation only took into account Buckingham's non-bonded interactions of amylose chains, while the contribution of the electrostatic interactions and the interactions with solvent/complexing molecules are not involved in the calculation. For this reason, the minima identified here might not be the minima of the whole system but should be very close to them.

By comparing the experimental XRD profile with those calculated from the models, it was found that the models with a L6 or R6 helix centered at the $(0.00,0.06)$ fractional coordinates showed the best agreement. Strictly, these models did not correspond to an energy minimum but their packing energy was very close (**Table III.2**). Therefore, these models were also selected as starting models for structure refinement. For an easy identification of each model, a name was given based on the helix type and position. In total, eight models were selected, shown in **Figure III.7**, and their features were summarized in **Table III.2**.

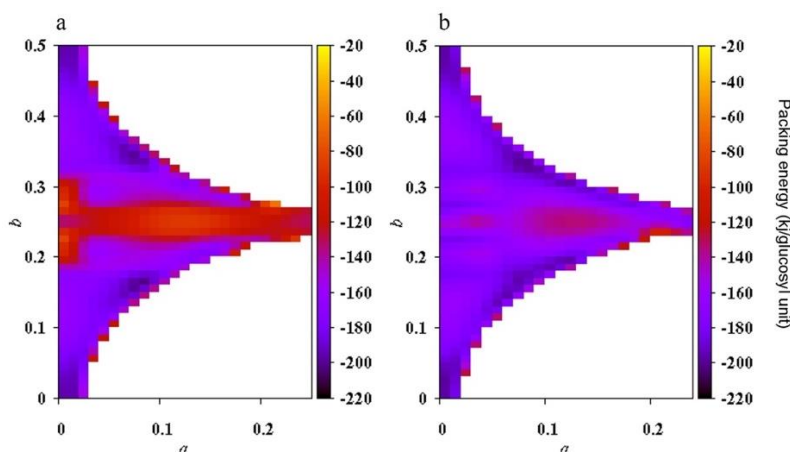
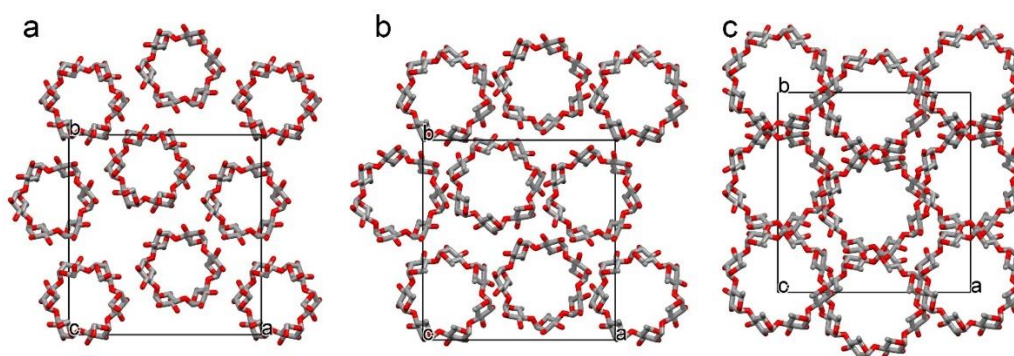
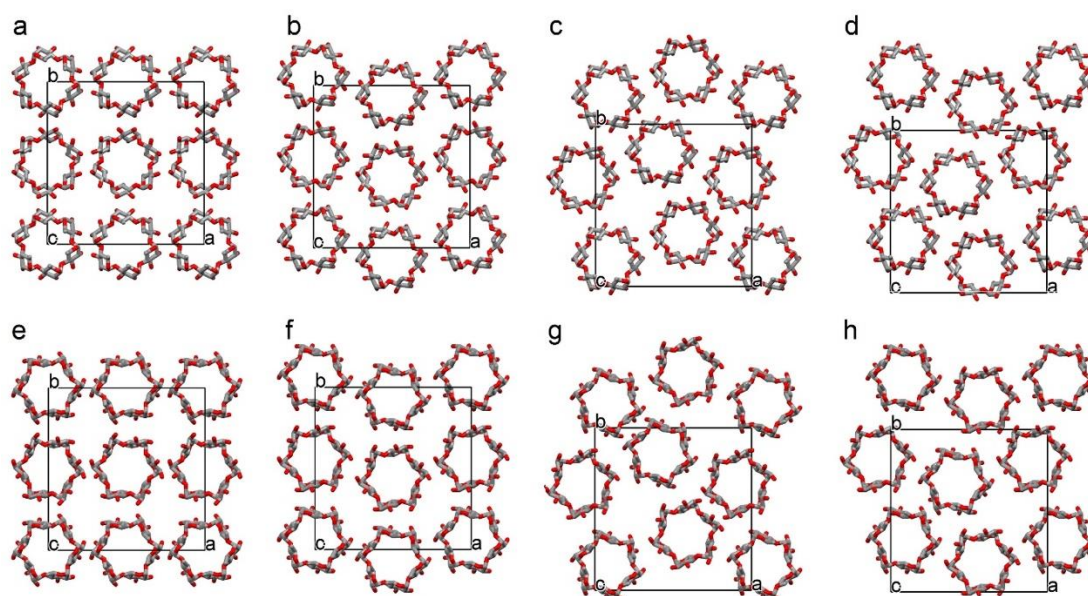


Figure III.5. Color packing energy map for left- handed (a) and right-handed (b) 6-fold helices when they are rotated and translated along the a - and b -axis in $1/8^{\text{th}}$ of the unit cell.

Table III.1. Lowest packing energy for different models built with rigid amylose helices.

Helix	L6	R6	L7	R7	L8	R8
Packing energy (kJ/glucosyl unit)	-205.9	-207.6	821.9	761.1	>10000	>10000

**Figure III.6.** Comparison of the projection on the (a,b) plane of the unit cell with the lowest packing energy models for 6- (a), 7- (b) and 8-fold (c) left-handed amylose helices with C6 hydroxyl groups removed. Hydrogens were omitted for clarity.**Figure III.7.** Selected starting models for structural refinement: a) L6_0000; b) L6_0006; c) L6_0817; d) L6_0833; e) R6_0000; f) R6_0006; g) R6_0817; h) R6_0833.

III.2.3.3. Addition of the C6 hydroxyl group, 1-butanol and water

Since the C6 hydroxyl group would adopt a wide range of orientations in the $V_{6\text{II}}$ structure, it was added with random conformation at each glucosyl residue. For 1-butanol and water, an initial rough number of these molecules inserted into the structure was estimated from the crystal density. The experimental density was $1.38 \pm 0.02 \text{ g.cm}^{-3}$, in agreement with the

value reported by Helbert and Chanzy (1994). Considering the total volume of the unit cell ($5.8088 \times 10^{-21} \text{ cm}^3$) and the total mass of the four amylose chains ($6.4588 \times 10^{-21} \text{ g}$), the total mass of water and 1-butanol would consequently be $1.5574 \times 10^{-21} \text{ g}$. Previously, Helbert and Chanzy (1994) estimated, based on the decrease in cell volume after drying, that each unit cell of $V_{1\text{-butanol}}$ would contain four 1-butanol molecules, along with some water molecules, located in the inter-helical space. If there is one 1-butanol located within each helical cavity, then the remaining mass corresponds to about 16 interstitial water molecules per unit cell.

After the addition of the C6 hydroxyl group, 1-butanol and water into the selected models, the molecular geometry was optimized using the Universal Force Field in two steps. First, the atoms of the rigid amylose helix were constrained and only 1-butanol and water molecules were allowed to move. In the second step, all the atoms were free to move. **Figure III.8** shows the example of the L6_0817 and L_0006 packing models of rigid helices (**a,d**) and the corresponding geometry-optimized ones after addition of C6 hydroxyl group, 1-butanol and water (**b,e**). It is noted that after the geometry optimization, the helix is more relaxed, losing the regular hexagonal symmetry while the hydroxymethyl conformation can be *gg* or between *gg* and *tg*.

Table III.2. Helix position and packing energy of selected models.

Model name	Helix center position (fractional coordinates)		Packing energy (kJ/glucosyl unit)
	<i>a</i>	<i>b</i>	
L6_0000*	0.00	0.00	-196.4
L6_0006	0.00	0.06	-177.3
L6_0817*	0.08	0.17	-205.9
L6_0833*	0.08	0.33	-199.0
R6_0000*	0.00	0.00	-205.2
R6_0006	0.00	0.06	-180.7
R6_0817*	0.08	0.17	-203.0
R6_0833*	0.08	0.33	-207.6

* corresponding to the local minima

III.2.3.4. Structure refinement

The geometry-optimized structures were input to the refinement against ED data using SHELX (see **Chapter II, § II.3.8.1.3**). In general, the refinement procedure allowed to find the atomic arrangements that increased the matching between observed and calculated intensities, indicated by a decrease in the *R**I*-factor. However, the refined structures and the corresponding *R**I*-factor depended on the starting models.

The 1-butanol and water molecules were directly inserted in the models and their positions were refined independently of the biopolymer molecules themselves. Using the average ED intensities to a resolution of 0.24 nm (72 diffraction spot) and the default value of the effective standard deviation ($sd = 0.02$ defined in the DEFS command) for restrained parameters, no model converged to the experimental diffraction intensities.

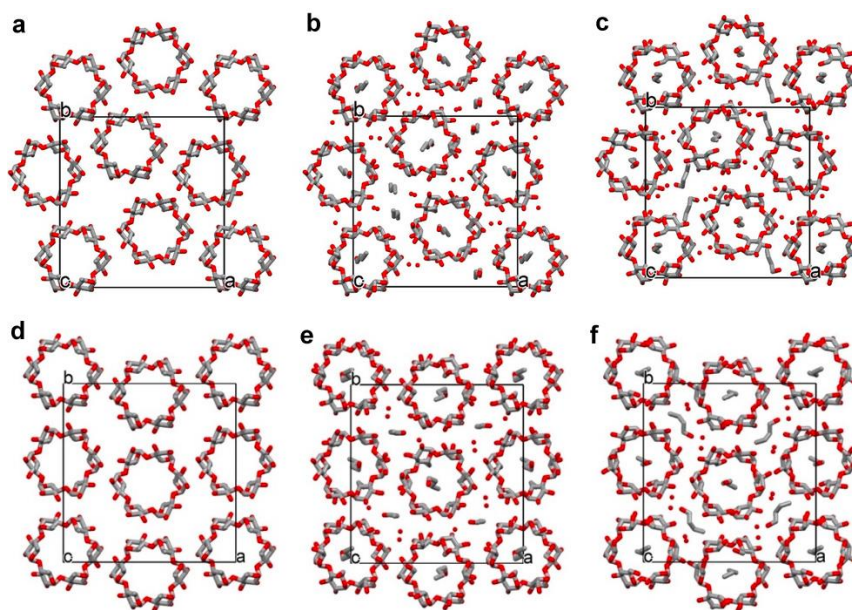


Figure III.8. Projection on the (a,b) plane of L6_0817 (a-c) and L6_0006 (d-f) models: a,d) initial packing of rigid helices with C6 hydroxyl groups removed, b,e) geometry-optimized model after addition of C6 hydroxyl groups, 1-butanol and water molecules; c,f) final structure refined with SHELX.

The R I -factor measures the agreement between the experimental and calculated structure factors after minimization (see **Chapter II**, § II.3.8.1.3). R I is close to 1 when the helical conformation is completely lost. Therefore, in the first several refinement steps, the sd was fixed 10 times lower than the default value in order to preserve the starting molecular conformations, *i.e.* helical conformation. At the same time, the resolution was first limited to 0.35 nm, then to 0.30 nm and finally to 0.24 nm. In the final refinement step, the default value of sd was used to allow the helix to relax while the resolution remained limited to 0.24 nm.

The refinement results are summarized in **Table III.3** and the examples of the L6_0817 and L6_0006 refined models are presented in **Figure III.8c,f**. The L6_0006 refined structure gave the best fit with the experimental data, with the lowest R I -factor of 0.13. Note that the L6_0817 model, which initially had the lowest packing energy in the grid-search (**Table III.2**) did not exhibit the lowest R I after refinement (**Table III.3** and **Figure III.9**).

Table III.3. *R*₁-factor of selected models refined against ED data using SHELX. *d* is the resolution of used reflections; *sd* is the effective standard deviation for restraints of distances between bonded atoms and bond angles, defined in the DEFS instruction in SHELX. The model with the lowest *R*₁ is in boldface.

Model	<i>R</i> ₁ -factor			
	<i>d</i> > 0.35 nm <i>sd</i> = 0.002	<i>d</i> > 0.30 nm <i>sd</i> = 0.002	<i>d</i> > 0.24 nm <i>sd</i> = 0.002	<i>d</i> > 0.24 nm <i>sd</i> = 0.02
L6_0000	0.60	0.40	0.42	0.20
L6_0006	0.23	0.28	0.33	0.13
L6_0817	0.71	0.64	0.60	0.40
L6_0833	0.68	0.60	0.54	0.43
R6_0000	0.63	0.61	0.58	0.42
R6_0006	0.47	0.45	0.42	0.34
R6_0817	0.78	0.77	0.74	0.33
R6_0833	0.88	0.80	0.77	0.57

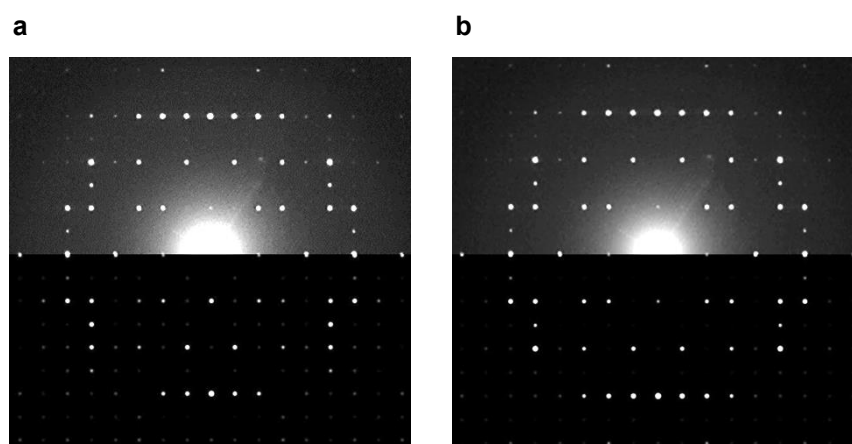


Figure III.9. Observed ED pattern of *V*₁-butanol (upper half) and a calculated pattern (lower half) of the final model after SHELX refinement: a) L6_0817; b) L6_0006.

Figure III.10 shows the observed XRD pattern recorded on a film of crystals (**a**) and those simulated from L6_0006 final structure with/without including the *c*-axis preferred orientation (**b** and **c**). The observed and calculated patterns fit better when a preferred orientation was considered. This result is consistent with the fact that the lamellar *V*-amylose crystals favor a flat-on orientation when settling in the form of a mat, which is demonstrated by a fiber-like XRD pattern when the X-ray beam is directed parallel to the film surface. Since the pattern shown in **Figure III.10a** was recorded when the X-ray beam was perpendicular to the film surface (parallel to the *c*-axis), *hkl* (*l* ≠ 0) reflections were almost not observed and the pattern was thus consistent with that including a preferred orientation.

Figure III.11 shows the projection of the final molecular structure on the (a,b) and (a,c) planes of the unit cell. The atomic coordinates are given in **Annex 1, Table S.III.2** whereas a selection of conformational parameters defining the helix geometry is listed in **Table III.4**. Consistent with the ^{13}C CP/MAS NMR data, the present results confirm that the $V_{1\text{-butanol}}$ structure consists of 6-fold left-handed helices in which the hydroxyl groups exhibit some conformational disorder. Inside the $P2_12_12_1$ orthorhombic unit cell, the helices are organized in an antiparallel fashion and in rows parallel to the b axis. These results validate the tentative model previously proposed by Helbert and Chanzy (1994). In addition, there are four 1-butanol and 16 water molecules distributed into four elongated interstitial pockets, and one 1-butanol molecule located inside each helix.

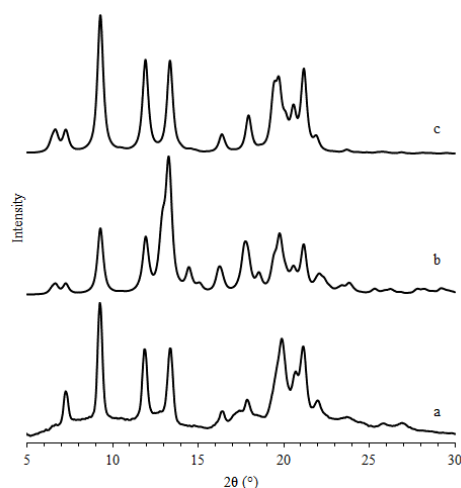


Figure III.10. a) XRD profile recorded on a hydrated film of $V_{1\text{-butanol}}$ crystals; b) calculated powder profile; c) calculated profile with an imposed c -axis preferred orientation.

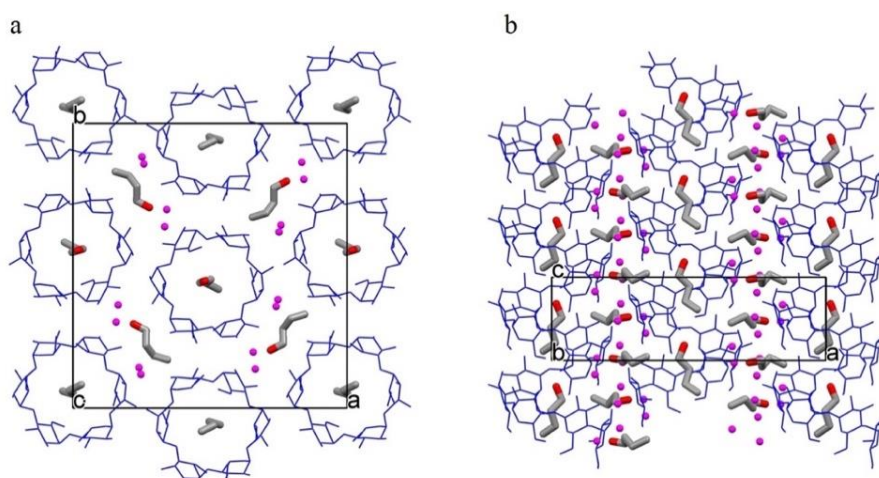


Figure III.11. Projection on the (a,b) (a) and (a,c) (b) planes of the final structure of $V_{1\text{-butanol}}$. Hydrogen atoms were omitted. Amylose and water molecules are in blue and in pink respectively.

The parameters of hydrogen bonds (H-bonds) in the final structure of $V_{1\text{-butanol}}$ are listed in **Table III.5** and illustrated in **Figure III.12**. All the H-bonds correspond to strong and moderate interactions with the $\text{O}\cdots\text{O}$ distances ranging from 2.2 to 3.3 Å (Jeffrey, 1997). There are several intramolecular H-bonds, especially those between the O6 with the O1, O5 and O6 of the adjacent glucosyl residue. In addition, some H-bonds occur between glucosyl residues of contiguous helical turns such as $\text{O31}\cdots\text{O61}[x,y,1+z]$, $\text{O63}\cdots\text{O23}[x,y,1+z]$, $\text{O64}\cdots\text{O34}[x,y,1+z]$. However, there is no evidence for H-bonds between O2 and O3 of each pair of contiguous glucosyl residues which were reported in previous studies for the $V_{6\text{I}}$ structure (Brisson et al., 1991; Rappenecker & Zugenmaier, 1981). Besides, several intermolecular H-bonds between neighboring helices were also found for $V_{6\text{II}}$ while they are absent in $V_{6\text{I}}$ (**Table III.5**) (Brisson et al., 1991). In addition, water and 1-butanol molecules in the interstitial space form an H-bonding network between themselves and with the adjacent single helices. These H-bonds together with the interhelical ones would ensure the stability of the orthorhombic packing in $V_{6\text{II}}$ structure. The removal of water would break down the H-bonding network leading to the disruption of the crystal structure and a conversion to hexagonal $V_{6\text{a}}$.

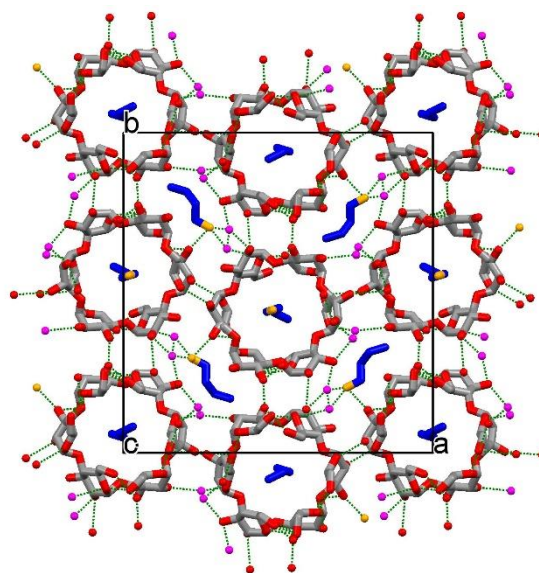


Figure III.12. Hydrogen bonds in the final structure of $V_{1\text{-butanol}}$ projected on the (a, b) plane of the unit cell.

Table III.5. Hydrogen bonding in the final structure of *V*₁-butanol.

Bond		Length (Å)	Symmetry operation of atom 1	Symmetry operation of atom 2
Atom1	Atom2			
Intrahelical hydrogen bonds				
O61	O12	3.3	x,y,z	x,y,z
O61	O52	2.7	x,y,z	x,y,z
O61	O62	2.8	x,y,z	x,y,z
O63	O14	3.0	x,y,z	x,y,z
O63	O54	2.3	x,y,z	x,y,z
O64	O15	3.0	x,y,z	x,y,z
O64	O55	2.3	x,y,z	x,y,z
O64	O65	2.3	x,y,z	x,y,z
O66	O11	2.9	x,y,z	x,y,1+z
O11	O36	2.9	x,y,z	x,y,-1+z
O51	O66	2.4	x,y,z	x,y,-1+z
O31	O62	2.6	x,y,z	x,y,-1+z
O63	O23	3.3	x,y,z	x,y,1+z
O64	O34	3.3	x,y,z	x,y,1+z
O11	O51	2.2	x,y,1+z	x,y,1+z
O11	O21	3.0	x,y,1+z	x,y,1+z
Interhelical hydrogen bonds				
O56	O26	3.0	x,y,z	-1/2-x,-y,1/2+z
O63	O33	3.3	x,y,z	1/2-x,-y,1/2+z
O34	O31	3.3	x,y,z	-x,-1/2+y,-1/2-z
O25	O22	3.3	x,y,z	-x,-1/2+y,-1/2-z
Hydrogen bonds with 1-butanol and water				
O36	O_Bu2	3.2	x,y,z	-1/2+x,1/2-y,-z
O32	OW1	2.8	x,y,z	x,y,z
O25	OW1	3.2	x,y,z	-x,-1/2+y,-1/2-z
O55	OW2	3.1	x,y,z	-x,-1/2+y,1/2-z
O32	OW3	3.0	x,y,z	x,y,-1+z
O23	OW3	2.5	x,y,z	x,y,-1+z
O53	OW4	2.3	x,y,z	x,y,-1+z
O24	OW4	3.1	x,y,z	1/2-x,-y,-1.5+z
O_Bu2	OW1	2.3	x,y,z	x,y,z
O_Bu2	OW2	2.3	x,y,z	x,y,z
OW1	OW2	2.3	x,y,z	x,y,z
OW3	OW4	2.5	x,y,z	x,y,-1+z

Table III.4. Selected geometrical parameters of the six glucosyl residues of the 6-fold helix in the final structure. The glucosidic torsion angles Φ and Ψ are defined by (O5-C1-O1-C4) and (C1-O1-C4-C5) respectively. The bond angle τ is defined by (C1-O1-C4). The torsion angle describing the hydroxymethyl conformation ω is defined by (O5-C5-O6-C6) which is -60 , 60 and 180° for *gg*, *gt* and *tg* respectively (**Annex 1, Figure S.III.1**).

Residue number	Φ ($^\circ$)	Ψ ($^\circ$)	τ ($^\circ$)	ω ($^\circ$)	O1-O4 (nm)
1	93(1)	-129(0)	117(4)	-154(1)	0.43
2	91(2)	-113(9)	118(6)	40(8)	0.44
3	96(3)	-114(3)	119(3)	-142(0)	0.44
4	100(1)	-143(8)	117(0)	-179(8)	0.44
5	76(0)	-112(8)	117(3)	26(2)	0.43
6	103(3)	-103(2)	117(2)	-93(4)	0.44

III.3. Conclusions

The present structure determination yielded a satisfactory model for $V_{1\text{-butanol}}$ regarding the diffraction data in combination with ^{13}C CP/MAS NMR, density value and packing energy analysis. Since the refinement is based on base-plane ED, the atomic positions along *c*-axis are less certain than those in the (*a*,*b*) plane. In order to ascertain the 3D information on the structure, ED patterns must be recorded on crystals rotated about selected axes of the reciprocal space, *e.g.* a^* and b^* to observed the *hkl* ($l \neq 0$) reflections. Our final model confirms the hypothesis made by Helbert and Chanzy (1994).

$V_{6\text{II}}$ crystals could be obtained with other complexing agents (see **Chapters IV** and **V**) but some variation in the diffracted intensities was observed. Different guest molecules may result in some variation in atomic positions of amylose chains but the helical conformation and the helix position are expected to remain closely similar. The procedure described in this chapter can be applied to determine the structure of these isomorphous crystals, which can help to know the correlation between the nature of guest and the variation in diffraction data.

Chapter IV

Morphology and crystal structure of different forms of V-amylose

IV.1. Introduction

The polymorphism of V-amylose has been the subject of many studies (Bear, 1944; Biais, 2006; Bluhm & Zugenmaier, 1981; Brisson et al., 1991; Buléon et al., 1990; Helbert, 1994; Mikus et al., 1946; Oguchi et al., 1998; Rappenecker & Zugenmaier, 1981; Rutschmann & Solms, 1990; Sarko & Biloski, 1980; Simpson et al., 1972; Takeo et al., 1973; Takeo & Kuge, 1969, 1971; Uchino et al., 2002; Winter & Sarko, 1974; Yamashita & Hirai, 1966; Yamashita & Monobe, 1971; Zaslów, 1963; Zobel et al., 1967). As reviewed in Chapter I, only five allomorphic families containing compact 6-, 7- and 8-fold single helices have been identified: V6_I (V_h), V6_{II} (V_{n-butanol}), V6_{III} (V_{glycerol}), V7 (V_{2-propanol}) and V8 (V_{1-naphthol}). On the other hand, previous modeling works suggested that V-amylose can exist in other forms. For instance, it was proposed that a structure with as many as 10 residues per turn could form if appropriate larger guests were used (French, 1979; French et al., 1978). So far, knowing the nature of a complexing agent is not enough to predict the structure of the resulting complex, although there are some indications of the dependence of the helical conformation on the size of the guest molecule. However, the crystallization of amylose into new structures likely requires testing new complexing agents and explore specific crystallization conditions. Some evidence showed that the structure of complexes may vary with the concentration of complexing agent and DMSO (Helbert, 1994; Takeo et al., 1973), but in previous investigations, the different complexes were usually prepared in similar conditions.

This chapter describes the preparation of different families of lamellar V-amylose crystals and the collection of their crystallographic data in order to propose a conformation and packing arrangement of amylose helices in each allomorph. We have tested the crystallization of amylose in the presence of 121 organic molecules (see **Chapter II, Table II.2**) in different crystallization conditions. Their morphology was characterized using TEM and, for a few of them, AFM. The unit cell parameters and symmetry were determined in hydrated/solvated and dry states from ED and XRD data. The complexes were also studied by FT-IR and the amylose conformation was determined by ¹³C solid-state NMR. Finally, tentative molecular models built with symmetrical rigid amylose helices were proposed based on the collected crystallographic data, showing probable arrangements of helices in the unit cells. The conditions of formation of the complexes and the crystallization parameters affecting the complex structure will be discussed in **Chapter V**.

IV.2. V_{6I} complexes

IV.2.1. Complexing agents

This allomorph was obtained with complexing agents that contain linear carbon chains with different functional groups such as carboxylic acids (-COOH), amides (-CONH₂), alcohols (-OH), amines (-NH₂) or aldehydes (-CHO). No tested alkanes and esters yielded V_{6I} despite containing linear carbon chains. This suggested that the functional groups play a role in the formation of the complexes. Quinoline, (-)-borneol and *trans*-decalin did not yield V_{6I} crystals although they were previously reported to induce this allomorph (Helbert, 1994). In addition, no branched or cyclic molecules produced V_{6I}. This result was expected as the size of these molecules is not compatible with the cavity of the 6-fold helices or the inter-helical spaces in V_{6I}.

IV.2.2. Morphology and crystal structure

Figure IV.1 shows TEM micrographs of typical V_{6I} crystals with a well-defined hexagonal shape (Figure IV.1a-c). They were monolamellar or, more frequently, multilamellar due to the spiral growth with a screw dislocation center. They usually resulted from a slow crystallization at relatively high temperatures or successive recrystallizations. In other cases, the crystals exhibited an overall round or less defined hexagonal shape. Sometimes elongated or undefined shapes were also observed (Figure IV.1d-f). The lamellar thickness determined by

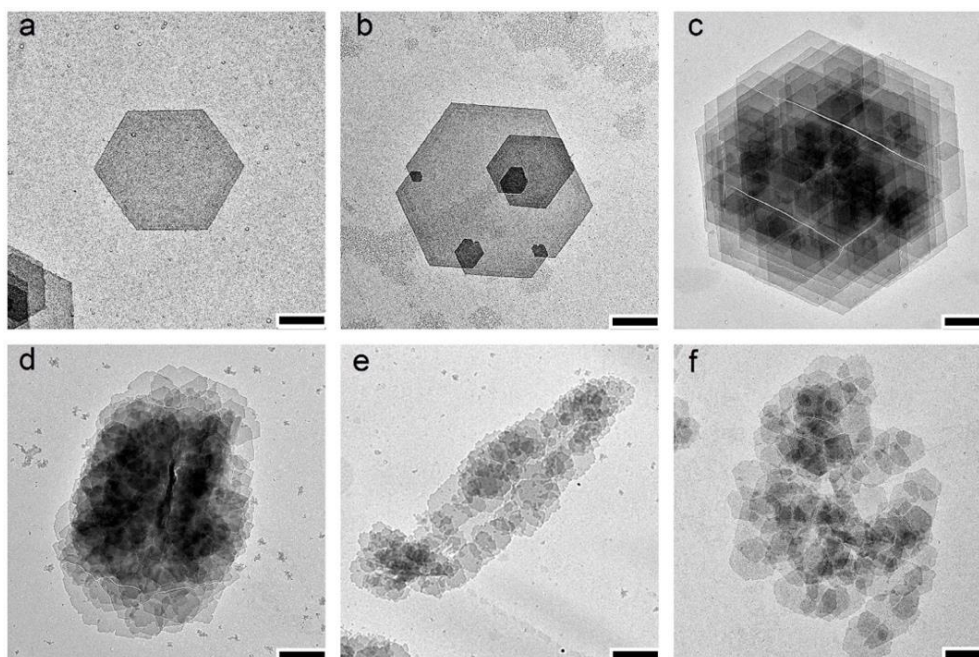


Figure IV.1. TEM images of V_{6I} crystals of native amylose complexed with tetradecanoic acid (a-c), octadecanoic acid (d,e) and octanoic acid (f). Scale bars: 1 μm .

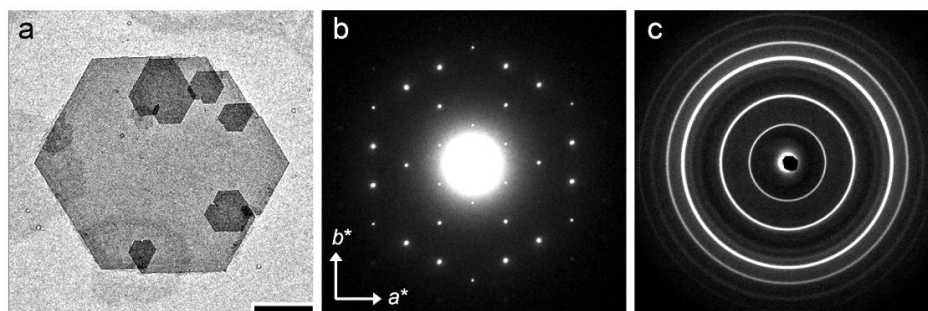


Figure IV.2. a) TEM image of a V_{6I} crystal of native amylose complexed with tetradecanoic acid (scale bar: 1 μm); b) corresponding base-plane ED pattern correctly oriented with respect to the crystal in (a); c) corresponding powder XRD diagram recorded from hydrated crystals.

AFM and averaged from 4 different samples is 9.5 ± 0.4 nm (**Annex 2, Table S.IV.4** and **Figure S.IV.1a**). The ED (**Figure IV.2b**) and XRD (**Figure IV.2c**) patterns were indexed on the basis of a hexagonal unit cell with $a = b = 1.37 \pm 0.01$ nm and $c = 0.81 \pm 0.01$ nm, or an orthorhombic unit cell with $a = 1.37 \pm 0.01$ nm, $b = a\sqrt{3} = 2.37 \pm 0.01$ nm and $c = 0.81 \pm 0.01$ nm, in agreement with previous works ([Brisson et al., 1991](#); [Helbert, 1994](#); [Mikus et al., 1946](#); [Takeo et al., 1973](#)). The Miller indices of the XRD reflections are given for V_{tetradecanoic acid} in **Annex 2, Table S.IV.1**.

IV.2.3. Effect of drying and rewetting on the crystal structure

Figure IV.3 shows the XRD profiles of V_{6I} crystals in their initial hydrated state (a), after drying (b) and after rehydration (c). After thorough drying, the peaks became broader and located at higher diffraction angles compared to those of the hydrated crystals, indicating a slight loss of crystallinity and a decrease in unit cell parameters. This result is in agreement with the previous studies that, upon drying, V_{6I} transforms into V_{6a} (V_a), which exhibits a smaller unit cell ([Mikus et al., 1946](#); [Shogren et al., 2006](#); [Takeo et al., 1973](#); [Takeo & Kuge, 1969](#)). Indeed, the diffraction profile of the dry complex shown in **Figure IV.3b** is typical for V_{6a} and was indexed on the basis of a hexagonal unit cell with $a = b = 1.32$ nm and $c = 0.81 \pm 0.01$ nm, or an orthorhombic unit cell with $a = 1.32$ nm, $b = a\sqrt{3} = 2.29$ nm and $c = 0.81 \pm 0.01$ nm. The slight difference in unit cell parameters between V_{6I} and V_{6a} would result from the loss of water molecules from V_{6I} which reduces the inter-helix space but does not alter the helical conformation ([Booy et al., 1979](#)). Besides, the transition from V_{6I} to V_{6a} would not depend on the release of the complexing agent since some guests such as long-chain fatty acids and alcohols would not be removed from the complexes by drying. After rewetting with water, the complexes yielded an XRD profile identical to the initial hydrated complexes (**Figure IV.3c**), supporting the fact that water is the key factor that controls the structural transition.

Figure I.4 shows the model proposed for V6_I (Rappenecker & Zugenmaier, 1981) and corresponding V6_a (Murphy et al., 1975) projected on the (*a*,*b*) plane of the orthorhombic unit cells. V6_a is more compact than V6_I. In both structures (space group $P2_12_12_1$), each unit cell contains two anti-parallel 6-fold left-handed helices packed onto a hexagonal lattice with guest molecules located inside the helix cavity. If the hexagonal symmetry is used, the crystal would have a statistical arrangement of 'up-and-down' amylose helices (Brisson et al., 1991).

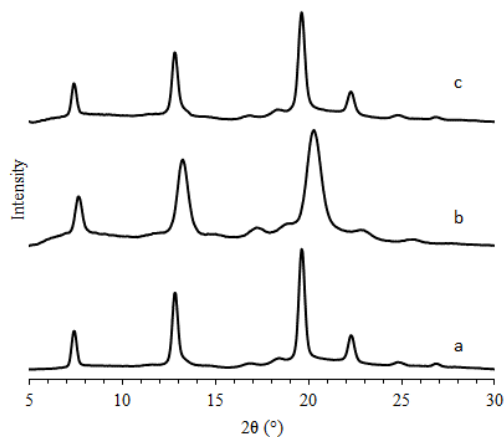


Figure IV.3. XRD profiles of a) hydrated V6_I crystals prepared with octadecanoic acid, b) crystals as in (a) after thorough drying in vacuum, c) crystals as in (b) after rewetting.

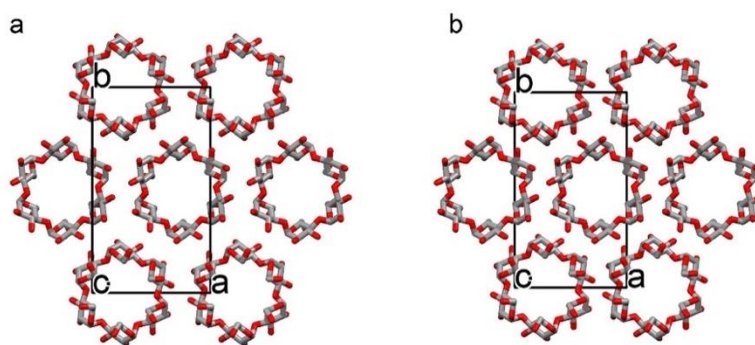


Figure IV.4. Packing of amylose helices in V6_I (a) (Rappenecker & Zugenmaier, 1981) and corresponding V6_a (b) (Murphy et al., 1975), projected on the (*a*,*b*) plane of the orthorhombic unit cells. Hydrogen atoms were removed for clarity.

IV.3. V6_{II} complexes

IV.3.1. Complexing agents

Similar to those of V6_I, V6_{II} complexes were obtained with linear compounds like fatty acids, alcohols, amines, aldehydes and stearamide. Indeed, most of these compounds yielded both V6_I and V6_{II}. This result is unexpected as only a few complexing agents with such ability have been reported, including *n*-propanol, *n*-butanol and *n*-pentanol (Helbert, 1994), adipic,

suberic and sebacic acids (Takeo et al., 1973), and hexanoic acid (Biais, 2006; Takeo et al., 1973). In addition, the long-chain fatty acids and alcohols (8-18 carbons) which were previously reported to yield only V6_I (Helbert, 1994; Takeo et al., 1973), were shown to induce V6_{II} in this study. V6_{II} was also obtained with some esters, which did not induce V6_I. Interestingly, isopropyl myristate yielded V6_{II} although the molecule contains a branched-chain moiety (isopropyl). V6_{II} was maybe formed because the molecule contains a long straight-chain aliphatic part (myristyl) that predominantly interacts with the helical cavity and controls the helicity. The remaining part with a larger size would be located outside the helix. In fact, other branched molecules including isopentyl acetate and cyclic compounds did not yield the V6 complex. This result agrees with previous conclusions that the 6-fold helix complexes are obtained with linear complexing agents whose diameter in cross-section is about 0.3 nm (Takeo & Kuge, 1969).

IV.3.2. Morphology and crystal structure

Figure IV.5 shows TEM images of typical rectangular V6_{II} lamellar crystals. The lamellar thickness determined by AFM and averaged from 4 different samples is 9.4 ± 1.2 nm (Annex 2, Table S.IV.4 and Figure S.IV.1b). Individual lamellae were rarely seen. Indeed, the crystal were usually built as compact stacks of lamellae that may result from an epitaxial growth. The rectangular platelets were isolated (Figure IV.5a,b) or occurred as twinned structures at an angle of about 60 or 90° (Figure IV.5c-f). This morphology is similar to that previously described for V6_{II} complexes of *n*-butanol and *n*-pentanol (Booy et al., 1979; Helbert, 1994; Manley, 1964; Yamashita et al., 1973; Yamashita, 1965). Besides, cracks were observed along the longer dimension of the lamellae. These cracks are associated with the stress due to the shrinkage which occurs when the crystals are dehydrated in vacuum (Helbert, 1994; Manley, 1964). The cracks were observed by TEM on dry crystals prepared in pure water with most complexing agents yielding the V6_{II} structure. However, if the crystals were prepared in the presence of 1-2% of DMSO as a co-solvent, they became more stable and the cracks were observed after several hours of exposure in vacuum.

In contrast, the V6_{II} crystals prepared with diols (Figure IV.5b-c) and diethyl malonate were as stable as those obtained with other complexing agents prepared in the presence of DMSO. This suggests that the complexing agents and co-solvent DMSO play an important role to stabilize the crystal structure. The drying behavior of V6_{II} crystals will be further discussed in the next section.

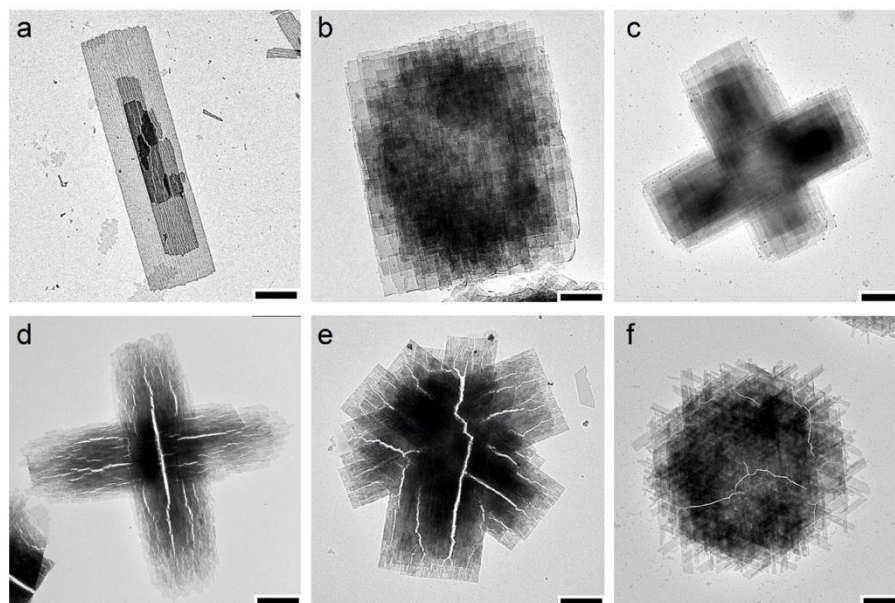


Figure IV.5. TEM images of V_{6II} crystals obtained with dodecanoic acid (a), 1,6-hexanediol (b), 1,3-butanediol (c), pentanoic acid (d), 2-propanol (e), and octadecanoic acid (f). Bars: 1 μm.

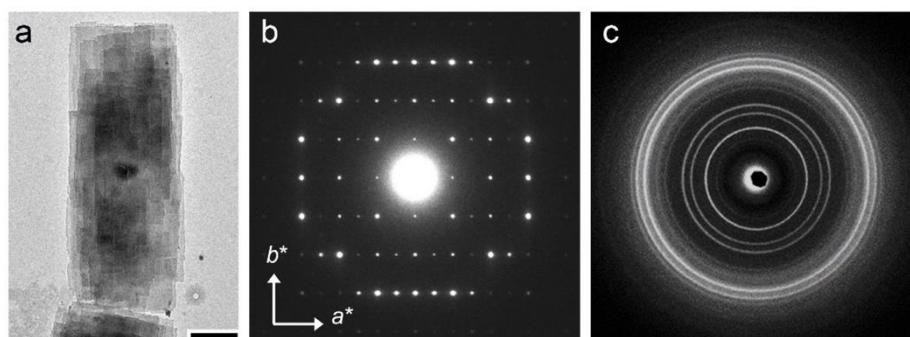


Figure IV.6. a) TEM image of V_{6II} crystals obtained with 1,3-butanediol (scale bar: 1 μm); b) corresponding base-plane ED pattern correctly oriented with respect to the crystal in (a); c) corresponding powder XRD diagram recorded from hydrated crystals.

When probed by ED under frozen-hydrated conditions, these crystals yield almost identical diffraction patterns such as those of V_{1,3-butanediol} shown in **Figure IV.6b**. The diffraction pattern is also identical to that previously reported for V_{6II} prepared with *n*-butanol and *n*-pentanol (Booy et al., 1979; Helbert & Chanzy, 1994), and thus can be described with an orthorhombic unit cell (space group $P2_12_12_1$). However, for consistency with the other V-amylose allomorphs described in this work, and following the convention proposed by Donnay (1943), *i.e.* $a < b$, we have switched the a and b values with respect to those given in the previous studies. Consequently, the average unit cell parameters are $a = 2.65 \pm 0.04$ nm and $b = 2.69 \pm 0.03$ nm, in good agreement with those calculated from the XRD pattern shown in

Figure IV.6c ($a = 2.646 \pm 0.009$ nm, $b = 2.705 \pm 0.013$ nm, and $c = 0.807 \pm 0.009$ nm). The Miller indices of the XRD reflections for V_{1,3}-butanediol are given in **Annex 2, Table S.IV.1**.

In **Chapter III**, we have described the molecular structure of V₁-butanol crystals based on analyses of the conformational and packing energy, combined with classical polymer structure refinement against ED data. The antiparallel helices are organized in rows parallel to the b axis, with 1-butanol molecules located inside and between helices (**Figure III.8**).

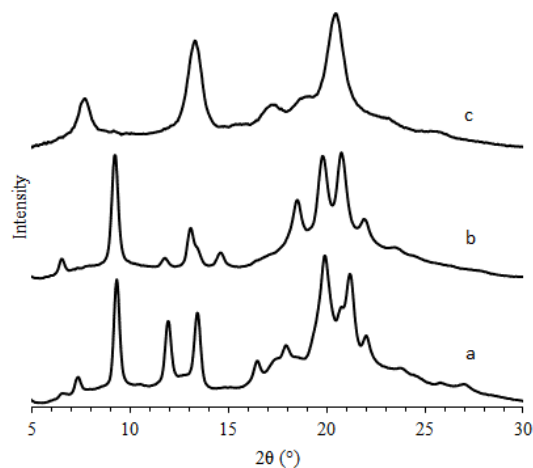


Figure IV.7. XRD profiles of a) hydrated V_{6II} crystals prepared with 1,4-butanediol, b) crystals as in (a) after partial drying in vacuum, c) crystals as in (b) after thorough drying.

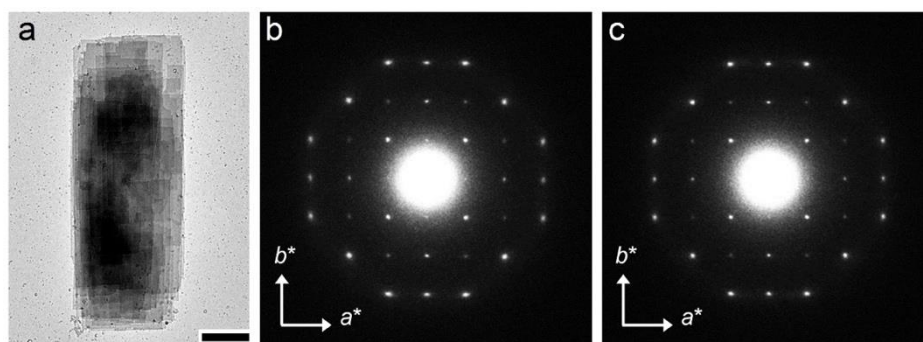


Figure IV.8. a) TEM image of a V_{6II} crystal prepared with 1,3-butanediol, partially dried in vacuum (scale bar: 1 μ m); b) corresponding base-plane ED pattern correctly oriented with respect to the crystal in (a); c) base-plane ED pattern recorded from a V_{6II} crystal obtained with 1,4-butanediol after partial drying in vacuum.

IV.3.3. Effect of drying on the crystal structure

As noted above, there are two different drying behaviors observed for V_{6II} complexes: i) crystals show the cracks just after being exposed to vacuum, and ii) crystals are more stable and the cracks are observed after keeping the crystals for long time in vacuum. In both cases, the cracks occur along the longer dimension of the lamellae and the crystals yield diffraction

patterns almost identical to that of V6_a obtained by drying the V6_I crystals (**Figure IV.7c**). Following the drying process of the more stable crystals, it is noted that the crystals rapidly yielded XRD (**Figure IV.7b**) and ED diagrams (**Figure IV.8**) exhibiting a tetragonal symmetry. These patterns were almost identical to those reported for V6_{III} prepared with glycerol, DMSO or ethylenediamine (Hulleman et al., 1996; Simpson, 1970; Winter & Sarko, 1974) (see § IV.3). This structure was rather stable and slowly transformed into V6_a (**Figure IV.7c**).

Figure IV.9 shows the schematic representation of the rectangular crystal in different states and the corresponding amylose packing arrangement. In the initial V6_{II}, amylose helices are organized in rows parallel to the *b*-axis of the unit cell or to the longer-dimension of the rectangular crystal. Upon partial drying, amylose helices are aligned along both *a*- and *b*-axes, leading to a small enlargement of *a*-parameter from 2.65 nm to 2.72 nm, while the *b*-parameter remained unchanged (2.72 nm). The small change in *a*-parameter does not cause any cracks on the crystal. Upon thorough drying, amylose helices are reorganized into a close-packed hexagonal arrangement, forming V6_a. There is a slight decrease of *b* (0.08 nm) while *a* significantly decreases (0.43 nm), which is consistent with the formation of cracks along the *b*-axis. In addition, the present models show that V6_a and the isomorphous V6_{III} obtained by drying V6_{II} would have orthorhombic unit cells with space group $P2_12_12_1$, containing four amylose chains per unit cell. These unit cells are larger than those proposed for the V6_a prepared by drying V6_I and the V6_{III} of glycerol, DMSO or ethylenediamine, which contain only two helices.

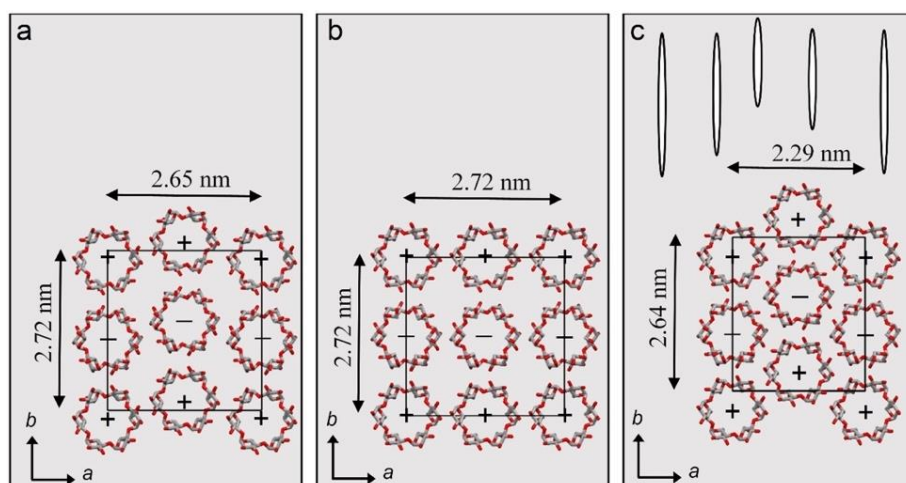


Figure IV.9. Schematic representation of a rectangular V6_{II} crystal and corresponding amylose helices packing (*insert*) during the drying process. a) Initial uncracked crystal having an orthorhombic V6_{II} structure (Helbert & Chanzy, 1994). b) Partial dry uncracked crystal having a pseudo-tetragonal V6_{III} structure (Hulleman et al., 1996; Winter & Sarko, 1974). c) Thoroughly dried crystal, exhibiting cracks running parallel to the long dimension of the crystals, having a pseudo-hexagonal structure V6_a.

The above results reveal that the pseudo-tetragonal V6_{III} is much more stable compared to the orthorhombic V6_{II} and thus the transition into V6_a takes a longer time. Interestingly, V6_{III} exhibits a larger inter-helix space but requires a lower water content to stabilize the structure. Previous studies on the transition of V6_{II} into V6_a during drying did not report the presence of V6_{III} as an intermediate structure (Booy et al., 1979; Hinkle & Zobel, 1968). In fact, our results show that the transition from V6_{II} to V6_{III} only occurs for complexes with specific guests such as diols and diethyl malonate or complexes prepared in the presence of 1-2% of DMSO as a co-solvent. The role of complexing agents and DMSO as well as the driving forces that allow for the formation of V6_{III} are still unclear.

According to Helbert and Chanzy (1994), the transition from V6_{II} to V6_a observed for complexes with *n*-butanol or *n*-pentanol would be promoted by the removal of the volatile complexing agents located in the inter-helix spaces from the crystals. However, such release may not be observed for non-volatile complexing agents such as long-chain mono- or dicarboxylic acids. This suggests that the departure of water would be the major cause of the structural transition rather than that of the complexing agent. Indeed, after rewetting in water, the crystals recovered the V6_{II} structure, as shown in **Figure IV.10**.

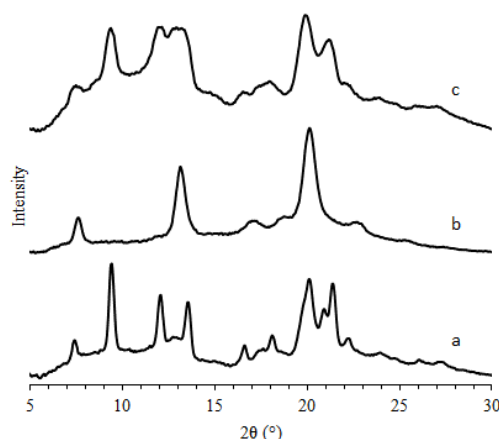


Figure IV.10. XRD profiles of a) hydrated V6_{II} crystals obtained with pentanoic acid, b) crystals as in (a) after thorough drying in vacuum, c) crystals as in (b) after rewetting.

IV.4. V6_{III} complexes with glycerol

IV.4.1. Formation of complexes

In the present study, V6_{III} lamellar crystals were directly obtained only with glycerol. Analogous molecules such as 1,3-propanediol, 1,2-propanediol, 2-propanol did not yield V6_{III} in the similar crystallization conditions. So far, V6_{III} have been obtained with three complexing agents: DMSO (French & Zobel, 1967; Winter & Sarko, 1972) and ethylenediamine (Simpson,

1970) in the form of crystalline films, and glycerol in the form of lamellar crystals. A common preparation condition of V6_{III} with these complexing agents is that water is nearly absent. For example, Hulleman et al. (1996) prepared V6_{III} lamellar crystals in glycerol at 100 °C in the presence of less than 0.2 wt% water. In the present study, V6_{III} could be prepared with glycerol in the presence of up to 10 wt% water but at a lower temperature (40 °C). With a higher concentration of water, V6_I was formed instead. In addition, V6_{III} crystals were also prepared by dissolving amylose in DMSO at 100 °C, and addition of 9 or 999 volumes of glycerol at 90-100 °C. This method is simple and does not require a removal of water.

IV.4.2. Morphology and crystal structure

Figure IV.11a shows a typical V6_{III} crystal prepared with glycerol. This crystal has a more or less square contour, consisting of a stack of square-shaped layers that may have grown by a dislocation-induced spiral growth. This morphology is similar to that previously reported for V_{glycerol} (Hulleman et al., 1996).

The V_{glycerol} crystals had a good stability in vacuum, *i.e.*, they did not exhibit any cracks or important decomplexation phenomenon. The corresponding base-plane ED pattern recorded at room temperature is shown in **Figure IV.11b**. This diagram can be indexed for a two-dimensional pseudo-tetragonal orthorhombic unit cell of space group $P2_12_12_1$ with $a = b = 1.92 \pm 0.01$ nm, in good agreement with data calculated from the powder XRD pattern shown in **Figure IV.1c** ($a = b = 1.91 \pm 0.01$ nm) (**Figure IV.1c, Annex 2, Table S.IV.1**). The unit cell parameters found in the present study are different from those determined by Hulleman et al. (1996) who reported that $a \neq b$ ($a = 1.93$ nm, $b = 1.8$ nm). Our results also confirm that V_{glycerol} is isomorphous to V_{DMSO} (French & Zobel, 1967; Winter & Sarko, 1974) and V_{ethylenediamine} (Simpson, 1970). V_{DMSO} has similar unit cell parameters ($a = b = 1.92$ nm) (Winter & Sarko, 1972) while those of V_{ethylenediamine} are slightly smaller ($a = b = 1.89$ nm) (Simpson, 1970). In the present study, both base-plane ED and XRD data did not allow identifying the *c*-parameter of the unit cell. Hulleman et al. (1996) reported $c = 0.83$ nm for V_{glycerol} (corresponding to one helical pitch), which is about three times lower than that of V_{DMSO} ($c = 2.24$ nm, corresponding to 3 helical pitches) (Winter & Sarko, 1972).

The detailed molecular structure of V_{glycerol} is still unknown. However, the packing of amylose helices in V_{glycerol} should be similar to that of V_{DMSO} described by Winter and Sarko (1974). Within the unit cell, there are two antiparallel left-handed 6-fold helices close-packed on a tetragonal lattice, as shown **Figure IV.12**. The complexing agent can be located both inside and between the helices.

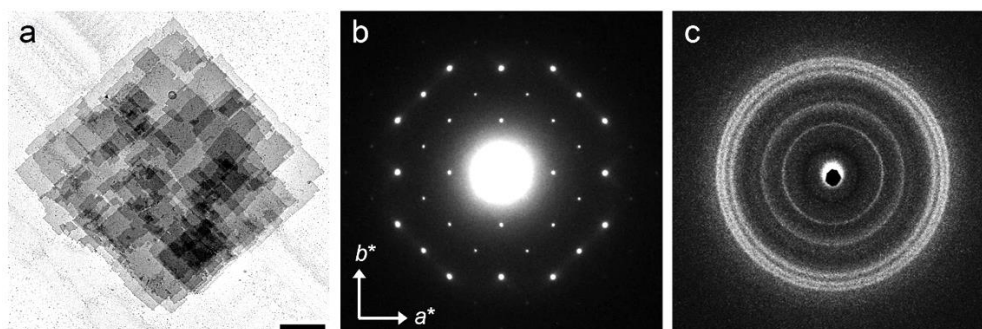


Figure IV.11. a) TEM images of a V_{6III} crystal prepared with glycerol (scale bar: 1 μm); b) corresponding base-plane ED pattern correctly oriented with respect to the crystal in (a); c) corresponding powder XRD diagram recorded from hydrated crystals.

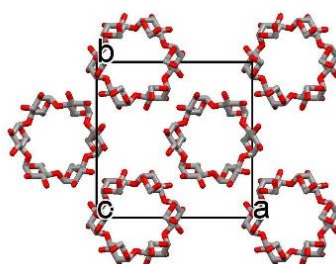


Figure IV.12. Packing of amylose helices in V_{6III} structure, projected on the (a,b) plane of the pseudo-tetragonal orthorhombic unit cell. Hydrogen atoms were removed for clarity.

IV.5. V7 complexes

IV.5.1. Complexing agents

V7 complexes were obtained with a variety of complexing agents with a cross-sectional diameter of in the range of 0.36-0.70 nm: linear saturated and unsaturated fatty acids having 3 to 20 carbons, linear ketones (2-pentanone), linear alcohols with the hydroxyl group located at endo-positions such as 2-propanol and 1,3-butanediol, and many branched and cyclic compounds. In general, this result is in agreement with the previous investigations (Helbert, 1994; Nuessli et al., 2003a; Takeo et al., 1973; Takeo & Kuge, 1969, 1971; Yamashita & Hirai, 1966). However, V7 lamellar crystals were also successfully prepared with some of molecules which were previously reported as unable to form a complex with amylose, such as citral, 2-naphthol and quinoxaline (Kuge & Takeo, 1968). In addition, V7 was also obtained with fatty acids having 6-20 carbons and quinoline which have been reported to form 6- and 8-fold complexes, respectively (Helbert, 1994; Takeo et al., 1973).

IV.5.2. Morphology and crystal structure

V7 lamellar crystals prepared with different complexing agents had an almost identical morphology (Figure IV.13). Typical crystals were long rectangular lamellae, usually grown

from the same nucleation site and forming flower-like aggregates. Individual lamellae were rarely seen. However, the crystals were more individual after successive recrystallizations. Stacks twinned at about 90° were sometimes observed. The lamellar thickness determined by AFM and averaged from 2 different samples is 7.9 ± 0.9 nm (Annex 2, Table S.IV.4 and Figure S.IV.1c).

The corresponding ED pattern recorded from individual V7 crystals prepared with different complexing agents were similar, such as that of $V_{\text{pentanoic acid}}$ shown in Figure IV.14b. They all resemble those previously reported for complexes prepared with 2-propanol and acetone (Buléon et al., 1990), fenchone, menthone and geraniol (Nuessli et al., 2003a), thymol, linalool and terpineol (Putaux et al., 2008). They can be accounted for a two-dimensional orthorhombic unit cell, with average parameters $a = 2.81 \pm 0.03$ nm and $b = 2.95 \pm 0.05$ nm. The powder XRD patterns of different complexes are similar as well (Figure IV.14c) and can be indexed on the basis of an orthorhombic unit cell with $a = 2.813 \pm 0.013$ nm, $b = 2.973 \pm 0.011$ nm and $c = 0.797 \pm 0.011$ nm (Annex 2, Table S.IV.2). In the model determined for $V_{2\text{-propanol}}$ (Nishiyama et al., 2010), each unit cell contains four left-handed 7-fold helices packed in the $P2_12_12_1$ symmetry with an alternation of up and down chains, as shown in Figure IV.15. This arrangement can be described by alternating motifs of 4 hexagonally-packed helices along with other 4 helices with a larger interhelical space. The complexing agent would be located both inside and between the helices, together with some water molecules.

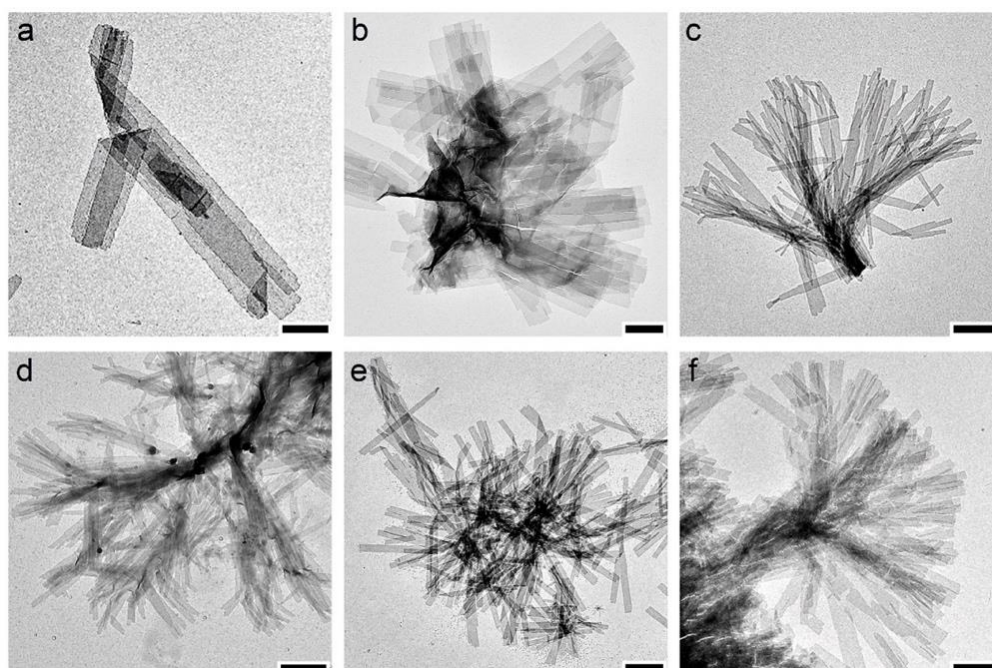


Figure IV.13. TEM images of V7 crystals prepared with 1,3-butanediol (a), pentanoic acid (b), β -citronellol (c), (*S*)-perillaldehyde (d), *cis*-decahydro-1-naphthol (e), 2-naphthol (f). Bars: 1 μm .

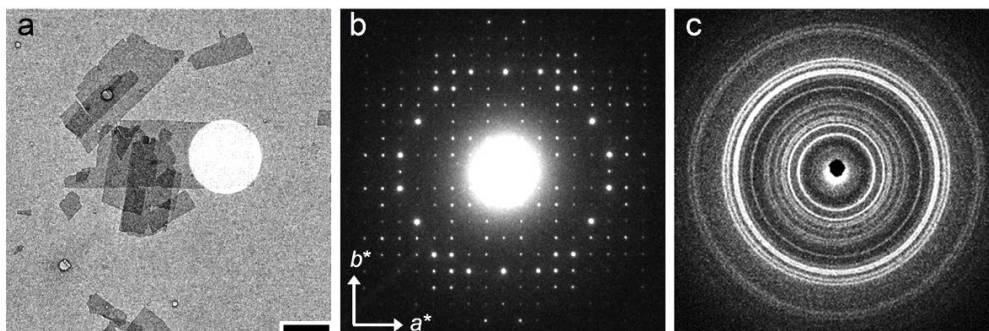


Figure IV.14. a) TEM image of V7 crystals prepared with pentanoic acid (scale bar: 1 μm); b) corresponding base-plane ED pattern correctly oriented with respect to the crystal in (a); c) corresponding powder XRD diagram recorded from hydrated crystals.

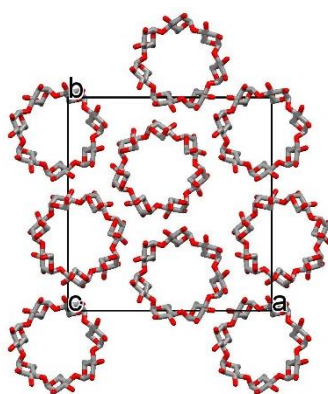


Figure IV.15. Packing of amylose helices in the V7 structure projected on the (a,b) plane of the orthorhombic unit cell. Hydrogen atoms were removed for clarity.

IV.5.3. Effect of drying on the crystal structure

All V7 complexes were sensitive to drying. The dry crystals yielded a XRD pattern different from that of the initial hydrated state, suggesting a structural transition. However, depending on the complexing agents, two drying behaviors were observed for the V7 complexes. Upon thorough drying, the complexes of all complexing agents, except 1,3-butanediol, exhibited similar XRD profiles, as shown for decahydro-2-naphthol in **Figure IV.16b**. These diagrams are nearly identical to those previously reported for the V7_a obtained by drying the V7 complexes with branched alcohols, ketones, fatty acids and ring compounds (Nuessli et al., 2003b; Takeo et al., 1973; Takeo & Kuge, 1969, 1971; Yamashita & Hirai, 1966; Zaslow, 1963). They can be indexed based on a hexagonal unit cell with $a = b = 1.480 \pm 0.014$ nm and $c = 0.794 \pm 0.008$ nm or a pseudo-hexagonal orthorhombic unit cell with $a = 1.480 \pm 0.014$ nm, $b = 2.563 \pm 0.024$ nm and $c = 0.794 \pm 0.008$ nm. However, since the 7-fold helix cannot be crystallographically located onto the 6-fold or 2-fold screw axes of $P2_12_12_1$, only the pseudo-hexagonal orthorhombic unit cell with the space group $P1$ can be considered. Alternatively, V7_a

can adopt the space group $P2_12_12_1$ by doubling the unit cell ($a = 2.563 \pm 0.024$ nm, $b = 2.960 \pm 0.028$ nm and $c = 0.794 \pm 0.008$ nm). In both cases, the 7-fold amylose helices would be organized in a hexagonal net, similar to that of the $V6_a$ structure, as shown in **Figure IV.17**.

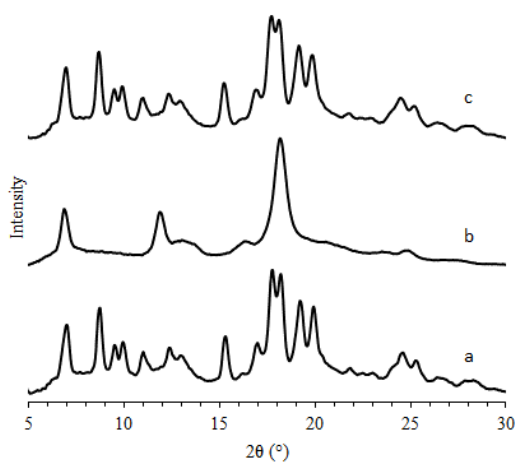


Figure IV.16. XRD profiles of a) hydrated V7 crystals prepared with decahydro-2-naphthol, b) crystals as in (a) after thorough drying in vacuum, c) crystals as in (b) after rewetting.

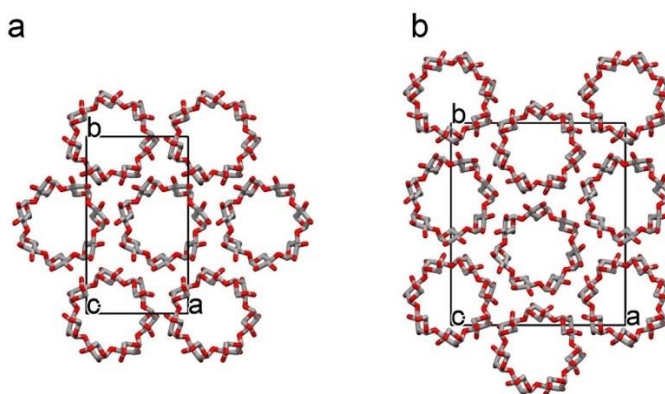


Figure IV.17. Possible packings of helices in the $V7_a$ structure projected on the (a,b) plane of an orthorhombic unit with space group $P1$ (a) or a larger orthorhombic unit cell with space group $P2_12_12_1$ (b).

On the other hand, the thoroughly dry V7 complex with 1,3-butanediol yielded a diffraction diagram different from that of other complexes, as shown in **Figure IV.18b**. This diffraction pattern contains characteristic reflections of both $V6_a$ and $V7_a$, indicating a partial transition of 7- to 6-fold helical conformation occurring during drying. The different drying behavior of V7 crystals with 1,3-butanediol would be due the ability of the complexing agent to adapt with both 6- and 7-fold helical conformation. Indeed, 1,3-butanediol was shown to induce the formation of both 6- and 7-fold helices.

The above structural transition behavior of V7 complexes would be the result of the departure of water rather than complexing agent. Indeed, the solid complexing agents such as *cis*-decahydro-1-naphthol or 2-naphthol are unlikely to be removed by drying. In addition, the V7 structure is completely recovered after rewetting with water (**Figure IV.16**), suggesting that the guest molecules remained inside the complexes. However, the above results raise the question of the location of complexing agents in the V7 crystals. If the complexing agent is located between the helices in V7 crystals and is not removed after drying, it is expected to disturb the hexagonal arrangement of amylose helices. The limited inter-helix space in V7_a would not allow the accommodation of the complexing agent.

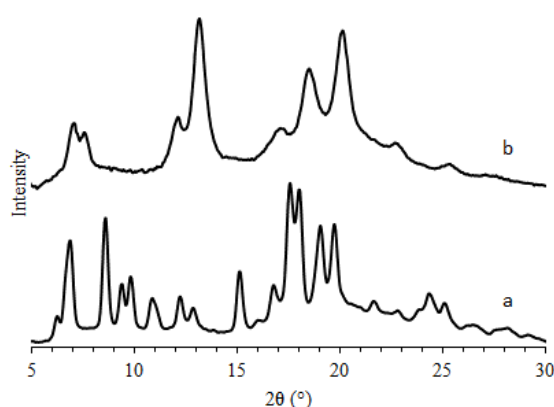


Figure IV.18. XRD profiles of a) hydrated V7 crystals prepared with 1,3-butanediol; b) crystals as in (a) after thorough drying in vacuum.

IV.6. V8 complexes

IV.6.1. Complexing agents and formation of complexes

V8 lamellar crystals were prepared by crystallization of amylose in the presence of 1-naphthol, quinoline and salicylic acid. To our knowledge, salicylic acid is the third complexing agent that yields this V-amylose allomorph. In addition, although Kuge and Takeo (1968) reported that salicylic acid did not form crystalline complexes from amylose solutions, we have successfully prepared V_{salicylic acid} lamellar crystals for the first time.

IV.6.2. Morphology and crystal structure

Figure IV.19a-c shows TEM images of single crystals of V8 complexes prepared with 1-naphthol, salicylic acid, and quinoline, respectively. The crystals have a square shape and consist of a stack of many thin lamellae. They are usually very thick, even when prepared in highly dilute condition (0.025 wt% amylose). For V_{quinoline}, mono- and multilamellar crystals were observed. This morphology is very similar to that observed for V6_{III} of glycerol.

Typical based-plane ED patterns recorded on lamellar single crystals of V8 complexes obtained with 1-naphthol, salicylic acid, and quinoline are presented in **Figure IV.19d-f**, respectively. They all resemble regarding the tetragonal symmetry and the positions of the corresponding reflections, and are similar to those previously reported for $V_{1\text{-naphthol}}$ and $V_{\text{quinoline}}$ (Cardoso et al., 2007; Helbert, 1994; Putaux et al., 2008; Yamashita & Monobe, 1971). These patterns are accounted for a tetragonal unit cell of space group $P4_32_12$ with average parameters $a = b = 2.30 \pm 0.01$ nm. The XRD patterns are similar as well, as shown in **Figure IV.19g-i**. The average unit cell parameters calculated from XRD data are $a = b = 2.313 \pm 0.006$ nm and $c = 0.790 \pm 0.001$ (Annex 2, Table S.IV.3), in good agreement with the ED data.

However, differences in relative intensities of the ED spots could be noted between the different complexes. Some reflections in the ED pattern of $V_{1\text{-naphthol}}$ and $V_{\text{salicylic acid}}$ are absent in the pattern of $V_{\text{quinoline}}$. This would be due to the double diffraction that occurs when the crystals are thick, as previously noted for $V_{1\text{-naphthol}}$ crystals (Putaux et al., 2011). A slight difference in reflection intensity was also observed in XRD patterns. Especially, the 1 1 0 reflection at d -spacing of 1.628 nm ($2\theta = 5.43^\circ$) is observed for $V_{\text{salicylic acid}}$ but is absent for the other complexes. These differences would be accounted for the contribution of the complexing agent.

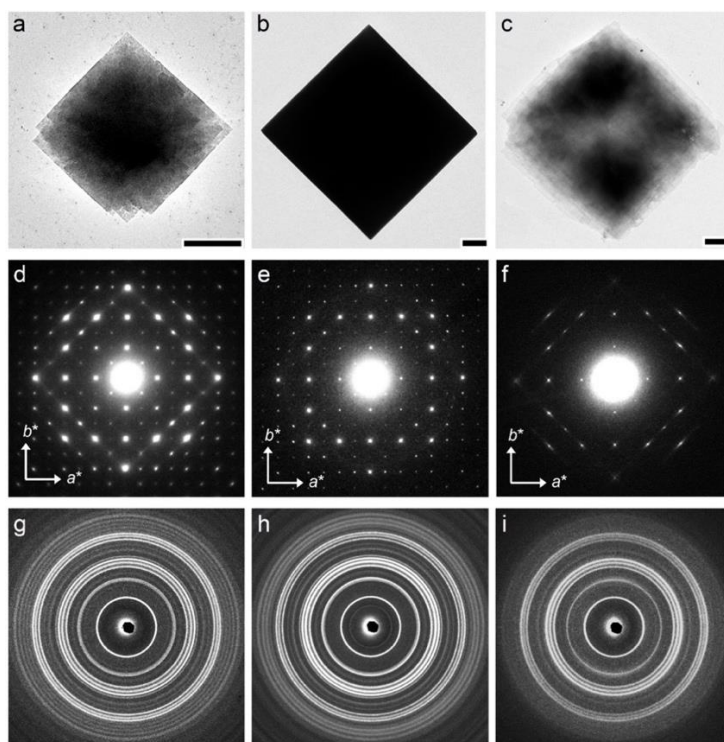


Figure IV.19. a-c) TEM images of V8 crystals prepared with 1-naphthol (a), salicylic acid (b) and quinoline (c) (scale bars: 1 μm). d-f) base-plane ED patterns of V8 crystals prepared with 1-naphthol (d), salicylic acid (e) and quinoline (f). g-i) powder XRD diagram recorded from hydrated V8 crystals prepared with 1-naphthol (g), salicylic acid (h) and quinoline (i).

Since their structures are isomorphous, the three complexes would have similar packings of amylose helices such as that proposed for $V_{1\text{-naphthol}}$ (Cardoso et al., 2007; Helbert, 1994; Yamashita & Monobe, 1971). The model in **Figure IV.20** shows that one unit cell contains two antiparallel left-handed 8-fold helix packed along space group $P4_32_12$. The complexing agents would be located both inside and between the helices. The complexing agent:glucosyl unit stoichiometry was determined by UV spectroscopy after extraction of complexing agent from the freeze-dried complexes using ethanol. The value was measured to be 1:6.2, 1:5.0, and 1:8.3 for $V_{1\text{-naphthol}}$, $V_{\text{salicylic acid}}$, and $V_{\text{quinoline}}$, respectively.

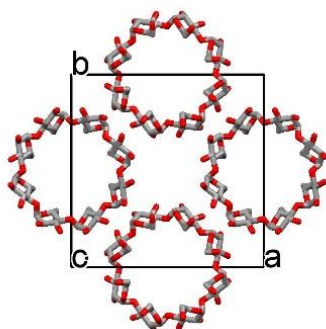


Figure IV.20. Packing of amylose helices in V8 structure projected on the (a,b) plane of the orthorhombic unit cell. Hydrogen atoms were removed for clarity.

IV.6.3. Effect of drying on the crystal structure

Figure IV.21 shows the effect of drying on the XRD pattern of the V8 complex with 1-naphthol. When the complex was freeze-dried, the diffraction peaks became broader, indicating a significant loss in crystallinity (**Figure IV.21b**). After rewetting with water, the complex yielded a diffraction pattern that was almost identical to that of the initial wet state (**Figure IV.21a,c**). The result implied that the complexing agent was not removed during drying and that water is essential for the crystallinity and stability of the complexes. Similar behaviors were observed for $V_{\text{salicylic acid}}$ and $V_{\text{quinoline}}$.

IV.7. A new V-amylose allomorph obtained with 4-hydroxybenzoic acid

The interaction between amylose and 4-hydroxybenzoic acid (HBA) has been the subject of several studies (Goudah & Guth, 1965; Zhu et al., 2008). However, no study have reported the existence of crystalline complexes. Besides, the investigation conducted by Kuge and Takeo (1968) showed that HBA was unable to form the complexes with amylose. In the present study, V_{HBA} was successfully prepared in the form of lamellar crystals. Moreover, it appears to be a new V-amylose allomorph, exhibiting unique morphological features, and distinct XRD and ED patterns.

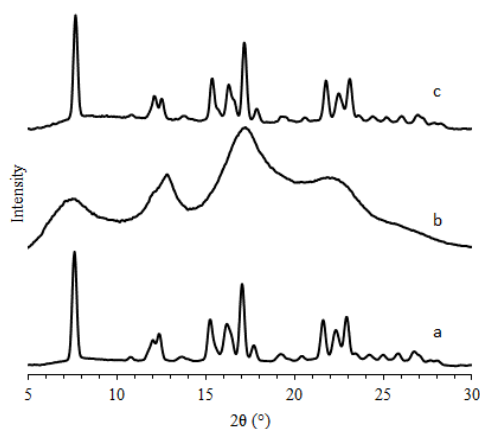


Figure IV.21. XRD profiles of a) hydrated V8 crystals prepared with 1-naphthol; b) crystals as in (a) after thorough drying in vacuum; c) crystals as in (b) after rewetting.

IV.7.1. Formation of complexes

The preparation of HBA complexes conducted in pure water and in DMSO/water mixture gave similar results. In the presence of 0.1-0.5 wt% of amylose and a saturation of HBA, the complexes crystallized out slowly at a relatively low temperature ≤ 50 °C. The crystals appeared after about one week of incubation and the crystallization finished after two weeks. In comparison to other complexes, nucleation and growth rates of V_{HBA} seem to be slower. Kuge and Takeo (1968) may not have waited for enough time to observe the formation of crystals.

IV.7.2. Morphology and crystal structure

Figure IV.22 shows lamellar V_{HBA} crystals prepared at 40 °C from a 0.2 wt% native amylose solution. The crystals are needle-shaped lamellae that radiate from a common nucleation site forming flower-like aggregates. Each lamella is about 0.1-0.3 μm wide and 10-20 μm long. This morphology is quite similar to that previously reported for some V7 crystals, but the V_{HBA} crystals do not have a well-defined rectangular shape.

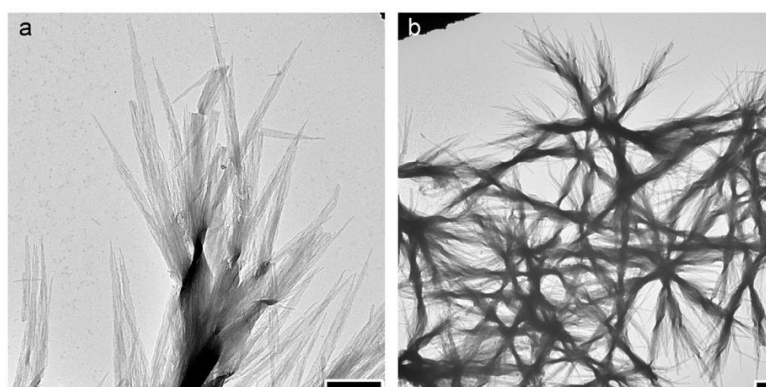


Figure IV.22. TEM images of a new form of V-amylose complexed with 4-hydroxybenzoic acid. Scale bars: 1 μm .

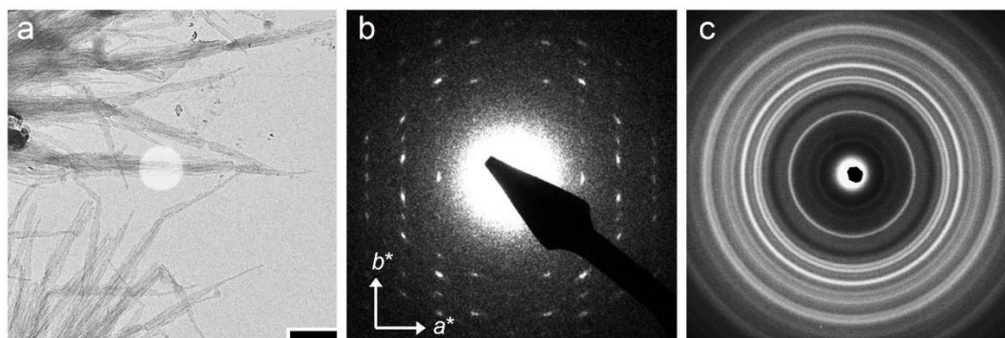


Figure IV.23. a) TEM image of V-amylose complexed with 4-hydroxybenzoic acid (scale bar: 1 μm); b) corresponding base-plane ED pattern correctly oriented with respect to the crystal in (a); c) corresponding powder XRD diagram recorded from hydrated crystals.

Figure IV.23b shows the base-plane ED pattern recorded from frozen-hydrated V_{HBA} crystals while **Figure IV.23c** shows the powder XRD diagram of hydrated crystals. These patterns clearly differ from those of $V_{6\text{I}}$, $V_{6\text{II}}$, $V_{6\text{III}}$, V_7 and V_8 , indicating that this is a new V-amylose allomorph. If the helices are perpendicular to the lamellae as reported for other allomorphs, then the ED pattern shown in **Figure IV.23b** corresponds to a two-dimensional lattice in the zero layer of the reciprocal lattice. It can be indexed on the basis of an orthorhombic unit cell with $a = 1.54 \pm 0.01$ nm and $b = 2.81 \pm 0.01$ nm. These cell parameters are in good agreement with those calculated from XRD data ($a = 1.550 \pm 0.001$ nm, $b = 2.836 \pm 0.001$ nm and $c = 0.790 \pm 0.001$ nm) (**Annex 2, Table S.IV.1**). In addition, the $h00$, $0k0$ reflections are systematically absent when h , k were odd, suggesting the $P2_12_12_1$ or $P2_12_12_1$ space group.

The orthorhombic unit cell would contain 2 amylose helices. Assuming a regular close-packed array of helices, the helix packing diameter would be 1.55 nm, smaller than the diameter of an 8-fold helix (1.62 nm) (Yamashita & Monobe, 1971) but larger than that of a 7-fold helix (1.50 nm) (Yamashita & Hirai, 1966) and a 6-fold helix (1.37 nm) (Mikus et al., 1946). Therefore, only 7-fold or 6-fold helices can be packed in the unit cell. If the crystal contains 7-fold helices, the space group would be $P1$ rather than $P2_12_12_1$ since 7-fold helices cannot be located on 2-fold screw axes. In contrast, if it contains 6-fold helices, the $P2_12_12_1$ space group is possible but the inter-helical space will be larger since the helices have a smaller diameter. A tentative model of V_{HBA} with $P2_12_12_1$ space group containing left-handed 6-fold helices is shown in **Figure IV.24**. The complexing agent would be located only in the inter-helix space with some water molecules. The quantification of HBA in the complex showed that there is about 1 HBA molecule for 6 glucose units, corresponding to 2 HBA molecule per unit cell. Our diffraction data is insufficient to determine the helical conformation of amylose. Further consideration of this point will be made using the solid-state NMR data presented in § IV.13.

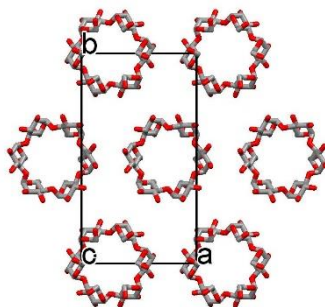


Figure IV.24. Proposed model of V₄-hydroxybenzoic acid, composed of left-handed 6-fold helices packed into the orthorhombic unit cell, space group $P2_12_12_1$. The model is projected on the (a,b) plane of the unit cell. Hydrogen atoms are not shown.

IV.7.3. Effect of drying on the crystal structure

Figure IV.25 shows the effect of different drying processes on the crystal structure of V_{HBA}. The XRD profiles of the complexes before and after drying in vacuum at room temperature (**Figures IV.25a,b**) is generally the same. The crystal is thus stable upon drying in vacuum and only a slight decrease of crystallinity was observed. On the other hand, freeze-drying led to a remarkable loss of crystallinity, together with a disappearance of the characteristic peaks of the initial structure. The resulting diagram (**Figure IV.25c**) contains broad peaks that can be indexed on the basis of a hexagonal unit cell with $a = b = 1.61 \pm 0.01$ nm and $c = 7.97 \pm 0.01$ nm or a pseudo-hexagonal orthorhombic unit cell with $a = 1.61 \pm 0.01$ nm, $b = a\sqrt{3} = 2.79 \pm 0.01$ nm and $c = 7.97 \pm 0.01$ nm. The helical conformation of amylose would remain unchanged, but amylose would form a more compact hexagonal arrangement, as shown in **Figure IV.26**. After rewetting in water, the complexes yielded a diffraction pattern that was almost identical to that of the initial structure (**Figure IV.25d**). As previously mentioned for other complexes, these results suggest that water plays an important role in the stability of the crystals. In addition, water appeared to be bound more tightly in V_{HBA} compared to other allomorphs, as it was not readily removed by vacuum-drying at room temperature.

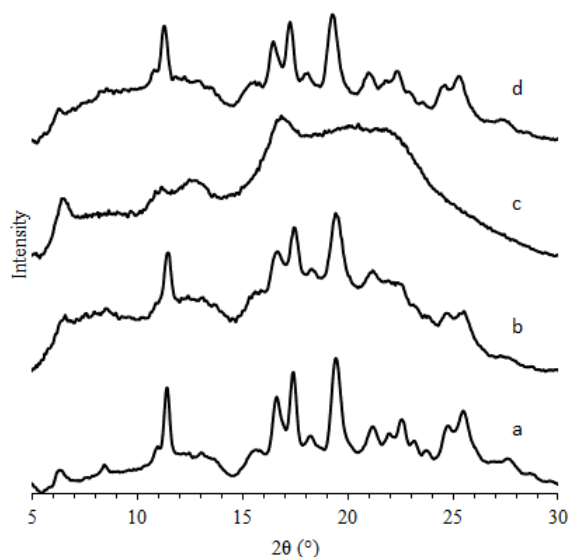


Figure IV.25. XRD profiles of a) hydrated V-amylose complexes with 4-hydroxybenzoic acid; b) crystals as in (a) after thorough drying in vacuum; c) crystals in (a) after freeze-drying; d) crystals as in (c) after rewetting.

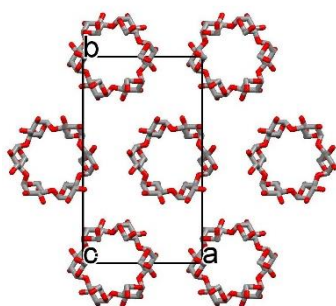


Figure IV.26. Proposed model of the dry form of V₄-hydroxybenzoic acid, composed of left-handed 6-fold helices packed into a pseudo-hexagonal orthorhombic unit cell. The model is projected on the (a,b) plane of the unit cell. Hydrogen atoms are not shown.

IV.8. A new V-amylose allomorph obtained with (-)-borneol, R-(+)-camphor, *cis*-decahydro-1-naphthol, decahydro-2-naphthol, and 1,3-butanediol

A new allomorphic family of V-amylose lamellar crystals was obtained by crystallization of amylose in the presence of (-)-borneol, R-(+)-camphor, *cis*-decahydro-1-naphthol, decahydro-2-naphthol and 1,3-butanediol. These complexes are isomorphous, having characteristic morphological features and ED and XRD patterns.

IV.8.1. Morphology and crystal structure

Figure IV.27 shows lamellar crystals of V-amylose prepared with (-)-borneol, R-(+)-camphor, *cis*-decahydro-1-naphthol, decahydro-2-naphthol and 1,3-butanediol. The crystals have a more or less hexagonal shape. They can be monolamellar or more frequently

consist of many superimposed lamellae involving a dislocation-centered spiral growth. This morphology is similar to that previously described for V6_I crystals.

When probed by ED in frozen-hydrated state at low temperature, these crystals give almost identical sharp diffraction patterns, as shown in **Figures IV.28b** and **IV.29a-c**. Furthermore, these diffraction patterns are similar to those of V6_I, exhibiting a hexagonal symmetry. However, the corresponding reflections appear at smaller diffraction angles (2θ) suggesting a larger unit cell compared to V6_I. Indeed, these ED patterns can be accounted for by a two-dimensional hexagonal unit cell with average parameters $a = b = 1.50 \pm 0.02$ nm, or a pseudo-hexagonal orthorhombic unit cell with $a = 1.50 \pm 0.02$ nm, $b = a\sqrt{3} = 2.61 \pm 0.03$ nm. The XRD patterns of these complexes are nearly identical as well (**Figure IV.28c**) and can be indexed along a hexagonal unit cell with average parameters $a = b = 1.526 \pm 0.017$ nm, or a pseudo-hexagonal orthorhombic unit cell with $a = 1.526 \pm 0.017$ nm, $b = a\sqrt{3} = 2.643 \pm 0.029$ nm and $c = 0.803 \pm 0.008$ nm (**Annex 2, Table S.IV.2**). It can be noted that the unit cell parameters of this allomorph are slightly larger than those of V7_a obtained by drying the V7 complexes. The XRD patterns are also similar suggesting that the two crystal structures are closely similar. Therefore, this new allomorph would contain a hexagonal arrangement of statistically or regularly antiparallel 7-fold helices.

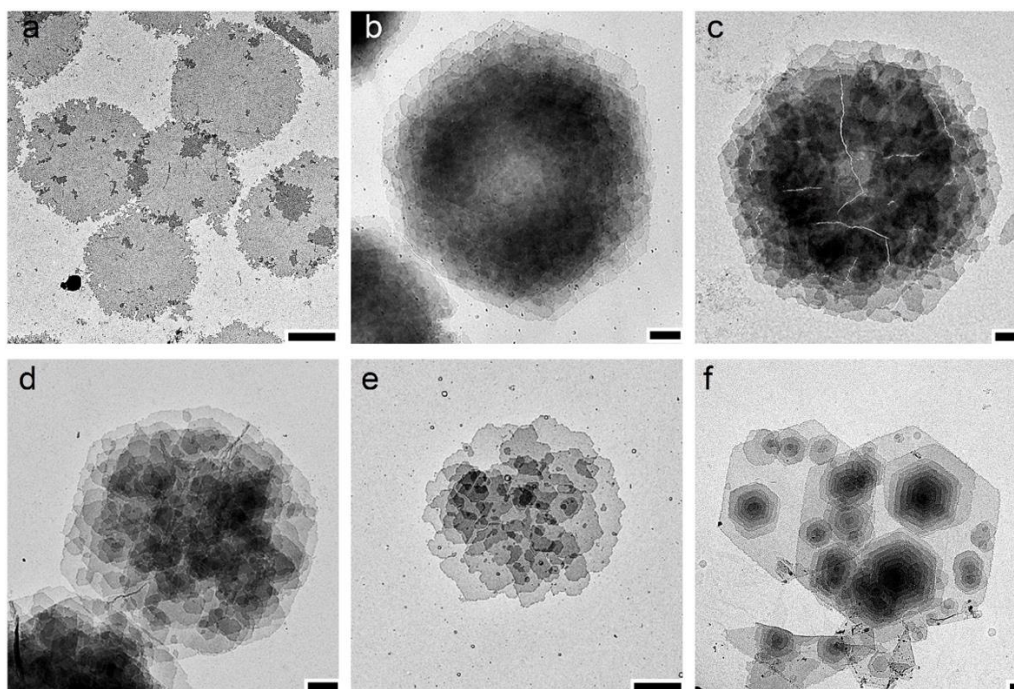


Figure IV.27. TEM images of a new form of V-amylose obtained with (-)-borneol (a,b), *R*-(+)-camphor (c), *cis*-decahydro-1-naphthol (d), decahydro-2-naphthol (e), 1,3-butanediol (f). Scale bars: 1 μ m.

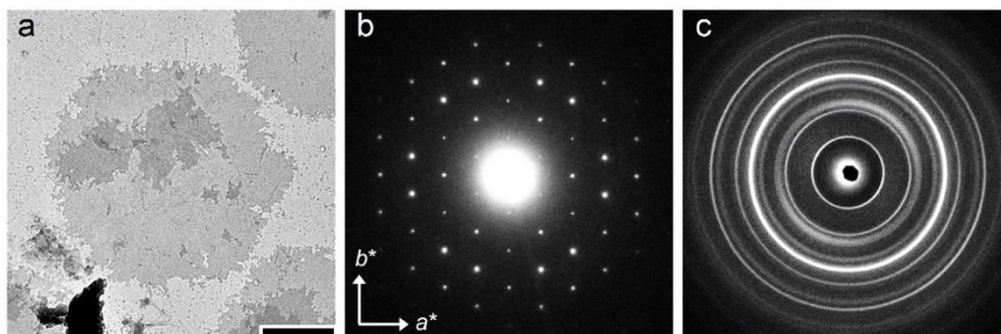


Figure IV.28. a) TEM image of V-amylose complexed with (-)-borneol (scale bar: 1 μm); b) corresponding base-plane ED pattern correctly oriented with respect to the crystal in (a); c) corresponding powder XRD diagram recorded from hydrated crystals.

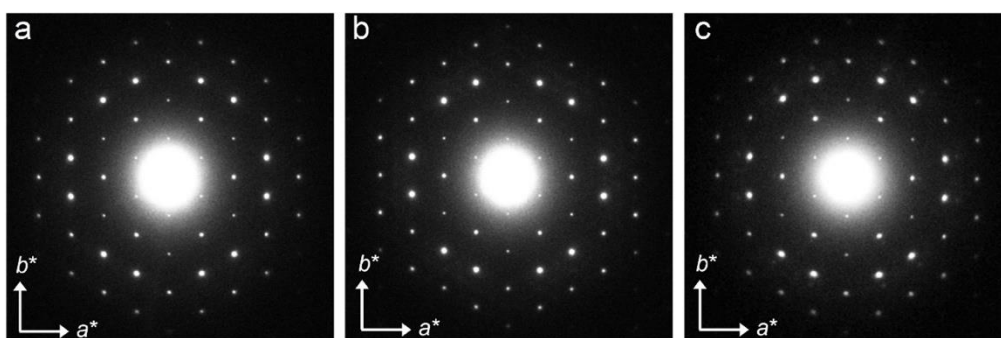


Figure IV.29. Base-plane ED patterns of V-amylose crystals obtained with *cis*-decahydro-1-naphthol (a); decahydro-2-naphthol (b); 1,3-butanediol (c).

IV.8.2. Effect of drying on the crystal structure

Upon drying, the complexes with (-)-borneol, *R*-(+)-camphor, *cis*-decahydro-1-naphthol, decahydro-2-naphthol yielded similar XRD patterns as that shown in **Figure IV.30b**. This pattern is almost identical to that of V7_a obtained by drying V7 complexes, and can be indexed using a pseudo-hexagonal orthorhombic unit cell with $a = 1.505 \pm 0.005$ nm, $b = a\sqrt{3} = 2.607 \pm 0.009$ nm and $c = 0.795 \pm 0.006$ nm. In contrast, the XRD pattern (**Figure IV.31b**) recorded on the dry complexes with 1,3-butanediol contains characteristic reflections of both V6_a and V7_a, which is similar to that obtained by drying the V7 complexes of 1,3-butanediol. After rewetting, the initial structures were recovered (**Figure IV.30c**).

The above results strongly support that the present crystals contain 7-fold helices like in previously known V7 structures. Therefore, they would have orthorhombic unit cells rather than hexagonal ones, and the space group would be *P1*. The arrangement of amylose helices would be essentially similar to that of V7_a but with more inter-helix space, as shown in model in **Figure IV.32**. The complexing agent would be located inside the helical cavity while the inter-helix space would accommodate some water molecules.

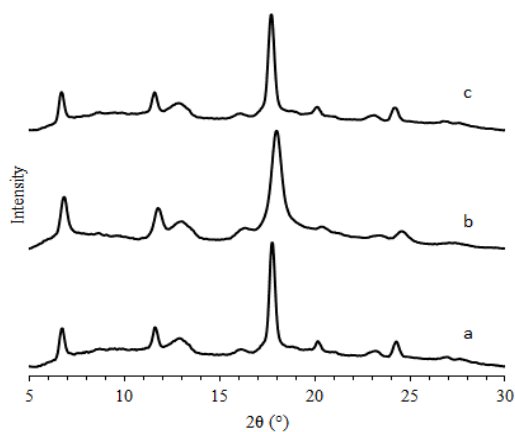


Figure IV.30. XRD profiles of a) hydrated V-amylose complexes with (-)-borneol, b) crystals as in (a) after thorough drying in vacuum, c) crystals as in (b) after rewetting.

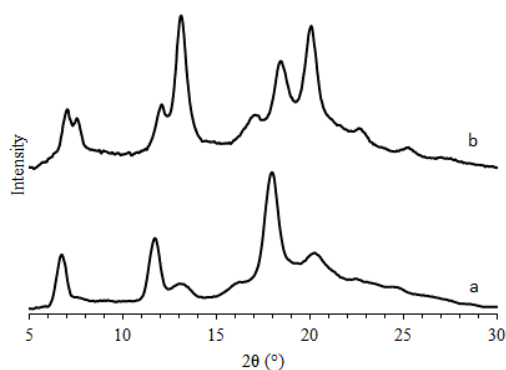


Figure IV.31. XRD profiles of a) hydrated V-amylose complexes with 1,3-butanediol, b) crystals as in (a) after thorough drying in vacuum.

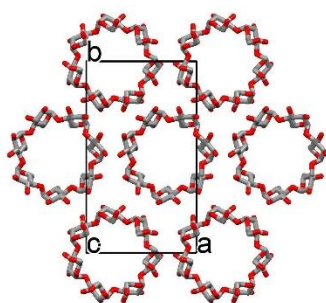


Figure IV.32. Proposed model of $V_{(-)\text{-borneol}}$ and the isomorphous complexes projected on the (a,b) plane of the unit cell. Hydrogen atoms are not shown.

IV.9. A new V-amylose allomorph obtained with 1-naphthol

The crystallization of amylose in the presence of 1-naphthol allowed obtaining a new allomorph, in addition to the well-known tetragonal V8 complex. Details of the crystallization of $V_{1\text{-naphthol}}$ are presented in **Chapter V**. The new allomorph shows unique morphological features and ED and XRD patterns that are easily distinguishable from those of other allomorphs.

IV.9.1. Morphology and crystal structure

Figure IV.33 shows the morphology of the new form of V_{1-naphthol}. The crystals consist of stacks of many lamellae, having a rhombohedral habit with an average angle of about 64°. The average thickness of each lamella is about 10.3 ± 0.6 nm (**Annex 2, Table S.IV.4** and **Figure S.IV.1d**), determined by AFM. Dislocation-centered spiral growth was not observed and the crystals likely thickened via epitaxial growth. Besides, twinned structures at an angle of about 64° were also observed (**Figure IV.33b,c**). This morphology is clearly different from that of the lamellar crystals of other V-amylose allomorphs.

In addition, the base-plane ED (**Figure IV.34b**) and XRD (**Figure IV.34c**) patterns recorded on frozen-hydrated crystals clearly differ from those of other allomorphs. The ED pattern can be indexed along an orthorhombic unit cell with $a = 1.66 \pm 0.01$ nm, and $b = 2.50 \pm 0.01$ nm, in agreement with the values calculated from the XRD pattern ($a = 1.663 \pm 0.001$ nm, $b = 2.518 \pm 0.001$ nm and $c = 0.856 \pm 0.001$ nm) (**Annex 2, Table S.IV.2**). The c -parameter is slightly larger than those of other allomorphs that are between 0.79 and 0.83 nm. In addition, only $h00$, $0k0$, and $00l$ reflections with even indices were observed, suggesting that the space group is either $P212121$ or a lower symmetry $P1$. The unit cell would contain 2 amylose helices. Assuming a close packing of helices, the helix packing diameter is about 1.50 nm which is identical to that found for the 7-fold helix of V7 complexes. Therefore, the present complex probably contains 7-fold helices in a compact arrangement or 6-fold helices with a looser packing. **Figure IV.35** shows a possible packing of left-handed 7-fold helices in the unit cell with space group $P1$. Such arrangement allows for a statistical or regular alternation of up and down chains. 1-Naphthol can be located inside the helices. The stoichiometry of 1-naphthol determined by UV spectroscopy is 1 molecule of 1-naphthol per 7.3 glucosyl units. From this geometrical analysis, it is not possible to conclude whether the complexes contain 6-fold or 7-fold helices. The helical conformation will be further studied by solid-state NMR, as presented in § IV.13.

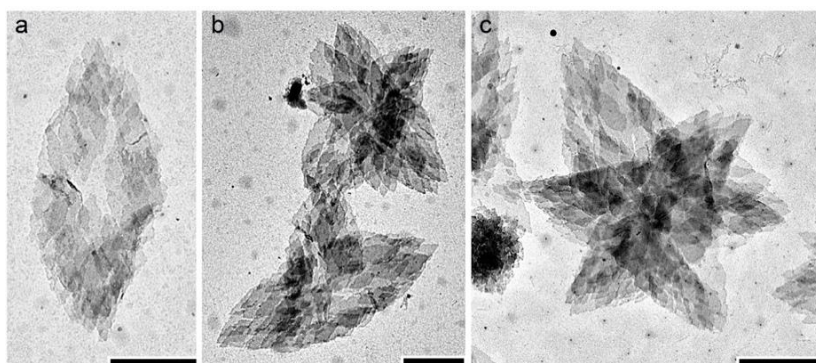


Figure IV.33. TEM images of a new form of V-amylose complexed with 1-naphthol. Bars: 1 μm.

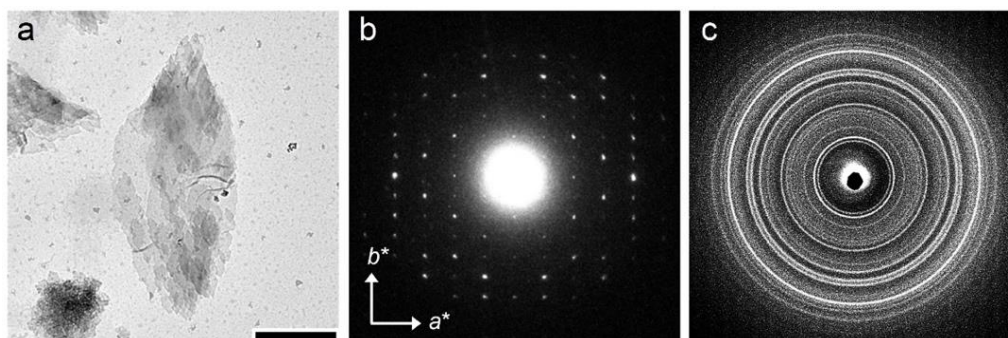


Figure IV.34. a) TEM image of V-amylose complexed with 1-naphthol (scale bar: 1 μm); b) corresponding base-plane ED pattern correctly oriented with respect to the crystal in (a); c) corresponding powder XRD diagram recorded from hydrated crystals.

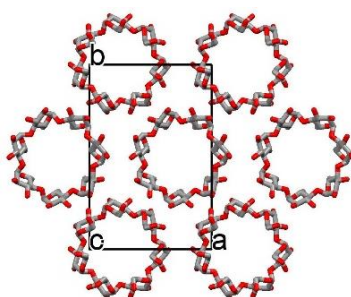


Figure IV.35. Proposed model for a new allomorph of $V_{1\text{-naphthol}}$ based on 7-fold left-handed helices. The model is projected on the (a, b) plane of the unit cell of space group $P1$. Hydrogen atoms are not shown.

IV.9.2. Effect of drying on the crystal structure

Figure IV.36 shows the effect of drying and rewetting on the XRD diagram of the complexes. Upon drying in vacuum at room temperature, the diffraction pattern remained nearly unchanged (**Figure IV.36b**), suggesting that the crystal structure was stable. However, when the complexes were freeze-dried, a significant loss in crystallinity was observed (**Figure IV.36c**). After rewetting with water, the complexes yielded a diffraction pattern that was almost identical to that of the initial hydrated state (**Figure IV.36d**). The drying behavior of the present complexes is very similar to that observed for V_{HBA} . Water is thus bound rather tightly and plays an important role on the stability of the crystal structure.

IV.10. A new V-amylose allomorph obtained with quinoline

In addition to the tetragonal V8 crystals, quinoline was shown to induce another type of allomorph which appeared to be a new one which exhibits ED and XRD patterns different from those of other V-amylose allomorphic families. Details of the crystallization of the two forms of $V_{\text{quinoline}}$ are presented in **Chapter V**.

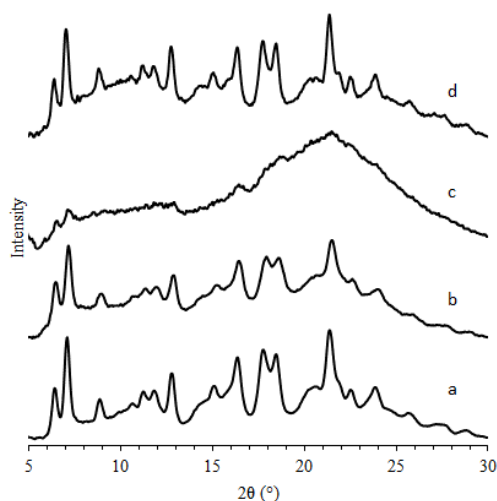


Figure IV.36. XRD profiles of a) hydrated V-amylose complexed with 1-naphthol; b) crystals as in (a) after thorough drying in vacuum; c) crystals as in (a) after freeze-drying; d) crystals as in (c) after rewetting.

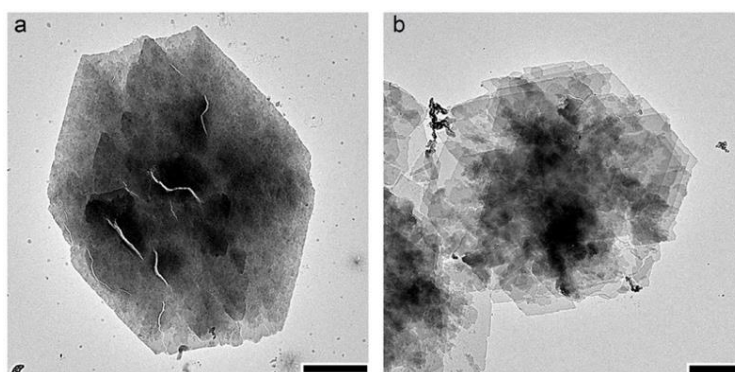


Figure IV.37. TEM images of crystals of a new form of V-amylose complexed with quinoline prepared from DP80 (a) and D130 (b) amylose. Scale bars: 1 μm .

IV.10.1. Morphology and crystal structure

Figure IV.37 shows TEM images of typical crystals of the new form of $V_{\text{quinoline}}$. The crystal shown in **Figure IV.37a** was prepared with DP80 amylose. It has a more or less rhombic shape and consists of many superimposed very small lamellae. The crystal thickens through epitaxial growth of new lamellae. On the other hand, the crystals prepared with longer amylose usually contain larger lamellae with more or less hexagonal shape such as that prepared with DP130 amylose shown in **Figure IV.37b**. The crystals thicken via a dislocation-centered spiral growth. This morphology is very similar to that of V_{6I} , $V_{(-)\text{-borneol}}$ and isomorphous complexes.

Typical ED and powder XRD patterns recorded from hydrated crystals of the new form of $V_{\text{quinoline}}$ are shown in **Figures IV.38b** and **IV.38c**, respectively. These patterns differ from those of other V-amylose allomorphs described above. It seems certain that the crystals contain helical amylose chains because complexes of quinoline also crystallized into the helical V8

structure. If the helices are oriented perpendicular to the lamellae as reported for other V-amylose complexes, the ED pattern represents a two-dimensional net in the zero layer of the reciprocal lattice and can be indexed on the basis of an orthorhombic unit cell with $a = 2.62 \pm 0.01$ nm and $b = 3.21 \pm 0.01$ nm, in agreement with those calculated from XRD data ($a = 2.702 \pm 0.001$ nm, $b = 3.291 \pm 0.001$ nm and $c = 0.786 \pm 0.001$ nm (Annex 2, Table S.IV.2). In addition, the $h00$, $0k0$, $00l$ reflections are absent when the indices are odd, suggesting a $P2_12_12_1$ space group. Each unit cell would contain four amylose helices. Assuming a close-packed structure, the helix packing diameter would be 1.58 nm, which is smaller than the helix diameter of 8-fold helix and higher than those of 6- and 7-fold helices. Therefore, the complexes could be composed of 6- or 7-fold helices. A tentative model based on left-handed 7-fold helices is shown in Figure IV.39. Quinoline would be located inside the helix cavity. The stoichiometry measured by UV spectroscopy is 1 quinoline for 12.5 glucosyl units, which is lower than that found for the previously described V8 structure (1 quinoline for 8.3 glucosyl units).

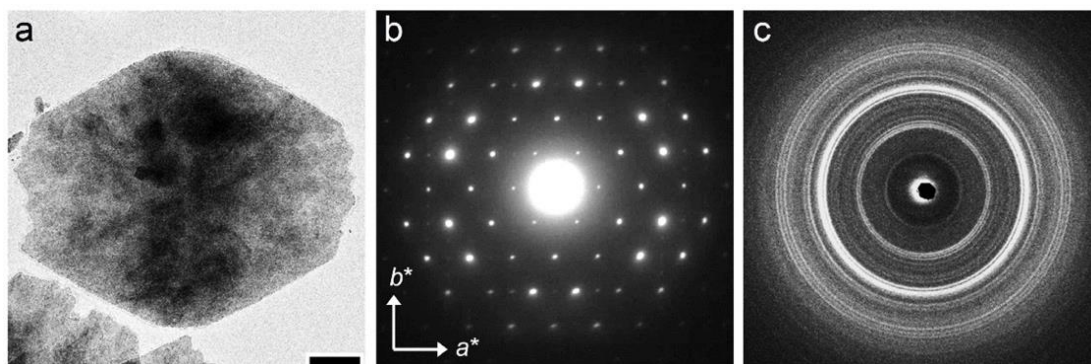


Figure IV.38. a) TEM image of a crystal of DP80 amylose complexed with quinoline (scale bar: 1 μm); b) corresponding base-plane ED pattern correctly oriented with respect to the crystal in (a); c) corresponding powder XRD diagram recorded from hydrated crystals.

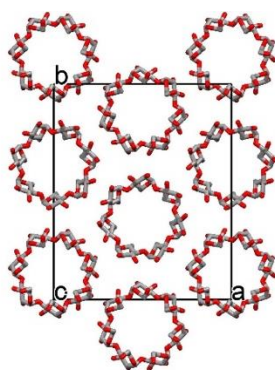


Figure IV.39. Proposed model for a new allomorph of $V_{\text{quinoline}}$ based on 7-fold left-handed helices. The model is projected on the (a,b) plane of the unit cell of space group $P2_12_12_1$. Hydrogen atoms are not shown.

IV.10.2. Effect of drying on the crystal structure

Figure IV.40 illustrates the effect of drying on the new form of $V_{\text{quinoline}}$. Upon drying, the complexes yielded a XRD diagram almost identical to those of $V7_a$ obtained by drying the $V7$ complexes or $V_{(-)\text{-borneol}}$ and isomorphous complexes. This supports the hypothesis that the complexes are composed of 7-fold rather than 6-fold helices. After rewetting in water, the initial structure was recovered, giving a diffraction diagram identical to that of the initial hydrated state. The results suggests that the complexing agent is not removed during the drying process and the structural transition is due to the departure of water located in the inter-helical space. In addition, it is interesting to note that the present $V_{\text{quinoline}}$, $V7$ complexes and $V_{(-)\text{-borneol}}$ and isomorphous complexes are commonly transformed into $V7_a$, but after rewetting, the $V7_a$ is reverted into the corresponding initial structure and not other allomorphs. The mechanism for this selective transition is still unknown, but the presence of water is essential for the process.

IV.11. A new V-amylose allomorph obtained with salicylic acid

In addition to the previously described $V8$ allomorph, the crystallization of amylose in the presence of salicylic acid allowed obtaining another type of crystals, with a structure differing from other known allomorphs.

IV.11.1. Morphology and crystal structure

Figure IV.41 shows TEM images of typical crystals of the new form of $V_{\text{salicylic acid}}$. The crystals consist of stacks of many lamellae with both epitaxial and dislocation-centered spiral growths. The shape of individual lamellae cannot be defined with precision. In general, the crystals exhibit an overall shape that is close to those of $V6_1$ type, $V_{(-)\text{-borneol}}$ type and the new allomorph of $V_{\text{quinoline}}$.

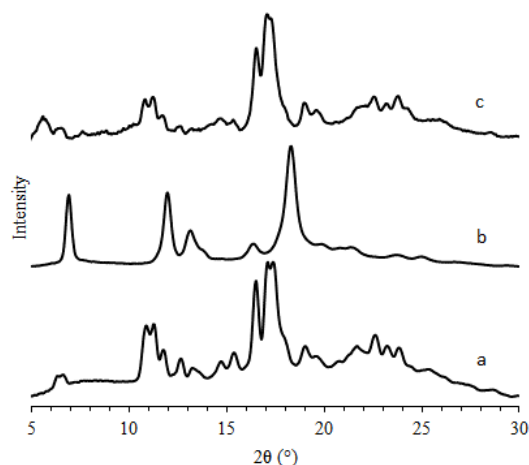


Figure IV.40. XRD profiles of a) hydrated V-amylose complexed with quinoline; b) crystals as in (a) after thorough drying in vacuum; c) crystals as in (b) after rewetting.

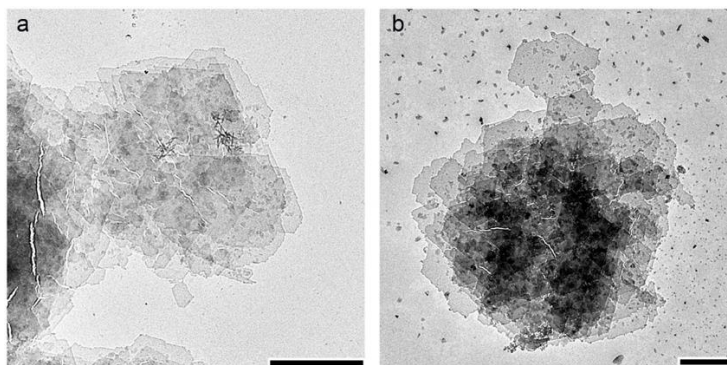


Figure IV.41. TEM images of a new form of V-amylose complexed with salicylic acid. Bars: 1 μm .

Figure IV.42b shows the typical base-plane ED pattern recorded from one frozen-hydrated lamella of $V_{\text{salicylic acid}}$. This pattern shows a centrosymmetry ($I_{hkl} = I_{\bar{h}\bar{k}\bar{l}}$) and is different from those of other V-amylose allomorphs. If the crystals are composed of helical amylose chains perpendicular to the lamellar surface, then the ED pattern can be indexed based on a monoclinic unit cell with $a = 3.21 \pm 0.01$ nm, $b = 3.23 \pm 0.01$ nm, and $\gamma = 116.9 \pm 0.3^\circ$. The unit cell parameters well agree with those calculated from powder XRD pattern (**Figure IV.42c**) (**Annex 2, Table S.IV.3**), given as $a = 3.245 \pm 0.006$ nm, $b = 3.246 \pm 0.005$ nm, $c = 0.793 \pm 0.001$ and $\gamma = 116.62 \pm 0.13^\circ$. Since there is no systematic absence based on the h and k indices, the space group would be $P2$ or $P2_1$. Each unit cell would contained four amylose helices. Assuming a close packing, the center-center distance of helices is 1.62 nm which is equal to the helix diameter of 8-fold helices. Therefore, all 6-, 7- and 8-fold helices could be packed into the unit cell. A tentative packing model of left-handed 8-fold helices in space group $P2_1$ is shown in **Figure IV.43**. Salicylic acid may be located inside the helix cavity. The stoichiometry of the complexes determined by UV spectroscopy is 1 salicylic acid per 6.1 glucosyl units. Additional details on the helical conformation obtained by solid-state NMR will be given in § IV.13.

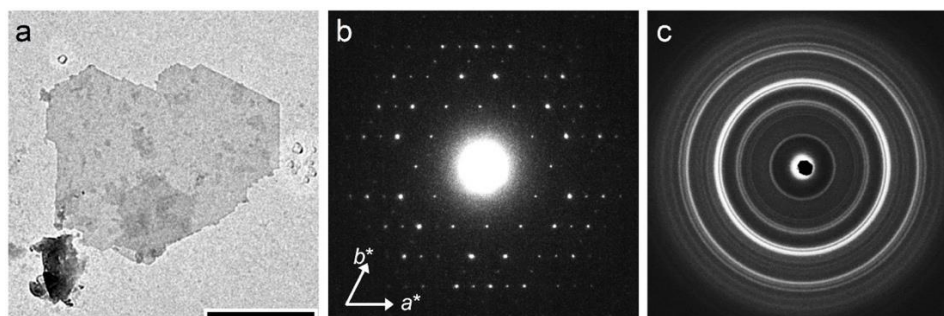


Figure IV.42. a) TEM image of V-amylose complexed with salicylic acid (scale bar: 1 μm); b) corresponding base-plane ED pattern correctly oriented with respect to the crystal in (a); c) corresponding powder XRD diagram recorded from hydrated crystals.

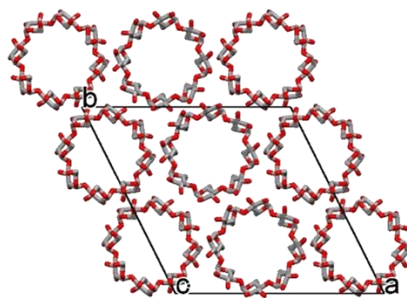


Figure IV.43. Proposed model for a new allomorph of $V_{\text{salicylic acid}}$ based on 8-fold left-handed helices. The model is projected on the (a,b) plane of the monoclinic unit cell of space group $P2_1$. Hydrogen atoms are not shown.

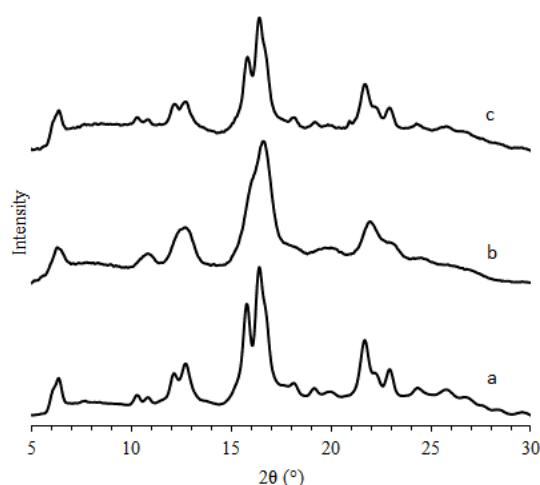


Figure IV.44. XRD profiles of a) hydrated V-amylose complexed with salicylic acid; b) crystals as in (a) after thorough drying in vacuum; c) crystals as in (b) after rewetting.

IV.11.2. Effect of drying on the crystal structure

Figure IV.44 shows the drying effect on the crystals structure of the allomorph of $V_{\text{salicylic acid}}$. Upon thorough drying, the diffraction peaks become broader but the peak positions remain the same, suggesting that the structure is rather stable upon drying. The slight decrease of crystallinity would be because the amylose helix would be less ordered due to the loss of water. After rewetting, the peaks sharpen like in the initial hydrated state. It is interesting to note that the diffraction pattern of the dry complexed is similar to that previously reported for complexes of salicylic acid and some analogues prepared by sealed-heating method (Oguchi et al., 1998; Uchino et al., 2002). As noted, the XRD diffraction data obtained from the polycrystalline aggregates prepared by sealed-heating was not resolved enough for the authors to determine the crystal structure. However, they proposed the formation of 8-fold helices showing some similarities with γ -cyclodextrin complexes with salicylic acid.

IV.12. Study the complexes by FT-IR spectroscopy

We have studied the IR spectra of different allomorphs of V-amylose. In addition, we also compared the IR spectra of V-amylose complexes to those of A- and B-amylose and DP6500 amylose which contains mainly amorphous amylose together with small fraction of B-amylose.

The IR spectra of untreated DP6500 amylose, A- and B-amylose and different allomorphs of V-amylose complexes in the hydrated state are shown in **Figures IV.45** and **IV.46**. The observed bands attributed to amylose in these spectra are listed in **Table IV.1**. In addition, the band near 1645 cm^{-1} is attributed to the adsorbed water. In V-amylose complexes, additional bands correspond to contributions from the complexing agents. **Figure IV.45** shows that the spectra of different allomorphs of amylose and V-amylose are very similar. However, some differences between V-amylose complexes and the uncomplexed amylose forms were noted in the fingerprint region from 1500 to 400 cm^{-1} . As observed in **Figure IV.46**, lines near 1408 , 1370 , 1295 , 1104 , 1022 , 946 cm^{-1} observed for V-amylose complexes are nearly absent or have a lower intensity by comparison to those of DP6500 amylose, A- and B-amylose. The variation in the vibrational frequencies would be related to the structure of different forms of amylose. As being reviewed in **Chapter I**, one of the main differences between V-amylose and other forms lies in the conformation of amylose. In the V-amylose complexes, amylose exists as compact single helices which are stabilized by intra-molecular hydrogen bonds, *i.e.* $O6\dots O2'$ and $O2\dots O3'$. On the other hand, A- and B-amylose have a more extended helical conformation which does not allow intra-molecular H-bonds. DP6500 amylose is almost amorphous and thus exists in a random coil state, in which H-bonds occur in an irregular manner. The difference in conformation and hydrogen bonds results in differences in length and strength of the related bonds, especially C1-O-C4' bridge and those related to O2, O3 and O6, leading to differences in vibrational frequencies of these bonds. In previous works, the frequencies around 1408 , 1370 , 1295 , 1104 and 1022 cm^{-1} have been assigned for the C-H, CH_2 , C-C and C-O-H related modes while that at 946 cm^{-1} is due to the $\alpha(1\rightarrow4)$ linkage (Cael et al., 1975; Cael et al., 1973; Santha et al., 1990).

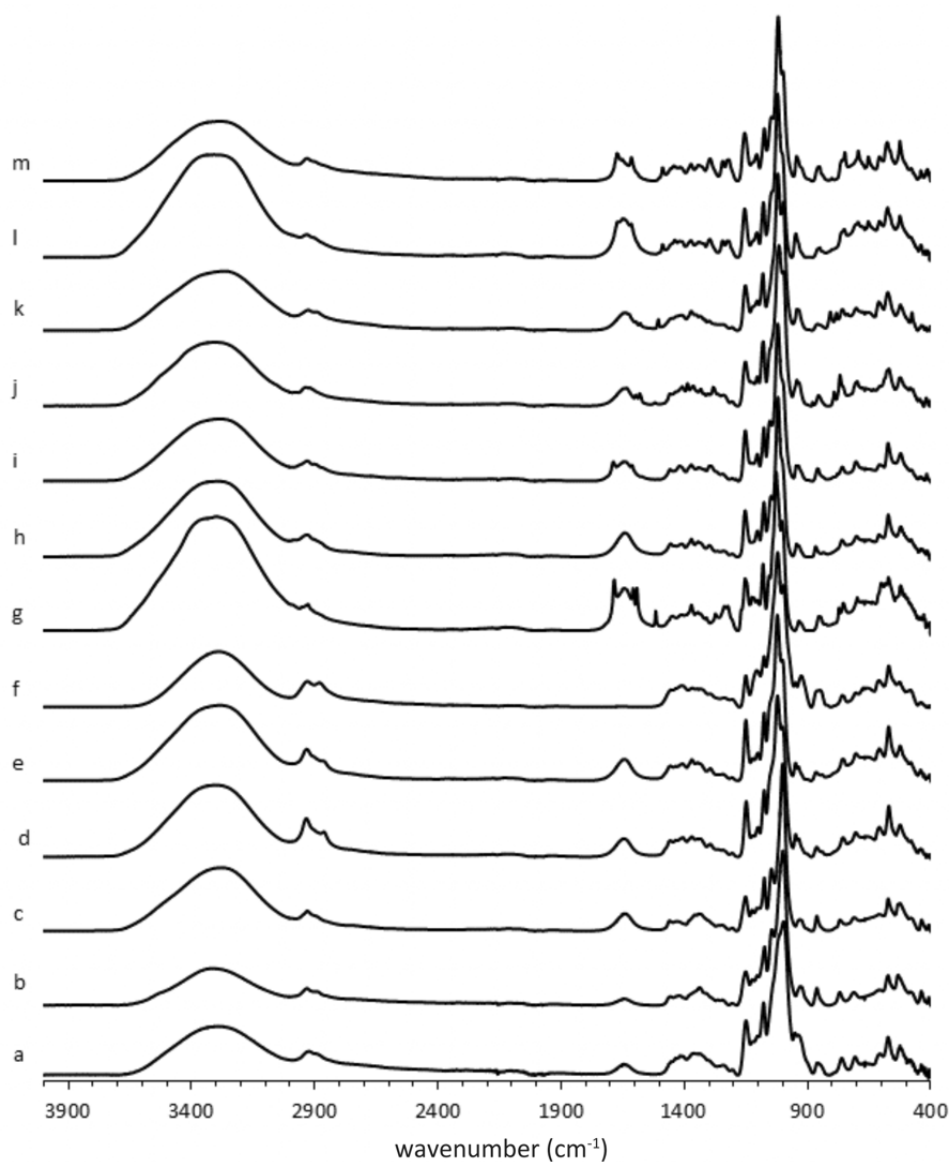


Figure IV.45. FT-IR absorbance spectra of untreated DP6500 amylose (a), A-amylose (b), B-amylose (c), V6_I of 1,6-hexanediol (d); V6_{II} of 1,6-hexanediol (e); V6_{III} of glycerol (f); V7 of 4-*tert*-butylbenzoic acid (g); V8 of salicylic acid (h); (i-m): new allomorphs of V₄-hydroxybenzoic acid (i), V₍₋₎-borneol (j), V₁-naphthol (k), V_{quinoline} (l) and V_{salicylic acid} (m).

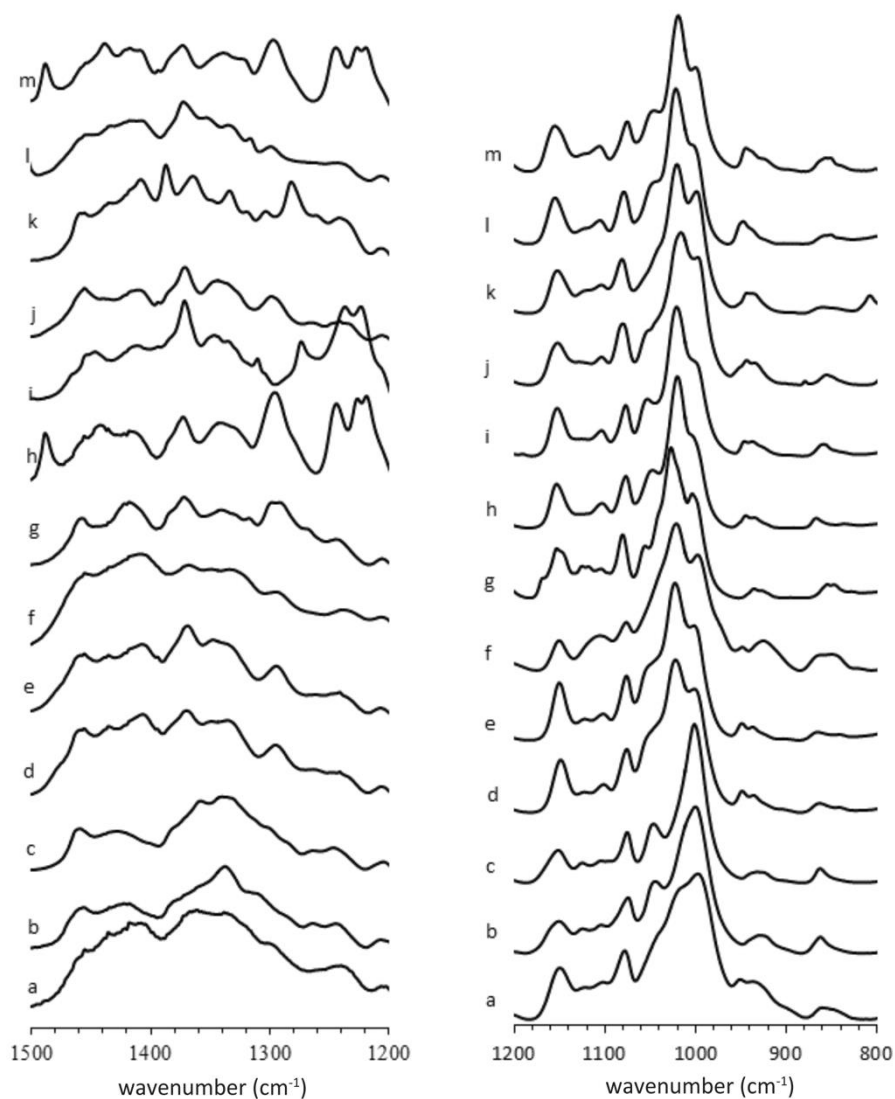


Figure IV.46. FT-IR absorbance spectra of untreated DP6500 amylose (a), A-amylose (b), B-amylose (c), V6_I of 1,6-hexanediol (d); V6_{II} of 1,6-hexanediol (e); V6_{III} of glycerol (f); V7 of 4-*tert*-butylbenzoic acid (g); V8 of salicylic acid (h); new allomorphs of V₄-hydroxybenzoic acid (i), V₍₋₎-borneol (j), V₁-naphthol (k), V_{quinoline} (l) and V_{salicylic acid} (m).

Table IV.1. FT-IR wavenumbers (cm⁻¹) of untreated DP6500 amylose, A- and B-amylose and V-amylose complexes.

Amylose ^a	A-type	B-type	V6 ^b	V6 ^{II} ^b	V6 ^{III} ^c	V7 ^d	V8 ^e	V _{HBA} ^f	V _{(-)-borneol} ^f	V _{1-naphthol} ^f	V _{quinoline} ^f	V _{salicylic acid} ^f	Assignment
3306.3	3306.8	3306.0	3307.0	3306.3	3306.5	3306.5	3305.8	3296.8	3306.5	3307.5	3306.0	3296.5	O-H stretching
2923.5	2931.5	2929.8	2933.8	2932.3	2929.8	2930.3	2930.8	2927.5	2931.8	2919.5	2926.3	2931.8	C-H stretching
1455.0	1456.0	1459.0	1455.5	1455.5	1455.0	1458.0	ND	ND	1455.5	1455.5	1452.0	1455.5	CH ₂ sym def.
1408.0	1418.0	1428.0	1406.5	1407.0	1407.5	1413.3	-	1411.5	1408.5	1408.5	1407.5	1408.5	C-H def.
1367.0	-	-	1370.0	1368.5	1368.0	1372.0	1373.0	1371.5	1371.0	1365.0	1372.5	1373.5	C-H def.
-	-	1358.0	-	-	-	-	-	-	-	-	-	-	
1338.0	1337.5	1340.0	1335.5	1335	1334.5	1336.5	1342.0	1335.5	1343.0	1334.0	1335.0	1339.0	C3-O-H and C6-H def
1302.5	-	-	1295.0	1294.5	1295.0	1298.3	1296.0	-	1298.8	1303.5	1299.5	1297.3	C-H def of ring hydrogens
1240.3	1244.8	1246.8	1241.5	1241.5	1238.0	1242.8	ND	ND	1241.5	1242.0	1244.8	ND	C-O-H and C-H def of ring H
1206.8	1207.3	1204.8	1207.0	1207.3	1206.5	1206.0	ND	ND	1206.0	1207.0	1207.0	ND	
1149.8	1151.0	1151.5	1149.0	1150.5	1150.5	1153.0	1155.5	1153.5	1153.5	1152.5	1152.5	1155.0	C-O-H, CH ₂ def
1121.5	1124.8	1125.0	1122.8	1122.3	ND	ND	ND	1118.5	ND	ND	ND	ND	
1101.3	1104.3	1104.5	1101.5	1102.3	1105.5	1104.0	1106.0	1104.3	1103.5	1104.0	1104.0	1105.5	
1078.3	1074.5	1075.5	1076.0	1076.5	1076.5	1077.0	1075.5	1080.5	1077.0	1080.3	1081.3	1079.0	C-O and C-C stretching, C-O-H def
-	1044.8	1046.5	ND	ND	ND	1053.0	1046.0	1055.5	1047.5	ND	ND	ND	
-	-	-	1022.0	1022.5	1021.5	1021.0	1019.0	1027.0	1020.0	1016.3	1020.5	1022.0	C-O-H def., CH ₂ (related modes)
997.5	1000.0	1001.3	1001.3	1001.5	997.5	ND	1000.0	1004.0	ND	997.5	999.0	ND	
950.8	-	-	948.5	949.0	948.5	946.0	944.5	-	944.5	943.5	943.3	947.5	Skeletal mode involving α-(1-4) linkage
937.5	929.0	932.0	936.0	937.0	ND	937.0	ND	935.5	935.0	935.0	937.3	ND	
859.8	862.3	862.5	863.0	865.0	860.3	859.0	856.0	854.5	866.8	855.5	855.5	856.8	C-H and CH ₂ def
761.0	769.3	768.0	755.8	756.0	759.3	759.3	759.0	755.0	759.8	759.3	758.8	759.3	C-C stretching
707.8	712.3	710.8	704.5	703.0	703.8	703.0	694.5	698.3	700.5	699.0	702.3	695.0	
605.5	606.8	610.5	608.5	608.3	610.0	608.5	607.5	ND	610.5	605.5	611.0	608.3	
573.8	573.0	572.5	570.3	571.0	571.0	573.5	577.0	572.0	572.5	572.5	574.0	574.8	Skeletal modes (ring bending)
525.0	532.5	526.5	524.5	524.5	525.5	522.3	525.5	522.3	521.0	523.8	524.0	526.0	

^a native amylose, almost amorphous; ^b complexes obtained with 1,6-hexanediol; ^c complexes obtained with glycerol; ^d complexes obtained with 4-tert-butylbenzoic acid; ^e complexes obtained with salicylic acid; ^f new allomorphs; ^g referenced from Cael et al. (1973) and Cael et al. (1975).

-: not observed; ND: not determined because the bands are present as shoulders or superimposed to those of complexing agents.

Among the vibrational lines, the one near 1022 cm^{-1} which is assigned to the C-O-H deformation shows the most remarkable difference between V-amylose and other amylose forms and thus can be used as a fingerprint for V-amylose. However, the relative intensity and the position of this line vary with the hydration state of V-amylose. As shown for V7 of ibuprofen in **Figure IV.47**, there is a decrease in intensity and the band is slightly shifted to lower frequencies upon drying, suggesting a decrease in bond strength. As presented above, V7 is transformed into a more compact hexagonal structure V7_a upon removal of water. As amylose helices get closer, intermolecular H-bonds between the hydroxyl groups would be formed, leading to a shift of the position of the C-O-H deformation bands.

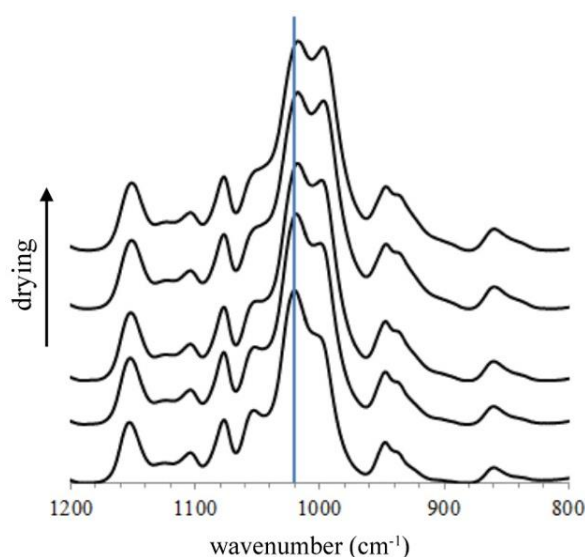


Figure IV.47. Effect of drying on the FT-IR spectra of V_{ibuprofen}.

IV.13. Study of the helical conformation by ^{13}C CP/MAS NMR spectroscopy

Typical ^{13}C CP/MAS NMR spectra of hydrated V-amylose complexes are shown in **Figure IV.48** and **Annex 2, Figure S.IV.2**. The resolved chemical shifts of carbons of the glucosyl residues are summarized in **Table IV.2**. The assignment was made based on the corresponding liquid-state spectra (Gidley & Bociak, 1985; Jane et al., 1985). A shoulder or a weak peak at 100.4 ppm was also observed in spectra of several complexes corresponding to C1 resonance of B-type amylose (Gidley & Bociak, 1988; Horii et al., 1987; Veregin et al., 1987a). In addition, resonances assigned to complexing agents were observed in the spectrum of V6_I (1,6-hexanediol) and V6_{II} (1,6-hexanediol) at 62.1 ppm, V6_{III} (glycerol) at 60.1 ppm and 72.8 ppm, and V_{R-(+)-camphor} at 57.9 ppm.

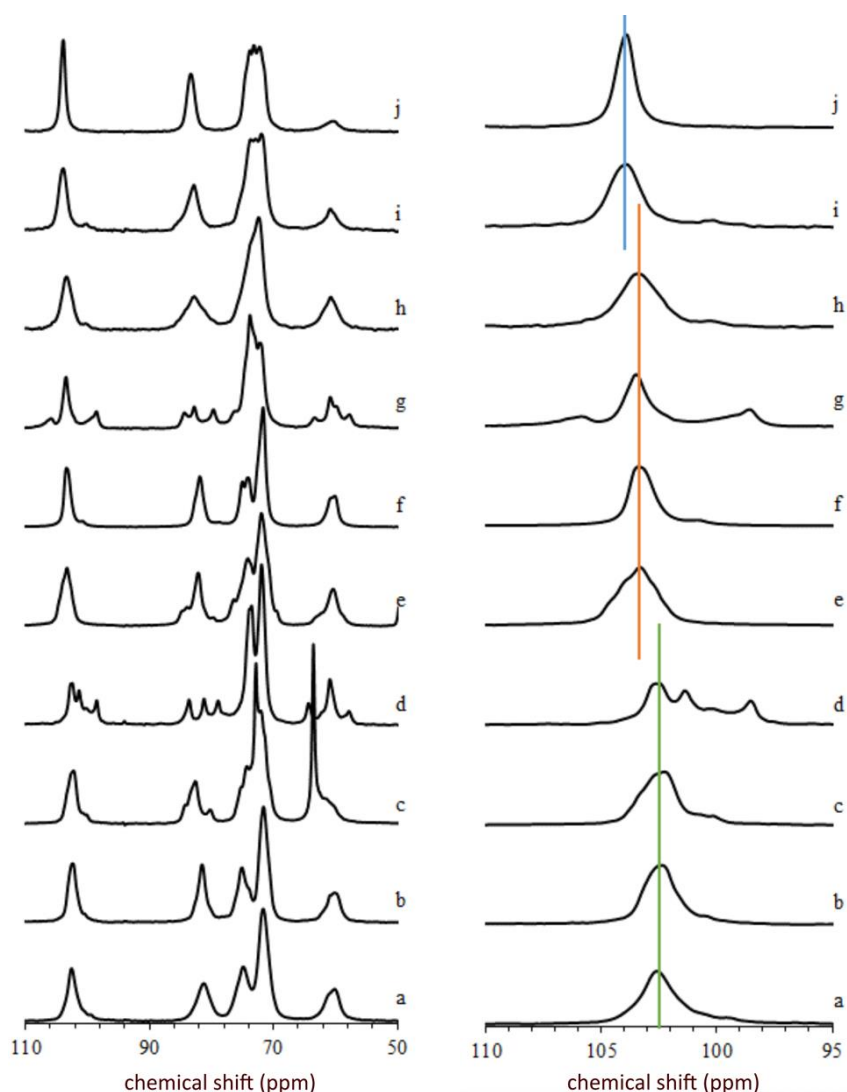


Figure IV.48. ^{13}C CP/MAS NMR spectra in two different regions of V6_I of hexadecanoic acid (a), V6_II of hexanoic acid (b), V6_III of glycerol (c), new allomorph V_4 -hydroxybenzoic acid (d), new allomorph V_borneol (e), V_7 of butanoic acid (f), new allomorph V_1 -naphthol (g), $\text{V}_\text{quinoline}$ (h), new allomorph $\text{V}_\text{salicylic acid}$ (i), V_8 of salicylic acid (j).

Previous ^{13}C CP/MAS NMR studies of crystalline carbohydrates have revealed that the C1 and C4 chemical shifts are particularly correlated with the torsion angles ϕ (O5-C1-O1-C4) and ψ (O1-C1-C4-C5) about the glucosidic linkages and thus reflect the helical conformation (Gidley & Bociek, 1988; Horii et al., 1987; Veregin et al., 1987a). Our results show that the C1 resonance is shifted downfield with increasing helicity of amylose chain (Figure IV.48, Annex 2, Figure S.IV.2, Table IV.2). In particular, V6_I , V6_II and V6_III complexes have a C1 signal in closely equal range 102.3-102.7 ppm, regardless the nature of complexing agents, while the C1-site in V_7 and V_8 complexes gives rise to resonance at 103.3-103.6 ppm and 103.9-104.3 ppm, respectively. On the other hand, we found no significant correlation between

C4 resonances and the helical conformations. V_{6I}, V_{6II} and V₇ have C4 signals in the range of 81.3-81.9 ppm, thus at higher field than that of V_{6III} (80.2-84.6 ppm) and V₈ (82.9-83.4 ppm). Our results partially agrees with the report of Gidley and Bociek (1988) that mentions that the C1 and C4 chemical shifts are not sensitive to expansion of the amylose helix from a 6- to a 7-fold repeat, but are shifted downfield by ~1 ppm in the V₈ complex obtained with 1-naphthol.

The conformation of V-amylose in the new allomorphs was determined based on the position of the C1 resonance. V_{(-)-borneol}, the isomorphous V_{(R)(+)-camphor} and V_{quinoline} have C1 resonances centered at a position similar to that of V₇ complexes, and thus would contain 7-fold helix, in agreement with the fact that these complexes are commonly transformed into V_{7a} upon drying. The new allomorph V_{salicylic acid} has the same C1 resonance with V₈ complexes, suggesting an 8-fold helical conformation. Difficulties arise for V_{4-hydroxybenzoic acid} and V_{1-naphthol} which C1 resonance is a multiplet rather than only one signal observed in other allomorphs. The splitting of the resonance reflects the presence of inequivalent environments within the material (Gidley & Bociek, 1988; Horii et al., 1987; Veregin et al., 1987a). Therefore, we can assume that the single helices in V_{4-hydroxybenzoic acid} and V_{1-naphthol} are less symmetrical than those in other allomorphs. However, it must be noted that the C1 resonance is rather broad in most spectra, suggesting that the residues are in a number of environments described by a range of conformations averaging about the highest peak. Considering the highest signal of C1, V_{4-hydroxybenzoic acid} and V_{1-naphthol} would contain 6- and 7-fold amylose helix, respectively. In general, the helical conformation determined from the C1 resonance in solid-state NMR is in good agreement with that predicted on the basis of helix packing diameter. Further works, such as a structural refinement using diffraction data, should be conducted to confirm the helicity of amylose in new allomorphs.

In previous works, the C6 chemical shift was found to be correlated with the exocyclic angle ω (C4-C5-C6-O6) of glucosyl residues and thus reflected the hydroxymethyl group conformation (*gg*, *gt* and *tg*) determined from single-crystal XRD data. For cellulose, three C6 chemical shifts are observed at 60-62.6 ppm, 62.5-64.5 ppm, and 65.5-66.5 ppm, which are related to the *gg*, *gt* and *tg* conformations, respectively (Horii et al., 1983). These values are in agreement with those proposed for cyclodextrins: 59.6-61.7 ppm for *gg*, and 62.7-65.9 for *gt* (Veregin et al., 1987b). In V-amylose, all allomorphs have the C6 resonance (singlet or multiplet) that covers a wide range (57-66 ppm), and centers at 60.2-61.8 ppm. Therefore, it seems that all *gg*, *gt* and *tg* conformations are present in V-amylose but *gg* is the major conformation.

Table IV.2. ^{13}C chemical shifts (ppm) of carbons of glucosyl residues of hydrated V-amylose allomorphs.

Complex	C1	C4	C2,3,5	C6
V6 _I of hexadecanoic acid	102.7	81.3	75.0, 71.8	60.2
V6 _I of 1,6-hexanediol	102.6	81.8	74.7, 72.0	62.1
V6 _{II} of 1-butanol	102.4	81.8	74.7, 71.7	61.0
V6 _{II} of 1,6-hexanediol	102.4	81.9	74.8, 71.7	60.8
V6 _{II} of hexanoic acid	102.4	81.5	75.1, 71.7	60.1
V6 _{III} of glycerol	102.3	82.6 ^{a,b}	74.3, 72.1	61.8
New allomorph of 4-hydroxybenzoic acid	102.4 ^{a,c}	81.2 ^{a,d}	73.8, 73.5, 72.0	61.0 ^{a,e}
New allomorph of (-)-borneol	103.3	82.2 ^{a,f}	76.4, 74.1, 72.0	60.4
New allomorph of (R)-(+)-camphor	103.3	82.2 ^{a,f}	74.4, 72.0	60.4
V7 of ibuprofen	103.3	81.9	74.3, 71.8	60.1
V7 of isopropanol	103.6	81.9	74.6-74.3, 71.8	60.3
V7 of butanoic acid	103.4	81.9	74.9-74.1, 71.7	60.1
New allomorph of 1-naphthol	103.4 ^{a,g}	82.8 ^{a,h}	76.1, 73.8, 72.2	60.8 ^{a,i}
New allomorph of quinoline	103.4	82.8	72.4	60.7
New allomorph of salicylic acid	103.9	83.1	73.7, 72.8, 72.0	60.8
V8 of salicylic acid	103.9	83.4	73.8, 73.1, 72.2	60.5
V8 of quinoline	104.3	82.9	75.1, 74.0, 72.1	60.3

^a weight-highest values; ^b individual values: 84.2, 82.6, 80.2 ppm; ^c individual values: 102.4, 101.4, 98.5 ppm; ^d individual values: 83.7, 81.2, 78.9 ppm; ^e individual values: 64.3, 61.0, 57.8 ppm; ^f individual values: 83.9, 82.2, 79.8 ppm; ^g individual values: 105.9, 103.4, 98.5 ppm; ^h individual values: 84.4, 82.8, 79.8 ppm; ⁱ individual values: 63.4, 60.8, 59.8, 57.8 ppm.

Finally, V6_I and V6_{II} complexes exhibit very similar spectra, with a slightly upfield shift observed for the C1 resonance of V6_{II} (102.4 ppm) with respect to that of V6_I (102.6-102.7 ppm), in agreement with the conclusions of Le Bail et al. (2005). The complexing agents appear to have no significant effect on the chemical shifts of the glucosyl carbons in these allomorphs. On the other hand, the V6_{III} spectrum exhibits by a triplet C4 resonance at lower field than that of V6_I and V6_{II}. V_{4-hydroxybenzoic acid} yielded a distinctive spectrum with triplet resonances of C1, C4 and C6. For 7-fold complexes, V_{(-)-borneol}, the isomorphous V_{(R)-(+)-camphor} and V_{1-naphthol} can also easily be recognized by the multiplicity of C4 resonance in V_{(-)-borneol} and the isomorphous V_{(R)-(+)-camphor} and of C1, C4 and C6 resonances in V_{1-naphthol}. In the spectra of V7 complexes and the new allomorph V_{quinoline}, only one signal was observed for each carbon. However, the resonances are much broader and the C4 resonance is found at lower field for V_{quinoline}. As for V8 families, the new allomorph of V_{salicylic acid} has a spectrum closely similar to V8 of the same complexing agent, with a slight shift in C4 resonance. However, the differences in spectral features between V8 complexes of salicylic acid and quinoline are recognizable (Annex 2,

Figure S.IV.2), which is consistent with slight differences in unit cell parameters and peaks intensity observed in ED and XRD. This suggests that the chemical shifts in V8 complexes are sensitive not only to the crystal structure but also to the nature of the complexing agents.

IV.14. Classification of complexes – proposition of a nomenclature

In the present study, 5 new V-amylose allomorphs have been identified, increasing the number of known allomorphic families to 10. In order to facilitate the identification of different allomorphs, we have established a nomenclature system on the basis of that proposed by Helbert (1994), in which the complexes are classified as a function of their helical conformation, interstitial space in the unit cell and complexing agent. Each allomorph is named "V_x_y", where "V" represents V-amylose, "x" is an Arabic number (6, 7, 8) representing the helicity of amylose, subscript "y" is Roman (I, II, III, etc.) referring to an ascending order of interstitial space of "unit cell" containing the same number of helices.

Table IV.3 summarizes the helical conformation and the unit cell parameters and the name assigned for each allomorph. According to the present nomenclature, the name of V6_I, V6_{II}, V6_{III} remains the same while V7 and V8 will be called V7_{II} and V8_{II}, respectively. The new allomorphs V_{4-hydrobenzoic acid}, V_{(-)-borneol}, V_{1-naphthol}, V_{quinoline} and V_{salicylic acid} are named V6_{IV}, V7_I, V7_{III}, V7_{IV} and V8_I, respectively. Since one allomorph can be obtained with different complexing agents, it is necessary to add the name of the complexing agent in order to clearly define a complex (Helbert, 1994). For example, V6_I obtained with ethanol will be named V6_I(ethanol). It is important to note that the present crystallographic data did not allow an unambiguous determination of the helical conformation V6_{IV}(4-hydroxybenzoic acid) and V7_{III}(1-naphthol). The nomenclature may thus be temporary and depend on future results.

Figure IV.49 shows the models proposed for V6_I (Brisson et al., 1991; Rappenecker & Zugenmaier, 1981), V6_{II} (Helbert & Chanzy, 1994), V6_{III} (Winter & Sarko, 1974), V7_{II} (Nishiyama et al., 2010), V8_{II} (Cardoso et al., 2007), as well as the new allomorphs. In all constructed V-amylose models, left-handed helices are arranged as antiparallel pairs, consistent with the concept of chain-folding. For V6_I, V7_I, V7_{III}, V7_{IV} and V8_I, the proposed arrangements of amylose are rather compact, and the complexing agents would only be located inside the helix. In contrast, there is more interstitial space in V6_{II}, V6_{III}, V6_{IV}, V7_{II} and V8_{II}, to accommodate guest molecules. Besides, since V6_{IV} was obtained with 4-hydroxybenzoic acid whose size appears to be incompatible with the cavity of a 6-fold helix, the cyclic complexing agent should be located in interstitial space. For other complexes, the complexing agents can possibly be located inside the helix.

Table IV.3. Symmetry, unit cell parameters and interhelical space per helix of V-amylose allomorphs determined from XRD powder data.

Allomorph	Name	Space group	Crystal system	Unit cell parameters			Number of helices per unit cell	Interhelical space per helix (nm ³) ^c
				<i>a</i> (nm)	<i>b</i> (nm)	<i>c</i> (nm)		
V6 _I	V6_I	<i>P2</i> ₁ <i>2</i> ₁ <i>2</i> ₁	orthorhombic	1.372 ± 0.006	2.376 ± 0.006	0.809 ± 0.008	2	0.126
		<i>P6</i> ₅ <i>22</i>	hexagonal	1.372 ± 0.006	1.372 ± 0.006	0.809 ± 0.008	1	
V6 _{II}	V6_{II}	<i>P2</i> ₁ <i>2</i> ₁ <i>2</i> ₁	orthorhombic	2.646 ± 0.009	2.705 ± 0.013	0.807 ± 0.009	4	0.254
V6 _{III}	V6_{III}	<i>P2</i> ₁ <i>2</i> ₁ <i>2</i> ₁	orthorhombic	1.913 ± 0.006	1.913 ± 0.010	0.814 ± 0.002	2	0.290
V ₄ -hydroxybenzoic acid ^a	V6_{IV}	<i>P2</i> ₁ <i>2</i> ₁ <i>2</i> ₁	orthorhombic	1.550 ± 0.001	2.836 ± 0.001	0.790 ± 0.001	2	0.572
V ₍₋₎ -borneol ^a	V7_I	<i>P1</i>	orthorhombic	1.526 ± 0.017	2.643 ± 0.029	0.803 ± 0.008	2	0.200
V7	V7_{II}	<i>P2</i> ₁ <i>2</i> ₁ <i>2</i> ₁	orthorhombic	2.813 ± 0.013	2.973 ± 0.011	0.797 ± 0.001	4	0.258
V ₁ -naphthol ^a	V7_{III}	<i>P1</i>	orthorhombic	1.663 ± 0.001	2.518 ± 0.001	0.856 ± 0.001	2	0.280
V _{quinoline} ^a	V7_{IV}	<i>P2</i> ₁ <i>2</i> ₁ <i>2</i> ₁	orthorhombic	2.702 ± 0.001	3.291 ± 0.001	0.786 ± 0.001	4	0.358
V _{salicylic acid} ^a	V8_I	<i>P2</i> ₁	monoclinic ^b	3.245 ± 0.006	3.246 ± 0.005	0.793 ± 0.001	4	0.232
V8	V8_{II}	<i>P4</i> ₃ <i>2</i> ₁ <i>2</i>	tetragonal	2.313 ± 0.006	2.313 ± 0.006	0.790 ± 0.001	2	0.485

^a new allomorphs^b $\gamma = 116.62 \pm 0.13^\circ$ ^c interhelical space per helix = [unit cell volume - N.(π .d²/4)]/N, where N is the number of helix per unit cell; d is the external helix diameter and is 1.37, 1.50 and 1.62 nm for V6, V7, and V8 helix, respectively.

It is important to note that the proposed models describe possible arrangements of amylose helices in the allomorphs rather than their precise atomic positions. For example, as suggested from ^{13}C solid-state NMR data, the amylose helices are likely less symmetrical than the rigid ones used in the models, especially for V6_{IV} and V7_{III}. However, these models can be used as starting hypotheses for other studies by molecular dynamics or structure refinement.

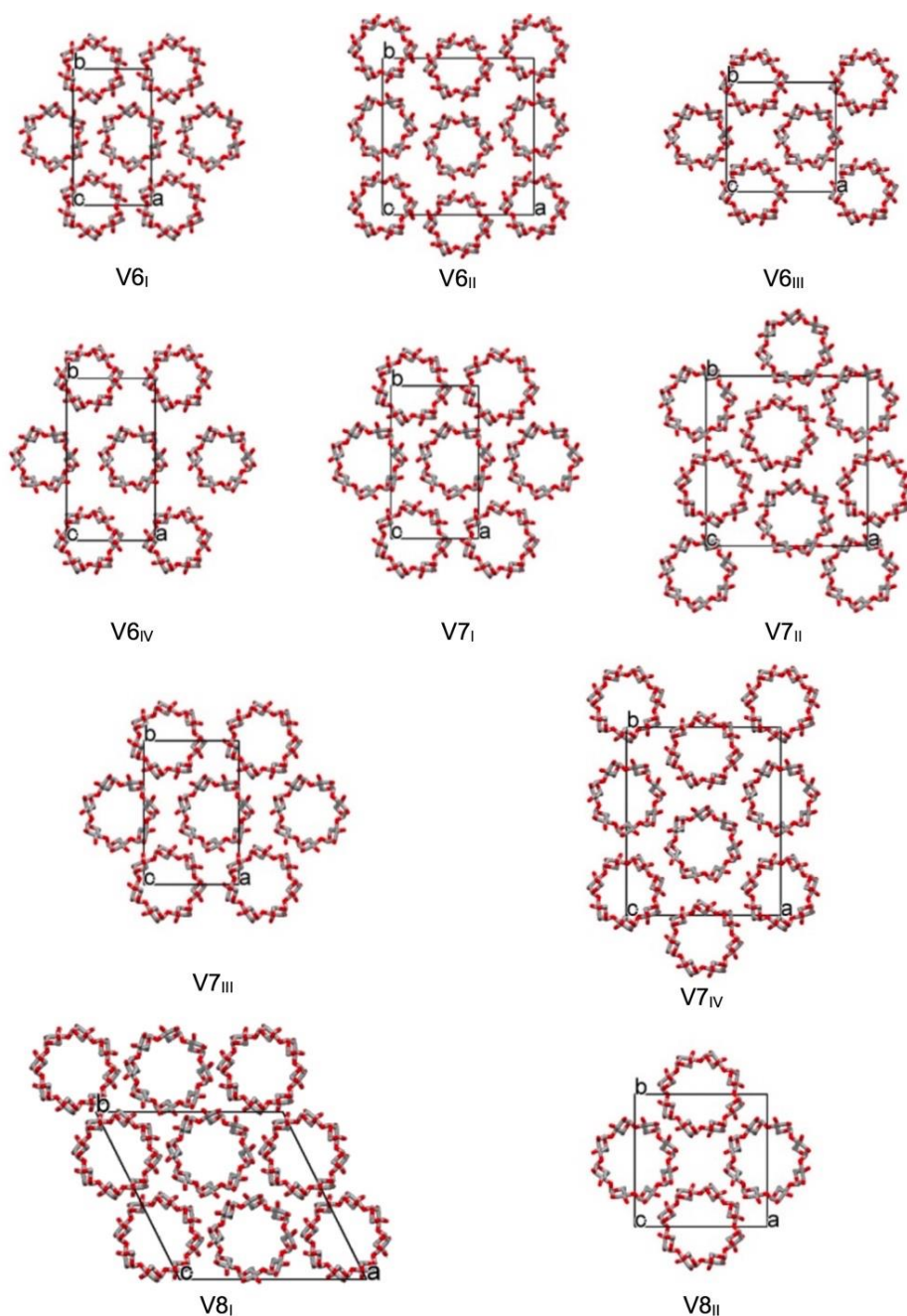


Figure IV.49. Tentative geometrical molecular models projected on the (a,b) plane of the unit cell of V-amylose allomorphs. Symmetrical left-handed helices with the hydroxymethyl group in *gg* conformation were used. Hydrogen atoms were removed for clarity.

IV.15. Conclusions

The investigation of the complexation of amylose with about 120 small organic molecules allowed identifying 10 different allomorphic families of lamellar V-amylose crystals. Interestingly, five of them are new allomorphs. A new nomenclature was proposed for these allomorphs based on the helical conformation and relative interhelical space of unit cells. Consequently, the 10 allomorphs were named: V6_I, V6_{II}, V6_{III}, V6_{IV}, V7_I, V7_{II}, V7_{III}, V7_{IV}, V8_I and V8_{II}. Each allomorph can be obtained with different complexing agents. However, V6_I, V6_{II} and V7_{II} appear to be more prevalent. Our results also confirmed that the helical conformation is related to the size of the complexing agent. V6 complexes were obtained with molecules with straight carbon chains, while branched-chain and cyclic molecules tended to yield 7-fold complexes. V8 complexes were obtained with 1-naphthol, quinoline and salicylic acid. However, it is still difficult to predict the crystal structure based on the nature of the guest since many complexing agents were shown to induce different crystal structures, helical conformation or helix packing.

The model lamellar crystals corresponding to V6_{II}, V6_{IV}, V7_{II}, and V7_{III} exhibited distinct morphologies. On the other hand, those with the V6_I, V7_I, V7_{IV} and V8_I structures showed very similar shapes. The morphology of V6_{III} and V8_{II} were similar as well. However, the different allomorphs could be distinguished without ambiguity by their base-plane ED or powder XRD patterns.

The FT-IR spectroscopy data showed an increase in intensity of vibrational bands near 1408, 1370, 1295, 1104, 1022 and 946 cm⁻¹ for V-amylose compared to amorphous or A- and B-amylose. These differences can be accounted for different amylose helical conformations in these forms. In addition, the band near 1022 cm⁻¹ can be used as a fingerprint for V-amylose.

The ¹³C solid-state NMR study showed a significant correlation between C1 resonances and the helicity of amylose. The C1 resonance shifted downfield with increasing number of glucosyl units per turn from 6 to 8. The result thus allowed determining the helical conformation of the new allomorphs. In addition, the C1 resonance appears as a multiplet in V6_{IV} and V7_{III} while it is a singlet in other allomorphs suggesting that V6_{IV} and V7_{III} would contain helices that are less symmetrical than those in other allomorphs.

Based on the above crystallographic data, tentative models were proposed for each allomorph. Water was shown to play an important role on the stability and the crystallinity of the complexes. Upon drying, V6_I, V6_{II}, V6_{IV}, V7_I, V7_{II}, V7_{IV} were transformed into compact hexagonal structures. For V7_{III}, V8_I and V8_{II}, a significant loss in crystallinity was observed, but the crystal structure remained the same. V6_{III} is the only structure that was stable upon drying.

Chapter V

Factors affecting the crystallization and crystal structure of V-amylose

V.1. Introduction

The crystal structure of V-amylose depends not only on the nature of the complexing agent but also on the conditions of crystallization (Helbert, 1994; Simpson et al., 1972; Takeo et al., 1973). Evidence supports that the helical conformation of amylose is related to the size of the complexing molecules (Helbert, 1994; Rutschmann & Solms, 1990; Takeo et al., 1973; Takeo & Kuge, 1969; Yamashita et al., 1973; Yamashita & Hirai, 1966). Indeed, isomorphous complexes can be obtained with molecules with a similar size. The amylose helices are thought to be in a minimum-energy conformation stabilized by complexing agents and water (Helbert, 1994).

On the other hand, with a given molecule, V-amylose may occur in more than one crystal structure with different helical conformations or packing arrangements (Helbert, 1994; Oguchi et al., 1998; Simpson et al., 1972; Takeo et al., 1973). This phenomenon is called *polymorphism* and has been observed for many other organic and inorganic systems, as reviewed by Bernstein (2002). The formation of different allomorphs requires applying a variety of crystallization conditions (Bernstein, 2002, 2011). The conventional crystallization of V-amylose in solution generally allows varying the following parameters: concentration of complexing agent and amylose, solvent, solvent mixture, temperature, cooling rate and DP of amylose. However, only concentration of complexing agent and solvent (with or without DMSO) have been reported to affect the resulting crystal structure (Helbert, 1994; Oguchi et al., 1998; Simpson et al., 1972; Takeo et al., 1973), whereas other factors control the yield, morphology and crystallinity of the complexes (Bhosale & Ziegler, 2010; Biliaderis & Galloway, 1989; Buléon et al., 1984; Cardoso, 2007; Dvonch et al., 1950; Gelders et al., 2004; Godet et al., 1995b; Karkalas et al., 1995; Nuessli et al., 2003; Whittam et al., 1989). It must also be noted that there is still a lack of systematic studies of V-amylose polymorphism. In most of the previous investigations, the different complexes were usually prepared in similar conditions (Biais, 2006; Helbert, 1994; Takeo et al., 1973; Takeo & Kuge, 1969, 1971).

In the present study, the complexes were prepared in different conditions of solvent (with or without DMSO), concentration of complexing agents and amylose, temperature and DP of amylose. This method allowed identifying for the first time five new allomorphs of V-amylose (see Chapter IV) and complexes with molecules that had been reported to be unable to form V-amylose from solution (ethyl butyrate, citral, 4-hydroxybenzoic acid, salicylic acid, 2-naphthol and quinoxaline). Furthermore, by comparison to what was reported in the literature,

polymorphism was observed for a large number of complexes. These results provide unique data on the factors that govern the formation of crystals and their structure.

V.2. Complexes with straight-chain *n*-alcohols, *n*-diols, *n*-amines, dicarboxylic acids, octanal, stearamide

The complexation of amylose with homologous series of straight-chain saturated *n*-alcohols (2-16 carbons), *n*-diols (2-6 carbons), *n*-amines (4-12 carbons), dicarboxylic acids (2-12 carbons), octanal and stearamide were conducted in 0.1 wt% aqueous amylose solutions at different temperatures and concentrations of complexing agent. As shown in **Table V.1**, all complexing agents, except *n*-amines having 2-4 carbons and dicarboxylic acids having 2-6 carbons, formed crystalline complexes with amylose. It is still unclear why the short-chain dicarboxylic acids do not complex amylose while diols and monocarboxylic acids with the same number of carbons do. For the water-miscible short-chain *n*-amines, it is possible that the amylose complexes may be not stable in basic solutions of these complexing agents due to the increased solubility of amylose. Longer *n*-amines are more hydrophobic and thus favor a localization in the hydrophobic cavity of amylose helices. Therefore, their inclusion complexes may be more stable and able to crystallize.

All molecules having complexing ability induced V6-type complexes. The result agrees with the previous conclusion of Takeo and Kuge (1969) that linear molecules, whose cross-sectional diameter is about 0.30 nm, form 6-fold helices. Interestingly, most of them can form both V6_I and V6_{II} crystals, some examples of which are shown in **Figure V.1**. This rather general complexing behavior is unexpected as it had only been previously observed for some dicarboxylic acids, *n*-alcohols having 3-5 carbons and hexanoic acid while other *n*-alcohols and diols were reported to form only V6_I (Biais, 2006; Helbert, 1994; Takeo et al., 1973).

In these polymorphic systems, the formations of V6_I and V6_{II} depend on the crystallization temperature. A general rule is that V6_{II} is preferred at relatively lower temperature (25-50 °C) while an incubation of the same complexation mixture at higher temperature (60-75 °C) favors the formation of V6_I (**Table V.1** and **Annex 3, Figure S.V.1**). The result suggests that the compact structure V6_I is more thermally stable than V6_{II}.

The crystal structure of complexes with 1-propanol, 1,4-butanediol and 1,6-hexanediol also varies with the concentration of complexing agent: V6_I is favored with a higher concentration of complexing agent compared to V6_{II} (**Table V.1** and **Annex 3, Figure S.V.2**). Helbert (1994) reported a similar result for 1-propanol. However, for 1,4-butanediol, the author only obtained

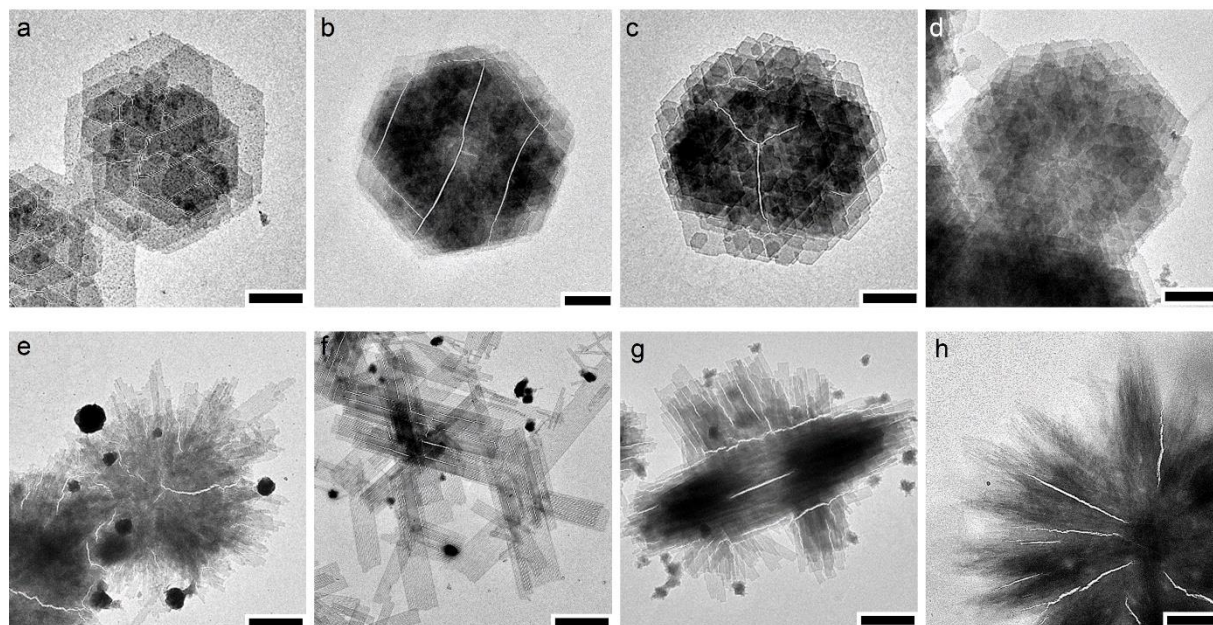


Figure V.1. TEM images of V_{6I} (a-d) and V_{6II} crystals (e-h) obtained with 1-hexadecanol (a,e), dodecanedioic acid (b,f), octanal (c,g) and stearamide (d,h). Scale bars: 1 μm .

V_{6I} for all tested concentrations of complexing agent. In fact, in the study of Helbert (1994), the complexes were prepared at 50 °C while the present study showed that 1,4-butanediol induces the formation of V_{6II} at ≤ 40 °C. The variation of crystal structure with the concentration of complexing agent may be related to a dehydration effect (Helbert, 1994). A sufficiently high concentration of complexing agents may capture water molecules, leading to a dehydration of amylose. This effect favors the formation of the compact structure V_{6I} over the looser V_{6II} (Helbert, 1994). Indeed, previous studies showed that V_{6II} was transformed into V_{6I} upon a release of water molecules (Booy et al., 1979; Helbert & Chanzy, 1994; Hinkle & Zobel, 1968). The hypothesis can also be accounted for the fact that ethanol or 1,2-ethanediol, which have to be used at a high concentration (≥ 40 vol%) for the complexation, only yield V_{6I}.

Furthermore, the crystallization of homologous series of *n*-alcohols and *n*-diols showed that the critical concentration required for the complex formation decreased with increasing chain length. This would be due to the increased hydrophobicity of the complexing agent which favors its association with amylose helices instead of water. In addition, the increase of complexing agent concentration allowed the crystallization to occur at higher temperature. This would be due to a higher dehydration effect which would decrease the solubility of amylose.

Moreover, the maximum crystallization temperature also increases with the chain length of complexing agents. For example, V_{*n*-butanol} crystallized at ≤ 50 °C, while V_{*n*-pentanol} crystallized at ≤ 60 °C and the complexes with longer *n*-alcohols could crystallize at up to 75 °C. A similar

effect was also observed for *n*-amines. This result suggests that the thermal stability of the V-amylose crystals increases with the chain length of the complexing agents. The lack of stability of V_{*n*-butanol} at high temperature (60-75 °C) would be the reason why V6_I crystals cannot be obtained with the complexing agent from the crystallization in aqueous solution. Indeed, Helbert (1994) reported that to obtain V6_I with *n*-butanol, DMSO must be added to increase the solubility of *n*-butanol and thus increases the concentration of the complexing agent. In that case, the formation of V6_I would be a result of a dehydration effect on amylose.

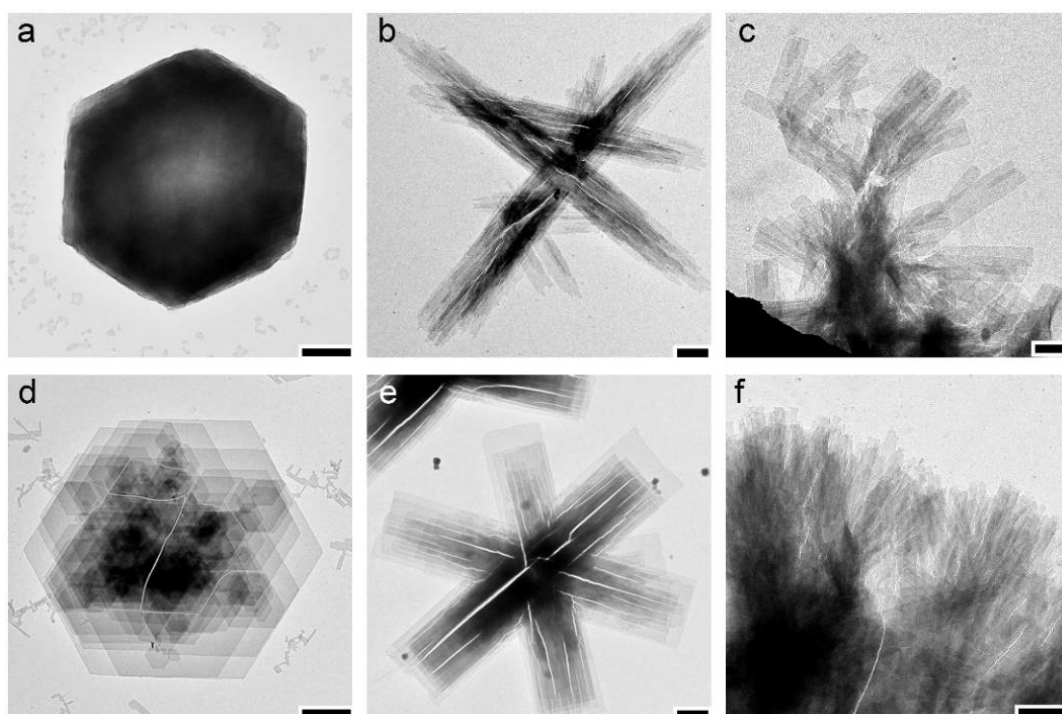


Figure V.2. TEM images of V6_I (a,d), V6_{II} (b,e) and V7_{II} (c,f) crystals obtained with butanoic acid (C4) (a-c) and decanoic acid (C10) (d-f). Scale bars: 1 μm.

V.3. Complexes with straight-chain saturated fatty acids

The crystallization of amylose from dilute solutions in the presence of a series of linear saturated fatty acids (C3 to C20) was investigated by varying the fatty acid concentration, crystallization temperature and solvent composition (DMSO:water in various ratios). **Table V.2** summarizes the allomorphic types observed for complexes formed with each fatty acid. A general observation is that all complexing agents could induce more than one crystalline structure. Specifically, propanoic acid (C3) formed V6_I and V7_{II} while all longer-chain fatty acids (C4-C20) promoted the formation of V6_I, V6_{II} and V7_{II}, such as those shown for V_{butanoic acid} and V_{decanoic acid} (**Figure V.2**).

Table V.1. V-type complexes with *n*-alcohols, *n*-amines, dicarboxylic acids, octanal and stearamide as a function of crystallization temperature and concentration of complexing agent (C). The amylose solutions and complexing agents were mixed at 90 °C, then kept at a given crystallization temperature, or allowed to slowly cool down to room temperature in a Dewar container. For mixtures, the major and minor allomorphs are indicated.

Complexing agent	C (%)	Incubation temperature (°C)					Cooling
		25	40	50	60	75	
ethanol	40-50	n. t.	V6 _I	V6 _I	V6 _I	V6 _I	n. t.
1-propanol	20-25	n. t.	V6 _{II}	V6 _{II}	-	-	n. t.
"	30	n. t.	V6 _I > V6 _{II}	V6 _I > V6 _{II}	V6 _I > V6 _{II}	-	n. t.
1-butanol	*	n. t.	V6 _{II}	V6 _{II}	-	-	n. t.
1-pentanol	*	n. t.	V6 _{II}	V6 _{II}	V6 _I > V6 _{II}	-	n. t.
<i>n</i> -alcohols (8-16 carbons)	*	n. t.	V6 _{II}	V6 _{II}	V6 _I > V6 _{II}	V6 _I	n. t.
<i>n</i> -amines (2-4 carbons)	10-60	n. t.	-	-	-	-	n. t.
1-hexylamine	*	n. t.	V6 _{II}	V6 _{II}	V6 _I > V6 _{II}	-	n. t.
<i>n</i> -amines (7-12 carbons)	*	n. t.	V6 _{II}	V6 _{II} > V6 _I	V6 _I > V6 _{II}	V6 _I	n. t.
dicarboxylic acids (2-6 carbons)	*	n. t.	-	-	-	-	n. t.
dicarboxylic acids (9-12 carbons)	*	n. t.	V6 _{II}	V6 _{II} > V6 _I	V6 _I > V6 _{II}	V6 _I	n. t.
octanal	*	n. t.	V6 _{II}	V6 _{II}	V6 _I > V6 _{II}	V6 _I	n. t.
stearamide	*	n. t.	V6 _{II}	V6 _{II}	V6 _I > V6 _{II}	V6 _I	n. t.
1,2-ethanediol	30	-	-	-	-	-	n. t.
"	40	V6 _I	-	-	-	-	n. t.
"	50	V6 _I	V6 _I	-	-	-	n. t.
"	60	V6 _I	V6 _I	V6 _I	-	-	n. t.
"	80	V6 _I	V6 _I	V6 _I	V6 _I	V6 _I	n. t.
1,4-butanediol	10	V6 _{II}	-	-	-	-	V6 _{II}
"	15	V6 _{II}	-	-	-	-	V6 _{II}
"	20	V6 _{II}	-	-	-	-	V6 _{II}
"	25	V6 _{II}	V6 _{II}	-	-	-	V6 _{II}
"	30	V6 _{II} > V6 _I	V6 _I > V6 _{II}	-	-	-	V6 _I > V6 _{II}
"	35	V6 _I	V6 _I	V6 _I	-	-	V6 _I
"	40	V6 _I	V6 _I	V6 _I	V6 _I	-	V6 _I
"	50-60	V6 _I	V6 _I	V6 _I	V6 _I	V6 _I	V6 _I
1,6-hexanediol	0.5	-	-	n. t.	-	-	-
"	1	V6 _{II}	V6 _{II}	-	-	-	V6 _{II}
"	2.5	n. t.	V6 _{II}	V6 _{II}	-	-	V6 _{II}
"	5.0	n. t.	V6 _{II}	V6 _{II}	V6 _{II}	-	V6 _{II}
"	10.0	n. t.	V6 _{II}	V6 _{II}	V6 _{II} > V6 _I	-	V6 _{II}
"	15.0	n. t.	V6 _{II}	V6 _{II}	V6 _I > V6 _{II}	V6 _I	V6 _{II}
"	20.0	n. t.	V6 _{II}	V6 _{II}	V6 _I > V6 _{II}	V6 _I	V6 _I > V6 _{II}

* The complexing agent was used at saturated; n. t.: not tested; -: no precipitate was observed

Table V.2. Summary of the allomorphs observed for the crystalline complexes of V-amylose with linear fatty acids as a function of the number of carbon atoms in the fatty chain and comparison with previous works.

Fatty acid	Previous works	This work
propionic / propanoic acid (C3)	V6 _I ^{a,b} , V7 _{II} ^{a,b}	V6 _I , V7 _{II}
butanoic / butyric acid (C4)	V6 _I ^b , V7 _{II} ^{a,b}	V6 _I , V6 _{II} , V7 _{II}
pentanoic / valeric acid (C5)	V7 _{II} ^{a,b}	V6 _I , V6 _{II} , V7 _{II}
hexanoic / caproic acid (C6)	V6 _I ^a , V6 _{II} ^c	V6 _I , V6 _{II} , V7 _{II}
octanoic / caprylic acid (C8)		
decanoic / capric acid (C10)		
dodecanoic / lauric acid (C12)		
tetradecanoic / myristic acid (C14)	V6 _I ^{a,b}	V6 _I , V6 _{II} , V7 _{II}
hexadecanoic / palmitic acid (C16)		
octadecanoic / stearic acid (C18)		
icosanoic / arachidic acid (C20)*		

^a Takeo et al. (1973), ^b Helbert (1994), ^c Biais (2006);

* The crystal type of V_{icosanoic acid} has not previously been reported.

This result is unexpected as polymorphism was only previously reported for propanoic, butanoic and hexanoic acids (Table V.2). In addition, all the tested fatty acids induced the formation of both 6- and 7-fold helices whereas earlier works reported that the amylose conformation depended on the chain length of the complexing agent. In particular, the occurrence of V7_{II} with long-chain fatty acids C6-C20 has never been reported.

Considering the cross-sectional diameter of the linear fatty acids (*ca.* 0.30 nm), V6 structures are expected rather than V7_{II}. V7_{II} is usually obtained with bulkier molecules such as branched alcohols or monoterpenes whose cross-sectional diameter is about 0.45-0.60 nm (Takeo & Kuge, 1969). In this context, Shogren et al. (2006) proposed that the formation of 7-fold helices with fatty acids was due to the interaction of amylose with fatty acid "dimers", the association of which would be promoted by hydrophobic interactions between the alkyl moieties (Mukerjee, 1965). However, our results showed that V7_{II} was favored by water-miscible fatty acids (C3 and C4) than by the poorly-soluble ones. Moreover, several complexes formed at high temperature (90 °C) at which the existence of fatty acid "dimers" in solution was unlikely. Therefore, the 7-fold helical conformation is more likely controlled by a specific interaction between fatty acids and amylose rather than by the molecular dimension of the guest. As proposed by Takeo et al. (1973), the inclusion of the polar head (*i.e.* the carboxyl group) of the fatty acid in the amylose helix could be responsible for its enlargement to the V7 conformation.

In contrast, straight-chain molecules bearing a different functional group such as aliphatic *n*-alcohols and aldehydes have been reported to only induce the formation of 6-fold helices (Conde-Petit et al., 2006; Helbert, 1994). Besides, previous numerical simulations and NMR data concluded that the linear alkyl moiety was included inside the 6-fold helix while the polar head remained outside (Godet et al., 1993; Kawada & Marchessault, 2004; Lebail et al., 2000; Snape et al., 1998). In addition, the hypothesis that the inclusion of the carboxyl group controls the helical conformation somewhat agrees with the fact that V7_{II} is preferred with shorter fatty acids (C3-C5) while V6_I is favored with C6-C20 fatty acids. It is possible that with a longer chain length, the influence of the linear aliphatic chain gets predominant over that of the carboxyl group in determining the size of helix and thus would induce mainly 6-fold helical complexes (Takeo et al., 1973). Expanding from the modeling work of Godet et al. (1993), further simulations must be carried out to elucidate the role of the carboxyl group and its interaction with amylose in the determination of its helical conformation.

Tables V.3 to V.5 summarize the results obtained with different solvent compositions, fatty acid concentrations and crystallization temperatures. For a given fatty acid, different allomorphs can crystallize alone or concomitantly, depending on the crystallization conditions. Selected examples of coexistences of the allomorphs are illustrated by TEM images (**Figure V.3**) and XRD diagrams (**Figure V.4**). The concomitant crystallization has previously been reported for many polymorphic systems as reviewed by Bernstein et al. (1999). The phenomenon has been explained by the fact that so-called occurrence domains, defined by sets of conditions at which specific allomorphs crystallize, could be independent or overlap. When the occurrence domain is unique, only one form is obtained, which is usually the most thermodynamically stable. In contrast, in regions where the domains overlap, two or more forms would crystallize under identical conditions. These concomitant allomorphs are energetically close and their relative amount is mainly governed by kinetic stability (Bernstein et al., 1999; Bučar et al., 2015).

Since we have only characterized the morphology and structure of the final products, the precise chronology of crystallization events was lost. The possibility that the amylose chains form nuclei and crystallize under conditions that depend on their length (so-called fractionated crystallization) or on the temperature (during cooling) cannot be ruled out. One allomorph would crystallize after the other and the allomorph formed first may even act as a seed for nucleation and epitaxial growth of the second one. As illustrated by **Figures V.3a** and **V.3b**, rectangular V6_{II} and hexagonal V6_I crystals are often associated with specific orientation

Table V.3. Allomorphic type of $V_{\text{fatty acid}}$ crystals formed in water at different fatty acid concentrations ($C_{\text{fatty acid}}$) and temperatures. The amylose solutions and fatty acids were mixed at 90 °C, then kept at a given crystallization temperature, or allowed to slowly cool down to room temperature in a Dewar container. For mixtures, the major and minor allomorphs are indicated.

Fatty acids	Physical state of the fatty acid at 25 °C	$C_{\text{fatty acid}}$	Crystallization temperature (°C)					
			40	50	60	75	90	Slow cooling
C3	water-miscible liquid	30 vol%	$V_{7\text{II}} > V_{6\text{I}}$	-	-	-	-	$V_{7\text{II}} > V_{6\text{I}}$
"	"	40 vol%	$V_{7\text{II}} > V_{6\text{I}}$	$V_{6\text{I}} > V_{7\text{II}}$	$V_{6\text{I}} > V_{7\text{II}}$	$V_{6\text{I}} > V_{7\text{II}}$	-	$V_{7\text{II}} > V_{6\text{I}}$
"	"	50 vol%	$V_{6\text{I}} > V_{7\text{II}}$	$V_{6\text{I}} > V_{7\text{II}}$	$V_{6\text{I}} > V_{7\text{II}}$	$V_{6\text{I}} > V_{7\text{II}}$	-	$V_{6\text{I}} > V_{7\text{II}}$
C4	water-miscible liquid	5-10 vol%	$V_{7\text{II}} > V_{6\text{II}} > \text{B}$	-	-	-	-	$V_{7\text{II}} > V_{6\text{II}} > \text{B}$
"	"	20-40 vol%	$V_{7\text{II}} > V_{6\text{I}}$	$V_{7\text{II}} > V_{6\text{I}}$	$V_{7\text{II}} > V_{6\text{I}}$	$V_{7\text{II}} > V_{6\text{I}}$	-	$V_{7\text{II}} > V_{6\text{I}}$
"	"	50 vol%	$V_{6\text{I}} > V_{7\text{II}}$	$V_{6\text{I}} > V_{7\text{II}}$	$V_{6\text{I}} > V_{7\text{II}}$	$V_{6\text{I}} > V_{7\text{II}}$	-	$V_{6\text{I}} > V_{7\text{II}}$
C5	water-immiscible liquid	2.5-5 vol%	$V_{6\text{II}}$	$V_{6\text{I}} > V_{6\text{II}}$	$V_{6\text{I}} > V_{6\text{II}}$	-	-	$V_{6\text{II}}$
C6	water-immiscible liquid	*	$V_{6\text{II}}$	$V_{6\text{II}} > V_{6\text{I}}$	$V_{6\text{I}}$	-	-	$V_{6\text{II}} > V_{6\text{I}}$
C8	water-immiscible liquid	*	$V_{6\text{II}}$	$V_{6\text{II}}$	$V_{6\text{I}}$	$V_{6\text{I}}$	-	$V_{6\text{II}} > V_{6\text{I}}$
C10-C20	solid	*	$V_{6\text{II}}$	$V_{6\text{II}}$	$V_{6\text{I}} > V_{6\text{II}}$	$V_{6\text{I}}$	$V_{6\text{I}}$	$V_{6\text{II}} > V_{6\text{I}}$

C3: propanoic acid, C4: butanoic acid, C5: pentanoic acid, C6: hexanoic acid, C8: octanoic acid, C10: decanoic acid, C12: dodecanoic acid, C14: tetradecanoic acid, C16: hexadecanoic acid, C18: octadecanoic acid, C20: icosanoic acid.

*: the fatty acid was used at saturation

-: no precipitation

Table V.4. Allomorphic type of V_{fatty acid} crystals formed in the presence of 2 vol% DMSO at different fatty acid concentrations (C_{fatty acid}) and temperatures. The amylose solutions and fatty acids were mixed at 90 °C, then kept at a given crystallization temperature. For mixtures, the major and minor allomorphs are indicated.

Fatty acid	C _{fatty acid}	Crystallization temperature (°C)			
		40	60	75	90
C3	n. t.	n. t.	n. t.	n. t.	n. t.
C4	n. t.	n. t.	n. t.	n. t.	n. t.
C5	2.5 vol%	V7 _{II}	V7 _{II}	-	-
"	3 vol%	V7 _{II} > V6 _{II}	V7 _{II}	-	-
"	4-5 vol%	V6 _{II}	V7 _{II}	-	-
C6	*	V6 _{II}	V6 _I > V7 _{II}	V6 _I > V7 _{II}	-
C8-C20	*	n. t.	n. t.	V6 _I > V7 _{II}	V6 _I > V7 _{II}

C3: propanoic acid, C4: butanoic acid, C5: pentanoic acid, C6: hexanoic acid, C8: octanoic acid, C10: decanoic acid, C12: dodecanoic acid, C14: tetradecanoic acid, C16: hexadecanoic acid, C18: octadecanoic acid, C20: icosanoic acid.

*: the fatty acid was used at saturation

- : no precipitate was observed

n. t.: not tested

Table V.5. Allomorphic type of $V_{\text{fatty acid}}$ crystals formed in the presence of 10 vol% DMSO at different fatty acid concentrations ($C_{\text{fatty acid}}$) and temperatures. The amylose solutions and fatty acids were mixed at 90 °C, then kept at a given crystallization temperature, or allowed to slowly cool down to room temperature in a Dewar container. For mixtures, the major and minor allomorphs are indicated.

Fatty acid	$C_{\text{fatty acid}}$	Crystallization temperature (°C)					
		40	50	60	75	90	Slow cooling
C3	30 vol%	-	-	-	-	-	-
"	40-50 vol%	$V_{6I} > V_{7II}$	$V_{6I} > V_{7II}$	$V_{6I} > V_{7II}$	$V_{6I} > V_{7II}$	-	$V_{6I} > V_{7II}$
C4	5-10 vol%	$V_{7II} > V_{6II} > B$	-	-	-	-	$V_{7II} > V_{6II} > B$
"	20-30 vol%	$V_{7II} > V_{6I}$	$V_{7II} > V_{6I}$	$V_{7II} > V_{6I}$	$V_{7II} > V_{6I}$	-	$V_{7II} > V_{6I}$
"	40-50 vol%	$V_{6I} > V_{7II}$	$V_{6I} > V_{7II}$	$V_{6I} > V_{7II}$	$V_{6I} > V_{7II}$	-	$V_{6I} > V_{7II}$
C5	2.5 vol%	$V_{7II} > V_{6II}$	$V_{7II} > V_{6I}, V_{6II}$	-	-	-	n. t.
"	5 vol%	$V_{6II} > V_{7II}$	$V_{6II} > V_{6I}, V_{7II}$	$V_{6I} > V_{7II}$	-	-	$V_{6II} > V_{6I}$
C6	*	$V_{6I} > V_{6II}$	$V_{6I} > V_{6II}$	$V_{6I} > V_{7II}$	$V_{6I} > V_{7II}$	-	$V_{6I} > V_{6II}$
C8	*	$V_{6I} > V_{6II}$	V_{6I}	V_{6I}	$V_{6I} > V_{7II}$	-	$V_{6I} > V_{6II}$
C10, C12	*	V_{6I}	V_{6I}	V_{6I}	$V_{6I} > V_{7II}$	$V_{6I} > V_{7II}$	$V_{6I} > V_{7II}$
C14-C20	*	V_{6I}	V_{6I}	V_{6I}	V_{6I}	$V_{6I} > V_{7II}$	$V_{6I} > V_{7II}$

C3: propanoic acid, C4: butanoic acid, C5: pentanoic acid, C6: hexanoic acid, C8: octanoic acid, C10: decanoic acid, C12: dodecanoic acid, C14: tetradecanoic acid, C16: hexadecanoic acid, C18: octadecanoic acid, C20: icosanoic acid.

*: the fatty acid was used at saturation

-: no precipitate was observed

n. t.: not tested

relationships that were not precisely analyzed in the present study. However, since the images are projections of the crystal assemblies, one cannot clearly identify the crystallization sequence of each allomorph. In the case of coexisting V6_I and V7_{II} crystals, the latter ones are mostly observed as outgrowths of the former (**Figure V.3d**), suggesting that they formed the last. V6_{II} and V7_{II} crystals did not appear to be associated but rather independent from one another (**Figure V.3e,f**).

In our study, the fatty acid concentration, temperature, and solvent composition were shown to play important roles to regulate the formation and crystal structure of V_{fatty acids}. In general, the V6_I structure was favored at higher concentrations of fatty acid and DMSO (10 vol%), and at higher temperature (60-90 °C), whereas milder conditions of these parameters resulted in the formation of V6_{II} and V7_{II} (**Tables V.3-V.5** and **Annex 3, Figures S.V.3-S.V.6**). This result is in agreement with those previously obtained for other straight chain molecules (see § V.2): higher concentrations of complexing agent and higher temperatures favor more compact structures. Therefore, this supports the hypotheses on the effect of dehydration and the relative thermal stability of allomorphs. In the case of butanoic acid (C4), we observed that V6_{II} was more sensitive to dehydration than V7_{II}, the former appearing only with a fatty acid concentration ≤ 10 vol% while the latter was formed at higher concentrations. This also explains why V6_{II} could not be obtained with propanoic acid for which at least 30 vol% was required to form the complexes. In addition, for C5-C8 fatty acids, V6_{II} is formed at a lower temperature compared to V7_{II} (**Tables V.4** and **V.5**, and **Annex 3, Figure S.V.5**).

The impact of DMSO on the formation of specific allomorphs has been clearly highlighted. This molecule is a good solvent of amylose but also of fatty acids which results in an increase of concentration of the weakly soluble fatty acids and therefore, their availability for complexation. Helbert (1994) also observed different allomorphs for complexes prepared with *n*-butanol and *n*-pentanol that exhibited a V6_{II} structure when crystallized in water and V6_I in DMSO:water mixtures. It must also be noted that DMSO can form crystalline complexes with amylose (French & Zobel, 1967; Simpson et al., 1972). While Simpson et al. (1972) mentioned the occurrence of two allomorphs based on 6- and 7-fold amylose helices, Winter and Sarko (1974) described the V_{DMSO} unit cell as pseudo-tetragonal and containing antiparallel 6-fold helices, with DMSO molecules located inside and between helices. However, these complexes were only formed under anhydrous conditions by casting amylose / DMSO solutions and letting them to dry in a vacuum oven. Nevertheless, this shows that in specific conditions, DMSO no longer acts as a solvent of amylose but rather like a complexing agent that specifically interacts with amylose chains to form helical inclusion compounds.

The most remarkable effect of DMSO was its crucial role in the formation of V7_{II}. Our results showed that the complexes with C5-C20 fatty acids exhibited a V7_{II} structure only if DMSO was present, preferably 1-2 vol%. A significant role of DMSO on the conformation of amylose has been suggested by other authors (Cheetham & Tao, 1998; Germino & Valletta, 1964; Helbert, 1994; Jane et al., 1985; Simpson et al., 1972). DMSO may induce specific conformations for both amylose and fatty acids, although, so far, the nature of the interactions remains unknown and no evidence were produced regarding the presence of DMSO in the crystal structure of V_{fatty acids} complexes.

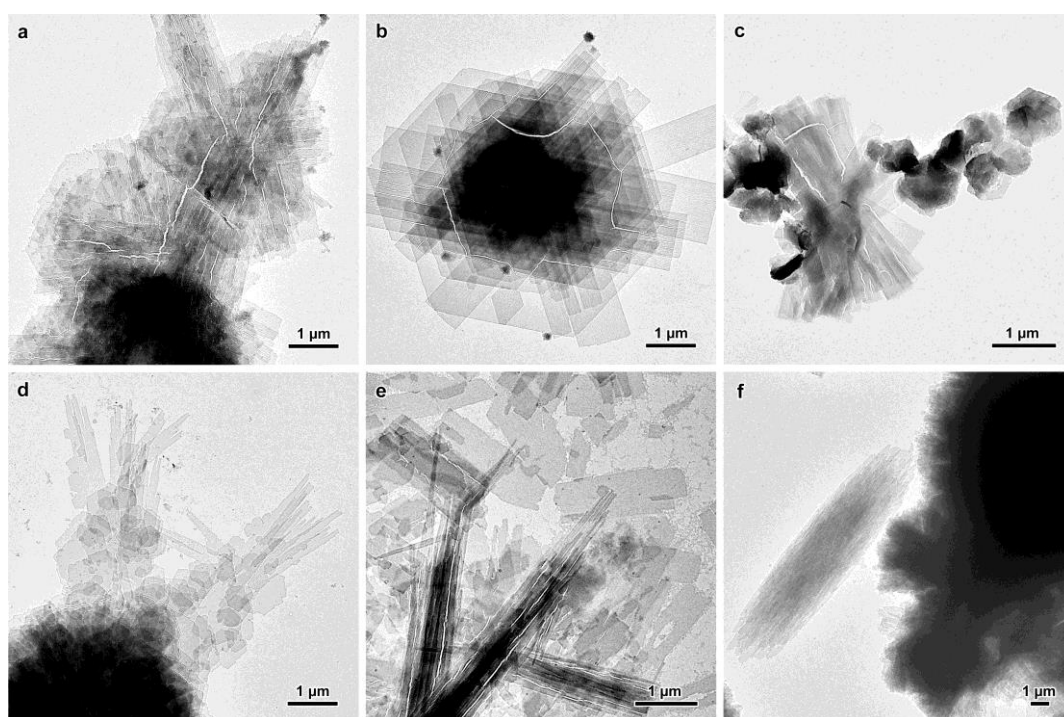


Figure V.3. Examples of coexisting crystals with different morphologies and allomorphic types prepared with a given fatty acid: a,b) V6_I and V6_{II} prepared in water with the saturation of hexanoic acid at 50 °C and tetradecanoic acid at 60 °C, respectively; c,d) V6_I and V7_{II} prepared in the presence of 10 vol% DMSO with 50% of butanoic acid at 60 °C and octadecanoic acid at 90 °C, respectively; e,f) V6_{II} and V7_{II} prepared with 5 vol% butanoic acid in water and 3 vol% pentanoic acid at 40 °C in the presence of 2 vol% DMSO, respectively (TEM images).

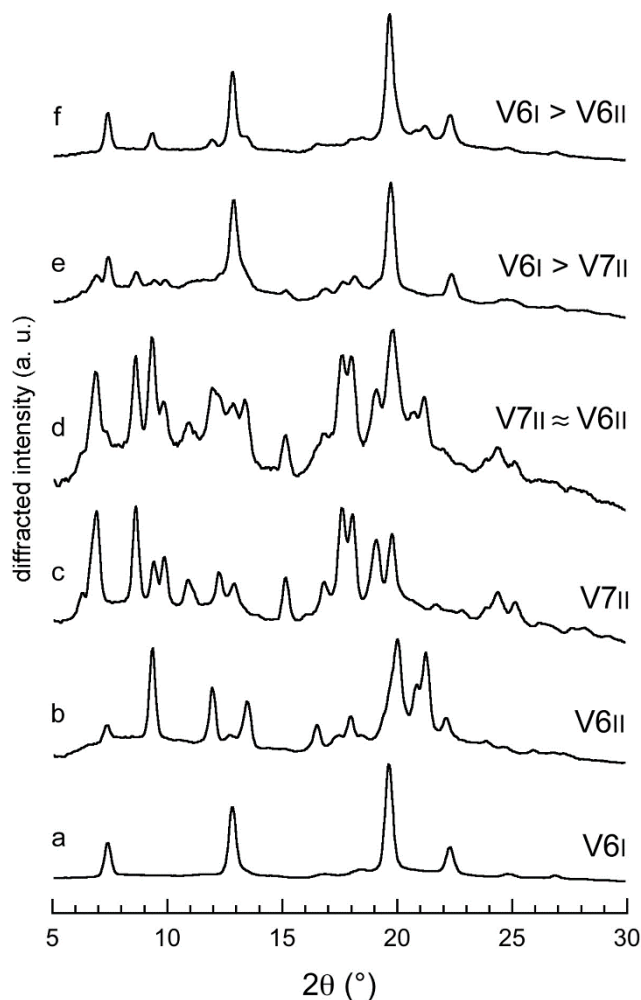


Figure V.4. XRD profiles of V-amylose crystallized from aqueous solutions in the presence of a series of linear fatty acids. Unique allomorphs: a) V6_I prepared with tetradecanoic acid; b) V6_{II} prepared with hexanoic acid; c) V7_{II} prepared with pentanoic acid. Coexisting allomorphs: d) V6_{II} and V7_{II} prepared with 3 vol% pentanoic acid at 40 °C in the presence of 2 vol% DMSO; e) V6_I and V7_{II} prepared in the presence of 2 vol% DMSO with octadecanoic at 90 °C; f) V6_I and V6_{II} prepared in water with tetradecanoic acid at 60 °C. The crystals have been equilibrated at 95% RH. For mixtures (d-f), the major and minor allomorphs are indicated.

V.4. Complexes with 1,3-butanediol

The crystallization of amylose in dilute aqueous solution (0.1 wt% amylose) in the presence of different concentrations of 1,3-butanediol (10-80 vol%) at different temperatures (25-75 °C) allowed obtaining four different V-amylose allomorphs: V6_I, V6_{II}, V7_I and V7_{II}. Examples of crystals are shown in **Figure V.5**. 1,3-Butanediol is also the only complexing agent that can form up to four crystal types.

The formation of both 6- and 7-fold helices would be due to the fact the molecular size of the complexing agent is compatible with both helical conformations. As mentioned above, 6-fold helices are expected to be obtained with molecules with straight-chain moieties while branched-chain or cyclic molecules usually used 7-fold complexes (Biais et al., 2006; Takeo & Kuge, 1969, 1971; Yamashita & Monobe, 1971; Zaslów, 1963). In case of 1,3-butanediol, the complexing agent is composed of a straight chain of carbons, but the presence of a hydroxyl group at the endo-position enlarges its diameter in cross section. Therefore, the molecule has an intermediate size between those that favor 6-fold helix (straight-chain molecules) and 7-fold helix (branched-chain molecules). In this thesis, other molecules which have similar structural features such as 2-propanol and 1,2-propanediol also induced both 6- and 7-fold complexes.

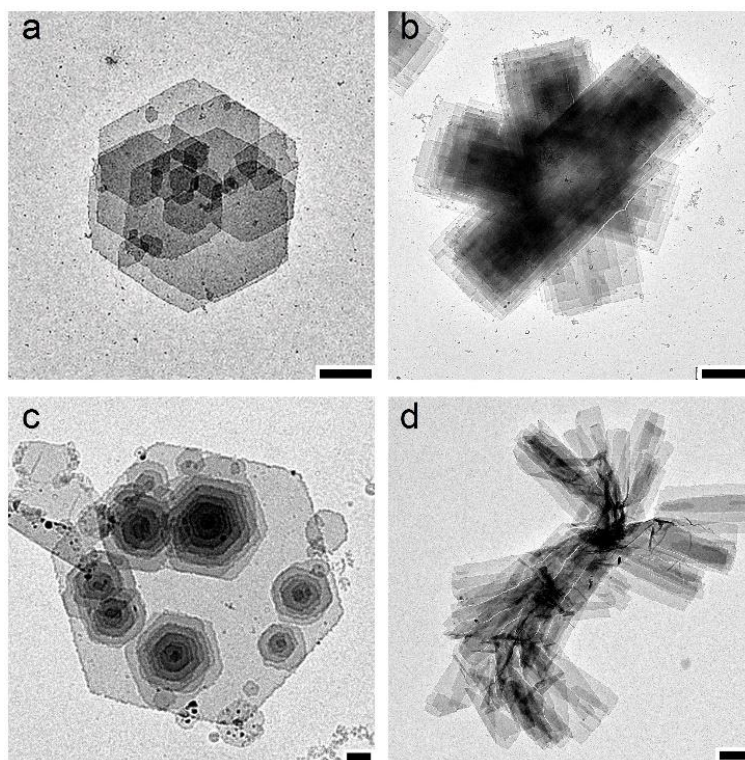


Figure V.5. TEM images of V6_I (a), V6_{II} (b), V7_I (c) and V7_{II} (d) V-amylose crystals prepared with 1,3-butanediol. Scale bars: 1 µm.

Similar to other polymorphic V-amylose presented previously, the structure of V_{1,3-butanediol} is dependent on the concentration of the complexing agent and the crystallization temperature, as shown in **Table V.6** and **Annex 3, Figures S.V.7 and S.V.8**. In general, the concentration of 1,3-butanediol necessary for the formation of different allomorphs can be arranged in the order: $V7_I \geq V6_I \geq V7_{II} \geq V6_{II}$. The effect of concentration of complexing agent on the structure of V_{1,3-butanediol} is thus similar to that observed for complexes prepared with *n*-propanol, 1,4-butanediol, 1,6-hexanediol, propanoic acid and butanoic acid, that the more compact allomorphs are formed at higher concentrations of complexing agent relative to the less dense ones. As discussed above, this effect can be explained by the dehydration effect of the complexing agent on amylose. Besides, the result also revealed that 6-fold complexes are preferred with lower concentrations of 1,3-butanediol than 7-fold ones for both orthorhombic ($V6_{II} < V7_{II}$) and compact hexagonal structures ($V6_I < V7_I$). The reason for this is still unclear.

On the other hand, the crystallization in the presence of the same concentration of 1,3-butanediol showed that the 7-fold complexes ($V7_I, V7_{II}$) are favored at higher temperature than 6-fold complexes ($V6_I, V6_{II}$). Previously, we also observed that $V7_{II}$ was preferred at higher temperature than $V6_{II}$ obtained with fatty acids. However, for the complexes of fatty acids such as propanoic acid or pentanoic acid, the occurrence domain of $V7_{II}$ was at relatively lower temperatures than $V6_I$; this is different from the crystallization behavior of V_{1,3-butanediol}.

Table V.6. Allomorphic type of V_{1,3-butanediol} crystals as a function of crystallization temperature and concentration of 1,3-butanediol.

Concentration (%vol)	Incubation temperature (°C)				
	25	40	60	75	Slow cooling
20	-	-	-	-	-
25	$V6_{II} > V7_{II}$	-	-	-	$V6_{II} > V7_{II}$
30	$V6_{II} > V7_{II}$	$V7_{II}$	-	-	$V7_{II} > V6_{II}$
35	$V6_{II} > V7_{II}, V6_I$	$V7_{II}$	-	-	$V6_I > V7_{II}, V6_{II}$
40	$V6_I$	$V7_{II} > V6_I$	-	-	$V6_I > V7_{II}$
45	$V6_I$	$V6_I > V7_{II}$	-	-	$V6_I > V7_{II}$
50	$V6_I$	$V6_I$	$V6_I, V7_I$	-	$V6_I > V7_I$
60	$V6_I, V7_I$	$V6_I, V7_I$	$V7_I$	$V7_I$	$V7_I > V6_I$

V.5. Complexes with esters

In this study, several esters were selected for investigating the complexing ability with amylose including: linear monoesters (ethyl hexanoate, ethyl valerate, ethyl caproate, propyl

acetate, butyl acetate and pentyl acetate), branched monoesters (isopentyl acetate, isopropyl myristate) and a diester (diethyl malonate). The complexes were prepared in aqueous solution having different concentrations of native amylose (0.1-0.5%) by incubation at different temperature (25-75 °C) or slowly cooling down to room temperature in a Dewar bottle.

The results are summarized in **Table V.7** and TEM images of typical crystals are shown in **Figure V.6**. Apart from propyl acetate, all linear monoesters, isopropyl myristate and diethyl malonate could form V6_{II}. Different from the results of Arvisenet et al. (2002), we did not observe the formation of V7_{II} with ethyl hexanoate. Besides, the complexes of ethyl butyrate were successfully prepared although this molecule was previously reported to have no complexing ability (Biais et al., 2006; Kuge & Takeo, 1968). This can be because the concentration of amylose used in this study (0.1-0.5 wt%) is lower than in the previous works (1.0%). Isopentyl acetate is the only ester that forms V7_{II}. This result agrees with previous observations that linear carbon chains induce 6-fold helices, while branched chains enlarge the helix to 7-fold (Takeo & Kuge, 1969). Six-fold helices form with isopropyl myristate maybe because the linear chain (myristate), not the branched part, predominates the helix.

As shown in **Table V.7** and **Annex 3, Figure S.V.9**, the formation of V_{esters} is significantly affected by the crystallization temperature and concentration of amylose. In general, the complexes formed very slowly (1-2 weeks) at relatively low temperatures ($\leq 40^\circ\text{C}$), suggesting a weak interaction between amylose and the complexing agents. In addition, the precipitated product usually contained a mixture of V- and B-amylose, indicating a competition between complexation and retrogradation. In addition, the complexation of each ester is favored at a specific range of amylose concentration, usually between 0.1-0.5 wt%. Out of this range, B-amylose predominantly forms. Nuessli et al. (2003) reported a similar effect of amylose concentration on the formation of complexes with geraniol. When the concentration was $> 0.5\%$, the retrogradation rate of amylose into B-type was much faster than the formation of complex.

V.6. Complexes with some bicyclic compounds

The complexes of amylose with several bicyclic compounds (*trans*-decalin, β -pinene, *cis*-decahydro-1-naphthol, decahydro-2-naphthol, (-)-borneol and *R*(+)-camphor) were prepared at different temperature (25-115 °C). The result is presented in **Table V.8**. *trans*-Decalin and β -pinene formed V7_{II} at relatively low temperature ($\leq 40^\circ\text{C}$). (-)-Borneol and *R*(+)-camphor yielded V7_I at $\leq 75^\circ\text{C}$. On the other hand, *cis*-decahydro-1-naphthol and decahydro-2-naphthol produced both V7_I and V7_{II} (**Figure V.7**), and V7_I was preferred at higher temperatures. In addition, the crystallinity of the complexes increased with the crystallization temperature

(Figure V.8), which would be due to a slower nucleation and growth at higher temperatures. Our results disagree with those of Helbert (1994) who observed the formation of hexagonal V6_I with *trans*-decalin and (-)-borneol. However, the retrieval of V7 lamellar crystals was consistent with the molecular dimension of the bicyclic compounds (Takeo & Kuge, 1969).

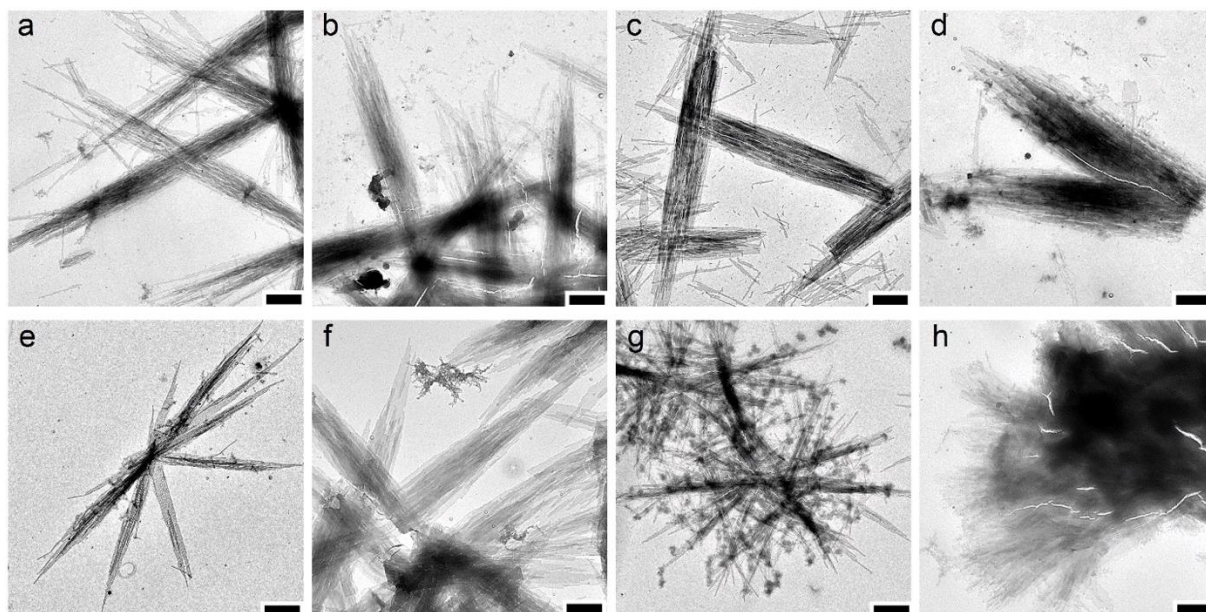


Figure V.6. TEM images of V-amylose complexed with ethyl butyrate (a), ethyl valerate (b), ethyl caproate (c), butyl acetate (d), pentyl acetate (e), diethyl malonate (f), isopropyl myristate (g) and isopentyl acetate (h). Scale bars: 1 μm .

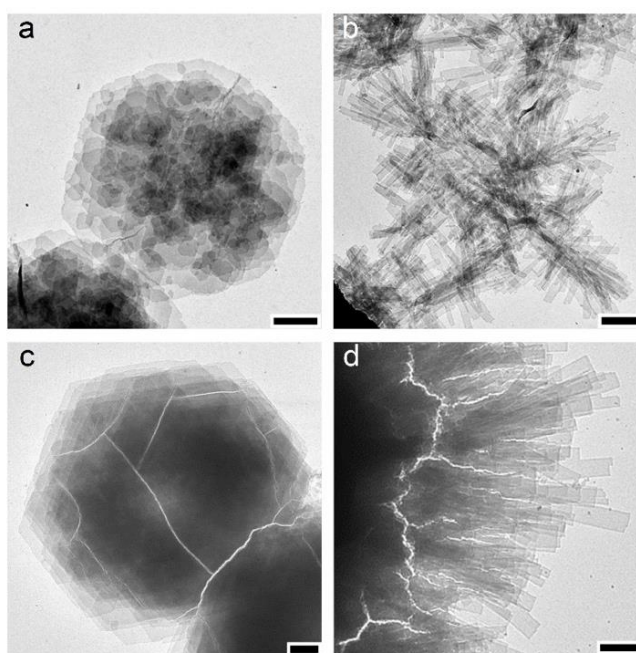


Figure V.7. TEM images of V7_I (a,c) and V7_{II} (b,d) crystals prepared with *cis*-decahydro-1-naphthol (a,b), and decahydro-2-naphthol (c,d). Scale bars: 1 μm .

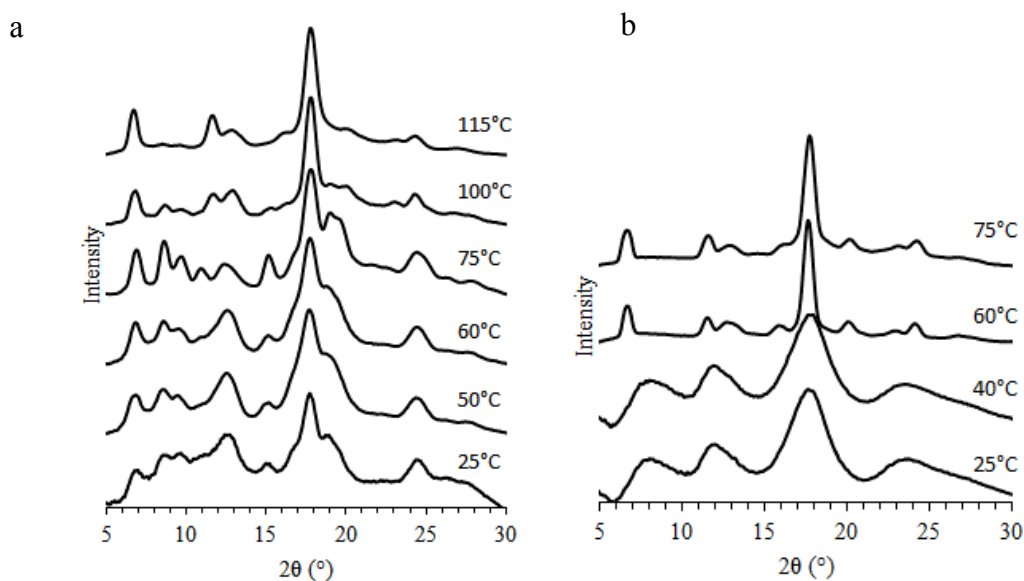
Table V.7. Allomorphic type of the V-amylose complexed with esters as a function of amylose concentration (C) and incubation temperature.

Esters	C (vol%)	Incubation temperature (°C)			
		25	40	60	Slow cooling
Ethyl butyrate	0.1	B	-	-	V6 _{II} > B
	0.2	B	-	-	V6 _{II}
	0.3	B	-	-	V6 _{II}
	0.4	B	B > V6 _{II}	-	V6 _{II}
	0.5	B	B > V6 _{II}	-	B > V6 _{II}
Ethyl valerate	0.1	B	V6 _{II}	-	B > V6 _{II}
	0.2	B	V6 _{II}	-	B > V6 _{II}
	0.3	B	V6 _{II}	-	B > V6 _{II}
	0.4	B	B > V6 _{II}	-	V6 _{II} > B
	0.5	B	B > V6 _{II}	-	B > V6 _{II}
Ethyl caproate	0.1	B > V6 _{II}	V6 _{II} > B	-	B > V6 _{II}
	0.2	B > V6 _{II}	V6 _{II}	-	B > V6 _{II}
	0.3	B > V6 _{II}	V6 _{II}	-	V6 _{II}
	0.4	B > V6 _{II}	V6 _{II}	-	B > V6 _{II}
	0.5	B > V6 _{II}	V6 _{II} > B	-	B > V6 _{II}
Propyl acetate	0.1-0.5	-	-	-	-
Butyl acetate	0.1	B > V6 _{II}	-	-	B > V6 _{II}
	0.2	B > V6 _{II}	-	-	V6 _{II}
	0.3	B > V6 _{II}	-	-	B > V6 _{II}
	0.4	B > V6 _{II}	B > V6 _{II}	-	B > V6 _{II}
	0.5	B > V6 _{II}	B	-	B > V6 _{II}
Pentyl acetate	0.1	B > V6 _{II}	-	-	B > V6 _{II}
	0.2	B > V6 _{II}	-	-	B > V6 _{II}
	0.3	B > V6 _{II}	B > V6 _{II}	-	V6 _{II}
	0.4	B > V6 _{II}	B > V6 _{II}	-	B > V6 _{II}
	0.5	B > V6 _{II}	B	-	B > V6 _{II}
Isopentyl acetate	0.1	B	B > V7 _{II}	-	B > V7 _{II}
	0.2	B	B > V7 _{II}	-	B > V7 _{II}
	0.3	B	V7 _{II}	-	V7 _{II}
	0.4	B	V7 _{II}	-	V7 _{II}
	0.5	B	B > V7 _{II}	-	B > V7 _{II}
Isopropyl myristate	0.1	B > V6 _{II}	-	-	B > V6 _{II}
	0.2	B > V6 _{II}	-	-	B > V6 _{II}
	0.3	B > V6 _{II}	-	-	B > V6 _{II}
	0.4	B	B	-	B
	0.5	B	B	-	B
Diethyl malonate	0.1	V6 _{II} > B	-	-	V6 _{II} > B
	0.2	V6 _{II}	-	-	V6 _{II} > B
	0.3	V6 _{II}	-	-	V6 _{II} > B
	0.4	B > V6 _{II}	-	-	B > V6 _{II}
	0.5	B > V6 _{II}	-	-	B > V6 _{II}

Table V.8. Allomorphic type of the V-amylose complexed with bicyclic compounds as a function of incubation temperature.

Complexing agent	Incubation temperature (°C)						
	25	40	50	60	75	100	115
<i>trans</i> -Decalin	V7 _{II}	V7 _{II}	-	-	-	-	-
β -Pinene	V7 _{II}	V7 _{II}	-	-	-	-	-
<i>cis</i> -Decahydro-1-naphthol	V7 _{II}	V7 _{II}	V7 _{II}	V7 _{II}	V7 _{II}	V7 _I , V7 _{II}	-
Decahydro-2-naphthol	V7 _{II}	V7 _{II}	V7 _{II}	V7 _{II}	V7 _{II}	V7 _I , V7 _{II}	V7 _I , V7 _{II}
(-)-Borneol	V7 _I	V7 _I	V7 _I	V7 _I	V7 _I	-	-
<i>R</i> -(+)-Camphor	V7 _I	V7 _I	V7 _I	V7 _I	V7 _I	-	-

Along with 1,3-butanediol, the above bicyclic compounds (*cis*-decahydro-1-naphthol, decahydro-2-naphthol, (-)-borneol and *R*-(+)-camphor) are among a few complexing agents that can produce V7_I. In contrast, V7_{II} appears to be more prevalent as having been obtained with a variety of molecules such as linear fatty acids (Takeo et al., 1973) and ketones (Takeo & Kuge, 1971), 2-propanol and branched alcohols (Yamashita & Hirai, 1966), monoterpenes and many cyclic compounds (Biais, 2006; Conde-Petit et al., 2006; Helbert, 1994; Nuessli et al., 2003; Putaux et al., 2008). As noted, the main difference between the structure of V7_I and V7_{II} stays in the more or less compact packing arrangements of 7-fold amylose helix. In V7_I structure, amylose helix would be closely packed on a hexagonal net with small inter-helix spaces which allow the location of some water molecules and not the bulky complexing bicyclic compounds.

**Figure V.8.** XRD profiles of hydrated V-amylose complexes prepared with decahydro-2-naphthol (a) and (-)-borneol (b) at different temperatures.

In contrast, the V7_{II} exhibits more interstitial spaces which accommodate for an occupation of both complexing agents and water (Nishiyama et al., 2010). Some authors believed that the location of complexing agents between amylose helices would disturb the hexagonal arrangement of amylose helices leading to the formation of the orthorhombic structures (Booy et al., 1979; Godet et al., 1995a; Simpson et al., 1972). Based on that hypothesis, the possibility of complexing agent to be located only inside the helix or both inside and between the helix is the decisive factor that controls the crystallization into V7_I or V7_{II}. Since V7_{II} have been obtained with numerous hydrophilic and hydrophobic complexing agents of different chemical structures, it may be impossible to figure out the specific interactions or structural features that allow their localization between the helix. However, the dimension of the complexing agents must be compatible with the inter-helix space they occupy (Helbert, 1994). As noted previously, (-)-borneol and R-(+)-camphor yielded V7_I but not V7_{II}. It is probable that these complexing agents are too bulky to enter the inter-helix void of V7_{II}. A few molecules could induce both V7_I and V7_{II} such as *cis*-decahydro-1-naphthol, decahydro-2-naphthol and 1,3-butanediol. In these cases, V7_I is preferred with a higher crystallization temperature (100-115 °C for *cis*-decahydro-1-naphthol and decahydro-2-naphthol) or higher concentration of complexing agent (60 vol% for 1,3-butanediol). These drastic conditions would necessitate strong interactions between complexing agent and amylose to stabilize the structure at high temperature or to avoid the retrogradation of amylose caused by dehydration effect of high concentration of complexing agent. Most of complexing agents such as *trans*-decalin and β -pinene would not meet this requirement, would thus induce V7_{II} which is favored at milder conditions. In addition, it is interesting to note that *cis*-decahydro-1-naphthol and decahydro-2-naphthol are different from *trans*-decalin just by a hydroxyl group. Therefore, it is logical to assume that the functional group would have some specific interactions with amylose that increase the stability of the complexes.

V.7. Complexes with 1-naphthol

The complexes were prepared by addition of an excess amount of 1-naphthol into aqueous solutions of amylose having different DPs, equilibrated at a predetermined temperature varying from 60-90 °C. The complexing mixture was kept at the mixing temperature for 30-60 min, and then allowed cooling down in ambient air to induce the crystallization. Two different allomorphs were obtained V7_{III} and V8_{II} whose morphologies are presented in **Figure V.9**.

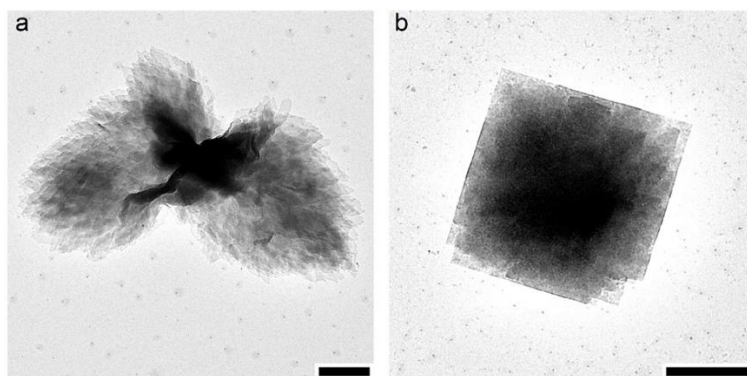


Figure V.9. TEM images of $V_{1\text{-naphthol}}$ crystals: a) $V7_{\text{III}}$ crystals prepared with DP6500 amylose; b) $V8_{\text{II}}$ crystals prepared with DP130 amylose.

Table V.9. Allomorphic structure of $V_{1\text{-naphthol}}$ as a function of weight-average degree of polymerization of amylose (DP_w) and mixing temperature at which 1-naphthol was added into amylose solution. The crystals were formed at cooling down to room temperature.

DP_w	Mixing temperature ($^{\circ}\text{C}$)		
	60	75	90
192-6500	$V7_{\text{III}} > V8_{\text{II}}$	$V7_{\text{III}} > V8_{\text{II}}$	$V8_{\text{II}} > V7_{\text{III}}$
130	$V8_{\text{II}} > V7_{\text{III}}$	$V8_{\text{II}} > V7_{\text{III}}$	$V8_{\text{II}} > V7_{\text{III}}$
60-86	$V8_{\text{II}}$	$V8_{\text{II}}$	$V8_{\text{II}}$

The type of allomorph depends on the DP of amylose and mixing temperature (Table V.9 and Annex 3, Figure S.V.10). $V8_{\text{II}}$ is preferred with lower DP and higher mixing temperature compared to $V7_{\text{III}}$. Amylose with an average DP_w of 60-86 yielded only $V8_{\text{II}}$ while DP130 amylose produced a mixture of $V8_{\text{II}}$ and $V7_{\text{III}}$ in which $V8_{\text{II}}$ was the major form (> 95%) whatever the mixing temperature. In the case of DP192 and DP6500 amylose, $V8_{\text{II}}$ and $V7_{\text{III}}$ also concomitantly crystallized but the major form depended on the mixing temperature. In particular, $V8_{\text{II}}$ was the major form if the mixing temperature was 90 $^{\circ}\text{C}$ while at lower temperatures, $V7_{\text{III}}$ was the main product. Previous studies revealed that the formation of crystalline V-amylose required a critical value of DP of amylose (about DP 20-30) (Dvonch et al., 1950; Gelders et al., 2004; Godet et al., 1995b). However this is the first time that the variation of the V-amylose crystal structure (both helical conformation and molecular packing in the case of $V_{1\text{-naphthol}}$) with the DP of amylose has been reported. The reason for this effect of DP of amylose is still unclear.

On the other hand, as previously suggested by Yamashita and Monobe (1971), the dependence of the crystal structure on the mixing temperature rather than the crystallization

temperature suggests that the association of the random-coil amylose chains with 1-naphthol into helical complexes occurs at high temperature. The helical conformation of amylose would be decided in this critical step and would not vary during the cooling down. The result also suggests that the 8-fold complex with 1-naphthol is more thermally-stable than the 7-fold one.

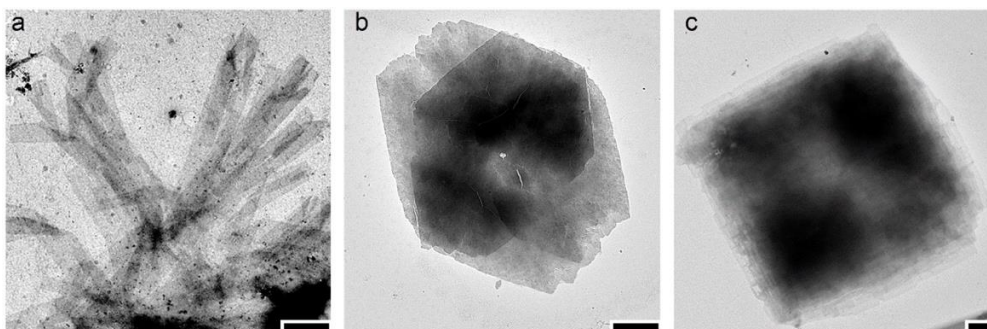


Figure V.10. TEM images of $V_{\text{quinoline}}$ crystals: a) $V7_{\text{II}}$ crystals prepared with DP6500 amylose, b) $V7_{\text{IV}}$ crystals obtained with DP80 amylose, c) $V8_{\text{II}}$ crystals obtained with DP6500 amylose.

Table V.10. Allomorphic type of the $V_{\text{quinoline}}$ prepared with DP6500 amylose at different incubation temperatures and DMSO concentrations. $V7_{\text{II}}$ was sometimes detected on TEM images but only as traces.

DMSO:water	Incubation temperature (°C)			
	25	40	50	60
0	$V7_{\text{IV}} > V8_{\text{II}}$	$V7_{\text{IV}} > V8_{\text{II}}$	-	-
10	$V7_{\text{IV}} > V8_{\text{II}}$	$V7_{\text{IV}} > V8_{\text{II}}$	-	-
15	$V7_{\text{IV}} > V8_{\text{II}}$	$V8_{\text{II}} > V7_{\text{IV}}$	$V8_{\text{II}} > V7_{\text{IV}}$	-
25	$V7_{\text{IV}} > V8_{\text{II}}$	$V8_{\text{II}} > V7_{\text{IV}}$	$V8_{\text{II}} > V7_{\text{IV}}$	-
30	$V7_{\text{IV}} > V8_{\text{II}}$	$V8_{\text{II}} > V7_{\text{IV}}$	$V8_{\text{II}} > V7_{\text{IV}}$	-

V.8. Complexes with quinoline

The $V_{\text{quinoline}}$ complexes were prepared with an excess amount of quinoline, using different fractions of amylose at different temperatures and solvent compositions (water or DMSO/water mixture). The crystallization always resulted in a mixture of 2 allomorphs: $V7_{\text{IV}}$, and $V8_{\text{II}}$ (**Figure V.10**), but their proportion depends on the crystallization conditions (**Table V.10**). Sometimes, $V7_{\text{II}}$ was also present as a trace and could only be identified by TEM.

Unlike for $V_{1\text{-naphthol}}$, the crystal structure of $V_{\text{quinoline}}$ does not depend on the DP of amylose. In fact, the parameter only affects the morphology of the crystals. In contrast, the solvent composition (DMSO concentration) and crystallization temperature appeared to be decisive factors that controlled the formation of different allomorphs. $V8_{\text{II}}$ was generally preferred at

higher concentrations of DMSO and higher crystallization temperatures. As shown in **Table V.10** and **Annex 3, Figure S.V.11**, the crystallization at 25 °C or in the presence of ≤ 10 vol% of DMSO mainly led to the formation of V7_{IV} while V8_{II} is the major form only in the presence of ≥ 15 vol% of DMSO at 40-50 °C. Helbert (1994) previously prepared V_{quinoline} by slowly cooling down the complexation mixture from 90 °C to room temperature. The author noted that the presence of 15 vol% of DMSO led to the formation of V8_{II}, while V6_I formed in the absence of DMSO. It is possible that the V7_{IV} was incorrectly identified as V6_I crystals in the previous study since the morphology of the two allomorphs is very similar. As discussed in previous sections, DMSO would increase the solubility of both amylose and the complexing agent, and thus increases the concentration of complexing agent in the solution. In addition, DMSO also affects the conformation of amylose in solution. These results would be accounted for by the effect of the solvent on the crystal structure of V_{quinoline} but the mechanism is still unknown.

V.9. Complexes with salicylic acid

The crystallization of amylose having a different DP was conducted in dilute solution in the presence of an excess amount of salicylic acid and in different conditions of crystallization temperatures and solvent compositions. Two crystalline allomorphs were identified, namely V8_I and V8_{II} whose morphology is shown in **Figure V.11**. Kuge and Takeo (1968) formerly reported that salicylic acid did not form complexes with amylose in solution. Later, Oguchi et al. (1998) prepared complexes with salicylic acid using the sealed-heating method and obtained two crystal types that, according to the authors, would consist of 7- and 8-fold amylose helices, respectively. The 7-fold complexes gave a powder XRD profile that is similar to that of V7_a while the 8-fold complexes gave a similar diffraction pattern to V8_I. Therefore, the result in the present study has been the first report of lamellar crystals of V_{salicylic acid} prepared by crystallization in solution. In addition, V_{salicylic acid} exhibited polymorphism but no 7-fold complex was identified. The crystallization conditions did probably not cover the occurrence domain of 7-fold complexes of V_{salicylic acid} or the complexes cannot form in aqueous solution.

Table V.11 presents the allomorphic type of V_{salicylic acid} corresponding to different crystallization conditions. It is observed that V8_I is favored with higher DP of amylose, higher concentrations of DMSO and higher crystallization temperatures, relative to V8_{II} (**Annex 3, Figures S.V.12 and S.V.13**). In terms of packing arrangement of amylose helices, V8_I is more compact than V8_{II} (see **Chapter IV**). Therefore, the crystallization behavior of V_{salicylic acid} also supports that higher crystallization temperatures favor the more compact structure. The effects

of DMSO and DP of amylose are not very clear, but these parameters may have an influence on the relative solubility between the two allomorphs. On the other hand, the crystallization behavior of $V_{\text{salicylic acid}}$ is similar to that of $V_{1\text{-naphthol}}$ regarding the preferred formation of $V8_{\text{II}}$ allomorph with the shorter amylose although both allomorphs of $V_{\text{salicylic acid}}$ consist of 8-fold helices while those of $V_{1\text{-naphthol}}$ have different helical conformations (7- and 8-fold). However, we did not observe any similar effect of DP of amylose on the formation of $V8_{\text{II}}$ in the case of $V_{\text{quinoline}}$. A similar remark can also be made regarding the effect of DMSO.

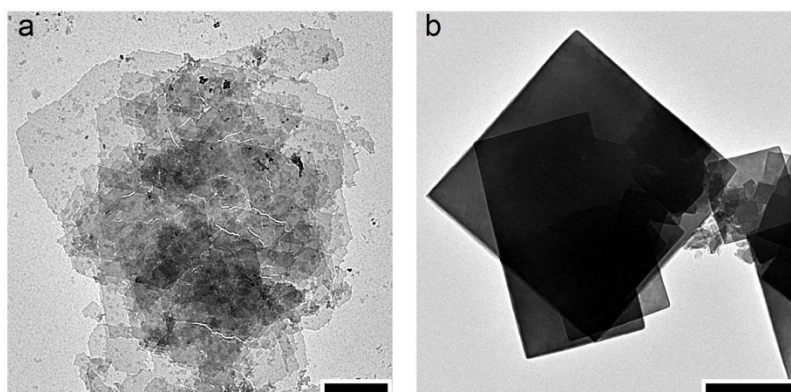


Figure V.11. TEM images of $V_{\text{salicylic acid}}$ crystals: a) $V8_{\text{I}}$ prepared with DP6500 amylose, b) $V8_{\text{II}}$ crystals prepared with DP86 amylose. Scale bars: 1 μm .

Table V.11. Allomorphic type of the $V_{\text{salicylic acid}}$ as a function of degree of polymerization (DP) of amylose, incubation temperature and DMSO concentration (C_{DMSO}).

Amylose	C_{DMSO} (vol%)	Incubation temperature ($^{\circ}\text{C}$)			
		25	40	60	75
DP86	0	$V8_{\text{II}}$	$V8_{\text{II}}$	-	-
	10	$V8_{\text{II}}$	$V8_{\text{II}} > V8_{\text{I}}$	-	-
	15	$V8_{\text{II}} > V8_{\text{I}}$	$V8_{\text{I}} > V8_{\text{II}}$	-	-
	25	$V8_{\text{II}} > V8_{\text{I}}$	$V8_{\text{I}} > V8_{\text{II}}$	-	-
DP130	0	$V8_{\text{II}}$	$V8_{\text{I}} > V8_{\text{II}}$	$V8_{\text{I}}$	-
DP200	0	$V8_{\text{I}} > V8_{\text{II}}$	$V8_{\text{I}} > V8_{\text{II}}$	$V8_{\text{I}}$	-
	10	$V8_{\text{I}} > V8_{\text{II}}$	$V8_{\text{I}} > V8_{\text{II}}$	$V8_{\text{I}}$	-
	15	$V8_{\text{I}} > V8_{\text{II}}$	$V8_{\text{I}}$	$V8_{\text{I}}$	-
	25	$V8_{\text{I}} > V8_{\text{II}}$	$V8_{\text{I}}$	$V8_{\text{I}}$	-
DP6500	0	$V8_{\text{I}} > V8_{\text{II}}$	$V8_{\text{I}} > V8_{\text{II}}$	$V8_{\text{I}}$	$V8_{\text{I}}$
	10	$V8_{\text{I}} > V8_{\text{II}}$	$V8_{\text{I}} > V8_{\text{II}}$	$V8_{\text{I}}$	$V8_{\text{I}}$
	15	$V8_{\text{I}} > V8_{\text{II}}$	$V8_{\text{I}}$	$V8_{\text{I}}$	$V8_{\text{I}}$
	25	$V8_{\text{I}} > V8_{\text{II}}$	$V8_{\text{I}}$	$V8_{\text{I}}$	$V8_{\text{I}}$

V.10. General conclusions

The results of the present study support the correlation between the dimensions of the complexing agent and the helical conformation: straight-chain molecules form 6-fold helices, while branched molecules and cyclic compounds induce 7-fold helical conformations, and some cyclic compounds form 8-fold helices (**Table V.12**). In addition, several molecules formed two different helical conformations. For example, straight-chain fatty acids and straight-chain alcohols with the hydroxyl group located at endo-position induced both V6 and V7 complexes. Quinoline and 1-naphthol formed both V7 and V8 complexes. These molecules likely have an intermediate size that is compatible with both helical conformations. An exception is the case of 4-hydroxybenzoic acid which complex is supposed to contain 6-fold helices although the size of the complexing agent is not compatible with helical cavity. In this case, the complexing agent would be located between the helices.

Polymorphism was observed for crystals prepared with a large number of complexing agents and is thus more general than what was previously reported in the literature. The tendency of a complex to exhibit a polymorphic behavior is not only related to the nature of complexing agent but also to the accessibility of the various structures through crystallization. Complexes of straight-chain molecules are more likely to exhibit polymorphism than the branched-chain or cyclic compounds. In addition, for straight-chain molecules, alcohols, fatty acids, aldehydes, amides, amines are likely more prone to form different allomorphs than esters and ketones. As noted, the occurrence domains usually varied between different allomorphs as well as between different complexing agents and are thus sometimes difficult to predict.

Therefore, a variety of crystallization conditions with the variation of different parameters (solvent composition, temperature of mixing and crystallization, concentration of complexing agent and amylose, DP of amylose, etc.) had to be explored in order to observe relevant structures. However, some general tendencies could be observed:

- i) more compact structures are favored at higher temperature;
- ii) the crystal structure of complexes with highly soluble or water-miscible molecules usually depends on the concentration of the complexing agent. In that case, the more compact structures with a larger helix (containing a higher number of glucosyl units per turn) are favored at a higher concentration of the complexing agent. The mechanism of polymorphic crystallization is still unclear. Future works should be conducted to understand the effect of the guest and several crystallization parameters on the formation and crystal structure of V-amylose.

The result of the present study suggests that more new V-amylose structure remain to be discovered. This can be done by testing new complexing agents, but more importantly, by varying the conventional crystallization method in solution. The influence of some parameters such as solvents and additives should be further explored. As noted, in this study, only DMSO was tested as additive. In addition, using different preparation techniques is also recommended, e.g. insertion of complexing agent into a preformed V-amylose, sealed-heating, etc.

Table V.12. Allomorphic types of V-amylose complexes with different complexing agents. "-" indicates that no complex was formed.

Complexing agent	Abbreviation	V-type
Alkanes		
Hexane	HAN	-
Decane	DEAN	-
Hexadecane	HEDAN	-
Straight-chain saturated monocarboxylic acid		
Propanoic acid (propionic acid)	PA	V6 _I , V7 _{II}
Butanoic acid (butyric acid)	BA	V6 _I , V6 _{II} , V7 _{II}
Pentanoic acid (valeric acid)	VA	V6 _I , V6 _{II} , V7 _{II}
Hexanoic acid (caproic acid)	COA	V6 _I , V6 _{II} , V7 _{II}
Octanoic acid (caprylic acid)	OA	V6 _I , V6 _{II} , V7 _{II}
Decanoic acid (capric acid)	CIA	V6 _I , V6 _{II} , V7 _{II}
Dodecanoic acid (lauric acid)	LA	V6 _I , V6 _{II} , V7 _{II}
Tetradecanoic acid (myristic acid)	MYA	V6 _I , V6 _{II} , V7 _{II}
Hexadecanoic acid (palmitic acid)	PMA	V6 _I , V6 _{II} , V7 _{II}
Octadecanoic acid (stearic acid)	SA	V6 _I , V6 _{II} , V7 _{II}
Icosanoic acid (arachidic acid)	ARA	V6 _I , V6 _{II} , V7 _{II}
Straight-chain unsaturated monocarboxylic acids		
Oleic acid	OLAN	V6 _I , V6 _{II} , V7 _{II}
Linoleic acid	LINA	V6 _I , V6 _{II} , V7 _{II}
Straight-chain saturated dicarboxylic acids		
Ethanedioic acid (oxalic acid)	OXA	-
Propanedioic acid (malonic acid)	MAA	-
Hexanedioic acid (adipic acid)	ADA	-
Nonanedioic acid (azelaic acid)	AZA	V6 _I , V6 _{II}
Dodecanedioic acid	DODA	V6 _I , V6 _{II}
Straight-chain saturated primary alcohols		
Ethanol	ET	V6 _I

1-Propanol (<i>n</i> -propanol)	POL	V _{6I} , V _{6II}
1-Butanol (<i>n</i> -butanol)	BU	V _{6II}
1-Pentanol (<i>n</i> -pentanol)	PENO	V _{6I} , V _{6II}
1-Octanol (<i>n</i> -octanol)	OCTO	V _{6I} , V _{6II}
1-Dodecanol (<i>n</i> -dodecanol)	DODO	V _{6I} , V _{6II}
1-Tetradecanol (<i>n</i> -tetradecanol)	TEDO	V _{6I} , V _{6II}
1-Hexadecanol (<i>n</i> -hexadecanol)	HEDO	V _{6I} , V _{6II}
Straight-chain unsaturated alcohols		
<i>cis</i> -3-Hexen-1-ol	HENOL	V _{6I} , V _{6II}
Straight-chain saturated primary diols		
1,2-Ethanediol (ethylene glycol)	EG	V _{6I}
1,3-Propanediol	PDIOL	V _{6I} , V _{6II}
1,4-Butanediol	BDIOL	V _{6I} , V _{6II}
1,5-Pentanediol	PEDIOL	V _{6I} , V _{6II}
1,6-Hexanediol	HDIOL	V _{6I} , V _{6II}
2-(2-Hydroxyethoxy)ethan-1-ol (diethylene glycol)	DEG	V _{6I}
Straight-chain secondary alcohols		
2-Propanol (isopropanol)	IP	V _{6I} , V _{6II} , V _{7II}
2-Butanol (sec-butanol)	SB	V _{7II}
Straight-chain secondary diols		
1,2-Propanediol (propylene glycol)	PG	V _{6I} , V _{7II}
1,3-Butanediol	BBOL	V _{6I} , V _{6II} , V _{7I} , V _{7II}
Triols		
1,2,3-Propanetriol (glycerol)	GOL	V _{6I} , V _{6III}
Halogeno-alcohols		
11-Bromo-1-undecanol	BUN	V _{6I}
Straight-chain esters		
Ethyl butanoate (ethyl butyrate)	EB	V _{6II}
Ethyl pentanoate (ethyl valerate)	EV	V _{6II}
Ethyl hexanoate (ethyl caproate)	EC	V _{6II}
Propyl acetate	PRAT	-
Butyl acetate	BAT	V _{6II}
Pentyl acetate	PAT	V _{6II}
Lysophosphatidylcoline	LYS	V _{6I}
Alkyl sulfate		
Sodium octadecyl sulfate	SODS	-
Diesters		
Diethyl malonate	DEM	V _{6II}
Triesters		

Triacetin	TAN	-
Tristearin	TSA	-
Ether		
Diethyl ether	DET	-
Ketones		
Pentan-2-one	PON	V7 _{II}
Aldehyde		
Octanal	OTAL	V6 _I , V6 _{II}
Straight-chain primary amines		
1-Butylamine (<i>n</i> -Butylamine)	BUA	-
1-Hexylamine (<i>n</i> -Hexylamine)	HEA	V6 _I , V6 _{II}
1-Heptylamine (<i>n</i> -Heptylamine)	HEPA	V6 _I , V6 _{II}
1-Octylamine (<i>n</i> -Octylamine)	OCTA	V6 _I , V6 _{II}
1-Nonylamine (<i>n</i> -Nonylamine)	NONA	V6 _I , V6 _{II}
1-Decylamine (<i>n</i> -Decylamine)	DECA	V6 _I , V6 _{II}
1-Dodecylamine (<i>n</i> -Dodecylamine)	DODEA	V6 _I , V6 _{II}
Straight-chain amide		
Stearamide	SAD	V6 _I , V6 _{II}
Branched-chain saturated alcohols		
2-Methylpropan-1-ol (isobutanol)	IB	V7 _{II}
2-Methylpropan-2-ol (<i>tert</i> -butanol)	TB	V7 _{II}
Branched-chained unsaturated alcohols		
β -Citronellol	BCIT	V7 _{II}
Linalool	LIN	V7 _{II}
Branched-chain secondary diols		
2-Methyl-2,4-pentanediol	MPDIOL	V7 _{II}
Branched-chain esters		
Isopropyl myristate	IPM	V6 _{II}
Isopentyl acetate	IPAT	V7 _{II}
Branched-chain ketones		
4-Methylpentan-2-one	MPON	V7 _{II}
3,3-Dimethylbutan-2-one	DMBON	V7 _{II}
Branched-chain aldehyde		
Citral (<i>cis</i> , <i>trans</i> mixture)	CI	V7 _{II}
Cycloalkanes		
Cyclohexane	CHAN	V7 _{II}
<i>trans</i> -Decahydronaphthalene (<i>trans</i> -decalin)	TDEC	V7 _{II}
β -Pinene	PIN	V7 _{II}
Aromatic hydrocarbons		

Limonene	LIMO	V7 _{II}
Toluene	TO	-
Aromatic carboxylic acids		
4- <i>tert</i> -Butylbenzoic acid	TBBA	V7 _{II}
4-Hydroxybenzoic acid	HBA	V6 _{IV}
Salicylic acid	SAL	V8 _I , V8 _{II}
Ibuprofen (isomer mixture)	IBU	V7 _{II}
(<i>S</i>)-(+)-Ibuprofen	SIBU	V7 _{II}
(<i>R</i>)-(-)-Ibuprofen	RIBU	V7 _{II}
Cinnamic acid	CINA	-
Ketoprofen	KETO	-
Aromatic amide		
Acetanilide	ACA	-
Cyclic alcohols		
Cyclohexanol	CHOL	V7 _{II}
(1 <i>S</i> ,2 <i>R</i> ,5 <i>S</i>)-(+)-Menthol	MEN+	V7 _{II}
(1 <i>R</i> ,2 <i>S</i> ,5 <i>R</i>)-(-)-Menthol	MEN-	V7 _{II}
(-)-Borneol	BOR	V7 _I
<i>cis</i> -Decahydro-1-naphthol	CDNAP	V7 _I , V7 _{II}
Decahydro-2-naphthol (isomer mixture)	DNAP	V7 _I , V7 _{II}
Terpineol	TER	V7 _{II}
(-)-Perillyl alcohol	PAL	V7 _{II}
Phenol	PhO	-
Benzyl alcohol	BAC	V7 _{II}
Carvacrol	CV	V7 _{II}
1-Naphthol	INAP	V7 _{III} , V8 _{II}
2-Naphthol	NAP	V7 _{II}
2,7-Dihydroxynaphthalene	DHN	-
1-Naphthalenemethanol	NM	-
Cyclic ketones		
Cyclohexanone	CHON	V7 _{II}
(+)-Camphor	CAM	V7 _I
(<i>S</i>)-(+)-Carvone	CARS	V7 _{II}
(<i>R</i>)-(-)-Carvone	CARR	V7 _{II}
Dihydrocoumarine	DHC	V7 _{II}
Cyclic aldehydes		
(<i>S</i>)-Perillaldehyde	PAD	V7 _{II}
Ethers		
<i>trans</i> -Anethol	AN	-

Eugenol	EU	-
Heterocyclic aromatic compounds		
8-Hydroxyquinoline	HQ	-
Quinoline	QN	V7 _{II} , V7 _{IV} , V8 _{II}
Quinoxaline	QNX	V7 _{II}
Cholesterol	CLS	-
Span 20	SZO	-
Span 60	SCO	-
Tween 80	TSO	-
D,L- α -tocopherol	TOCO	-
Tocopheryl linoleate	LITO	-
Curcumin	CUR	-

Chapter VI

Molecular structure and release properties of Vibuprofen

VI.1. Introduction

The property of amylose to form inclusion complexes with a variety of small organic molecules has been exploited for the encapsulation of a wide range of compounds that serve as flavor components, nutraceutical, pharmaceutical, or bioactive substances (Conde-Petit et al., 2006; Obiro et al., 2012; Panyoo & Emmambux, 2017; Putseys et al., 2010). In particular, complexes of amylose with ibuprofen (IBU), a widely used non-steroidal anti-inflammatory, analgesic and antipyretic agent, have been prepared by acidification of an alkali solution or *in situ* enzymatic polymerization (Yang et al., 2013; Zhang et al., 2016). The studies agree on the good *in vitro* stability of the complexes in a simulated gastric fluid and the gradual but sustained release of ibuprofen by enzymatic degradation of the amylose matrix in a simulated intestinal environment (Yang et al., 2013; Zhang et al., 2016). However, XRD profiles attested that the product prepared in previous studies contained a significant fraction of retrograded B-amylose along with semicrystalline V-type. Besides, the low crystallinity achieved with the preparation methods did not allow retrieving detailed information about the crystal structure.

We have studied the crystallization behavior of amylose with IBU in solution in order to prepare highly crystalline complexes and determine their structure. We have proposed models based on crystallographic and spectroscopic data as well as molecular modeling. Finally, in order to validate the potential of V-amylose as a delivery system, we have studied the *in vitro* release profiles of the guest molecule as a function of pH and in relation with the crystal structure.

VI.2. Crystallization behavior and morphology of *V*_{ibuprofen} complexes

Two batches of complexes were prepared. The first one was prepared from low amylose concentration solutions (0.1 wt%) with the aim of producing individualized lamellar single crystals for imaging (TEM and AFM) and ED crystallography analyses. Each crystallization was carried out using 10 mg amylose diluted in 10 mL of pure water. The second batch was prepared at a higher concentration (1 wt%) in order to produce a larger amount of complex (about 10 g). In that case, DMSO (10 vol%) was added as co-solvent to facilitate the dissolution of amylose. For spectroscopy characterization, the solid product was briefly washed to remove uncomplexed molecules and kept in suspension. However, for release studies, the complexes were extensively washed by centrifugation in water saturated with IBU prior to lyophilization.

VI.2.1. V_{IBU} crystals from dilute solutions

We have investigated the formation of lamellar V_{IBU} crystals as a function of the DP_w of amylose (60 to 6500), concentration of ibuprofen (0.0025 to 0.04 wt%) and at different temperatures (25, 40, 60, 75 and 90 °C). The complexes prepared with longer amylose crystallized at higher temperature (**Table V.1**). This would be due to the decrease of solubility of amylose with increasing DP. In addition, **Table VI.2** shows that the yield of complexation depended on the incubation temperature and concentration of IBU. When crystallized from a 0.1 wt% amylose solution and at a given temperature, the yield increased with IBU concentration and reached a maximum at saturation. However, the possibility that the initial amount of IBU has not been entirely complexed by amylose cannot be ruled out. Indeed, the crystallization at higher temperature required a higher amount of IBU. A similar behavior was observed for complexes with highly soluble fatty acids or alcohols. In the latter cases, the crystallization at high temperature was favored by the desolvation effect caused by the presence of high concentrations of complexing agent. In contrast, IBU being poorly water-soluble, the desolvation is negligible. The requirement of a higher concentration of IBU for complexation at higher temperature would likely be related to the increase in solubility of the complexing agent. As discussed in **Chapter V**, each complexing agent exhibits a critical concentration essential for the complexation which is correlated with its solubility in water. Indeed, as solubility increases, the association of complexing agent with water is favored. Therefore, a higher concentration of complexing agent is required to promote its association with amylose.

Figure VI.1 shows the optical and low-magnification TEM images of typical V_{IBU} crystals from DP6500 amylose prepared in the presence of saturated ibuprofen at 75 °C. These micrographs shows that the crystals radially grow from a common origin forming of flower-like aggregates. Higher magnification TEM images of crystals prepared at different crystallization temperatures are presented in **Figure VI.2**. The crystals are lamellae with a more or less rectangular shape. The size of the lamellae increases with the crystallization temperature. This would be a result of a slower nucleation and growth rate.

Considering the very large number of crystals per aggregate, recrystallization steps were used, resulting in more individual single crystals. The series of images in **Figure VI.3** shows that the length, width and "perfection" of the crystals vary with the DP of amylose. The crystals are longer for longer amylose chains while their rectangular shape is more clearly defined with the shorter chains. The morphology of these crystals appears to be characteristic of V_{7II} complexes ([Bul on et al., 1990](#); [Nishiyama et al., 2010](#)).

Table VI.1. Maximum crystallization temperature T_c of V_{IBU} in solution in the presence of saturated ibuprofen as a function of DP_w of amylose (0.1 wt% solutions).

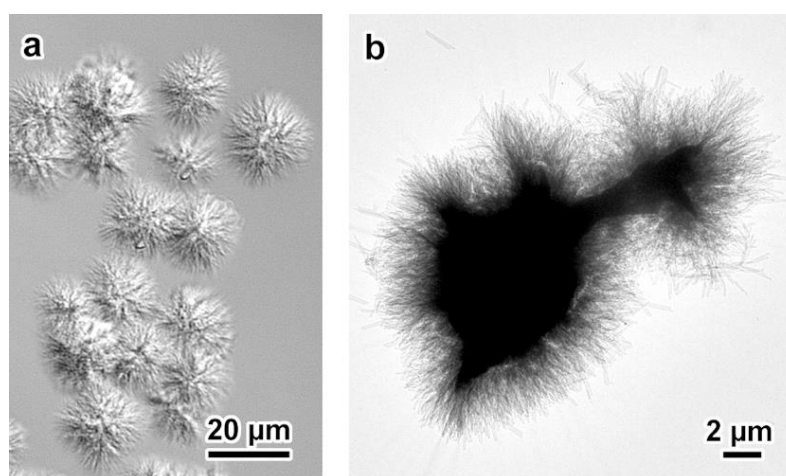
Fraction	DP60	DP130	DP192	DP600	DP6500
T_c (°C)	≤ 60	≤ 60	≤ 75	≤ 75	≤ 75

Table VI.2. Yield of complexation (%) of a 0.1 wt% DP6500 amylose solution as a function of incubation temperature and concentration of ibuprofen ($C_{ibuprofen}$). The results are expressed as a mean value \pm standard deviation from 3 independent assays.

$C_{ibuprofen}$ (wt%)	Incubation temperature (°C)			
	25	40	60	75
0.0025	-	-	-	-
0.0050	37.7 ± 4.5	23.3 ± 1.2	0.0 ± 0.0	0.0 ± 0.0
0.0100	84.0 ± 3.6	78.7 ± 5.9	22.5 ± 4.9	0.0 ± 0.0
0.0200	$93.3 \pm 0.6^*$	93.7 ± 1.5	90.7 ± 4.0	10.0 ± 1.3
0.0300	$97.0 \pm 2.6^*$	$96.7 \pm 1.5^*$	$91.3 \pm 1.2^*$	66.3 ± 3.1
0.0400	$95.0 \pm 1.0^*$	$94.7 \pm 2.1^*$	$93.0 \pm 1.0^*$	$84.7 \pm 4.5^*$

*: an excess of ibuprofen was observed.

-: no complexation was observed

**Figure VI.1.** a) Interference contrast optical micrograph (a) and low-magnification TEM image (b) of aggregates of V_{IBU} crystalline complexes (0.1 wt% DP6500 amylose, 75 °C).

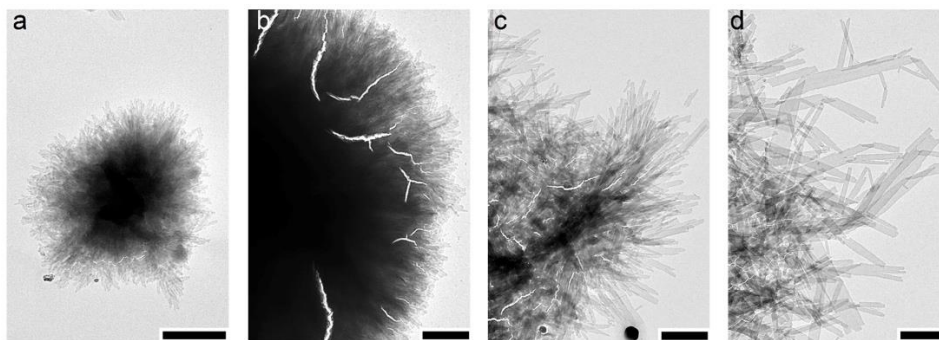


Figure VI.2. TEM images of lamellar single crystals of *V*_{IBU} prepared using DP6500 amylose at 25 °C (a), 40 °C (b), 60 °C (c) and 75 °C (d). Scale bars: 1 μ m.

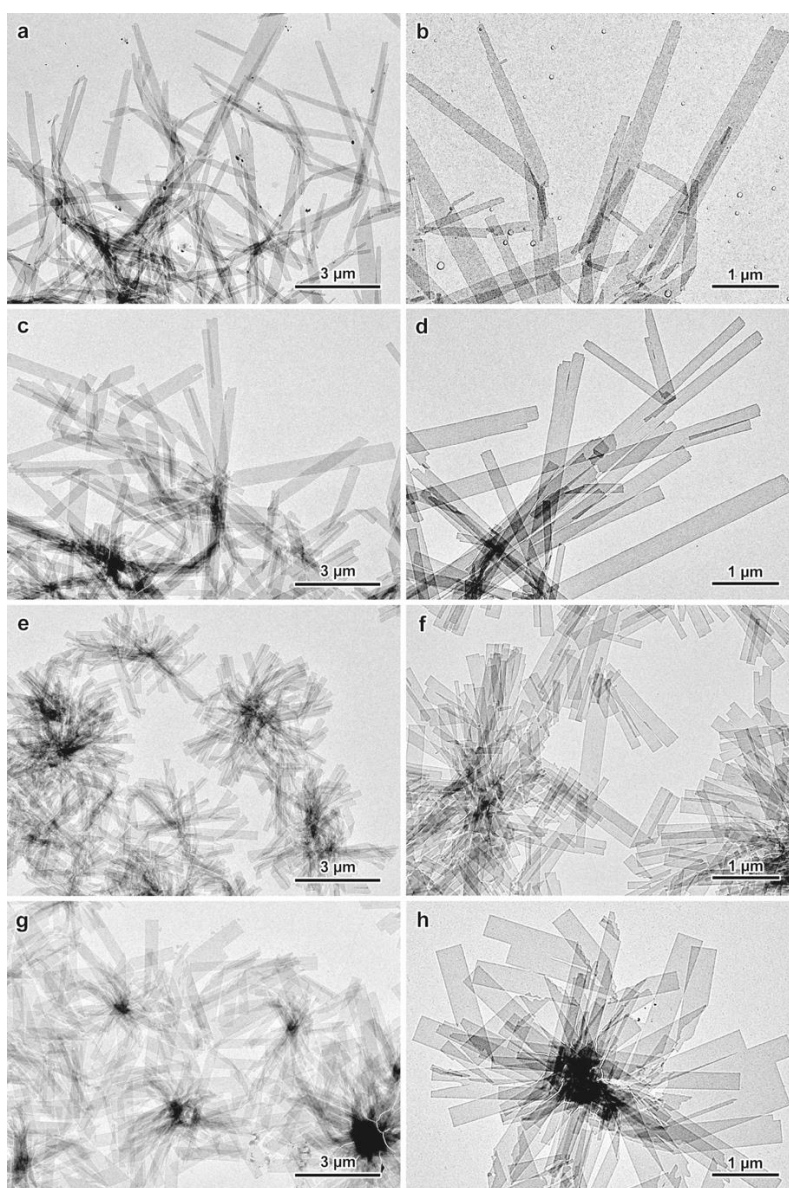


Figure VI.3. TEM images of lamellar single crystals of *V*-amylose complexed with ibuprofen: a,b) DP6500; c,d) DP192; e,f) DP130; g,h) DP60 (0.05 wt%, 75 °C for DP6500 amylose and 60 °C for others). More individual crystals were obtained by repeated recrystallization.

The general morphological features were confirmed by AFM images (**Figures VI.4**) from which height profiles were determined. As seen in **Table VI.3**, the lamellar thickness slightly increased with increasing amylose DP, from 5.5 (± 0.5) nm for DP60 to 7.0 (± 0.4) nm for DP6500. The roughness (0.7 nm) was fairly similar for all samples. Assuming that crystals contain 7-fold helices with a pitch of 0.8 nm and that there is no chain-folding, the theoretical thickness would be proportional to the DP of amylose (**Table VI.3**). The difference between the measured and calculated thickness supports the model of chain folding of amylose helices in V-amylose crystals.

Base-plane electron diffraction patterns were recorded at low temperature from individual frozen-solvated lamellar crystals. Despite some differences in terms of shape and size, the crystals prepared from all amylose fractions yielded similar patterns. A typical diagram recorded on a specimen area of about $1 \mu\text{m}^2$ of a single crystal prepared from DP60 amylose is shown in **Figure VI.5b**. It contains about 150 diffraction spots, up to a resolution of 0.35 nm, distributed along a rectangular network defined by two orthogonal reciprocal base vectors a^* and b^* very close in length. The stronger spots are located on the 5th and 6th rows and the odd reflections on the a^* and b^* axes are systematically absent. The calibration of about 40 spots allowed calculating the unit cell parameters $a = 2.83 \pm 0.01$ nm and $b = 2.96 \pm 0.01$ nm, in good agreement with previously published results (Buléon et al., 1990; Nishiyama et al., 2010; Nuessli et al., 2003; Putaux et al., 2008). The shape of the lamellar crystals and their base-plane ED and parameters are similar to those reported earlier for V7_{II} crystals (see **Chapter IV**). Consequently, we concluded that the unit cell was orthorhombic and that its three-dimensional space group was $P2_12_12_1$.

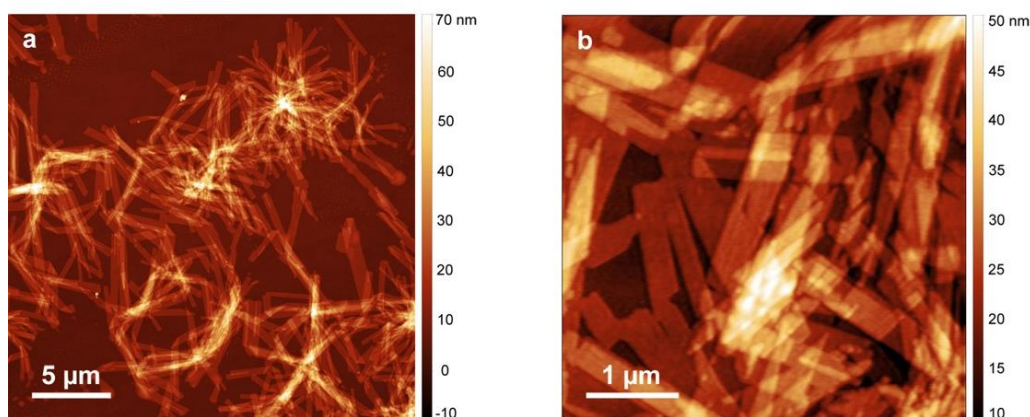


Figure VI.4. AFM images of lamellar single crystals of DP192 (a) and DP60 (b) amylose complexed with ibuprofen.

Table VI.3. Average thickness and roughness of V_{IBU} lamellar crystals measured from height profiles in AFM images. The roughness was calculated over $100 \times 100 \text{ nm}^2$ regions. The theoretical thickness has been estimated from the DP_w of amylose, assuming a non-folded 7-fold single helix with a pitch of $c = 0.80 \text{ nm}$.

Fraction	DP60	DP130	DP192	DP6500
Experimental thickness (nm)	5.5 ± 0.5	5.7 ± 0.4	6.5 ± 0.3	7.0 ± 0.4
Roughness (nm)	0.7	0.7	0.5	0.7
Theoretical thickness (nm)	6.9	14.9	21.9	743.0

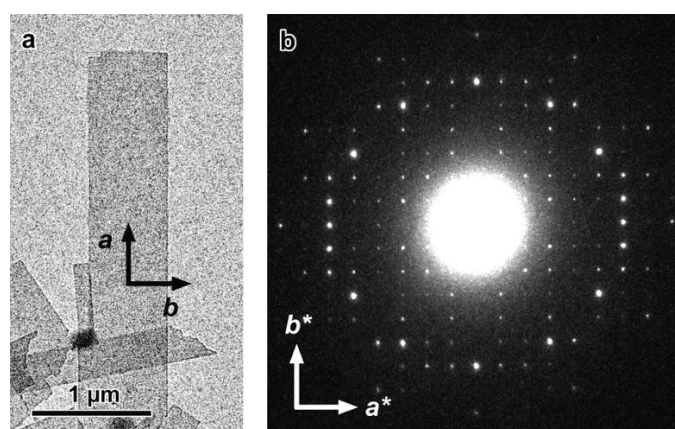


Figure VI.5. a) TEM image of a lamellar single crystal of DP60 amylose complexed with ibuprofen; b) corresponding base-plane electron diffraction pattern. The pattern is rotated by 90° with respect to the crystal in (a).

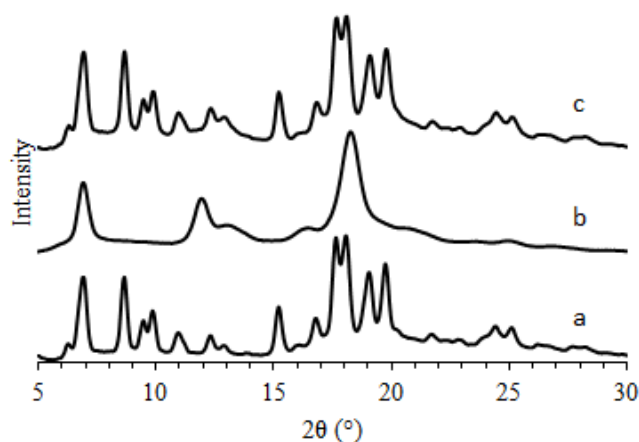


Figure VI.6. XRD profiles of hydrated V_{IBU} crystals (D6500 amylose) (a), after thorough drying in vacuum at room temperature (b), and rewetting (c).

The XRD powder profile of V_{IBU} crystals in the solvated state and recorded at room temperature is shown in **Figure V.6a**. After calibration and assuming an orthorhombic structure, as suggested by ED data, the unit cell parameters were determined as: $a = 2.824$ (± 0.001) nm, $b = 2.966$ (± 0.001) nm and $c = 0.800$ (± 0.001) nm (**Annex 4, Table S.VI.1**).

Upon freeze-drying, the complexes yielded a typical diffraction pattern for $V7_a$ (**Figure VI.6b**). Reflection peaks and corresponding Miller indices are listed in **Annex 4, Table SVI.1**. In addition, the reflections of the dry form are rather broad suggesting a slight loss in crystallinity. However, after rewetting in water or rehydrating in 95% RH chamber, the complexes produced a diffraction pattern that is almost identical to that of the wet sample. This result suggested that ibuprofen was retained in the crystal and the structural transition was due a loss of water molecules. Furthermore, water would not be bound very tightly since the structural transition occurred even when the crystal was exposed to the ambient air. The drying behavior of V_{IBU} was generally observed for $V7_{II}$ crystals obtained with many other complexing agents (see **Chapter IV**).

As noted in **Chapter IV**, the transition to $V7_a$ from a $V7_{II}$ complex with a non-volatile guest which is not easily removed by drying raises an ambiguity about the location of the complexing agent. Indeed, the presence of the bulky molecules in the inter-helix space may perturb the hexagonal arrangement in $V7_a$.

VI.2.2. V_{IBU} crystals from concentrated solutions

A batch of V_{IBU} crystals was prepared from a more concentrated aqueous solution of DP6500 amylose (1 wt%) in order to obtain a larger amount of material for the release experiments. DMSO (10 vol%) was used as co-solvent to facilitate the dissolution of amylose. The crystallization occurred at 75 °C in the presence of a saturation of IBU. The solid precipitate was recovered by decantation followed by centrifugation (3600 g, 15 min), washed three times with water saturated with IBU and then freeze-dried.

Figure VI.7 shows an optical micrograph and TEM images of the resulting crystals that exhibit a less defined rectangular shape and a smaller width compared to those prepared in a 0.1 wt% amylose aqueous solution at the same crystallization temperature (**Figure VI.2d**). This morphological difference can be due to a faster nucleation and growth since the crystallization was carried out in much higher amylose concentration (1 wt%) (**Mersmann, 2001**). The powder XRD profiles of hydrated V_{IBU} crystals (**Figure VI.8a**) is well defined and almost identical to that shown in **Figure VI.6a** for the sample prepared from 0.1 wt% amylose. After freeze-drying, the complexes yielded a typical diffraction pattern of $V7_a$ (**Figure VI.8b**). This diffraction

pattern is similar but contains broader peaks compared to that shown in **Figure VI.6b** for *V_{ibuprofen}* dried in vacuum at room temperature, suggesting a lower crystallinity. As discussed in **Chapter IV**, freeze-drying would be more efficient than vacuum-drying at room temperature in removal of water which is essential for the crystal structure and crystallinity. However, in both case, the initial crystal structure and crystallinity were recovered after rewetting or equilibrating at 95% RH.

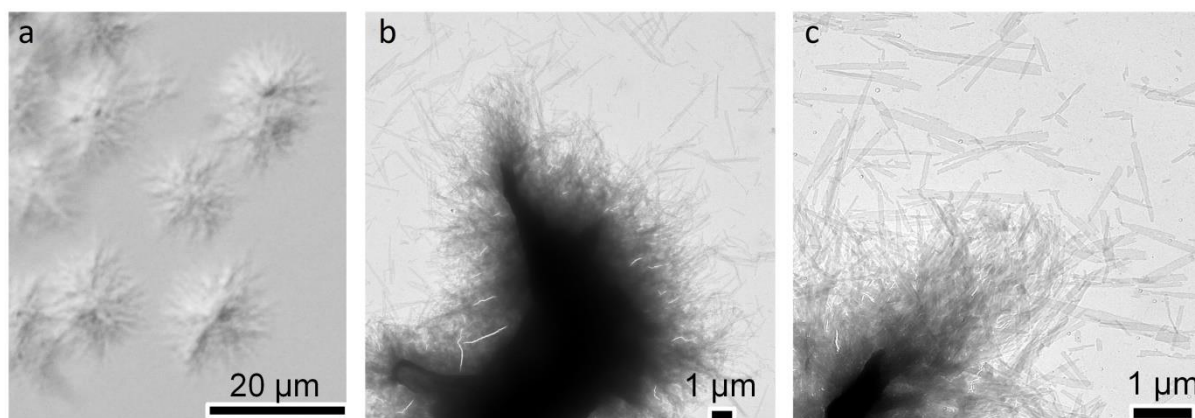


Figure VI.7. Optical (a) and TEM (b,c) images of aggregates of *V_{IBU}* crystalline complexes prepared in a 1 wt% amylose and 1:9 DMSO:water solution at 75 °C.

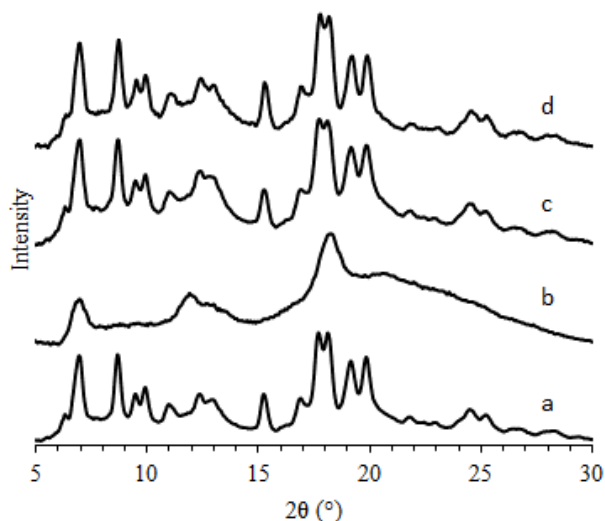


Figure VI.8. XRD profiles of: a) hydrated *V_{IBU}* crystals prepared in 1 wt% amylose and 1:9 DMSO:water mixture at 75 °C; b) crystals as (a) after freeze-drying; c) crystals as in (b) after partial dissolution in 0.1 M HCl at pH 1.2; d) crystals in (b) after partial dissolution in phosphate buffer at pH 5.5.

The FT-IR analysis supports the formation of an inclusion complex between amylose and IBU. The spectrum of *V*_{IBU} crystals prepared from DP6500 amylose shown in **Figure VI.9d** is compared to those of pure IBU, pure amylose and a physical mixture of amylose with 10 wt% IBU (**Figures VI.9a, VI.9b and VI.9c**, respectively). The carbonyl (C=O) stretching vibration band of pure IBU observed at 1707 cm⁻¹ is present in the spectra of the physical mixture and the complex but a new band appeared at 1730 cm⁻¹ in *V*_{IBU}'s spectrum. By analogy with the results from several studies of complexes between IBU and β-cyclodextrins, the band at 1707 cm⁻¹ would correspond to a very strong interaction between IBU through H-bonds between carbonyl groups while the band at 1730 cm⁻¹ would be attributed to less structured H-bonded carbonyls which are formed as a result of complexation (Braga et al., 2003; Bratu et al., 2005; Hussein et al., 2007; Mura et al., 1998; Tozuka et al., 2006).

In addition, the band assigned to aromatic C-C stretching shifted from 1507 cm⁻¹ in pure IBU or the physical mixture to 1512 cm⁻¹ in the complexes. Several bands attributed to IBU, and that still appeared in the physical mixture, disappeared from the *V*_{IBU} spectrum. This is the case for absorbances at 669 and 779 cm⁻¹, attributed to the deformation of the out-of-plane aromatic C-H bonds of IBU's phenyl group (Ghorab & Adeyeye, 2001) and bands that correspond to aromatic C-C stretching (1451 cm⁻¹), O-H bending (1418 and 934 cm⁻¹), C-O stretching (1268-1123 cm⁻¹) and in-plane C-H bending (1091-1007 cm⁻¹) (Coates, 2000). Furthermore, characteristic vibrational bands for *V*-amylose were observed at 1017, 1103, 1150, 1205, 1298, 1368 and 1411 cm⁻¹ (see **Chapter IV**).

The ¹³C CP/MAS NMR spectrum of never-dried *V*_{IBU} crystals shown in **Figure VI.10a** is typical of *V*-amylose. In particular, the C1 resonance at 103.3 ppm is a singlet, while those of the A- and B-amylose would be a triplet and a doublet, respectively (Gidley & Bociek, 1988; Veregin et al., 1987). Other clear peaks in the carbohydrate region can be assigned to specific carbons as summarized in **Chapter IV, Table IV.2**. Within the 50-110 ppm region, the spectrum is broadly similar to that shown by Zhang et al. (2016), although the resolution is higher in our case since, as can be judged from the XRD profiles, our specimen was significantly more crystalline. The contributions of guest IBU molecules appear at 20-40 ppm (CH/CH₂/CH₃) and 120-140 ppm (aromatic carbons). However, the peak corresponding to carbonyl groups (C=O), located in the spectrum of bulk ibuprofen at 181-183 ppm (Braga et al., 2003), is absent from the *V*_{IBU} spectrum, suggesting a high mobility of the IBU molecules in the crystal lattice.

A SP/MAS spectrum was recorded to quantify the guest IBU molecules included in the complex, (**Figure VI.9a**). The stoichiometry of IBU and glucosyl residues, calculated as the ratio of the integral area of the signal from the C1 contribution of amylose (103.3 ppm) to those from aromatic carbons of ibuprofen (121-134 ppm), was found to be 1:14.6. Note that a sharp peak corresponding to residual DMSO is present at 39.6 ppm in the SP/MAS spectrum while it is nearly absent in the CP/MAS spectrum, which suggests that the molecule is highly mobile.

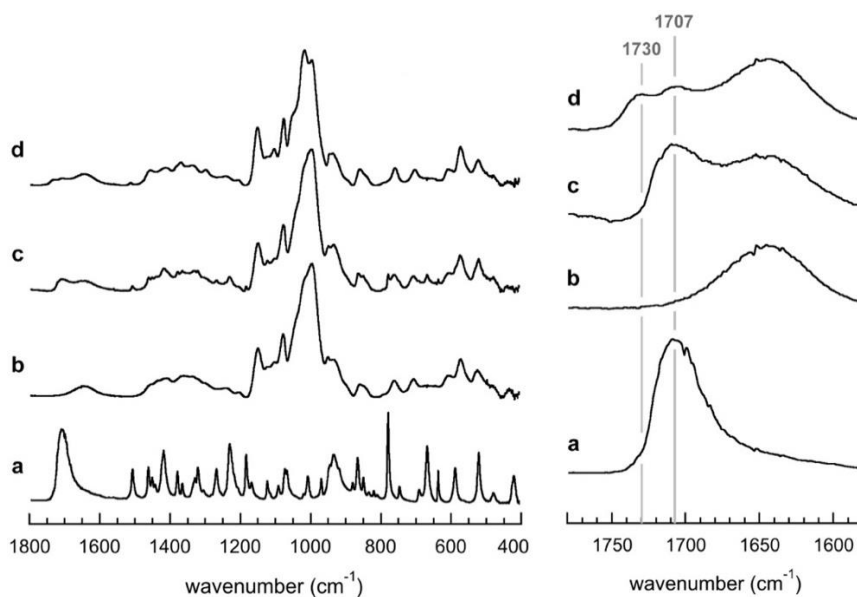


Figure VI.9. FT-IR spectra of racemic ibuprofen (a), DP6500 amylose (b), physical mixture of amylose and 10 wt% ibuprofen (c) and *V*_{IBU} crystalline complex (d). The series on the right focuses on the 1780-1580 cm^{-1} region corresponding to the contribution of carbonyl groups.

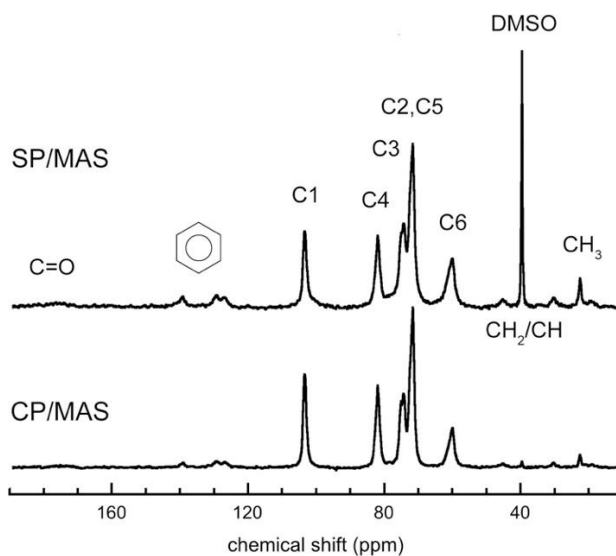


Figure VI.10. ^{13}C CP/MAS (a) and SP/MAS (b) NMR spectra of *V*_{IBU} crystalline complexes prepared from 1 wt% DP6500 amylose in 1:9 DMSO:water solution.

VI.3. Molecular modeling

Since the ED and XRD data of $V_{\text{ibuprofen}}$ and $V_{2\text{-propanol}}$ complexes have been shown to be nearly identical (**Annex 4, Figure S.VI.1**), the packing arrangement of amylose helices in the two complexes are expected to be similar. Therefore, the crystal structure of $V_{2\text{-propanol}}$ amylose was used to build the starting model for the simulation of the V_{IBU} crystal. In the $V_{2\text{-propanol}}$ model proposed by Nishiyama et al. (2010), antiparallel left-handed 7-fold helices are organized in an orthorhombic unit cell. The helix arrangement can be described by two alternating groups of four helices, organized into nearly close-packed hexagonal and tetragonal motifs, respectively. Two 2-propanol and two water molecules are located inside the helical cavity while two 2-propanol and four water molecules lie between the helices (**Annex 4, Figure S.VI.2**).

As noted above, the transition of $V_{\text{ibuprofen}}$ into the hexagonal $V7_a$ without removal of ibuprofen raised the ambiguity about the location of IBU in the inter-helix space. Consequently, we have studied two types of models: in **model 1**, IBU is only located inside the helix while in **model 2**, IBU lies both inside and between the helices. The ^{13}C SP/MAS NMR analysis showed that the stoichiometry was about 1 IBU per 14.6 glucosyl units. As there would be a small amount of amorphous amylose and to simplify the calculation, the stoichiometry of the complexes was rounded to 1 ibuprofen per 14 glucosyl units. In addition, the amount of water added was based on the measured density ($1.48 \text{ g}\cdot\text{cm}^{-3}$).

In **model 1**, built by Yu Ogawa (CERMAV), the unit cell structure of $V_{\text{ibuprofen}}$ was duplicated to build a $P1$ supercell having approximately 3 nm in each direction and containing 4 amylose chains. Each chain consisted of 28 glucose residues and was covalently bonded to its own periodic image to simulate an infinite chain. Periodic boundary conditions were applied in all three directions to model an infinite-size crystal. Two IBU molecules were placed inside each helix and water molecules were inserted both inside and between the helices. The supercell structure was first energy-minimized using the steepest-descent method, followed by the conjugate gradient method. The convergence criterion to stop minimization was a $10 \text{ kJ mol}^{-1}\text{nm}^{-1}$ maximum force. The structure was then heated at a rate of 0.2 K ps^{-1} , and equilibrated at 300 K and 1 atm. The production run was performed for 50 ns at the same temperature and pressure. The axial and longitudinal views of the final model are shown in **Figures VI.11a** and **VI.11b** respectively.

To construct **model 2**, a $P1$ supercell was generated by considering three helical turns. Thus, it has a c -axis of 2.40 nm and the same a and b parameters as those of the $V_{\text{ibuprofen}}$ unit cell with space group $P2_12_12_1$. One IBU molecule was inserted in each helical cavity and

interstitial pocket. Thus, the proposed ratio of intra-helical to inter-helical ibuprofen was 2:1. The stable positions of IBU were then searched by geometry minimization while constraining the amylose helices. Water were then placed into the structure and the structure was energy-minimized using the same method. Finally, the system was optimized with all atoms free to move. The final structure was presented in **Figures VI.11c,d**.

In both models, the amylose helices have positions very similar to those in the model of $V_{2\text{-propanol}}$ (**Annex 4, Figure S.VI.2**). On the other hand, in both cases, the helices are much more deformed because the helices are allowed to freely relax in the $P1$ symmetry. The above results suggest that the interstitial IBU is not essential for the stability of the crystal structures. **Figure VI.12** compares the observed and calculated EDs for the two models. There are noticeable differences in reflection intensities between both patterns. Model 2 seems to give a slightly better fit. In addition, for model 1, some reflections of the calculated pattern are absent in the experimental one. The difference may arise from the location of IBU and water molecules that should be considered as one local solution among many others differing by the distribution of the guest molecules. As revealed by solid-state NMR results, IBU is quite mobile in the crystal structure and thus would not occupy a precise crystallographic position. In addition, it is important to note that these models were built on the basis of packing energy. A combination with a structural refinement against diffraction data, such as that previously used to solve the structure of $V_{1\text{-butanol}}$ may help increase the matching between the observed and calculated diffraction pattern. However, the difficulty is that the diffraction data with several reflections at low angles would not be sufficient to solve the structure of V_{IBU} with a large number of parameters.

VI.4. *In vitro* release properties of ibuprofen from the complexes

VI.4.1. Ibuprofen content in the complexes

The amount of IBU in the complex was determined by UV spectroscopy using two different methods. Method 1 used ethanol to extract IBU from the complex without solubilizing amylose. In order to confirm the complete IBU extraction from the complex, a second method was implemented. The complex was dissolved in 0.1 M NaOH, resulting in the total release of IBU. The results obtained with both methods were in good agreement: IBU contents of 8.345 ± 0.089 wt% and 8.403 ± 0.132 wt% were determined by methods 1 and 2, respectively. The corresponding stoichiometry was calculated to be about 1 IBU molecule per 14 glucosyl units, in agreement with the value previously determined by ^{13}C SP/MAS NMR spectrometry (§ VI.2.2). The result suggests that ibuprofen was totally extracted by ethanol. In addition, all the above quantification methods are reliable for the determination of ibuprofen content in V_{IBU} .

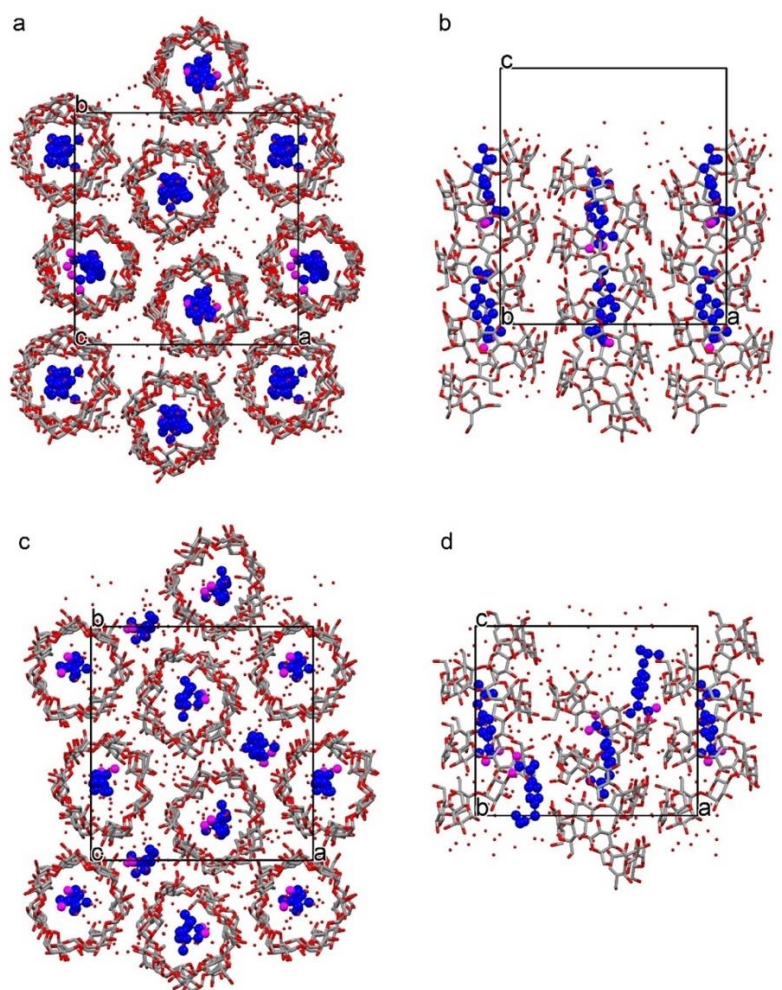


Figure VI.11. Projection on the (a,b) plane (a-c) and (a,c) plane (b-d) of the two molecular models proposed for *V_{ibuprofen}*. In model 1 (a-b), IBU is located only inside the helices. There are 2 IBUs per 4 turns of left-handed 7-fold helix. In model 2 (c-d), IBU is located both inside and between the helices. There is 1 intrahelical IBU per 3 turns of helix and another IBU located in the adjacent interstitial pocket.

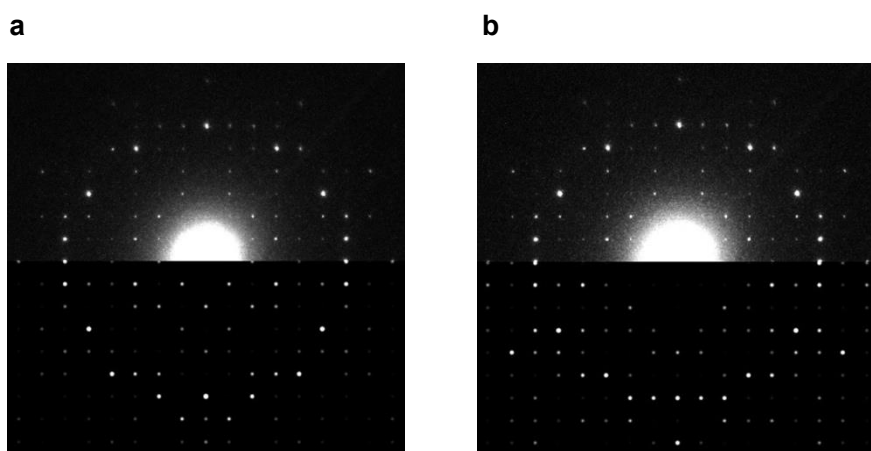


Figure VI.12. Composite of observed (upper) and calculated (lower) ED patterns from the two proposed models of *V_{ibuprofen}*: model 1 (a) and model 2 (b).

VI.4.2. *In vitro* dissolution studies

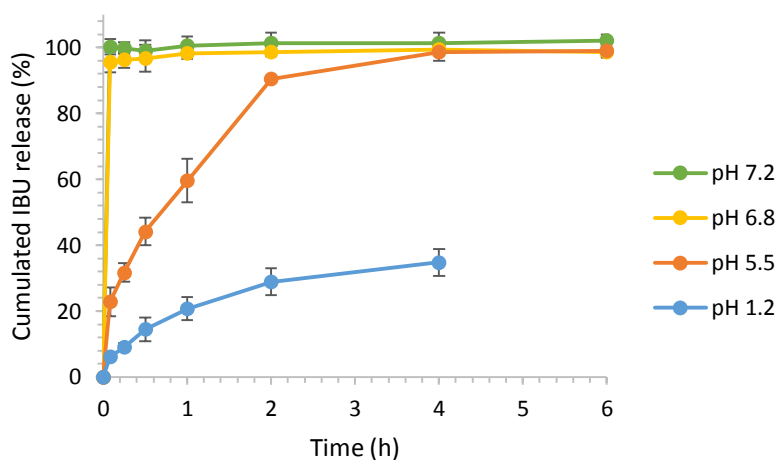
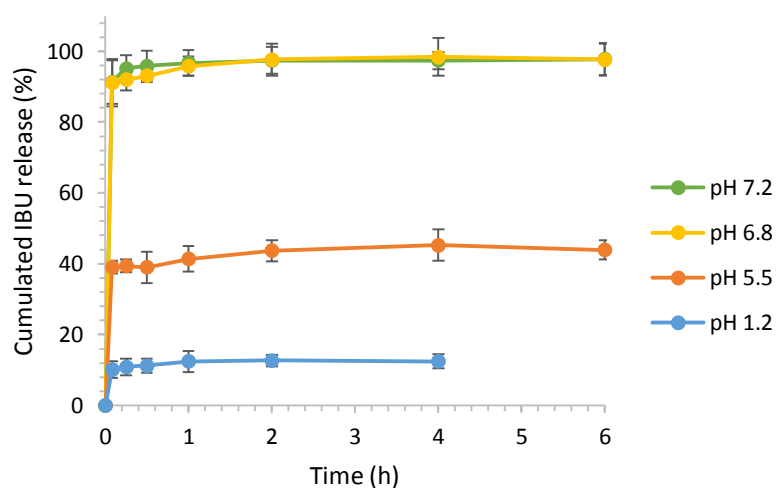
The solubility of raw IBU powder at 37 °C increased with increasing pH (**Table VI.4**), in agreement with previous studies (Levis et al., 2003; Qiu et al., 2001; Rivera-Leyva et al., 2012; Yiyun & Jiepin, 2006). The increase in solubility is due to the ionization of IBU. Indeed at pH higher than pKa (4.5) (Newton & Kluza, 1978; Ràfols et al., 1997), the ionized form of IBU is predominant. The lowest IBU solubility (75 mg.L⁻¹) was observed in 0.1 M HCl corresponding to the acidic form of IBU. In order to ensure sink conditions, all dissolution tests were performed in a sufficient volume of medium with respect to the amount of IBU to be dissolved, taking into account that the maximum concentration corresponding to the release of 100% IBU should not exceed 52.6 mg.L⁻¹. In these conditions, the dissolution medium would not reach saturation.

Figure VI.13 shows the dissolution profiles of the IBU raw powder in different media. The dissolution rate clearly increased with increasing pH. This result is expected to correlate with the solubility in these media. One can note that in acidic medium (pH 1.2), the dissolved IBU molecular fraction was about 40% after 4 h while in higher pH environments, it reached 100% within the same period of time. Indeed, at pH 1.2, residual IBU particles remained stuck to the basket and at the air/liquid surface due to the poor powder wettability.

The release profiles of the *V_{IBU}* complex were obviously different from those of pure IBU powder, as shown in **Figures VI.14** and **VI.15**. The variation of pH affected the amount of released IBU rather than the dissolution rate. The maximum percentage of released drug was only about 12% in 0.1 M HCl, but increased to about 45% in the buffer solution pH 5.5 and 100% in buffer solutions with pH > 6.8. The dramatic difference in percentage of released guest would mainly be attributed to the different solubilities of IBU in these pH solutions. The release profiles also suggest that IBU could be located at different positions within the complex. Three different IBU fractions were selectively released by controlling the pH of the dissolution medium. The first fraction (about 12% of total IBU) was readily released in the 0.1 M HCl. This fraction would be very loosely bound to *V*-amylose and may correspond to uncomplexed IBU entrapped inside amorphous regions of the sample. On the other hand, the fraction released at higher pH would correspond to complexed IBU that would comprise two distinct fractions: one that is further released upon increasing the pH to 5.5 (about 30% of total IBU) and the other is the remaining fraction (about 60%) that is released at pH 6.8-7.2 (**Figures VI.14** and **VI.15**). The latter would correspond to the most tightly bound molecules. In addition, the total release of IBU at pH 6.8-7.2 resulted in the complete dissolution of the *V_{IBU}* crystals. In contrast, the crystals appeared to be resistant in media pH 1.2 or pH 5.5.

Table VI.4. Solubility of ibuprofen in different dissolution media at 37 °C.

Medium	pH	Solubility (mg.L ⁻¹)
0.1 M HCl	1.2	75.28 ± 4.39
0.1 M phosphate buffer	5.5	427.74 ± 6.60
0.05 M phosphate buffer	6.8	3071.32 ± 18.65
0.05 M phosphate buffer	7.2	4609.90 ± 45.84

**Figure VI.13.** Partial dissolution of pure ibuprofen in 0.1 M HCl at pH 1.2, and phosphate buffers at pH 5.5 (0.1 M), pH 6.8 (0.05 M) and 7.2 (0.05 M) at 37 °C.**Figure VI.14.** Release of ibuprofen from V_{IBU} complexes in 0.1 M HCl at pH 1.2, and phosphate buffers at pH 5.5 (0.1 M), pH 6.8 (0.05 M) and 7.2 (0.05 M) at 37 °C.

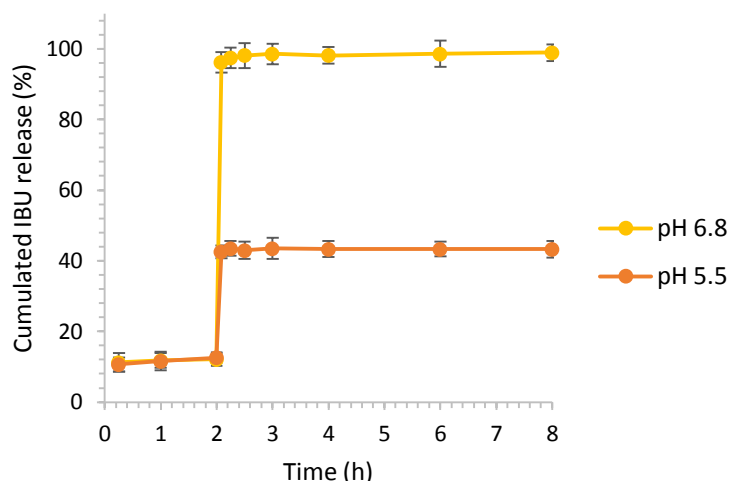


Figure VI.15. Release of ibuprofen from V_{IBU} complexes in a 2-stage dissolution test: acid stage (0-2 h): 0.1 M HCl; buffer stage (2-8 h): phosphate buffer at pH 5.5 (0.1 M) or pH 6.8 (0.05 M) at 37 °C.

Indeed, the XRD diagrams of the residues recovered after partial dissolution in these media were identical to those of the initial hydrated sample (**Figure VI.8c,d**). The result suggests that IBU molecules would not interact with amylose in the same manner in the crystal lattice. The most tightly bound fraction plays a crucial role in the stability of the complexes while the elimination of the loosely bound fraction does not cause any significant change in crystal structure. The interaction of IBU with amylose would depend on the location of the complexing agent. IBU can possibly be located both inside and between amylose helices (**Figure VI.11c,d**). Since the amylose helical cavity is a relatively hydrophobic environment, hydrophobic ibuprofen should be more tightly bound when located inside the helix than in the interhelical spaces. On the basis of this hypothesis, the ratio between intra- and inter-helical ibuprofen is approximately 2:1, thus supporting **model 2**. The result also suggests that the interstitial ibuprofen is not essential for the stability of the crystal structure, in agreement with the modeling study. However, it must be noted that our experimental data do not allow an unambiguous confirmation of the location of IBU in the complex.

Furthermore, as the release of IBU mainly occurred at pH 5.5-7.2, the V_{IBU} complexes can act as a delayed release system for intestinal targeting. The observation that V_{IBU} was stable in gastric pH 1.2 but released in simulated intestinal fluid has recently been made in other studies (Yang et al., 2013; Zhang et al., 2016). However, the authors showed a sustained release profile in pH 6.8-7.2 buffers by comparison with the instantaneous dissolution revealed in the present work. Similar instantaneous and sustained releases have also been observed for

complexes of ibuprofen with β -cyclodextrin (Charoenchaitrakool et al., 2002; Salústio et al., 2012). For V_{IBU} , the release rate is also most probably be related to the morphology of the complex. Indeed, the lamellar shape with a thickness lower than 10 nm, offers a high contact surface with the medium which should increase the release rate.

VI.5. Conclusions

Lamellar rectangular *V*-amylose single crystals were prepared by adding racemic IBU to hot dilute aqueous solutions of native and enzymatically-synthesized amylose (0.1 wt%) with an average DP_w varying from 60 to 6500. In addition, a highly crystalline fraction of V_{IBU} inclusion complexes was successfully prepared by crystallization in 1 wt% DP6500 amylose DMSO:water solution. The base-plane electron diffraction pattern, powder XRD profile, FT-IR and ^{13}C CP/MAS NMR spectra of the crystals concurred to show that the complex belongs to the $V7_{II}$ allomorphic family. Amylose is thus crystallized in an orthorhombic $P2_12_12_1$ space group with unit cell parameters $a = 2.824 (\pm 0.001)$ nm, $b = 2.966 (\pm 0.001)$ nm and $c = 0.800 (\pm 0.001)$ nm, corresponding to four 7-fold left-handed amylose single helices per unit cell. IBU would be located both inside and between the helices along with some water molecules. Water was shown to be an essential part of the complexes, its elimination resulting in the collapse of the original orthorhombic $V7_{II}$ structure and a generation pseudo-hexagonal $V7_a$ structure. The transition was reversible by rewetting the dry complexes. A stoichiometry of 1 ibuprofen molecule per 14.6 glucosyl residues was determined by SP/MAS NMR spectroscopy, in good agreement with the value quantified by UV spectrometry from *in vitro* release experiments (1 IBU per 14 glucosyl units). Two tentative models with or without interstitial IBU were built by molecular dynamics and geometry optimization using the previously published model of isomorphous for $V_{2\text{-propanol}}$ crystal as starting model. The organization of amylose helices were similar in both calculated structures, which suggests that the stability of the complex would not depend on the presence of IBU in the interstitial spaces.

In vitro dissolution studies showed that the amount of IBU released from the complexes increased with increasing pH. This correlated with possible locations of IBU in the complexes in relation with different interactions with amylose. For instance, the IBU molecules located inside the helix would be bound more tightly and have more important effect on the stability of the complexes than that located in the inter-helix space. The results also suggest that the inclusion complexes are potentially interesting for intestinal targeting which would thus be an advantage for improving the therapeutic effect of ibuprofen while avoiding stomach damage.

Conclusions and perspectives

Twenty four years after the work of William Helbert (PhD in CERMAV in 1994) and 12 years after that of Benoit Biais (PhD in INRA Nantes in 2006), we have carried out an extensive study on the fascinating property of amylose to form crystalline inclusion complexes with a large variety of small molecules. One of our objectives was to propose convincing molecular models of these complexes in order to better understand the interaction of amylose with the guest molecules, and if possible, be able to predict the structure that would result from the crystallization of amylose with a given complexing agent.

Since, so far, and as is generally the case with polymers, it has not been possible to grow single crystals large enough to allow their analysis by X-ray crystallography, our general approach has been to prepare model lamellar crystals from dilute aqueous solutions and characterize their morphology and structure by combining TEM and ED of these single crystals with XRD of hydrated powders.

The first part of this work has thus been devoted to optimizing the crystallization protocols by investigating the impact of several parameters (DP and concentration of amylose, nature of the solvent, crystallization temperature and time) on the morphology and structure of the crystals. The study of the complexes prepared with a homologous series of straight-chain saturated fatty acids (from C3 to C20) has brought an unexpected new result: a given fatty acid could induce the formation of different allomorphs containing 6- and 7-fold helices, and up to 3 allomorphs in some cases. This observation has prompted us to test more homologous series of molecules differing by their chemical structure (diols, esters, amines, ketones, aromatic compounds, etc.).

The second part of our work consisted in characterizing the large number of crystals prepared in various conditions and analyzing the significant amount of data collected using different techniques. Several conclusions could be drawn. Within the range of selected crystallization conditions, among the **121 agents** that were tested, 28 did not yield any crystals and 43 induced the formation of 2 to 4 allomorphs (**Table V.11**).

Ten different allomorphic families of lamellar V-amylose crystals containing 6-, 7- or 8-fold helices were identified, among which 5 corresponded to structures reported by previous authors and **5 were new allomorphs described for the first time**. In order to distinguish these allomorphs, we have augmented the previous nomenclature of V-amylose. The 10 allomorphs were named based on the helical conformation of amylose and relative interhelical space of unit

cells: **V6_I**, **V6_{II}**, **V6_{III}**, **V6_{IV}**, **V7_I**, **V7_{II}**, **V7_{III}**, **V7_{IV}**, **V8_I** and **V8_{II}**. The lamellar crystals corresponding to **V6_I**, **V7_I**, **V7_{IV}** and **V8_I** structures exhibited very similar shapes. Those of **V6_{III}** and **V8_{II}** were similar as well while **V6_{II}**, **V6_{IV}**, **V7_{II}**, and **V7_{III}** exhibited distinct morphologies. However, the allomorphs could be distinguished without ambiguity from their base-plane ED and powder XRD patterns.

Spectroscopy analyses were used to complement the crystallography data. FT-IR spectra of V-amylose showed an increase in intensity of specific vibrational bands compared to amorphous or A- and B-amylose. In addition, the band near 1022 cm⁻¹ could be used as a fingerprint of V-amylose. These differences can be accounted for different amylose helical conformations in the various allomorphs. However, we consider these FT-IR data to be preliminary and the complex spectra should be analyzed and compared in more details.

Expanding from previous results from the literature, we observed that there is a significant correlation between the helicity of V-amylose and its C1 resonance in ¹³C CP/MAS solid-state NMR spectra. The resonance is shifted downfield with increasing number of glucosyl units per turn. Three C1 chemical shifts were detected, likely corresponding to the 6-, 7- and 8-fold helices. In addition, the C1 resonance was a multiplet in **V6_{IV}** and **V7_{III}** while it was a singlet in other allomorphs, suggesting that **V6_{IV}** and **V7_{III}** would contain helices that are less symmetrical than those in other allomorphs. However, due to the multiplicity in the C1 chemical shift, the helical conformation of **V6_{IV}** and **V7_{III}** could not be unambiguously confirmed from the present data. Like for FT-IR spectroscopy, we consider these solid-state NMR results to be preliminary and they should be further investigated. In particular SP/MAS analyses are potentially interesting to evaluate the mobility of the guest molecules and determine the stoichiometry of the complexes.

Although we proposed tentative geometrical models for each allomorph, we have carried out a more detailed study of V_{1-butanol} (**Chapter III**). On the one hand, this complex is of historical importance since 1-butanol was one of the first agents used in the 1940's to fractionate native starch by selective crystallization with amylose. On the other hand, among the 5 previously known crystal forms, it was the only one for which the arrangement of helices was still hypothetical, and 43 of our tested complexing agents yielded the **V6_{II}** allomorph. Our structure determination approach was based on conformational and packing energy analyses, combined with classical crystalline polymer structure refinement. The resulting model with the lowest reliability factor was described by a *P2₁2₁2₁* orthorhombic lattice of antiparallel 6-fold left-handed single helices in which the hydroxyl groups exhibit some conformational disorder.

There are four 1-butanol and 16 water molecules distributed into four elongated interstitial pockets, and one 1-butanol molecule per unit cell located inside each helix. This result confirmed the model proposed by Helbert and Chanzy (1994). However, our structure was only refined against base-plane ED data. Therefore, the atomic positions along the *c*-axis are not precisely known. In order to ascertain the 3D structure, ED patterns must be recorded on crystals rotated about the main axes of the reciprocal space and the intensity of the diffraction spots quantitatively analyzed.

Due to time limitation and the large number of different guest molecules, we could not perform the same type of analysis for the 5 new allomorphs but we have proposed geometrical models based on the crystallographic and spectroscopic data. The helix packing in V6_I, V7_I, V7_{III}, V7_{IV} and V8_I structures is rather compact, and the complexing agents would only be located inside the helices. In contrast, there is more interstitial space in V6_{II}, V6_{III}, V6_{IV}, V7_{II} and V8_{II} to accommodate guest molecules. In addition the complexing agents can possibly be located inside the helices, except for V6_{IV}. In fact, since V6_{IV} was obtained with 4-hydroxybenzoic acid whose size appears to be incompatible with the cavity of a 6-fold helix, the cyclic complexing agent should be located only in interstitial spaces. All the tentative geometrical models remain to be validated by a detailed structural analysis combining experiments and modeling.

Our results show that each allomorph can be obtained with different complexing agents. However, V6_I, V6_{II} and V7_{II} were more prevalent. In addition, the helical conformation was found to be related to the size of the complexing agent. V6-type complexes were obtained with molecules with straight carbon chains, while branched-chain and cyclic molecules tended to yield 7-fold complexes. V8-type complexes were obtained with 1-naphthol, quinoline and salicylic acid. However, it is still difficult to predict the crystal structure based on the nature of the guest since a complexing agent could induce different crystal structures.

Indeed, **V-amylose polymorphism** was observed with a large number of complexing agents and **is thus a more general phenomenon than what was previously reported** in the literature. The tendency of a complex to exhibit a polymorphic behavior is not only related to the nature of the complexing agent but also to the accessibility of the various structures through crystallization. Complexes of straight-chain molecules are more likely to exhibit polymorphism than the branched-chain or cyclic compounds. In addition, straight-chain molecules, alcohols, fatty acids, aldehydes, amides or amines are likely more prone to form different allomorphs than esters and ketones.

Different parameters including solvent composition, temperature of mixing and crystallization, concentration of complexing agent and amylose, DP of amylose were revealed to have important impact on the formation and crystal structure of V-amylose. A variety of crystallization conditions had to be explored in order to observe relevant structures. However, the mechanism of polymorphic crystallization is still unclear. Future works combining experimental data and simulations should be conducted to understand the effect of the chemical nature of the guest and several crystallization parameters on the formation and crystal structure of V-amylose.

Water was shown to play a crucial role on the stability and the crystallinity of the complexes. Upon drying, V6_I, V6_{II}, V6_{IV}, V7_I, V7_{II} and V7_{IV} were transformed into compact hexagonal structures. For V7_{III}, V8_I and V8_{II}, a significant loss in crystallinity was observed, but the crystal structure remained the same. V6_{III} is the only structure that was stable upon drying. Surprisingly, in many cases, after drying in vacuum resulting in a loss of crystallinity, the original structure was reversibly restored by rehydration in humid atmosphere. In many previous studies, the focus was on the entrapment and release of the complexing agent but in view of our results, the role of water must be further studied and clarified.

Our results also suggest that **new allomorphs of V-amylose remain to be discovered**, which can be done by testing new complexing agents together with varying the conventional crystallization method in solution. The influence of factors such as solvent composition and additives should be further explored. As noted, in this study, only DMSO was tested as additive. In addition, using different preparation techniques is also recommended, *e.g.* insertion of complexing agent into a preformed V-amylose, sealed-heating, etc.

To evaluate the potential of V-amylose as a delivery system of bioactive agents, we have studied model amylose complexes prepared with racemic ibuprofen. Highly crystalline fractions of lamellar crystals were successfully prepared by crystallization in water or DMSO:water solution (0.1-1 wt% amylose). The base-plane electron diffraction pattern, powder XRD profile, FT-IR and ¹³C CP/MAS NMR spectra of the crystals showed that the complex belonged to the V7_{II} allomorphic family. Tentative models with or without interstitial ibuprofen were built by molecular dynamics and geometry optimization based on the arrangement that was previously published for the isomorphous V_{2-propanol} structure. The result suggests that the stability of the structure does not depend on the presence of ibuprofen in the interstitial spaces. However, the fit between the experimental ED pattern and those calculated from the proposed models is still not good enough and further work should be done to improve the model using a complementary analysis of packing energy.

In vitro dissolution studies revealed that $V_{\text{ibuprofen}}$ crystals exhibited different release profiles. In particular, the variation of the pH of the dissolution medium induced the selective release of different fractions of ibuprofen from the complexes. This result suggests that ibuprofen would reside in different locations and have different types of interactions with amylose. For instance, the ibuprofen molecules located inside the helix would be bound more tightly and play a more important role on the stability of the complexes than those located in the inter-helix space. Since the release mainly occurs at higher pH, the inclusion complexes seem to be a potentially interesting delivery system of ibuprofen for intestinal targeting and would thus be an advantage for improving its therapeutic effect.

Finally, since all validated models of V-amylose only involve left-handed helices, the **potential property of chiral selectivity** should also be investigated in the future. Our preliminary tests with enantiomers of ibuprofen, carvone, and menthol (results not shown in this manuscript) that all formed $V7_{\text{II}}$ complexes did not reveal any chiral discrimination. However, future works should investigate the interaction of amylose with stereoisomers of other molecules having different sizes and carefully consider the kinetics of the complex formation.

References

- Ades, H., Kesselman, E., Ungar, Y., & Shimoni, E. (2012). Complexation with starch for encapsulation and controlled release of menthone and menthol. *LWT - Food Science and Technology*, 45(2), 277-288.
- Akai, H., Yokobayashi, K., Misaki, A., & Harada, T. (1971). Complete hydrolysis of branching linkages in glycogen by *Pseudomonas* isoamylase: distribution of linear chains. *Biochimica et Biophysica Acta (BBA)-General Subjects*, 237(3), 422-429.
- Akkermans, R. L., Spensley, N. A., & Robertson, S. H. (2013). Monte Carlo methods in materials studio. *Molecular Simulation*, 39(14-15), 1153-1164.
- Andrew, E., Bradbury, A., & Eades, R. (1958). Nuclear magnetic resonance spectra from a crystal rotated at high speed. *Nature*, 182(4650), 1659.
- Arvisenet, G., Le Bail, P., Voilley, A., & Cayot, N. (2002). Influence of physicochemical interactions between amylose and aroma compounds on the retention of aroma in food-like matrices. *Journal of Agricultural and Food Chemistry*, 50(24), 7088-7093.
- Banks, W., & Greenwood, C. (1963). Hydrodynamic properties and dimensions of linear potato amylose molecules in dilute aqueous salt solution. *Die Makromolekulare Chemie: Macromolecular Chemistry and Physics*, 67(1), 49-63.
- Banks, W., & Greenwood, C. (1967). The fractionation of laboratory-isolated cereal gereal starches using dimethyl sulphoxide. *Starch-Stärke*, 19(12), 394-398.
- Banks, W., & Greenwood, C. (1968a). The conformation of amylose in neutral, aqueous salt solution. *Carbohydrate Research*, 7(3), 349-356.
- Banks, W., & Greenwood, C. (1968b). The hydrodynamic behaviour of native amylose in good solvents. *Carbohydrate Research*, 7(4), 414-420.
- Banks, W., & Greenwood, C. (1969). Viscosity and sedimentation studies on amylose in aqueous solution—further evidence for non-helical character. *European Polymer Journal*, 5(5), 649-658.
- Banks, W., & Greenwood, C. (1971a). The conformation of amylose in dilute solution. *Starch-Stärke*, 23(9), 300-314.
- Banks, W., Greenwood, C., & Thomson, J. (1959). The properties of amylose as related to the fractionation and subfractionation of starch. *Die Makromolekulare Chemie*, 31, 197-213.
- Banks, W., & Greenwood, C. T. (1966). The fine structure of amylose: the action of pullulanase as evidence of branching. *Archives of Biochemistry and Biophysics*, 117(3), 674-675.
- Banks, W., & Greenwood, C. T. (1971b). Amylose: a non-helical biopolymer in aqueous solution. *Polymer*, 12(2), 141-145.
- Bear, R. S. (1942). The significance of the “V” X-ray diffraction patterns of starches. *Journal of the American Chemical Society*, 64(6), 1388-1392.
- Bear, R. S. (1944). Complex formation between starch and organic molecules. *Journal of the American Chemical Society*, 66(12), 2122-2123.
- Berendsen, H. J., Postma, J. v., van Gunsteren, W. F., DiNola, A., & Haak, J. (1984). Molecular dynamics with coupling to an external bath. *The Journal of Chemical Physics*, 81(8), 3684-3690.
- Bernstein, J. (2002). *Polymorphism in molecular crystals*. Oxford University Press, p. 424.
- Bernstein, J. (2011). Polymorphism— a perspective. *Crystal Growth & Design*, 11(3), 632-650.
- Bernstein, J., Davey, R. J., & Henck, J.-O. (1999). Concomitant polymorphs. *Angewandte Chemie International Edition*, 38(23), 3440-3461.
- Bertoft, E. (2004). *Analysing starch structure*. In *Starch in Food: Structure, Function and Applications*, A.-C. Eliasson (Ed.). CRC Press, pp. 62-101.

- Bhatnagar, S., & Hanna, M. (1994). Extrusion processing conditions for amylose-lipid complexing. *Cereal Chemistry*, 71(6), 587-593.
- Bhosale, R. G., & Ziegler, G. R. (2010). Preparation of spherulites from amylose-palmitic acid complexes. *Carbohydrate Polymers*, 80(1), 53-64.
- Biais, B. (2006). Étude structurale et mécanismes de formation de complexes amylose-ligand Influence sur la rétention de composés d'arôme dans une matrice amyliacée. Doctoral dissertation, Université de Nantes.
- Biais, B., Le Bail, P., Robert, P., Pontoire, B., & Buléon, A. (2006). Structural and stoichiometric studies of complexes between aroma compounds and amylose. Polymorphic transitions and quantification in amorphous and crystalline areas. *Carbohydrate Polymers*, 66(3), 306-315.
- Biliaderis, C. G., & Galloway, G. (1989). Crystallization behavior of amylose-V complexes: structure-property relationships. *Carbohydrate Research*, 189, 31-48.
- Bluhm, T. L., & Zugenmaier, P. (1981). Detailed structure of the V_H-amylose-iodine complex: a linear polyiodine chain. *Carbohydrate Research*, 89(1), 1-10.
- Booy, F. P., Chanzy, H., & Sarko, A. (1979). Electron diffraction study of single crystals of amylose complexed with n-butanol. *Biopolymers*, 18(9), 2261-2266.
- Bourne, E., Donnison, G., Haworth, N., & Peat, S. (1948). 345. Thymol and cyclohexanol as fractionating agents for starch. *Journal of the Chemical Society (Resumed)*, 1687-1693.
- Braga, S. S., Gonçalves, I. S., Herdtweck, E., & Teixeira-Dias, J. J. (2003). Solid state inclusion compound of S-ibuprofen in β -cyclodextrin: structure and characterisation. *New Journal of Chemistry*, 27(3), 597-601.
- Bratu, I., Hernanz, A., Gavira, J., & Bora, G. (2005). FT-IR spectroscopy of inclusion complexes of beta-cyclodextrin with fenbufen and ibuprofen. *Romanian Journal of Physics*, 50(9/10), 1063.
- Brisson, J., Chanzy, H., & Winter, W. T. (1991). The crystal and molecular structure of V_H amylose by electron diffraction analysis. *International Journal of Biological Macromolecules*, 13(1), 31-39.
- Bučar, D.-K., Lancaster, R. W., & Bernstein, J. (2015). Disappearing polymorphs revisited. *Angewandte Chemie International Edition*, 54(24), 6972-6993.
- Buléon, A., Colonna, P., Planchot, V., & Ball, S. (1998). Starch granules: structure and biosynthesis. *International Journal of Biological Macromolecules*, 23(2), 85-112.
- Buléon, A., Delage, M. M., Brisson, J., & Chanzy, H. (1990). Single crystals of V amylose complexed with isopropanol and acetone. *International Journal of Biological Macromolecules*, 12(1), 25-33.
- Buléon, A., Duprat, F., Booy, F., & Chanzy, H. (1984). Single crystals of amylose with a low degree of polymerization. *Carbohydrate Polymers*, 4(3), 161-173.
- Buléon, A., Veronese, G., & Putaux, J.-L. (2007). Self-association and crystallization of amylose. *Australian Journal of Chemistry*, 60(10), 706-718.
- Burchard, V. W. (1963). Das viskositätsverhalten von amylose in verschiedenen lösungsmitteln. *Die Makromolekulare Chemie: Macromolecular Chemistry and Physics*, 64(1), 110-125.
- Byars, J. A., Fanta, G. F., & Felker, F. C. (2003). The effect of cooling conditions on jet-cooked normal corn starch dispersions. *Carbohydrate Polymers*, 54(3), 321-326.
- Byars, J. A., Fanta, G. F., & Felker, F. C. (2009). Rheological properties of dispersions of spherulites from jet-cooked high-amylose corn starch and fatty acids. *Cereal Chemistry*, 86, 76-81.

- Byars, J. A., Fanta, G. F., Kenar, J. A., & Felker, F. C. (2012). Influence of pH and temperature on the rheological properties of aqueous dispersions of starch–sodium palmitate complexes. *Carbohydrate Polymers*, 88(1), 91-95.
- Cael, J. J., Koenig, J. L., & Blackwell, J. (1975). Infrared and Raman spectroscopy of carbohydrates. Part VI. Normal coordinate analysis of V-amylose. *Biopolymers: Original Research on Biomolecules*, 14(9), 1885-1903.
- Cael, S., Koenig, J., & Blackwell, J. (1973). Infrared and Raman spectroscopy of carbohydrates. Part III: Raman spectra of the polymorphic forms of amylose. *Carbohydrate Research*, 29(1), 123-134.
- Cantor, S. M., Merion, T. L., & Wimmer, E. L. (1957). Alkaline earth hydroxide fractionation of starch. *U.S. Patent No. 2779692*.
- Carbinatto, F. M., Ribeiro, T. S., Colnago, L. A., Evangelista, R. C., & Cury, B. S. (2016). Preparation and characterization of amylose inclusion complexes for drug delivery applications. *Journal of Pharmaceutical Sciences*, 105(1), 231-241.
- Carciofi, M., Blennow, A., Jensen, S. L., Shaik, S. S., Henriksen, A., Buléon, A., Holm, P. B., & Hebelstrup, K. H. (2012). Concerted suppression of all starch branching enzyme genes in barley produces amylose-only starch granules. *BMC Plant Biology*, 12(1), 223.
- Cardoso, M. B. (2007). From rice starch to amylose crystals: alkaline extraction of rice starch, solution properties of amylose and crystal structure of V-amylose inclusion complexes. Doctoral dissertation. Université Joseph Fourier, Grenoble.
- Cardoso, M. B., Putaux, J.-L., Nishiyama, Y., Helbert, W., Hÿtch, M., Silveira, N. P., & Chanzy, H. (2007). Single crystals of V-amylose complexed with α -naphthol. *Biomacromolecules*, 8(4), 1319-1326.
- Charoenchaitrakool, M., Dehghani, F., & Foster, N. R. (2002). Utilization of supercritical carbon dioxide for complex formation of ibuprofen and methyl- β -cyclodextrin. *International Journal of Pharmaceutics*, 239(1-2), 103-112.
- Cheetham, N. W. H., & Tao, L. (1998). Amylose conformational transitions in binary DMSO/water mixtures. *Carbohydrate Polymers*, 35(3), 287-295.
- Chen, X., Yuan, C., Wong, C. K., & Zhang, G. (2012). Molecular modeling of temperature dependence of solubility parameters for amorphous polymers. *Journal of Molecular Modeling*, 18(6), 2333-2341.
- Cieřla, K., & Eliasson, A.-C. (2003). DSC studies of gamma irradiation influence on gelatinisation and amylose–lipid complex transition occurring in wheat starch. *Radiation Physics and Chemistry*, 68(5), 933-940.
- Coates, J. (2000). Interpretation of infrared spectra, a practical approach. *Encyclopedia of Analytical Chemistry*, 12, 10815-10837.
- Cohen, R., Orlova, Y., Kovalev, M., Ungar, Y., & Shimoni, E. (2008). Structural and functional properties of amylose complexes with genistein. *Journal of Agricultural and Food Chemistry*, 56(11), 4212-4218.
- Cohen, R., Schwartz, B., Peri, I., & Shimoni, E. (2011). Improving bioavailability and stability of genistein by complexation with high-amylose corn starch. *Journal of Agricultural and Food Chemistry*, 59(14), 7932-7938.
- Colonna, P., & Mercier, C. (1983). Macromolecular modifications of manioc starch components by extrusion-cooking with and without lipids. *Carbohydrate Polymers*, 3(2), 87-108.
- Colonna, P., & Mercier, C. (1984). Macromolecular structure of wrinkled-and smooth-pea starch components. *Carbohydrate Research*, 126(2), 233-247.

- Conde-Petit, B., & Escher, F. (1992). Gelation of low concentration starch systems induced by starch emulsifier complexation. *Food Hydrocolloids*, 6(2), 223-229.
- Conde-Petit, B., Escher, F., & Nuessli, J. (2006). Structural features of starch-flavor complexation in food model systems. *Trends in Food Science & Technology*, 17(5), 227-235.
- Conde-Petit, B., Handschin, S., Heinemann, C., & Escher, F. (2007). *Chapter 8 Self-assembly of starch spherulites as induced by inclusion complexation with small ligands*. In *Food Colloids: Self-Assembly and Material Science*, E. Dickinsin & E. M. Leser (Eds.). The Royal Society of Chemistry, pp. 117-126.
- Conde-Petit, B., & Escher, F. (1995). Complexation induced changes of rheological properties of starch systems at different moisture levels. *Journal of Rheology (1978-present)*, 39(6), 1497-1518.
- Cowie, J. (1960). Studies on amylose and its derivatives. Part I. Molecular size and configuration of amylose molecules in various solvents. *Die Makromolekulare Chemie: Macromolecular Chemistry and Physics*, 42(1), 230-247.
- Cowie, J. (1963). Studies on amylose and its derivatives. Part IV. The viscosity behaviour of amylose in mixed solvents. *Die Makromolekulare Chemie: Macromolecular Chemistry and Physics*, 59(1), 189-200.
- Cowley, J. M., Peng, L. M., Ren, G., Dudarev, S. L., & Whelan, M. J. (2004). 4.3.2. *Parameterizations of electron atomic scattering factors*. In *International Tables for Crystallography. Volume C: Mathematical, Physical and Chemical Tables*, E. Prince & A. J. C. Wilson (Eds.). Kluwer Academic Publishers, pp. 282.
- Creek, J. A., Benesi, A., Runt, J., & Ziegler, G. R. (2007). Potential sources of error in the calorimetric evaluation of amylose content of starches. *Carbohydrate Polymers*, 68(3), 465-471.
- Creek, J. A., Ziegler, G. R., & Runt, J. (2006). Amylose crystallization from concentrated aqueous solution. *Biomacromolecules*, 7(3), 761-770.
- Cui, R., & Oates, C. (1999). The effect of amylose-lipid complex formation on enzyme susceptibility of sago starch. *Food Chemistry*, 65(4), 417-425.
- D'Silva, T. V., Taylor, J. R., & Emmambux, M. N. (2011). Enhancement of the pasting properties of teff and maize starches through wet-heat processing with added stearic acid. *Journal of Cereal Science*, 53(2), 192-197.
- Dauchez, M., Derreumaux, P., & Vergoten, G. (1993). Vibrational molecular force field of model compounds with biologic interest. II. Harmonic dynamics of both anomers of glucose in the crystalline state. *Journal of Computational Chemistry*, 14(3), 263-277.
- De Montalk, G. P., Remaud-Simeon, M., Willemot, R.-M., Sarçabal, P., Planchot, V., & Monsan, P. (2000). Amylosucrase from *Neisseria polysaccharea*: novel catalytic properties. *FEBS Letters*, 471(2-3), 219-223.
- De Pilli, T., Jouppila, K., Ikonen, J., Kansikas, J., Derossi, A., & Severini, C. (2008). Study on formation of starch-lipid complexes during extrusion-cooking of almond flour. *Journal of Food Engineering*, 87(4), 495-504.
- DeLano, W. L. (2002). PyMOL. DeLano Scientific, San Carlos, CA, 700.
- Donnay, J. D. H. (1943). Rules for the conventional orientation of crystals. *American Mineralogist*, 28, 313-328.
- Dvornch, W., Yearian, H., & Whistler, R. L. (1950). Behavior of low molecular weight amylose with complexing agents. *Journal of the American Chemical Society*, 72(4), 1748-1750.
- Eliasson, A.-C., & Krog, N. (1985). Physical properties of amylose-monoglyceride complexes. *Journal of Cereal Science*, 3(3), 239-248.

- Erlander, S. R., & Purvinas, R. (1968). The polyelectrolyte behavior of amylose and its helix-to-coil transition in aqueous alkaline solutions. *Starch-Stärke*, 20(2), 37-45.
- Erlander, S. R., & Tobin, R. (1968). The stability of the helix of amylose and amylopectin in DMSO and water solutions. *Die Makromolekulare Chemie: Macromolecular Chemistry and Physics*, 111(1), 194-211.
- Etheridge, O.R., Wagoner, J.A., McDonald, J.W., Lippincott, D.A. (1962). Starch fractionation. *U.S. Patent No. 3067067*.
- Everett, W. W., & Foster, J. F. (1959). The conformation of amylose in solution. *Journal of the American Chemical Society*, 81(13), 3464-3469.
- Fanta, G., Shogren, R., & Salch, J. (1999). Steam jet cooking of high-amylose starch–fatty acid mixtures. An investigation of complex formation. *Carbohydrate Polymers*, 38(1), 1-6.
- Fanta, G. F., Felker, F. C., Hay, W. T., & Selling, G. W. (2017). Increased water resistance of paper treated with amylose–fatty ammonium salt inclusion complexes. *Industrial Crops and Products*, 105, 231-237.
- Fanta, G. F., Felker, F. C., & Selling, G. W. (2016). Films prepared from poly (vinyl alcohol) and amylose–fatty acid salt inclusion complexes with increased surface hydrophobicity and high elongation. *Starche-Stärke*, 68(9-10), 874-884.
- Fanta, G. F., Felker, F. C., & Shogren, R. L. (2002). Formation of crystalline aggregates in slowly-cooled starch solutions prepared by steam jet cooking. *Carbohydrate Polymers*, 48(2), 161-170.
- Fanta, G. F., Felker, F. C., Shogren, R. L., & Salch, J. H. (2008). Preparation of spherulites from jet cooked mixtures of high amylose starch and fatty acids. Effect of preparative conditions on spherulite morphology and yield. *Carbohydrate Polymers*, 71, 253-262.
- Felker, F. C., Kenar, J. A., Fanta, G. F., & Biswas, A. (2013). Comparison of microwave processing and excess steam jet cooking for spherulite production from amylose–fatty acid inclusion complexes. *Starch-Stärke*, 65(9-10), 864-874.
- Forcite. Material Studio 5.5. Accelrys Inc., San Diego, CA.
- Foster, J. F., & Serman, M. D. (1956). A light scattering investigation of the retrogradation of amylose. *Journal of Polymer Science*, 21(97), 91-101.
- Foster, J. F., & Zucker, D. (1952). Length of the amylose–iodine complex as determined by streaming dichroism. *The Journal of Physical Chemistry*, 56(2), 170-173.
- French, A. (1979). Allowed and preferred shapes of amylose. *Bakers Digest*, 53(1), 39-46.
- French, A., & Murphy, V. (1977a). Computer modeling in the study of starch. *Cereal Foods World*, 22(2), 61-70.
- French, A., & Murphy, V. (1977b). Intramolecular changes during polymorphic transformations of amylose. *Polymer*, 18(5), 489-494.
- French, A., Murphy, V., & Kainuma, K. (1978). Accessible conformations of amylose. *Journal of the Japanese Society of Starch Science*, 25(3), 171-176.
- French, A., & Zobel, H. (1967). X-Ray diffraction of oriented amylose fibers. I. Amylose dimethyl sulfoxide complex. *Biopolymers*, 5(5), 457-464.
- French, D., & Whelan, W. (1963). Starch fractionation by hydrophobic complex formation. *Starch-Stärke*, 15(10), 349-354.
- Freudenberg, K., Schaaf, E., Dumpert, G., & Ploetz, T. (1939). Neue ansichten über die stärke. *Naturwissenschaften*, 27(51), 850-853.
- Galloway, G., Biliaderis, C., & Stanley, D. (1989). Properties and structure of amylose–glyceryl monostearate complexes formed in solution or on extrusion of wheat flour. *Journal of Food Science*, 54(4), 950-957.

- Gelders, G., Vanderstukken, T., Goesaert, H., & Delcour, J. (2004). Amylose–lipid complexation: a new fractionation method. *Carbohydrate Polymers*, 56(4), 447-458.
- Gelders, G. G., Duyck, J. P., Goesaert, H., & Delcour, J. A. (2005a). Enzyme and acid resistance of amylose-lipid complexes differing in amylose chain length, lipid and complexation temperature. *Carbohydrate Polymers*, 60(3), 379-389.
- Gelders, G. G., Goesaert, H., & Delcour, J. A. (2005b). Potato phosphorylase catalyzed synthesis of amylose-lipid complexes. *Biomacromolecules*, 6(5), 2622-2629.
- Germino, F. J., & Valletta, R. M. (1964). Amylose V complexes from dimethyl sulfoxide solutions. *Journal of Polymer Science Part A: General Papers*, 2(11), 4757-4763.
- Gernat, C., Radosta, S., Anger, H., & Damaschun, G. (1993). Crystalline parts of three different conformations detected in native and enzymatically degraded starches. *Starch-Stärke*, 45(9), 309-314.
- Ghorab, M. K., & Adeyeye, M. C. (2001). Enhancement of ibuprofen dissolution via wet granulation with β -cyclodextrin. *Pharmaceutical Development and Technology*, 6(3), 305-314.
- Gidley, M. J., & Bociek, S. M. (1985). Molecular organization in starches: A carbon-13 CP/MAS NMR study. *Journal of the American Chemical Society*, 107(24), 7040-7044.
- Gidley, M. J., & Bociek, S. M. (1988). Carbon-13 CP/MAS NMR studies of amylose inclusion complexes, cyclodextrins, and the amorphous phase of starch granules: relationships between glycosidic linkage conformation and solid-state carbon-13 chemical shifts. *Journal of the American Chemical Society*, 110(12), 3820-3829.
- Gidley, M. J., & Bulpin, P. V. (1987). Crystallisation of malto-oligosaccharides as models of the crystalline forms of starch: minimum chain-length requirement for the formation of double helices. *Carbohydrate Research*, 161(2), 291-300.
- Godet, M., Tran, V., Colonna, P., Buleon, A., & Pezolet, M. (1995a). Inclusion/exclusion of fatty acids in amylose complexes as a function of the fatty acid chain length. *International Journal of Biological Macromolecules*, 17(6), 405-408.
- Godet, M. C., Bizot, H., & Buléon, A. (1995b). Crystallization of amylose-fatty acid complexes prepared with different amylose chain lengths. *Carbohydrate Polymers*, 27(1), 47-52.
- Godet, M. C., Bouchet, B., Colonna, P., Gallant, D. J., & Buléon, A. (1996). Crystalline amylose-fatty acid complexes: morphology and crystal thickness. *Journal of Food Science*, 61(6), 1196-1201.
- Godet, M. C., Buléon, A., Tran, V., & Colonna, P. (1993a). Structural features of fatty acid-amylose complexes. *Carbohydrate Polymers*, 21(2), 91-95.
- Godet, M. C., Tran, V., Delage, M. M., & Buléon, A. (1993b). Molecular modelling of the specific interactions involved in the amylose complexation by fatty acids. *International Journal of Biological Macromolecules*, 15(1), 11-16.
- Gotanda, R., Yamamoto, K., & Kadokawa, J. I. (2016). Amylose stereoselectively includes poly (d-alanine) to form inclusion complex in vine-twining polymerization: a novel saccharide–peptide supramolecular conjugate. *Macromolecular Chemistry and Physics*, 217(9), 1074-1080.
- Goudah, M. W., & Guth, E. P. (1965). Complex interaction of starches with certain drug pharmaceuticals. *Journal of Pharmaceutical Sciences*, 54(2), 298-301.
- Green, M. M., Blankenhorn, G., & Hart, H. (1975). Which starch fraction is water-soluble, amylose or amylopectin? *Journal of Chemical Education*, 52(11), 729.
- Greenwood, C., & Thomson, J. (1962). 42. Physicochemical studies on starches. Part XXIV. The fractionation and characterization of starches of various plant origins. *Journal of the Chemical Society (Resumed)*, 222-229.

- Gunning, A. P., Giardina, T. P., Faulds, C. B., Juge, N., Ring, S. G., Williamson, G., & Morris, V. J. (2003). Surfactant-mediated solubilisation of amylose and visualisation by atomic force microscopy. *Carbohydrate Polymers*, 51(2), 177-182.
- Guraya, H. S., Kadan, R. S., & Champagne, E. T. (1997). Effect of rice starch-lipid complexes on in vitro digestibility, complexing index, and viscosity. *Cereal Chemistry*, 74, 561-565.
- Hanashiro, I. (2015). *Fine structure of amylose*. In *Starch: Metabolism and Structure*, Y. Nakamura Ed., Springer Japan, pp. 41-60.
- Hanashiro, I., Sakaguchi, I., & Yamashita, H. (2013). Branched structures of rice amylose examined by differential fluorescence detection of side-chain distribution. *Journal of Applied Glycoscience*, 60(1), 79-85.
- Hanashiro, I., & Takeda, Y. (1998). Examination of number-average degree of polymerization and molar-based distribution of amylose by fluorescent labeling with 2-aminopyridine. *Carbohydrate Research*, 306(3), 421-426.
- Harada, T., Misaki, A., Akai, H., Yokobayashi, K., & Sugimoto, K. (1972). Characterization of Pseudomonas isoamylase by its actions on amylopectin and glycogen: comparison with Aerobacter pullulanase. *Biochimica et Biophysica Acta - Enzymology*, 268, 497-505.
- Hasjim, J., Lee, S. O., Hendrich, S., Setiawan, S., Ai, Y., & Jane, J. (2010). Characterization of a novel resistant-starch and its effects on postprandial plasma-glucose and insulin responses. *Cereal Chemistry*, 87(4), 257-262.
- Hathaway, R.J. (1971). Method for obtaining amylose from cooked starch solutions. *U.S. Patent No. 3556942*.
- Hayashi, A., Kinoshita, K., & Miyake, Y. (1981). The conformation of amylose in solution. I. *Polymer Journal*, 13(6), 537.
- Heinemann, C., Zinsli, M., Renggli, A., Escher, F., & Conde-Petit, B. (2005). Influence of amylose-flavor complexation on build-up and breakdown of starch structures in aqueous food model systems. *LWT-Food Science and Technology*, 38(8), 885-894.
- Helbert, W. (1994). Données sur la structure du grain d'amidon et des produits de recristallisation de l'amylose. Doctoral dissertation, Université de Grenoble 1.
- Helbert, W., & Chanzy, H. (1994). Single crystals of V-amylose complexed with n-butanol or n-pentanol: structural features and properties. *International Journal of Biological Macromolecules*, 16(4), 207-213.
- Helbert, W., Chanzy, H., Planchot, V., Buléon, A., & Colonna, P. (1993). Morphological and structural features of amylose spherocrystals of A-type. *International Journal of Biological Macromolecules*, 15(3), 183-187.
- Hess, B., Kutzner, C., Van Der Spoel, D., & Lindahl, E. (2008). GROMACS 4: algorithms for highly efficient, load-balanced, and scalable molecular simulation. *Journal of Chemical Theory and Computation*, 4(3), 435-447.
- Higginbotham, R., & Morrison, G. (1949). 12—The fractionation of starch. Part II—The separation of amylose and amylopectin. *Journal of the Textile Institute Transactions*, 40(4), T208-T219.
- Hinkle, M. E., & Zobel, H. F. (1968). X-ray diffraction of oriented amylose fibers. III. The structure of amylose-n-butanol complexes. *Biopolymers*, 6(8), 1119-1128.
- Hizukuri, S. (1991). Properties of hot-water-extractable amylose. *Carbohydrate Research*, 217, 251-253.
- Hizukuri, S., Takeda, Y., Maruta, N., & Juliano, B. O. (1989). Molecular structures of rice starch. *Carbohydrate Research*, 189, 227-235.
- Hizukuri, S., Takeda, Y., Yasuda, M., & Suzuki, A. (1981). Multi-branched nature of amylose and the action of debranching enzymes. *Carbohydrate Research*, 94(2), 205-213.

- Holló, J., & Szejtli, J. (1958). Die struktur der amylose-moleküle in wässrigen lösungen. *Starch-Stärke*, 10(3), 49-52.
- Holm, J., Björck, I., Ostrowska, S., Eliasson, A. C., Asp, N. G., Larsson, K., & Lundquist, I. (1983). Digestibility of amylose-lipid complexes in-vitro and in-vivo. *Starch-Stärke*, 35(9), 294-297.
- Horii, F., Hirai, A., & Kitamaru, R. (1983). Solid-state ^{13}C -NMR study of conformations of oligosaccharides and cellulose. *Polymer Bulletin*, 10(7-8), 357-361.
- Horii, F., Yamamoto, H., Hirai, A., & Kitamaru, R. (1987). Structural study of amylose polymorphs by cross-polarization-magic-angle spinning, ^{13}C -NMR spectroscopy. *Carbohydrate Research*, 160, 29-40.
- Hulleman, S., Helbert, W., & Chanzy, H. (1996). Single crystals of V amylose complexed with glycerol. *International Journal of Biological Macromolecules*, 18(1), 115-122.
- Humphrey, W., Dalke, A., & Schulten, K. (1996). VMD: visual molecular dynamics. *Journal of Molecular Graphics*, 14(1), 33-38.
- Hussein, K., Türk, M., & Wahl, M. A. (2007). Comparative evaluation of ibuprofen/ β -cyclodextrin complexes obtained by supercritical carbon dioxide and other conventional methods. *Pharmaceutical Research*, 24(3), 585-592.
- Imberty, A., Chanzy, H., Pérez, S., Buléon, A., & Tran, V. (1987). New three-dimensional structure for A-type starch. *Macromolecules*, 20(10), 2634-2636.
- Imberty, A., & Pérez, S. (1988). A revisit to the three-dimensional structure of B-type starch. *Biopolymers: Original Research on Biomolecules*, 27(8), 1205-1221.
- Itthisoponkul, T., Mitchell, J. R., Taylor, A. J., & Farhat, I. A. (2007). Inclusion complexes of tapioca starch with flavour compounds. *Carbohydrate Polymers*, 69(1), 106-115.
- Jacob, J., Geßler, K., Hoffmann, D., Sanbe, H., Koizumi, K., Smith, S. M., Takaha, T., & Saenger, W. (1998). Strain-induced "band flips" in cyclodecaamylose and higher homologues. *Angewandte Chemie International Edition*, 37(5), 605-609.
- Jane, J., Robyt, J. F., & Huang, D.-H. (1985). ^{13}C -NMR study of the conformation of helical complexes of amylopectin and of amylose in solution. *Carbohydrate Research*, 140(1), 21-35.
- Jane, J. (2009). *Structural features of starch granules II*. In *Starch: Chemistry and Technology*, J. N. BeMiller & R. L. Whistler (Eds.), Academic Press, pp. 193-237.
- Jeffrey, G. A. (1997). *An Introduction to Hydrogen Bonding*. New York: Oxford university press, p. 303.
- Jouquand, C., Ducruet, V., & Le Bail, P. (2006). Formation of amylose complexes with C6-aroma compounds in starch dispersions and its impact on retention. *Food Chemistry*, 96(3), 461-470.
- Kadokawa, J.-I. (2012). Preparation and applications of amylose supramolecules by means of phosphorylase-catalyzed enzymatic polymerization. *Polymers*, 4(1), 116-133.
- Kadokawa, J.-I., Kaneko, Y., Nakaya, A., & Tagaya, H. (2001). Formation of an amylose-polyester inclusion complex by means of phosphorylase-catalyzed enzymatic polymerization of α -D-glucose 1-phosphate monomer in the presence of poly(ϵ -caprolactone). *Macromolecules*, 34(19), 6536-6538.
- Kadokawa, J. I., Kaneko, Y., Nagase, S. I., Takahashi, T., & Tagaya, H. (2002). Vine-twining polymerization: amylose twines around polyethers to form amylose-polyether inclusion complexes. *Chemistry-a European Journal*, 8(15), 3321-3326.
- Kaneko, Y., Beppu, K., & Kadokawa, J.-I. (2007). Amylose selectively includes one from a mixture of two resemblant polyethers in vine-twining polymerization. *Biomacromolecules*, 8(10), 2983-2985.

- Kaneko, Y., Beppu, K., & Kadokawa, J.-I. (2009). Amylose selectively includes a specific range of molecular weights in poly (tetrahydrofuran) s in vine-twining polymerization. *Polymer Journal*, 41(9), 792.
- Kaneko, Y., Beppu, K., & Kadokawa, J. I. (2008a). Preparation of amylose/polycarbonate inclusion complexes by means of vine-twining polymerization. *Macromolecular Chemistry and Physics*, 209(10), 1037-1042.
- Kaneko, Y., Saito, Y., Nakaya, A., Kadokawa, J.-I., & Tagaya, H. (2008b). Preparation of inclusion complexes composed of amylose and strongly hydrophobic polyesters in parallel enzymatic polymerization system. *Macromolecules*, 41(15), 5665-5670.
- Karkalas, J., Ma, S., Morrison, W. R., & Pethrick, R. A. (1995). Some factors determining the thermal properties of amylose inclusion complexes with fatty acids. *Carbohydrate Research*, 268(2), 233-247.
- Karve, M. S., Bhide, S. V., & Kale, N. R. (1981). *Separation of starch components by affinity chromatography*. In *Solution Properties of Polysaccharides*, Vol. 150, D. A. Brant (Ed.). ASC Symposium Series; American Chemical Society, pp. 559-570.
- Katz, J., & Derksen, J. (1933). Physical chemistry of starch and bread making. XII. The conversion of starch preparations with the potato starch spectrum (B-spectrum) into those with the wheat starch spectrum (A-spectrum) and the reverse. *Zeitschrift fuer physikalische Chemie A*, 165, 228-233.
- Katz, J., & van Itallie, T. (1930). Alle Starkearten haben das gleiche retrogradationspektrum. *Z. Phys. Chem*, 150, 90-99.
- Kawada, J., & Marchessault, R. H. (2004). Solid-state NMR and X-ray studies on amylose complexes with small organic molecules. *Starch-Stuttgart*, 56(1), 13-19.
- Kenar, J. A., Eller, F. J., Felker, F. C., Jackson, M. A., & Fanta, G. F. (2014). Starch aerogel beads obtained from inclusion complexes prepared from high amylose starch and sodium palmitate. *Green Chemistry*, 16(4), 1921-1930.
- Kennedy, J. F., Rivera, Z. S., Lloyd, L. L., & Warner, F. P. (1992). Fractionation of starch amylopectin and amylose by high performance gel filtration chromatography. *Starch - Stärke*, 44(2), 53-55.
- Kjølberg, O., & Manners, D. (1963). Studies on carbohydrate-metabolizing enzymes. 9. The action of isoamylase on amylose. *Biochemical Journal*, 86(2), 258.
- Kong, L., & Ziegler, G. R. (2014). Molecular encapsulation of ascorbyl palmitate in preformed V-type starch and amylose. *Carbohydrate Polymers*, 111, 256-263.
- Krog, N. (1973). Influence of food emulsifiers on pasting temperature and viscosity of various starches. *Starch-Stärke*, 25(1), 22-27.
- Kuge, T., & Takeo, K. I. (1968). Complexes of starchy materials with organic compounds: Part II. Complex formation in aqueous solution and fractionation of starch by L-menthone. *Agricultural and Biological Chemistry*, 32(10), 1232-1238.
- Kurimoto, M., & Sugimoto, K. (1975). Process for producing amylose powders having a mean degree of polymerization between 20-30. *U.S. Patent No. 3881991*.
- Kurimoto, M., & Yoshida, M. (1973). Methods for the separation and purification of amyloses. *U.S. Patent No. 3766011*.
- Lalush, I., Bar, H., Zakaria, I., Eichler, S., & Shimoni, E. (2005). Utilization of amylose-lipid complexes as molecular nanocapsules for conjugated linoleic acid. *Biomacromolecules*, 6(1), 121-130.
- Lansky, S., Kooi, M., & Schoch, T. J. (1949). Properties of the fractions and linear subfractions from various starches. *Journal of the American Chemical Society*, 71(12), 4066-4075.

- Lau, E., Zhou, W., & Henry, C. J. (2016). Effect of fat type in baked bread on amylose–lipid complex formation and glycaemic response. *British Journal of Nutrition*, 115(12), 2122-2129.
- Laugier, J., & Bochu, B. LMGP-Suite. Suite of programs for the interpretation of X-ray experiments. ENSP/Laboratoire des Matériaux et du Génie Physique, Saint Martin d'Hères, France. <http://www.inpg.fr/LMGP> and <http://www.ccp14.ac.uk/tutorial/lmgp/>.
- Le Bail, P., Buléon, A., Shifan, D., & Marchessault, R. (2000). Mobility of lipid in complexes of amylose–fatty acids by deuterium and ^{13}C solid-state NMR. *Carbohydrate Polymers*, 43(4), 317-326.
- Le Bail, P., Chauvet, B., Simonin, H., Rondeau-Mouro, C., Pontoire, B., de Carvalho, M., & Le Bail, A. (2013). Formation and stability of amylose ligand complexes formed by high pressure treatment. *Innovative Food Science & Emerging Technologies*, 18, 1-6.
- Le Bail, P., Rondeau, C., & Buléon, A. (2005). Structural investigation of amylose complexes with small ligands: helical conformation, crystalline structure and thermostability. *International Journal of Biological Macromolecules*, 35(1-2), 1-7.
- Leiser, R. S., Macarus, D. P., & Wagoner, J. A. (1967). Process for separating amylaceous material into amylose and amylopectin. *U.S. Patent No. 3323949*.
- Leloir, L. F., Rongine de Fekete, M. A., & Cardini, C. E. (1961). Starch and oligosaccharide synthesis from uridine diphosphate glucose. *Journal of Biological Chemistry*, 236(3), 636-641.
- Lesmes, U., Barchechath, J., & Shimoni, E. (2008). Continuous dual feed homogenization for the production of starch inclusion complexes for controlled release of nutrients. *Innovative Food Science & Emerging Technologies*, 9(4), 507-515.
- Lesmes, U., Cohen, S. H., Shener, Y., & Shimoni, E. (2009). Effects of long chain fatty acid unsaturation on the structure and controlled release properties of amylose complexes. *Food Hydrocolloids*, 23(3), 667-675.
- Levis, K. A., Lane, M. E., & Corrigan, O. I. (2003). Effect of buffer media composition on the solubility and effective permeability coefficient of ibuprofen. *International Journal of Pharmaceutics*, 253(1), 49-59.
- Lii, C.-y., Stobinski, L., Tomasik, P., & Liao, C.-d. (2003). Single-walled carbon nanotube—potato amylose complex. *Carbohydrate Polymers*, 51(1), 93-98.
- Loewus, F. A., & Briggs, D. (1957). A potentiometric study of the change in iodine binding capacity of amylose while retrograding in dilute solution. *Journal of the American Chemical Society*, 79(6), 1494-1497.
- Lourdin, D., Putaux, J.-L., Potocki-Véronèse, G., Chevigny, C., Rolland-Sabaté, A., & Buléon, A. (2015). *Crystalline structure in starch*. In *Starch: Metabolism and Structure*, Y. Nakamura (Ed.). Springer Japan, pp. 61-90.
- Ma, U. V. L., Floros, J. D., & Ziegler, G. R. (2011). Formation of inclusion complexes of starch with fatty acid esters of bioactive compounds. *Carbohydrate Polymers*, 83, 1869-1878.
- Manley, R. St. J. (1964). Chain folding in amylose crystals. *Journal of Polymer Science Part A: General Papers*, 2(10), 4503-4515.
- Marotta, N. G., & Ryan, J. J. (1965). Method for the preparation of dustless starches. *U.S. Patent No. 3173807*.
- Matheson, N. K. (1996). The chemical structure of amylose and amylopectin fractions of starch from tobacco leaves during development and diurnally-nocturnally. *Carbohydrate Research*, 282(2), 247-262.

- Matheson, N. K., & Welsh, L. A. (1988). Estimation and fractionation of the essentially unbranched (amylose) and branched (amylopectin) components of starches with concanavalin A. *Carbohydrate Research*, 180(2), 301-313.
- Meng, S., Ma, Y., Sun, D.-W., Wang, L., & Liu, T. (2014). Properties of starch-palmitic acid complexes prepared by high pressure homogenization. *Journal of Cereal Science*, 59(1), 25-32.
- Mercier, C., Charbonniere, R., Grebaut, J., & De la Gueriviere, J. (1980). Formation of amylose-lipid complexes by twin-screw extrusion cooking of manioc starch. *Cereal Chem*, 57(1), 4-9.
- Mersmann, A. (2001). *Crystallization technology handbook* (2nd ed.). CRC Press, p. 840.
- Meyer, K. H., Bernfeld, P., & Wolf, E. (1940a). Recherches sur l'amidon III. Fractionnement et purification de l'amylose de maïs naturel. *Helvetica Chimica Acta*, 23(1), 854-864.
- Meyer, K. H., Brentano, W., & Bernfeld, P. (1940b). Recherches sur l'amidon II. Sur la nonhomogénéité de l'amidon. *Helvetica Chimica Acta*, 23(1), 845-853.
- Mikus, F., Hixon, R., & Rundle, R. (1946). The complexes of fatty acids with amylose. *Journal of the American Chemical Society*, 68(6), 1115-1123.
- Miles, M. J., Morris, V. J., & Ring, S. G. (1985). Gelation of amylose. *Carbohydrate Research*, 135(2), 257-269.
- Miller, D. P., & Brannon, R. C. (1980). *Accurate fiber X-ray diffraction data from films*. In *Fiber Diffraction Methods*, A. D. French & K. H. Gardner Eds. The American Chemical Society Washington, pp. 93-112.
- Mira, I., Persson, K., & Villwock, V. K. (2007). On the effect of surface active agents and their structure on the temperature-induced changes of normal and waxy wheat starch in aqueous suspension. Part I. Pasting and calorimetric studies. *Carbohydrate Polymers*, 68(4), 665-678.
- Mitchell, W. A. (1977). Starch solubility. *Journal of Chemical Education*, 54(2), 132.
- Montesanti, N. (2008). Système modèle de cristallisation de l'amylose A. Doctoral dissertation, Université Joseph Fourier, Grenoble.
- Montesanti, N., Véronese, G., Buléon, A., Escalier, P.-C., Kitamura, S., & Putaux, J.-L. (2010). A-type crystals from dilute solutions of short amylose chains. *Biomacromolecules*, 11(11), 3049-3058.
- Montgomery, E. M., & Senti, F. (1958). Separation of amylose from amylopectin of starch by an extraction-sedimentation procedure. *Journal of Polymer Science*, 28(116), 1-9.
- Morell, M. K., Kosar-Hashemi, B., Cmiel, M., Samuel, M. S., Chandler, P., Rahman, S., Buleon, A., Batey, I. L., & Li, Z. (2003). Barley sex6 mutants lack starch synthase IIa activity and contain a starch with novel properties. *The Plant Journal*, 34(2), 173-185.
- Morrison, W. R. (1988). Lipids in cereal starches: a review. *Journal of Cereal Science*, 8(1), 1-15.
- Mua, J., & Jackson, D. (1995). Fractionation of regular corn starch: a comparison of aqueous leaching and aqueous dispersion methods. *Cereal Chemistry*, 72(5), 508-511.
- Muetgeert, J., & Hiemstra, P. (1958). Amylose films. *U.S. Patent No. 2822581*.
- Mukerjee, P. (1965). Dimerization of anions of long-chain fatty acids in aqueous solutions and the hydrophobic properties of the acids. *The Journal of Physical Chemistry*, 69(9), 2821-2827.
- Mura, P., Bettinetti, G., Manderioli, A., Faucci, M., Bramanti, G., & Sorrenti, M. (1998). Interactions of ketoprofen and ibuprofen with β -cyclodextrins in solution and in the solid state. *International Journal of Pharmaceutics*, 166(2), 189-203.

- Murphy, V. G., Zaslow, B., & French, A. D. (1975). The structure of V amylose dehydrate: a combined X-ray and stereochemical approach. *Biopolymers*, 14(7), 1487-1501.
- Nakanishi, Y., Norisuye, T., Teramoto, A., & Kitamura, S. (1993). Conformation of amylose in dimethyl sulfoxide. *Macromolecules*, 26(16), 4220-4225.
- Navarro, A., Martino, M., & Zaritzky, N. (1996). Modelling of rheological behaviour in starch–lipid systems. *LWT-Food Science and Technology*, 29(7), 632-639.
- Nelles, E., Dewar, J., Bason, M., & Taylor, J. (2000). Maize starch biphasic pasting curves. *Journal of Cereal Science*, 31(3), 287-294.
- Nelles, E. M., Dewar, J., van der Merwe, C. F., & Taylor, J. (2003). Granule integrity and starch solubility during slow, extended pasting of maize starch -The second viscosity peak. *Starch-Stärke*, 55(2), 72-79.
- Newton, D. W., & Kluza, R. B. (1978). pKa values of medicinal compounds in pharmacy practice. *Drug Intelligence & Clinical Pharmacy*, 12(9), 546-554.
- Niemann, C., Saenger, W., & Pfannemüller, B. (1992). Enzymatic synthesis of low molecular weight amyloses with modified terminal groups. *Carbohydrate Research*, 226, 119-130.
- Nishiyama, Y., Mazeau, K., Morin, M., Cardoso, M. B., Chanzy, H., & Putaux, J.-L. (2010). Molecular and crystal structure of 7-fold V-amylose complexed with 2-propanol. *Macromolecules*, 43(20), 8628-8636.
- Nuessli, J., Conde-Petit, B., Trommsdorff, U. R., & Escher, F. (1995). Influence of starch flavour interactions on rheological properties of low concentration starch systems. *Carbohydrate Polymers*, 28(2), 167-170.
- Nuessli, J., Putaux, J.-L., Le Bail, P., & Buléon, A. (2003a). Crystal structure of amylose complexes with small ligands. *International Journal of Biological Macromolecules*, 33(4-5), 227-234.
- Nuessli, J., Putaux, J.-L., Le Bail, P., & Buléon, A. (2003b). Crystal structure of amylose complexes with small ligands. *International Journal of Biological Macromolecules*, 33(4), 227-234.
- Nunes, M. H. B., Moore, M. M., Ryan, L. A., & Arendt, E. K. (2009). Impact of emulsifiers on the quality and rheological properties of gluten-free breads and batters. *European Food Research and Technology*, 228(4), 633-642.
- Obiro, W. C., Sinha Ray, S., & Emmambux, M. N. (2012). V-amylose structural characteristics, methods of preparation, significance, and potential applications. *Food Reviews International*, 28(4), 412-438.
- Obiro, W. C., Sinha Ray, S., & Emmambux, M. N. (2012). Occurrence of amylose–lipid complexes in teff and maize starch biphasic pastes. *Carbohydrate Polymers*, 90, 616-622.
- Oguchi, T., Yamasato, H., Limmatvapirat, S., Yonemochi, E., & Yamamoto, K. (1998). Structural change and complexation of strictly linear amylose induced by sealed-heating with salicylic acid. *Journal of the Chemical Society, Faraday Transactions* 94, 923-927.
- Ohdan, K., Fujii, K., Yanase, M., Takaha, T., & Kuriki, T. (2006). Enzymatic synthesis of amylose. *Biocatalysis and Biotransformation*, 24(1-2), 77-81.
- Ohdan, K., Fujii, K., Yanase, M., Takaha, T., & Kuriki, T. (2007). Phosphorylase coupling as a tool to convert cellobiose into amylose. *Journal of Biotechnology*, 127(3), 496-502.
- Ong, M. H., Jumel, K., Tokarczuk, P. F., Blanshard, J. M. V., & Harding, S. E. (1994). Simultaneous determinations of the molecular weight distributions of amyloses and the fine structures of amylopectins of native starches. *Carbohydrate Research*, 260, 99-117.
- Ozcan, S., & Jackson, D. S. (2002). The impact of thermal events on amylose-fatty acid complexes. *Starch-Stärke*, 54(12), 593-602.

- Panyoo, A. E., & Emmambux, M. N. (2017). Amylose–lipid complex production and potential health benefits: a mini-review. *Starch-Stärke*, 69(7-8), 1600203.
- Peat, S., Pirt, S. J., & Whelan, W. J. (1952). 128. Enzymic synthesis and degradation of starch. Part XV. α -Amylase and the constitution of amylose. *Journal of the Chemical Society (Resumed)*, 705-713.
- Peat, S., Whelan, W. J., & Pirt, S. J. (1949). The amylolytic enzymes of soya bean. *Nature*, 164(4168), 499-499.
- Pfannemüller, B. (1987). Influence of chain length of short monodisperse amyloses on the formation of A-and B-type X-ray diffraction patterns. *International Journal of Biological Macromolecules*, 9(2), 105-108.
- Pfannemüller, B., Mayerhöfer, H., & Schulz, R. (1971). Conformation of amylose in aqueous solution: optical rotatory dispersion and circular dichroism of amylose–iodine complexes and dependence on chain length of retrogradation of amylose. *Biopolymers: Original Research on Biomolecules*, 10(2), 243-261.
- Plazinski, W., Lonardi, A., & Hünenberger, P. H. (2016). Revision of the GROMOS 56A6CARBO force field: improving the description of ring-conformational equilibria in hexopyranose-based carbohydrates chains. *Journal of Computational Chemistry*, 37(3), 354-365.
- Popov, D., Buléon, A., Burghammer, M., Chanzy, H., Montesanti, N., Putaux, J. L., Potocki-Veronese, G., & Riekkel, C. (2009). Crystal structure of A-amylose: a revisit from synchrotron microdiffraction analysis of single crystals. *Macromolecules*, 42(4), 1167-1174.
- Popov, D., Burghammer, M., Buléon, A., Montesanti, N., Putaux, J., & Riekkel, C. (2006). A-amylose single crystals: unit cell refinement from synchrotron radiation microdiffraction data. *Macromolecules*, 39(10), 3704-3706.
- Potocki-Veronese, G., Putaux, J.-L., Dupeyre, D., Albenne, C., Remaud-Siméon, M., Monsan, P., & Buleon, A. (2005). Amylose synthesized in vitro by amylosucrase: morphology, structure, and properties. *Biomacromolecules*, 6(2), 1000-1011.
- Potter, A., & Hassid, W. (1948a). Starch. I. End-group determination of amylose and amylopectin by periodate oxidation. *Journal of the American Chemical Society*, 70(10), 3488-3490.
- Potter, A., & Hassid, W. (1948b). Starch. II. Molecular weights of amyloses and amylopectins from starches of various plant origins. *Journal of the American Chemical Society*, 70(11), 3774-3777.
- Protzman, T. F., Wagoner, J. A., & Young, A. H. (1967). Process of casting amylose films. *U.S. Patent No. 3344216*.
- Purhagen, J. K., Sjöo, M. E., & Eliasson, A.-C. (2012). The anti-staling effect of pre-gelatinized flour and emulsifier in gluten-free bread. *European Food Research and Technology*, 235(2), 265-276.
- Putaux, J.-L., Montesanti, N., Véronèse, G., & Buléon, A. (2011a). Morphology and structure of A-amylose single crystals. *Polymer*, 52(10), 2198-2205.
- Putaux, J.-L., Nishiyama, Y., Mazeau, K., Morin, M., Cardoso, M. B., & Chanzy, H. (2011b). Helical conformation in crystalline inclusion complexes of V-amylose: a historical perspective. *Macromolecular Symposia*, 303(1), 1-9.
- Putaux, J.-L., Cardoso, M. B., Dupeyre, D., Morin, M., Nulac, A., & Hu, Y. (2008). Single crystals of V-amylose inclusion complexes. *Macromolecular Symposia*, 273(1), 1-8.

- Putseys, J. A., Derde, L. J., Lamberts, L., Goesaert, H., & Delcour, J. A. (2009). Production of tailor made short chain amylose-lipid complexes using varying reaction conditions. *Carbohydrate Polymers*, 78(4), 854-861.
- Putseys, J. A., Lamberts, L., & Delcour, J. A. (2010). Amylose-inclusion complexes: formation, identity and physico-chemical properties. *Journal of Cereal Science*, 51(3), 238-247.
- Qiu, X., Leporatti, S., Donath, E., & Möhwald, H. (2001). Studies on the drug release properties of polysaccharide multilayers encapsulated ibuprofen microparticles. *Langmuir*, 17(17), 5375-5380.
- Ràfols, C., Rosés, M., & Bosch, E. (1997). A comparison between different approaches to estimate the aqueous pKa values of several non-steroidal anti-inflammatory drugs. *Analytica Chimica Acta*, 338(1-2), 127-134.
- Rangelov, A., Stoyanov, S., Arnaudov, L., & Spassov, T. (2017). Novel mechanochemical approach for wheat starch-LPC complex formation. *Journal of Cereal Science*, 76, 72-75.
- Rao, V., & Foster, J. F. (1963). Studies of the conformation of amylose in solution. *Biopolymers*, 1(6), 527-544.
- Raphaelides, S. (1993). Rheological studies of starch-fatty acid gels. *Food Hydrocolloids*, 7(6), 479-495.
- Raphaelides, S., Arsenoudi, K., Exarhopoulos, S., & Xu, Z.-M. (2010). Effect of processing history on the functional and structural characteristics of starch-fatty acid extrudates. *Food Research International*, 43(1), 329-341.
- Raphaelides, S. N., Dimitreli, G., Exarhopoulos, S., Iliá, E., & Koutsomihali, P. (2015). A process designed for the continuous production of starch inclusion complexes on an industrial scale. *Food and Bioprocess Processing*, 96, 245-255.
- Raphaelides, S. N., & Georgiadis, N. (2007). Effect of fatty acids on the rheological behaviour of pea starch dispersions during heating. *Food Hydrocolloids*, 21(7), 1188-1200.
- Rappé, A. K., Casewit, C. J., Colwell, K., Goddard III, W. A., & Skiff, W. (1992). UFF, a full periodic table force field for molecular mechanics and molecular dynamics simulations. *Journal of the American Chemical Society*, 114(25), 10024-10035.
- Rappenecker, G., & Zugenmaier, P. (1981). Detailed refinement of the crystal structure of Vh-amylose. *Carbohydrate Research*, 89(1), 11-19.
- Recondo, E., & Leloir, L. F. (1961). Adenosine diphosphate glucose and starch synthesis. *Biochemical and Biophysical Research Communications*, 6(2), 85-88.
- Ribeiro, A. C., Rocha, Â., Soares, R. M. D., Fonseca, L. P., & da Silveira, N. P. (2017). Synthesis and characterization of acetylated amylose and development of inclusion complexes with rifampicin. *Carbohydrate Polymers*, 157, 267-274.
- Richardson, G., Langton, M., Bark, A., & Hermansson, A. M. (2003). Wheat starch gelatinization—the effects of sucrose, emulsifier and the physical state of the emulsifier. *Starch-Stärke*, 55(3-4), 150-161.
- Ring, S., Miles, M., Morris, V., Turner, R., & Colonna, P. (1987). Spherulitic crystallization of short chain amylose. *International Journal of Biological Macromolecules*, 9, 158-160.
- Rivera-Leyva, J. C., García-Flores, M., Valladares-Méndez, A., Orozco-Castellanos, L. M., & Martínez-Alfaro, M. (2012). Comparative studies on the dissolution profiles of oral ibuprofen suspension and commercial tablets using biopharmaceutical classification system criteria. *Indian Journal of Pharmaceutical Sciences*, 74(4), 312.
- Roblin, P., Potocki-Véronèse, G., Guieysse, D., Guerin, F., Axelos, M., Perez, J., & Buleon, A. (2012). SAXS conformational tracking of amylose synthesized by amylosucrases. *Biomacromolecules*, 14(1), 232-239.

- Rondeau-Mouro, C., Le Bail, P., & Buléon, A. (2004). Structural investigation of amylose complexes with small ligands: inter-or intra-helical associations? *International Journal of Biological Macromolecules*, 34(5), 251-257.
- Rongine, D. F. M., Leloir, L. F., & Cardini, C. E. (1960). Mechanism of starch biosynthesis. *Nature*, 187, 918-919.
- Rundle, R., Foster, J. F., & Baldwin, R. (1944). On the nature of the starch—iodine complex. *Journal of the American Chemical Society*, 66(12), 2116-2120.
- Rundle, R. E., & Edwards, F. C. (1943). The configuration of starch in the starch-iodine complex. IV. An X-ray diffraction investigation of butanol-precipitated amylose. *Journal of the American Chemical Society*, 65(11), 2200-2203.
- Rutschmann, M. A., & Solms, J. (1990). Formation of inclusion complexes of starch with different organic compounds. IV, ligand binding and variability in helical conformations of V amylose complexes. *Lebensmittel-Wissenschaft+ Technologie*, 23(1), 84-87.
- Salústio, P. J., Feio, G., Figueirinhas, J. L., Cabral-Marques, H. M., Costa, P. C., & Pinto, J. F. (2012). Release profile of ibuprofen in β -cyclodextrin complexes from two different solid dosage forms. *Powder Technology*, 221, 245-251.
- Santha, N., Sudha, K., Vijayakumari, K., Nayar, V., & Moorthy, S. (1990). Raman and infrared spectra of starch samples of sweet potato and cassava. *Journal of Chemical Sciences*, 102(5), 705-712.
- Sarko, A., Zeitlin, B. R., & Germino, F. J. (1963). Cold water soluble amylose. *U.S. Patent No. 3086890*.
- Sarko, A., & Biloski, A. (1980). Crystal structure of the KOH-amylose complex. *Carbohydrate Research*, 79(1), 11-21.
- Sarko, A., & Zugenmaier, P. (1980). *Crystal structures of amylose and its derivatives: a review*. In *Fiber Diffraction Methods*, Vol. 141, A. D. French & K. H. Gardner (Eds.), ASC Symposium Series; ACS Publications, pp. 459-482.
- Schoch, T. J. (1941). Physical aspects of starch. *Cereal Chemistry*, 18(2), 121-128.
- Schoch, T. J. (1942). Fractionation of starch by selective precipitation with butanol. *Journal of the American Chemical Society*, 64(12), 2957-2961.
- Schoch, T. J. (1944). The fractionation of starch. *Advances in Carbohydrate Chemistry*, 1, 247-277.
- Seneviratne, H. D., & Biliaderis, C. G. (1991). Action of α -amylases on amylose-lipid complex superstructures. *Journal of Cereal Science*, 13(2), 129-143.
- Senti, F., & Witnauer, L. (1948). Structure of alkali amylose. *Journal of the American Chemical Society*, 70(4), 1438-1444.
- Senti, F. R., & Witnauer, L. (1946). Oriented filaments of amylose and alkali amylose. *Journal of the American Chemical Society*, 68(11), 2407-2408.
- Senti, F. R., & Witnauer, L. P. (1952). X-ray diffraction studies of addition compounds of amylose with inorganic salts. *Journal of Polymer Science*, 9(2), 115-132.
- Sheldrick, G. M. (2015). Crystal structure refinement with SHELXL. *Acta Crystallographica Section C: Structural Chemistry*, 71(1), 3-8.
- Shibuya, T., Yamauchi, T., Chaen, H., Nakano, M., Sakai, S., & Kurimoto, M. (1993). The formation of amylose-granules from cyclomaltodextrin glucanotransferase by α -cyclodextrin. *Journal of Applied Glycoscience*, 40(4), 375-381.

- Shogren, R. L., Fanta, G. F., & Felker, F. C. (2006). X-ray diffraction study of crystal transformations in spherulitic amylose/lipid complexes from jet-cooked starch. *Carbohydrate Polymers*, 64(3), 444-451.
- Sievert, D., & Holm, J. (1993). Determination of amylose by differential scanning calorimetry. *Starch-Stärke*, 45(4), 136-139.
- Sievert, D., & Wursch, P. (1993). Thermal behavior of potato amylose and enzyme-resistant starch from maize. *Cereal Chemistry*, 70, 333-338.
- Simpson, T. (1970). X-Ray diffraction of ethylenediamine-amylose complex. *Biopolymers*, 9(9), 1039-1047.
- Simpson, T. D., Dintzis, F. R., & Taylor, N. W. (1972). A V7 conformation of dimethyl sulfoxide-amylose complex. *Biopolymers*, 11(12), 2591-2600.
- Singh, J., Singh, N., & Saxena, S. (2002). Effect of fatty acids on the rheological properties of corn and potato starch. *Journal of Food Engineering*, 52(1), 9-16.
- Singh, M., & Byars, J. A. (2009). Starch-lipid composites in plain set yogurt. *International Journal of Food Science & Technology*, 44(1), 106-110.
- Singh, M., Byars, J. A., & Kenar, J. A. (2014). Amylose-potassium oleate inclusion complex in plain set-style yogurt. *Journal of Food Science*, 79(5), E822-E827.
- Singh, M., & Kim, S. (2009). Yogurt fermentation in the presence of starch-lipid composite. *Journal of Food Science*, 74(2), C85-C89.
- Smernik, J. R., & Malcolm Oades, J. (2000). The use of spin counting for determining quantitation in solid state ^{13}C NMR spectra of natural organic matter 2. HF-treated soil fractions. *Geoderma*, 96, 159-171.
- Smernik, R. J., & Oades, J. M. (1999). Effects of added paramagnetic ions on the ^{13}C CP/MAS NMR spectrum of a de-ashed soil. *Geoderma*, 89(3-4), 219-248.
- Smernik, R. J., & Oades, J. M. (2000). The use of spin counting for determining quantitation in solid state ^{13}C NMR spectra of natural organic matter: 1. Model systems and the effects of paramagnetic impurities. *Geoderma*, 96(1-2), 101-129.
- Snape, C. E., Axelson, D. E., Botto, R. E., Delpuech, J., Tekely, P., Gerstein, B. C., Pruski, M., Maciel, G. E., & Wilson, M. A. (1989). Quantitative reliability of aromaticity and related measurements on coals by ^{13}C nmr A debate. *Fuel*, 68(5), 547-548.
- Snape, C. E., Morrison, W. R., Maroto-Valer, M. M., Karkalas, J., & Pethrick, R. A. (1998). Solid state ^{13}C NMR investigation of lipid ligands in V-amylose inclusion complexes. *Carbohydrate Polymers*, 36(2), 225-237.
- St.-Jacques, M., Sundararajan, P., Taylor, K., & Marchessault, R. (1976). Nuclear magnetic resonance and conformational studies on amylose and model compounds in dimethyl sulfoxide solution. *Journal of the American Chemical Society*, 98(15), 4386-4391.
- Szejtli, J., & Augustat, S. (1966). Über die konfiguration der amylosemoleküle in wäßriger lösung. *Starch-Stärke*, 18(2), 38-52.
- Szejtli, J., & Bánky-Elöd, E. (1975). Inclusion complexes of unsaturated fatty acids with amylose and cyclodextrin. *Starch-Stärke*, 27(11), 368-376.
- Takahashi, Y., Kumano, T., & Nishikawa, S. (2004). Crystal structure of B-amylose. *Macromolecules*, 37(18), 6827-6832.
- Takeda, Y., Hizukuri, S., & Juliano, B. O. (1986). Purification and structure of amylose from rice starch. *Carbohydrate Research*, 148(2), 299-308.
- Takeda, Y., Maruta, N., & Hizukuri, S. (1992a). Examination of the structure of amylose by tritium labelling of the reducing terminal. *Carbohydrate Research*, 227, 113-120.

- Takeda, Y., Maruta, N., & Hizukuri, S. (1992b). Structures of amylose subfractions with different molecular sizes. *Carbohydrate Research*, 226(2), 279-285.
- Takeda, Y., Maruta, N., Hizukuri, S., & Juliano, B. O. (1989). Structures of indica rice starches (IR48 and IR64) having intermediate affinities for iodine. *Carbohydrate Research*, 187(2), 287-294.
- Takeda, Y., Shirasaka, K., & Hizukuri, S. (1984). Examination of the purity and structure of amylose by gel-permeation chromatography. *Carbohydrate Research*, 132(1), 83-92.
- Takeda, Y., Shitaozono, T., & Hizukuri, S. (1990). Structures of sub-fractions of corn amylose. *Carbohydrate Research*, 199(2), 207-214.
- Takeo, K., Tokumura, A., & Kuge, T. (1973). Complexes of starch and its related materials with organic compounds. Part. X. X-ray diffraction of amylose-fatty acid complexes. *Starch-Stärke*, 25(11), 357-362.
- Takeo, K. i., & Kuge, T. (1969). Complexes of starchy materials with organic compounds: Part III. X-ray studies on amylose and cyclodextrin complexes. *Agricultural and Biological Chemistry*, 33(8), 1174-1180.
- Takeo, K. I., & Kuge, T. (1971). Complexes of starchy materials with organic compounds: Part VI. X-ray diffraction of amylose-n-aliphatic ketone complexes. *Agricultural and Biological Chemistry*, 35(4), 537-542.
- Tanaka, Y., & Akazawa, T. (1971). Enzymic mechanism of starch synthesis in ripening rice grains VI. Isozymes of starch synthetase. *Plant and Cell Physiology*, 12(4), 493-505.
- Tapanapunnitikul, O., Chaiseri, S., Peterson, D. G., & Thompson, D. B. (2007). Water solubility of flavor compounds influences formation of flavor inclusion complexes from dispersed high-amylose maize starch. *Journal of Agricultural and Food Chemistry*, 56(1), 220-226.
- Tester, R. F., Karkalas, J., & Qi, X. (2004). Starch-composition, fine structure and architecture. *Journal of Cereal Science*, 39(2), 151-165.
- Tomasik, P., & Schilling, C. H. (1998a). Complexes of starch with inorganic guests. *Advances in Carbohydrate Chemistry and Biochemistry*, 53, 263-343.
- Tomasik, P., & Schilling, C. H. (1998b). Complexes of starch with organic guests. *Advances in Carbohydrate Chemistry and Biochemistry*, 53, 345-426.
- Tozuka, Y., Fujito, T., Moribe, K., & Yamamoto, K. (2006a). Ibuprofen-cyclodextrin inclusion complex formation using supercritical carbon dioxide. *Journal of Inclusion Phenomena and Macrocyclic Chemistry*, 56(1), 33-37.
- Tozuka, Y., Takeshita, A., Nagae, A., Wongmekiat, A., Moribe, K., Oguchi, T., & Yamamoto, K. (2006b). Specific inclusion mode of guest compounds in the amylose complex analyzed by solid state NMR spectroscopy. *Chemical and Pharmaceutical Bulletin*, 54(8), 1097-1101.
- Uchino, T., Tozuka, Y., Oguchi, T., & Yamamoto, K. (2001). The change of the structure of amylose during the inclusion of 2-naphthol in sealed-heating process. *Journal of Inclusion Phenomena and Macrocyclic Chemistry*, 39(1-2), 145-149.
- Uchino, T., Tozuka, Y., Oguchi, T., & Yamamoto, K. (2002). Inclusion compound formation of amylose by sealed-heating with salicylic acid analogues. *Journal of Inclusion Phenomena and Macrocyclic Chemistry*, 43(1-2), 31-36.
- Ulmann, M., & Richter, M. (1962). Fragen der papierchromatographischen Untersuchung von Amylopektin und Amylose. *Starch-Stärke*, 14(12), 455-460.
- Utsumi, Y., Yoshida, M., Francisco, J. P. B., Sawada, T., Kitamura, S., & Nakamura, Y. (2009). Quantitative assay method for starch branching enzyme with biconchonic acid by

- measuring the reducing terminals of glucans. *Journal of Applied Glycoscience*, 56(3), 215-222.
- Van Dijk, J., Henkens, W. C. M., & Smit, J. A. M. (1976). The determination of the molecular weight distribution of amylose by gel permeation chromatography. *Journal of Polymer Science: Polymer Physics Edition*, 14(8), 1485-1493.
- Veregin, R. P., Fyfe, C. A., & Marchessault, R. H. (1987a). Investigation of the crystalline "V" amylose complexes by high-resolution ^{13}C CP/MAS NMR spectroscopy. *Macromolecules*, 20(12), 3007-3012.
- Veregin, R. P., Fyfe, C. A., Marchessault, R. H., & Taylor, M. G. (1987b). Correlation of ^{13}C chemical shifts with torsional angles from high-resolution, ^{13}C -CP-MAS NMR studies of crystalline cyclomalto-oligosaccharide complexes, and their relation to the structures of the starch polymorphs. *Carbohydrate Research*, 160, 41-56.
- Waldmann, H., Gygas, D., Bednarski, M. D., Randall Shangraw, W., & Whitesides, G. M. (1986). The enzymic utilization of sucrose in the synthesis of amylose and derivatives of amylose, using phosphorylases. *Carbohydrate Research*, 157, C4-C7.
- Walker, G. J., & Whelan, W. J. (1959). Synthesis of amylose by potato D-enzyme. *Nature*, 183(4653), 46-46.
- Whistler, R. L., & Hilbert, G. (1945). Separation of amylose and amylopectin by certain nitroparaffins. *Journal of the American Chemical Society*, 67(7), 1161-1165.
- Whistler, R. L., & Johnson, C. (1948). Effect of acid hydrolysis on the retrogradation of amylose. *Cereal Chemistry*, 25(6), 418-424.
- Whittam, M. A., Orford, P. D., Ring, S. G., Clark, S. A., Parker, M. L., Cairns, P., & Miles, M. J. (1989). Aqueous dissolution of crystalline and amorphous amylose-alcohol complexes. *International Journal of Biological Macromolecules*, 11(6), 339-344.
- Winter, W., & Sarko, A. (1972). The crystal structure of amylose-DMSO complex. *Biopolymers*, 11(4), 849-852.
- Winter, W. T., & Sarko, A. (1974a). Crystal and molecular structure of the amylose-DMSO complex. *Biopolymers*, 13(7), 1461-1482.
- Winter, W. T., & Sarko, A. (1974b). Crystal and molecular structure of V-anhydrous amylose. *Biopolymers*, 13(7), 1447-1460.
- Wulff, G. n., Avgenaki, G., & Guzman, M. S. P. (2005). Molecular encapsulation of flavours as helical inclusion complexes of amylose. *Journal of Cereal Science*, 41(3), 239-249.
- Würsch, P., & Hood, L. (1981). Structure of starch from mango seed. *Starch-Stärke*, 33, 217-221.
- Yamada, T., & Taki, M. (1976). Fractionation of maize starch by gel-chromatography. *Starch-Stärke*, 28(11), 374-377.
- Yamashita, Y.-H., Ryugo, J., & Monobe, K. (1973). An electron microscopic study on crystals of amylose V complexes. *Journal of Electron Microscopy*, 22(1), 19-26.
- Yamashita, Y. (1965). Single crystals of amylose V complexes. *Journal of Polymer Science Part A: General Papers*, 3(9), 3251-3260.
- Yamashita, Y., & Hirai, N. (1966). Single crystals of amylose V complexes. II. Crystals with 7_1 helical configuration. *Journal of Polymer Science Part A-2: Polymer Physics*, 4, 161-171.
- Yamashita, Y., & Monobe, K. (1971). Single crystals of amylose V complexes. III. Crystals with 8_1 helical configuration. *Journal of Polymer Science Part A-2: Polymer Physics*, 9(8), 1471-1481.
- Yanase, M., Takaha, T., & Kuriki, T. (2006). α -Glucan phosphorylase and its use in carbohydrate engineering. *Journal of the Science of Food and Agriculture*, 86(11), 1631-1635.

- Yanase, M., Takata, H., Fujii, K., Takaha, T., & Kuriki, T. (2005). Cumulative effect of amino acid replacements results in enhanced thermostability of potato type L α -glucan phosphorylase. *Applied and Environmental Microbiology*, 71(9), 5433-5439.
- Yang, L., Zhang, B., Liang, Y., Yang, B., Kong, T., & Zhang, L.-M. (2008). In situ synthesis of amylose/single-walled carbon nanotubes supramolecular assembly. *Carbohydrate Research*, 343(14), 2463-2467.
- Yang, L., Zhang, B., Yi, J., Liang, J., Liu, Y., & Zhang, L. M. (2013). Preparation, characterization, and properties of amylose-ibuprofen inclusion complexes. *Starch-Stärke*, 65(7-8), 593-602.
- Yang, Y., Gu, Z., & Zhang, G. (2009). Delivery of bioactive conjugated linoleic acid with self-assembled amylose-CLA complex. *Journal of Agricultural and Food Chemistry*, 57(15), 7125-7130.
- Yeo, L., Thompson, D. B., & Peterson, D. G. (2016). Inclusion complexation of flavour compounds by dispersed high-amylose maize starch (HAMS) in an aqueous model system. *Food Chemistry*, 199, 393-400.
- Yiyun, C., & Jiepin, Y. (2006). Solubilization of non-steroidal anti-inflammatory drugs in the presence of tween series surfactants. *Physics and Chemistry of Liquids*, 44, 249-256.
- Young, A. H. (1984). Fractionation of starch. *Starch: Chemistry and Technology*, 2, 249-283.
- Zabar, S., Lesmes, U., Katz, I., Shimoni, E., & Bianco-Peled, H. (2009). Studying different dimensions of amylose-long chain fatty acid complexes: molecular, nano and micro level characteristics. *Food Hydrocolloids*, 23(7), 1918-1925.
- Zaslow, B. (1963). Characterization of a second helical amylose modification. *Biopolymers*, 1(2), 165-169.
- Zaslow, B., Murphy, V. G., & French, A. D. (1974). The V amylose-H₂O system: structural changes resulting from hydration. *Biopolymers*, 13(4), 779-790.
- Zhang, L., Cheng, H., Zheng, C., Dong, F., Man, S., Dai, Y., & Yu, P. (2016). Structural and release properties of amylose inclusion complexes with ibuprofen. *Journal of Drug Delivery Science and Technology*, 31, 101-107.
- Zhao, Y., Ai, Y., Li, L., Jane, J.-L., Hendrich, S., & Birt, D. F. (2014). Inhibition of azoxymethane-induced preneoplastic lesions in the rat colon by a stearic acid complexed high-amylose cornstarch using different cooking methods and assessing potential gene targets. *Journal of Functional Foods*, 6, 499-512.
- Zhao, Y., Hasjim, J., Li, L., Jane, J.-L., Hendrich, S., & Birt, D. F. (2011). Inhibition of azoxymethane-induced preneoplastic lesions in the rat colon by a cooked stearic acid complexed high-amylose cornstarch. *Journal of Agricultural and Food Chemistry*, 59(17), 9700-9708.
- Zhu, F., Cai, Y.-Z., Sun, M., & Corke, H. (2008). Effect of phenolic compounds on the pasting and textural properties of wheat starch. *Starch-Stärke*, 60(11), 609-616.
- Zobel, H. F., French, A. D., & Hinkle, M. E. (1967). X-Ray diffraction of oriented amylose fibers. II. Structure of V amyloses. *Biopolymers*, 5(9), 837-845.

Annex 1

Supplementary material Chapter III

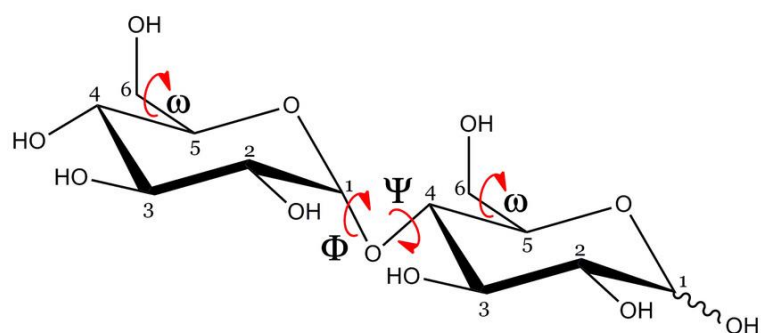


Figure S.III.1. Definition of the dihedral bond angles Φ , Ψ and ω for a maltose unit.

(from Muñoz-García, J.C. Insights on the structure and dynamics of glycosaminoglycans and their interactions with langerin: NMR and computational studies, Doctoral dissertation, 2013, University of Sevilla)

Table S.III.1. List of observed reflections and their intensities (I_{obs}) in the base-plane ED pattern ($l = 0$) of V_{1-butanol} crystals. σ is the estimated standard error.

h	k	I_{obs}	σ	h	k	I_{obs}	σ
1	1	0.00	0.00	5	6	27.54	0.10
0	2	30.95	0.46	0	8	0.00	0.00
2	0	33.49	0.32	1	8	0.00	0.00
1	2	7.76	1.50	4	7	2.03	0.32
2	1	0.00	0.00	2	8	13.62	0.15
2	2	242.34	0.18	3	8	3.19	0.32
1	3	0.00	0.00	5	7	0.00	0.00
3	1	0.00	0.00	4	8	3.71	0.20
2	3	0.00	0.00	5	8	0.00	0.00
3	2	254.15	0.20	6	0	433.05	0.15
0	4	0.00	0.00	6	1	22.05	0.12
1	4	163.88	0.12	6	2	265.98	0.16
4	0	186.04	0.13	6	3	2.91	0.46
4	1	0.00	0.00	6	4	7.04	0.17
3	3	0.00	0.00	6	5	3.79	0.27
2	4	0.00	0.00	6	6	5.83	0.19
4	2	1.98	0.46	6	7	0.90	0.57
3	4	140.35	0.13	6	8	7.28	0.14
1	5	3.15	0.45	7	1	0.00	0.00
4	3	2.14	0.68	7	2	0.00	0.00
5	1	0.00	0.00	7	3	0.00	0.00
2	5	0.00	0.00	7	4	6.01	0.19
5	2	254.51	0.15	7	5	0.00	0.00
4	4	11.92	0.18	7	6	1.35	0.31
3	5	2.78	0.41	7	7	2.15	0.28
5	3	55.99	0.11	7	8	0.00	0.00
0	6	509.27	0.17	8	0	30.08	0.10
1	6	279.37	0.13	8	1	0.00	0.00
2	6	292.87	0.12	8	2	0.00	0.00
4	5	3.60	0.32	8	3	0.00	0.00
5	4	527.36	0.17	8	4	1.55	0.29
3	6	102.05	0.10	8	5	0.00	0.00
1	7	3.04	0.30	8	6	5.50	0.15
5	5	6.58	0.21	8	7	0.00	0.00
4	6	10.41	0.17	8	8	1.96	0.29
3	7	0.00	0.00				

Table S.III.2. Fractional coordinates and thermal parameters of independent atoms in the $V_{1\text{-butanol}}$ unit cell. U_{iso} is the temperature factor.

Atom	x	y	z	U_{iso} (\AA^2)
O11_1	-0.13(7)	0.14(6)	-0.5(5)	0.355
C11_1	0.15(10)	0.19(7)	-0.5(5)	0.355
H11_1	-0.1823	0.1911	-0.4545	0.426
O51_1	0.13(11)	0.19(16)	-0.3(5)	0.355
C51_1	0.07(11)	0.19(10)	-0.3(5)	0.355
H51_1	-0.0573	0.1553	-0.2981	0.426
C61_1	0.06(11)	0.20(15)	-0.1(5)	0.355
H61A_1	-0.0935	0.1918	-0.0268	0.426
H61B_1	-0.0345	0.1874	-0.0471	0.426
O61_1	-0.1(3)	0.25(16)	-0.1(8)	0.355
H061_1	-0.0457	0.2621	-0.0039	0.426
C41_1	0.04(10)	0.23(14)	-0.4(6)	0.355
H41_1	-0.0478	0.2574	-0.3377	0.426
C31_1	0.07(11)	0.23(13)	-0.6(6)	0.355
H31_1	-0.055	0.2006	-0.632	0.426
C21_1	0.12(11)	0.23(9)	-0.6(6)	0.355
H21_1	-0.1323	0.2597	-0.4944	0.426
O21_1	-0.1(2)	0.2(2)	-0.7(7)	0.355
H021_1	-0.1379	0.2618	-0.7561	0.426
O31_1	0.05(18)	0.27(19)	-0.6(7)	0.355
H031_1	-0.0507	0.2697	-0.7437	0.426
O12_1	0.01(10)	0.21(16)	-0.4(7)	0.355
C12_1	0.04(10)	0.25(13)	-0.3(6)	0.355
H12_1	0.0289	0.2816	-0.3445	0.426
O52_1	0.04(14)	0.24(15)	-0.1(6)	0.355
C52_1	0.06(10)	0.20(11)	-0.1(6)	0.355
H52_1	0.0386	0.1701	-0.1283	0.426
C62_1	0.1(2)	0.2(2)	0.1(6)	0.355
H62A_1	0.0482	0.1654	0.1466	0.426
H62B_1	0.0833	0.2115	0.1561	0.426
O62_1	0.0(2)	0.2(3)	0.1(8)	0.355
H062_1	0.0195	0.2562	0.1433	0.426
C42_1	0.11(11)	0.19(10)	-0.1(7)	0.355
H42_1	0.1371	0.2025	-0.0664	0.426
C32_1	0.13(12)	0.20(13)	-0.3(7)	0.355
H32_1	0.1199	0.176	-0.3964	0.426
C22_1	0.10(10)	0.25(14)	-0.4(6)	0.355
H22_1	0.1127	0.2757	-0.3336	0.426
O22_1	0.1(2)	0.3(3)	-0.6(7)	0.355
H022_1	0.1286	0.2566	-0.5823	0.426

O32_1	0.18(12)	0.22(19)	-0.3(10)	0.355
H032_1	0.183	0.2424	-0.2935	0.426
O13_1	0.12(13)	0.13(10)	-0.1(8)	0.355
C13_1	0.17(13)	0.12(10)	-0.1(7)	0.355
H13_1	0.192	0.1478	-0.0921	0.426
O53_1	0.2(2)	0.11(10)	0.1(7)	0.355
C53_1	0.15(16)	0.06(11)	0.1(7)	0.355
H53_1	0.1165	0.0578	0.1083	0.426
C63_1	0.16(17)	0.05(11)	0.3(7)	0.355
H63A_1	0.1961	0.0594	0.3407	0.426
H63B_1	0.1407	0.0776	0.3713	0.426
O63_1	0.1(10)	0.0(3)	0.4(9)	0.355
H063_1	0.1417	-0.0108	0.2854	0.426
C43_1	0.17(13)	0.02(10)	0.0(7)	0.355
H43_1	0.2026	0.0021	0.0754	0.426
C33_1	0.19(12)	0.03(10)	-0.2(8)	0.355
H33_1	0.1606	0.0161	-0.2299	0.426
C23_1	0.19(14)	0.08(11)	-0.2(7)	0.355
H23_1	0.23	0.0882	-0.1991	0.426
O23_1	0.2(3)	0.09(15)	-0.4(7)	0.355
H023_1	0.1492	0.1005	-0.3681	0.426
O33_1	0.2(2)	0.00(19)	-0.2(12)	0.355
H033_1	0.2364	-0.0199	-0.1496	0.426
O14_1	0.13(15)	0.02(12)	0.0(8)	0.355
C14_1	0.14(12)	0.07(12)	0.1(8)	0.355
H14_1	0.1794	-0.0715	0.0981	0.426
O54_1	0.12(15)	0.06(18)	0.2(7)	0.355
C54_1	0.07(14)	0.07(13)	0.3(7)	0.355
H54_1	0.0526	-0.0384	0.2427	0.426
C64_1	0.06(16)	0.08(19)	0.4(7)	0.355
H64A_1	0.0908	-0.0934	0.4967	0.426
H64B_1	0.0503	-0.0517	0.5063	0.426
O64_1	0.02(15)	0.12(19)	0.5(8)	0.355
H064_1	-0.0059	-0.1038	0.4576	0.426
C44_1	0.04(11)	0.11(14)	0.1(7)	0.355
H44_1	0.0425	-0.139	0.1866	0.426
C34_1	0.06(13)	0.10(13)	0.0(7)	0.355
H34_1	0.0555	-0.0725	-0.0828	0.426
C24_1	0.12(13)	0.11(12)	0.0(8)	0.355
H24_1	0.1296	-0.1396	0.0337	0.426
O24_1	0.1(2)	-0.1(3)	-0.2(9)	0.355
H024_1	0.1562	-0.0805	-0.1957	0.426
O34_1	0.04(19)	-0.1(2)	-0.1(9)	0.355

H034_1	0.0514	-0.1354	-0.232	0.426
O15_1	0.01(11)	0.09(17)	0.1(8)	0.355
C15_1	0.05(11)	0.12(12)	0.2(7)	0.355
H15_1	-0.0357	-0.1581	0.1888	0.426
O55_1	0.06(15)	0.11(13)	0.4(7)	0.355
C55_1	0.08(12)	0.06(12)	0.4(8)	0.355
H55_1	-0.0546	-0.0392	0.3176	0.426
C65_1	0.08(15)	0.0(2)	0.6(8)	0.355
H65A_1	-0.079	-0.0143	0.5767	0.426
H65B_1	-0.104	-0.0649	0.6186	0.426
O65_1	0.0(2)	-0.1(4)	0.6(7)	0.355
H065_1	-0.0323	-0.0687	0.7294	0.426
C45_1	0.13(13)	0.06(10)	0.3(7)	0.355
H45_1	-0.155	-0.076	0.3472	0.426
C35_1	0.13(14)	0.07(13)	0.1(7)	0.355
H35_1	-0.1061	-0.0487	0.0432	0.426
C25_1	0.10(12)	0.12(12)	0.1(7)	0.355
H25_1	-0.1211	-0.1469	0.1421	0.426
O25_1	-0.1(2)	-0.1(2)	-0.1(8)	0.355
H025_1	-0.1177	-0.1412	-0.1194	0.426
O35_1	0.17(18)	-0.1(3)	0.0(9)	0.355
H035_1	-0.1705	-0.0863	-0.0643	0.426
O16_1	0.14(16)	0.01(11)	0.3(9)	0.355
C16_1	0.19(14)	0.01(10)	0.4(8)	0.355
H16_1	-0.2142	-0.0227	0.3394	0.426
O56_1	-0.2(2)	0.02(9)	0.5(7)	0.355
C56_1	0.16(11)	0.06(8)	0.6(6)	0.355
H56_1	-0.1249	0.055	0.5507	0.426
C66_1	-0.2(2)	0.07(17)	0.8(5)	0.355
H66A_1	-0.2033	0.0519	0.784	0.426
H66B_1	-0.145	0.047	0.8168	0.426
O66_1	-0.2(3)	0.1(2)	0.8(8)	0.355
H066_1	-0.1947	0.1281	0.7748	0.426
C46_1	-0.18(7)	0.11(6)	0.5(4)	0.355
H46_1	-0.2055	0.1208	0.5132	0.426
C36_1	0.18(15)	0.10(13)	0.3(5)	0.355
H36_1	-0.1521	0.0914	0.2231	0.426
C26_1	0.22(14)	0.05(14)	0.3(8)	0.355
H26_1	-0.2495	0.0543	0.2994	0.426
O26_1	-0.2(3)	0.0(2)	0.1(8)	0.355
H026_1	-0.1969	0.0171	0.0607	0.426
O36_1	-0.2(3)	0.13(18)	0.2(8)	0.355
H036_1	-0.2297	0.1468	0.2749	0.426

C1_2	0.0(3)	0.1(4)	0(3)	0.355
H11_2	0.0449	0.1094	0.3254	0.426
H12_2	0.0562	0.0576	0.3992	0.426
H13_2	0.0192	0.0929	0.4925	0.426
C2_2	0.0(4)	0.1(12)	0(2)	0.355
H12_2	-0.0263	0.0324	0.3422	0.426
H22_2	-0.0403	0.085	0.28	0.426
C3_2	0.0(5)	0.0(10)	0(2)	0.355
H13_2	0.0339	0.065	0.0816	0.426
H23_2	0.0107	0.0128	0.105	0.426
C4_2	0.0(2)	0.1(7)	0(2)	0.355
H14_2	-0.0655	0.0375	-0.0078	0.426
H24_2	-0.0485	0.0925	-0.0077	0.426
O_Bu1_2	0.0(9)	0.1(15)	0(2)	0.355
H04_2	0.0141	0.0543	-0.1791	0.426
C1_3	0.3(2)	0.2(2)	0.0(10)	0.355
H11_3	0.3408	0.1404	0.1085	0.426
H12_3	0.3564	0.1954	0.1192	0.426
H13_3	0.3699	0.1648	-0.0401	0.426
C2_3	0.3(2)	0.2(3)	0.0(10)	0.355
H12_3	0.2744	0.1558	-0.0497	0.426
H22_3	0.3014	0.1989	-0.1428	0.426
C3_3	0.3(2)	0.2(2)	0.1(14)	0.355
H13_3	0.2317	0.2108	0.0865	0.426
H23_3	0.2815	0.2222	0.1852	0.426
C4_3	0.3(2)	0.3(3)	0(3)	0.355
H14_3	0.2941	0.2915	0.0518	0.426
H24_3	0.2744	0.2706	-0.1189	0.426
O_Bu2_3	0.2(3)	0.3(3)	0.0(11)	0.355
H04_3	0.206	0.2831	0.1032	0.426
OW1_4	0.2(4)	0.3(3)	-0.2(10)	0.355
HW1_4	0.1(9)	0.3(5)	0(3)	0.426
HW2_4	0.18(19)	0.32(18)	-0.3(12)	0.426
OW2_5	0.2(4)	0.4(4)	0.0(13)	0.355
HW1_5	0.2(5)	0.4(19)	0(2)	0.426
HW2_5	0.2(9)	0.35(16)	0.1(18)	0.426
OW3_6	0.2(4)	0.1(4)	0(11)	0.355
HW1_6	0.2(8)	0.1(9)	1(3)	0.426
HW2_6	0.3(11)	0.1(11)	0(21)	0.426
OW4_7	0.2(2)	0.1(3)	1.2(9)	0.355
HW1_7	0.2(5)	0.1(6)	1.1(10)	0.426
HW2_7	0.3(3)	0.1(4)	1(4)	0.426

Annex 2

Supplementary material Chapter IV

Table S.IV.1. Observed and calculated diffraction angles (2θ) and corresponding Miller indices of V_{6I} of myristic acid (MYA), V_{6II} of 1,3-butanediol (BBOL), V_{6III} of glycerol (GOL), and the new allomorph of V₄-hydroxybenzoic acid (V_{6IV} (HBA)).

V _{6I} (MYA) ^a			V _{6II} (BBOL) ^b			V _{6III} (GOL) ^c			V _{6IV} (HBA) ^d		
<i>h k l</i>	$2\theta_{\text{obs}}$ (°)	$2\theta_{\text{cal}}$ (°)	<i>h k l</i>	$2\theta_{\text{obs}}$ (°)	$2\theta_{\text{cal}}$ (°)	<i>h k l</i>	$2\theta_{\text{obs}}$ (°)	$2\theta_{\text{cal}}$ (°)	<i>h k l</i>	$2\theta_{\text{obs}}$ (°)	$2\theta_{\text{cal}}$ (°)
0 1 0	7.42	7.41	2 2 0	6.65	6.65	0 2 0	9.30	9.28	0 2 0	6.23	6.23
1 1 0	12.86	12.86	1 2 0	7.31	7.30	2 2 0	13.07	13.14	1 1 0	6.49	6.50
1 1 1	16.85	16.87	2 2 0	9.31	9.31	1 3 0	14.65	14.69	1 2 0	8.44	8.45
0 2 1	18.47	18.45	3 2 0	11.93	11.93	0 4 0	18.62	18.62	1 3 0	10.97	10.96
1 2 0	19.70	19.69	1 4 0	13.45	13.45	3 3 0	19.80	19.76	2 0 0	11.42	11.42
0 3 0	22.36	22.36	3 4 0	16.44	16.44	2 4 0	20.85	20.84	2 2 0	13.05	13.02
0 3 1	24.91	24.93	1 4 1	17.45	17.45				1 3 1	15.70	15.70
1 3 0	26.95	26.95	5 2 0	17.93	17.92				1 5 0	16.63	16.64
			0 6 0	19.59	19.59				2 4 0	16.93	16.95
			1 6 0	19.90	19.88				3 1 0	17.45	17.45
			2 6 0	20.71	20.71				3 2 0	18.29	18.28
			4 5 0	21.11	21.12				2 5 0	19.47	19.39
			3 6 0	22.03	22.03				3 3 0	19.47	19.58
			7 1 0	23.69	23.67				3 4 0	21.25	21.28
			5 6 0	25.82	25.84				2 6 0	22.03	22.03
			7 4 0	26.89	26.90				4 1 0	23.23	23.17
									3 5 0	23.23	23.29
									4 2 0	23.81	23.81
									4 3 0	24.83	24.83

^a data indexed on the basis of the hexagonal unit cell: $a = b = 1.377 \pm 0.002$ nm, $c = 0.813 \pm 0.002$ nm. Root-mean-square error (RMSE) = $\sqrt{\sum(2\theta_{\text{obs}} - 2\theta_{\text{cal}})^2 / N_{\text{reflections}}} = 0.012$.

^b data indexed on the basis of the orthorhombic unit cell: $a = 2.656 \pm 0.002$ nm, $b = 2.724 \pm 0.003$ nm, $c = 0.790 \pm 0.004$ nm. RMSE = 0.042.

^c data indexed on the basis of the orthorhombic unit cell with $a = b = 1.906 \pm 0.006$ nm, c unknown. RMSE = 0.038.

^d data indexed on the basis of the orthorhombic unit cell with $a = 1.550 \pm 0.001$ nm, $b = 2.836 \pm 0.001$ nm and $c = 0.790 \pm 0.001$ nm. RMSE = 0.014.

Table S.IV.2. Observed and calculated diffraction angles (2θ) and corresponding Miller's index of the new allomorph of V_{(-)-borneol} (V7_{I(BOR)}), V7 of butanoic acid (V7_{II(BA)}), the new allomorph of V_{1-naphthol} (V7_{III(INAP)}), and the new allomorph of V_{quinoline} (V7_{IV(QN)}).

V7 _{I(BOR)} ^a			V7 _{II(BA)} ^b		
<i>h k l</i>	$2\theta_{\text{obs}} (^{\circ})$	$2\theta_{\text{cal}} (^{\circ})$	<i>h k l</i>	$2\theta_{\text{obs}} (^{\circ})$	$2\theta_{\text{cal}} (^{\circ})$
1 1 0	6.68	6.65	1 1 0	4.35	4.35
2 0 0	11.51	11.53	2 0 0	6.35	6.34
0 2 1	12.74	12.79	2 1 0	6.99	7.01
2 0 1	15.92	15.90	2 2 0	8.71	8.71
1 5 0	17.63	17.65	1 3 0	9.52	9.52
3 3 0	20.03	20.03	3 1 0	9.97	9.97
0 6 1	22.91	22.87	2 3 0	10.99	10.99
4 2 0	24.14	24.13	1 4 0	12.39	12.39
			2 0 1	12.78	12.76
			4 1 0	13.05	13.04
			1 5 0	15.32	15.31
			5 2 0	17.01	16.98
			3 5 0	17.77	17.77
			5 3 0	18.27	18.27
			6 1 0	19.32	19.32
			6 2 0	20.00	20.02
			5 5 0	21.88	21.90
			2 7 0	21.98	21.98
			4 7 0	24.64	24.64
			7 4 0	25.38	25.39
			6 6 0	26.37	26.35
			2 9 0	27.90	27.90

V7 _{III} (INAP) ^c			V7 _{IV} (QN) ^d		
<i>h k l</i>	$2\theta_{\text{obs}}$ (°)	$2\theta_{\text{cal}}$ (°)	<i>h k l</i>	$2\theta_{\text{obs}}$ (°)	$2\theta_{\text{cal}}$ (°)
1 1 0	6.37	6.37	1 2 0	6.27	6.29
0 2 0	7.03	7.02	2 0 0	6.55	6.54
1 2 0	8.81	8.81	0 4 0	10.76	10.75
2 0 0	10.64	10.64	3 2 0	11.20	11.20
2 1 0	11.21	11.20	1 0 1	11.70	11.72
1 0 1	11.61	11.63	2 4 0	12.59	12.60
1 3 0	11.81	11.81	4 0 0	13.12	13.11
2 2 0	12.75	12.76	4 1 0	13.41	13.38
1 4 0	15.04	15.05	3 4 0	14.58	14.58
3 1 0	16.37	16.37	2 3 1	15.34	15.34
2 4 0	17.68	17.67	0 6 0	16.16	16.16
1 5 0	18.40	18.41	1 6 0	16.49	16.49
2 5 0	20.60	20.62	4 4 0	16.98	16.98
0 0 2	20.76	20.75	5 2 0	17.27	17.27
3 4 0	21.36	21.35	0 5 1	17.55	17.57
4 2 0	22.52	22.52	1 5 1	17.95	17.88
3 5 0	23.87	23.87	3 6 0	18.95	18.94
			5 4 0	19.65	19.66
			5 2 1	20.63	20.66
			0 8 0	21.59	21.60
			4 5 1	21.99	21.98
			6 4 0	22.52	22.51
			5 6 0	23.10	23.11
			7 2 0	23.68	23.68
			1 3 2	24.28	24.27
			3 1 2	24.83	24.85
			4 8 0	25.34	25.35

^a data indexed on the basis of the orthorhombic unit cell with $a = b/\sqrt{3} = 1.53 \pm 0.002$ nm, $c = 0.812 \pm 0.002$ nm. Root-mean-square error (RMSE) = $\sqrt{\sum(2\theta_{\text{obs}} - 2\theta_{\text{cal}})^2 / N_{\text{reflections}}} = 0.027$.

^b data indexed on the basis of the orthorhombic unit cell: $a = 2.790 \pm 0.001$ nm, $b = 2.957 \pm 0.001$ nm, $c = 0.798 \pm 0.001$ nm. RMSE = 0.009.

^c data indexed on the basis of the orthorhombic unit cell with $a = 1.663 \pm 0.001$ nm, $b = 2.518 \pm 0.001$ nm and $c = 0.856 \pm 0.001$ nm. RMSE = 0.009.

^d data indexed on the basis of the orthorhombic unit cell with $a = 2.702 \pm 0.001$ nm, $b = 3.291 \pm 0.002$ nm. $c = 0.786 \pm 0.001$ nm. RMSE = 0.019.

Table S.IV.3. Observed and calculated diffraction angles (2θ) and corresponding Miller indices of the two allomorphs of V_{salicylic acid} (V8_{I(SAL)} and V8_{II(SAL)}).

V8 _{I(SAL)} ^a			V8 _{II(SAL)} ^b		
<i>h k l</i>	$2\theta_{\text{obs}}$ (°)	$2\theta_{\text{cal}}$ (°)	<i>h k l</i>	$2\theta_{\text{obs}}$ (°)	$2\theta_{\text{cal}}$ (°)
0 2 0	6.09	6.09	1 1 0	5.43	5.42
2 2 0	6.40	6.40	0 2 0	7.68	7.67
-2 2 0	10.37	10.38	2 2 0	10.88	10.85
4 2 0	10.93	10.92	0 1 1	11.86	11.86
4 0 0	12.23	12.20	1 3 0	12.15	12.14
0 2 1	12.73	12.73	1 1 1	12.45	12.47
4 4 0	12.81	12.82	0 2 1	13.63	13.60
-4 2 0	15.92	15.92	2 3 0	13.90	13.84
2 6 0	16.53	16.52	2 1 1	14.11	14.14
-1 5 0	16.87	16.87	0 4 0	15.39	15.37
-3 4 0	18.27	18.28	2 2 1	15.66	15.63
7 4 0	19.32	19.32	3 3 0	16.31	16.31
4 8 0	21.85	21.82	1 3 1	16.60	16.55
5 8 0	22.33	22.34	2 4 0	17.21	17.20
6 8 0	23.13	23.14	2 3 1	17.84	17.85
8 0 0	24.52	24.54	4 1 1	19.42	19.45
8 1 1	25.89	25.91	4 2 1	20.56	20.58
8 7 1	26.84	26.82	4 4 0	21.78	21.80
			3 5 0	22.54	22.48
			6 0 0	23.13	23.14
			2 6 0	24.46	24.41
			3 5 1	25.18	25.19
			1 6 1	26.04	26.08
			6 2 1	26.93	26.94

^a data were indexed on basis of the monoclinic unit cell: $a = 3.245 \pm 0.006$ nm, $b = 3.246 \pm 0.005$ nm, $c = 0.793 \pm 0.001$ nm, $\gamma = 63.38 \pm 0.14^\circ$. Root-mean-square error (RMSE) = $\sqrt{\sum(2\theta_{\text{obs}} - 2\theta_{\text{cal}})^2 / N_{\text{reflections}}} = 0.014$.

^b data were indexed on basis of the orthorhombic unit cell: $a = b = 2.306 \pm 0.002$ nm, $c = 0.789 \pm 0.001$ nm. RMSE = 0.028.

Table S.VI.4. Lamellar thickness of V-amylose crystals measured from atomic force microscopy images.

Allomorph	Complexing agent	Thickness (nm)
V6 _I	1,3-butanediol	9.2 ± 0.9
V6 _I	octadecanoic acid	9.8 ± 0.6
V6 _{II}	dodecanoic acid*	8.4 ± 1.2 10.5 ± 0.9
V6 _{II}	hexadecanoic acid	7.8 ± 1.1
V6 _{II}	octadecanoic acid	10.2 ± 0.5
V6 _{II}	dodecanedioic acid	9.9 ± 0.7
V7 ^a	ibuprofen	7.0 ± 0.5
V7 ^a	cis-decahydro-1-naphthol	7.1 ± 1.2
V7 ^a	decahydro-2-naphthol	8.6 ± 0.5
V7 ^a	1,3-butanediol	8.7 ± 0.6
V7 _{III} ^b	1-naphthol	10.3 ± 0.6

^a corresponding to V7_{II} in the new nomenclature.

^b a new allomorph of V_{1-naphthol}.

* two different preparations

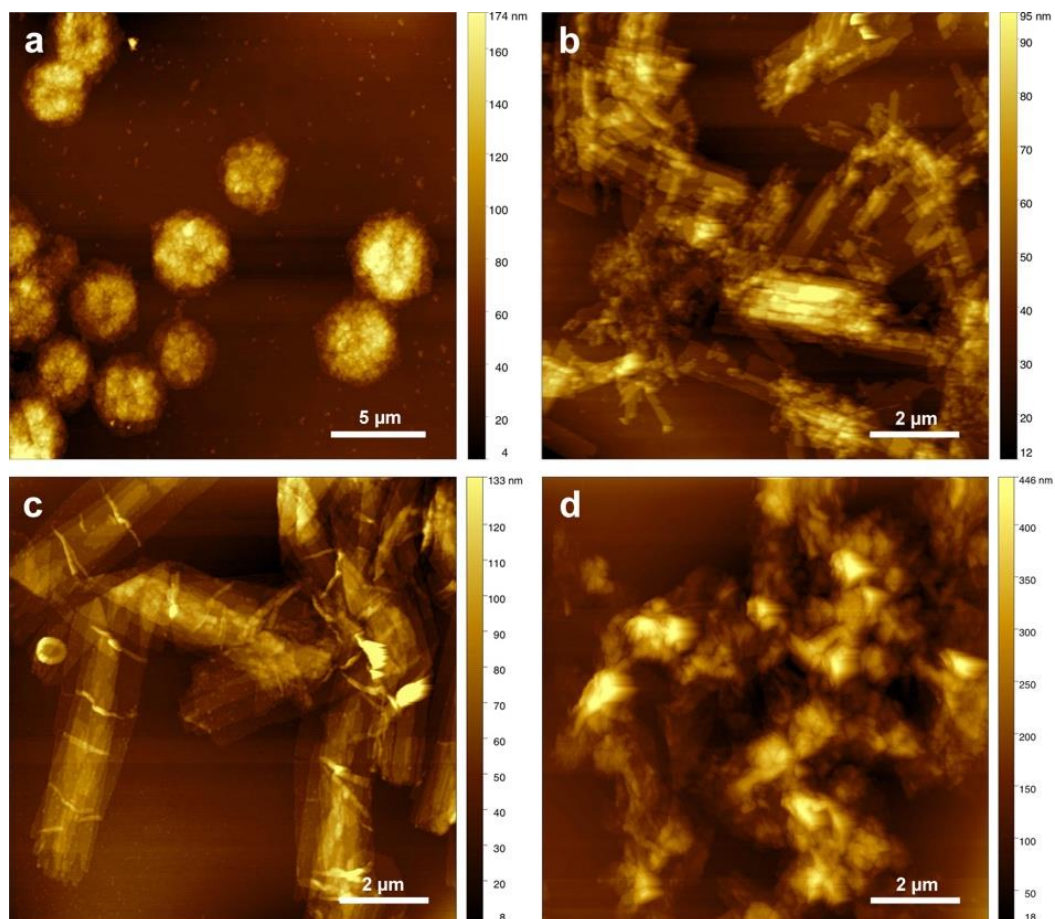


Figure S.IV.1. AFM images (tapping mode) of V-amylose crystals: a) V6_I of octadecanoic / stearic acid; b) V6_{II} of octadecanoic / stearic acid; c) V7_{II} of 1,3-butanediol; d) V7_{III} of 1-naphthol.

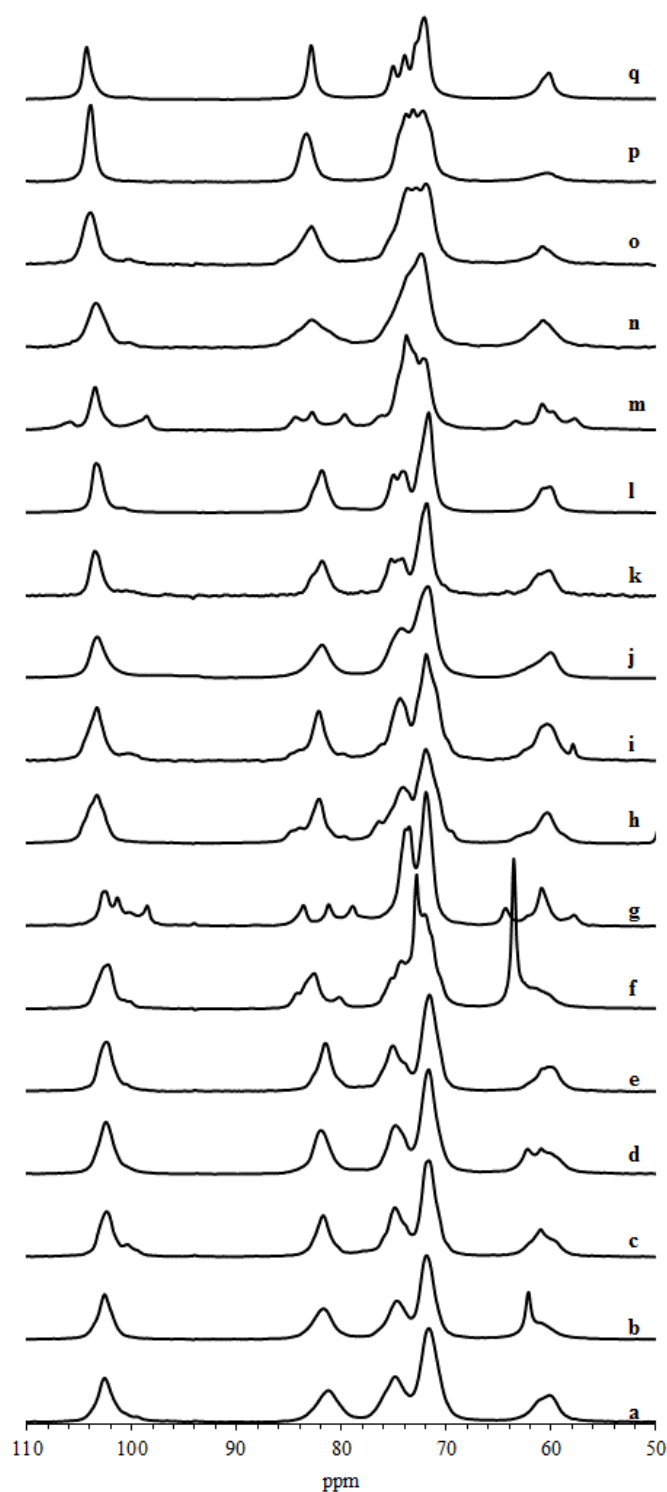


Figure S.IV.2. ^{13}C CP/MAS NMR spectra of: V6_I of hexadecanoic acid (a) and 1,6-hexanediol (b); V6_{II} of 1-butanol (c), 1,6-hexanediol (d) and hexanoic acid (e); V6_{III} of glycerol (g); V6_{IV} of 4-hydroxybenzoic acid; V7_I of (-)-borneol (h) and (R)-(+)-camphor (i); V7_{II} of ibuprofen (j), 2-propanol (k) and butanoic acid (l); V7_{III} of 1-naphthol (m); V7_{IV} of quinoline (n); V8_I of salicylic acid (o); V8_{II} of salicylic acid (p) and quinoline (q).

Annex 3

Supplementary material Chapter V

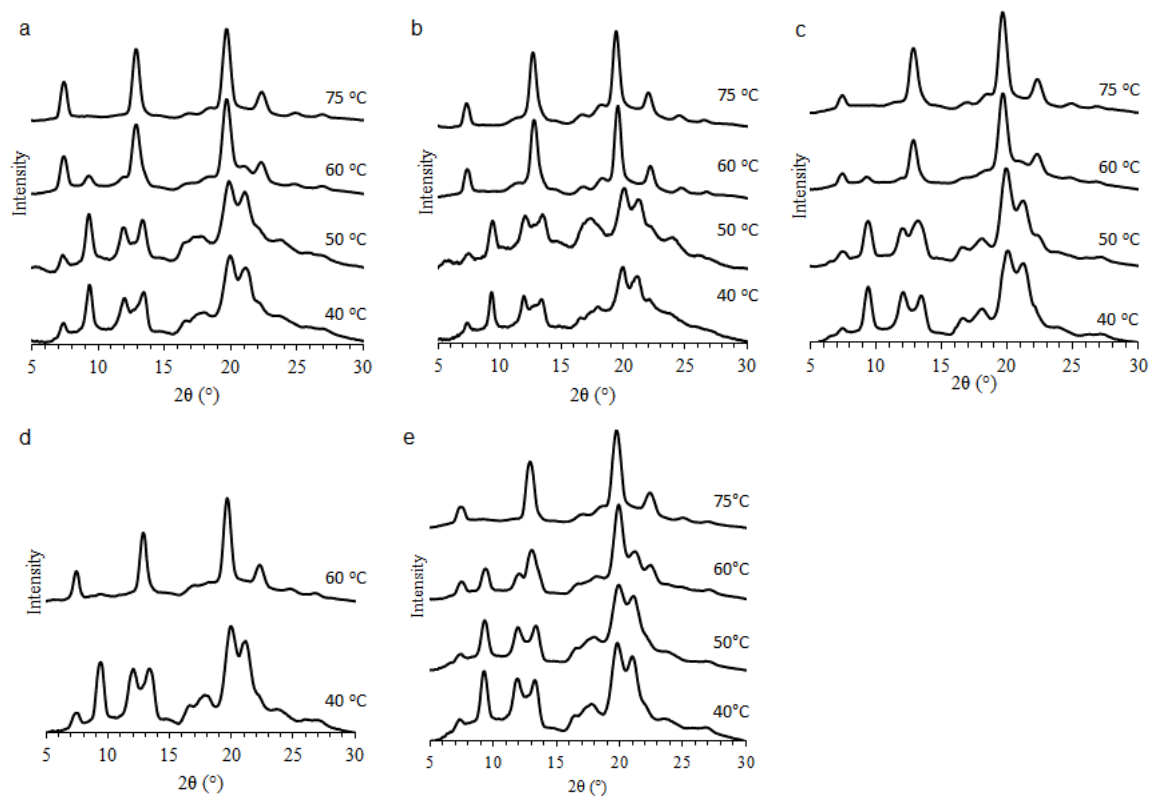


Figure S.V.1. XRD profiles of V-amylose prepared at different temperatures in the presence of saturation of complexing agent: 1-octanol (a), 1-heptylamine (b), nonanedioic acid (c), octanal (d) and 1,6-hexanediol (e).

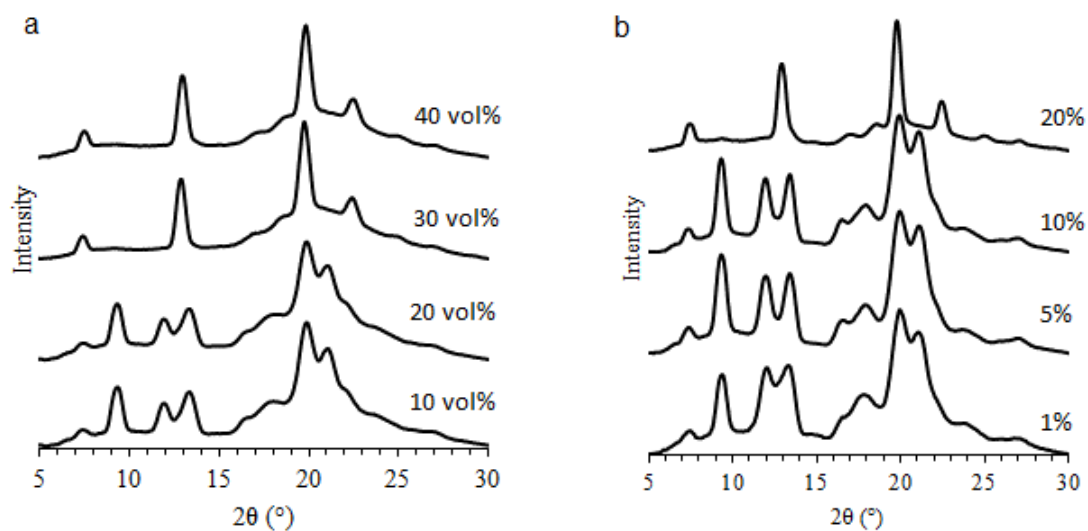


Figure S.V.2. XRD profiles of V-amylose prepared by slow cooling to room temperature in a Dewar bottle in the presence of different concentrations of 1,4-butanediol (a) and 1,6-hexanediol (b).

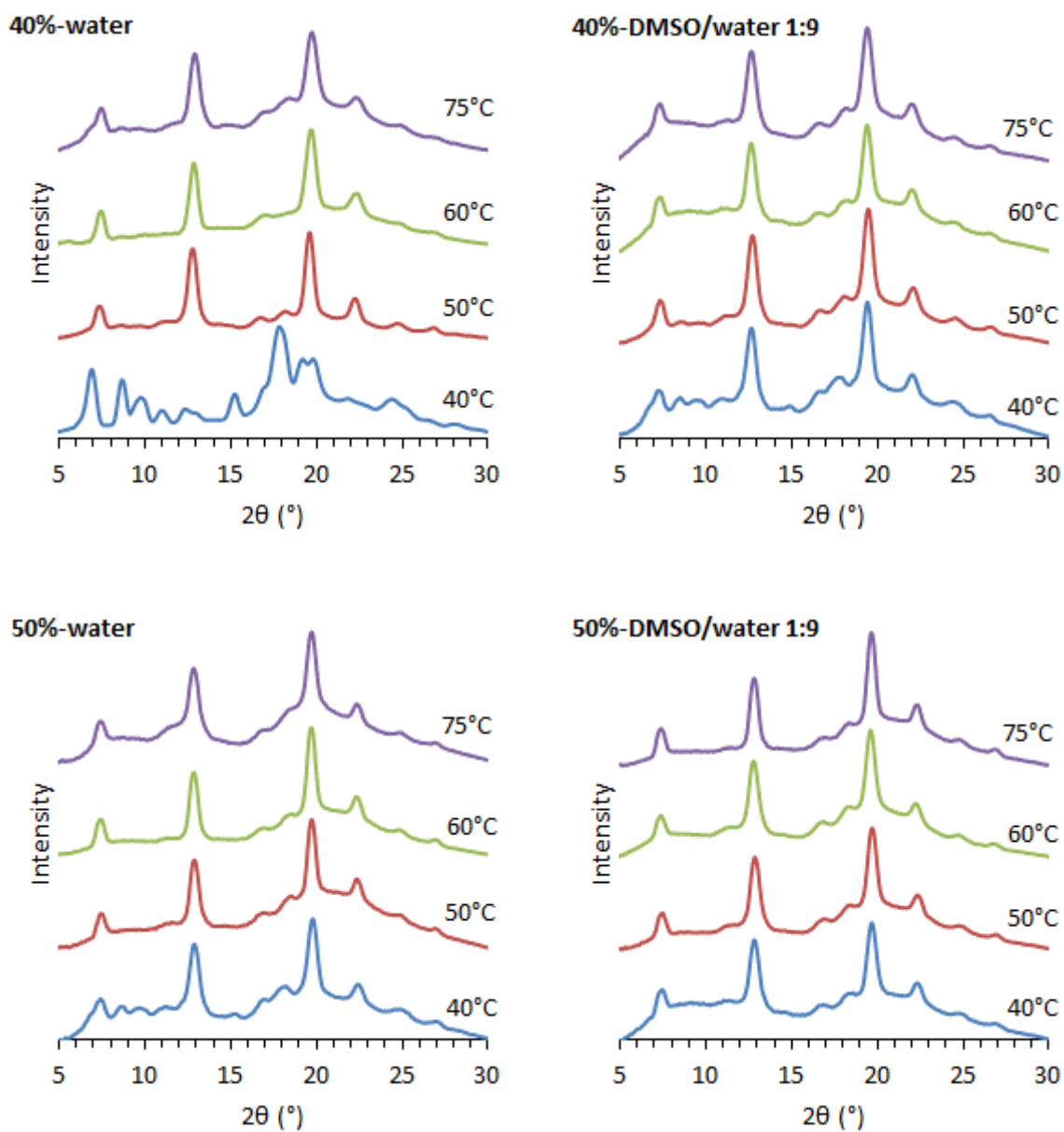


Figure S.V.3. XRD profiles of $V_{\text{propanoic acid}}$ (C3) complexes prepared at different temperatures in the presence of 40 and 50 vol% of propanoic acid in pure water or in a 1:9 DMSO:water mixture.

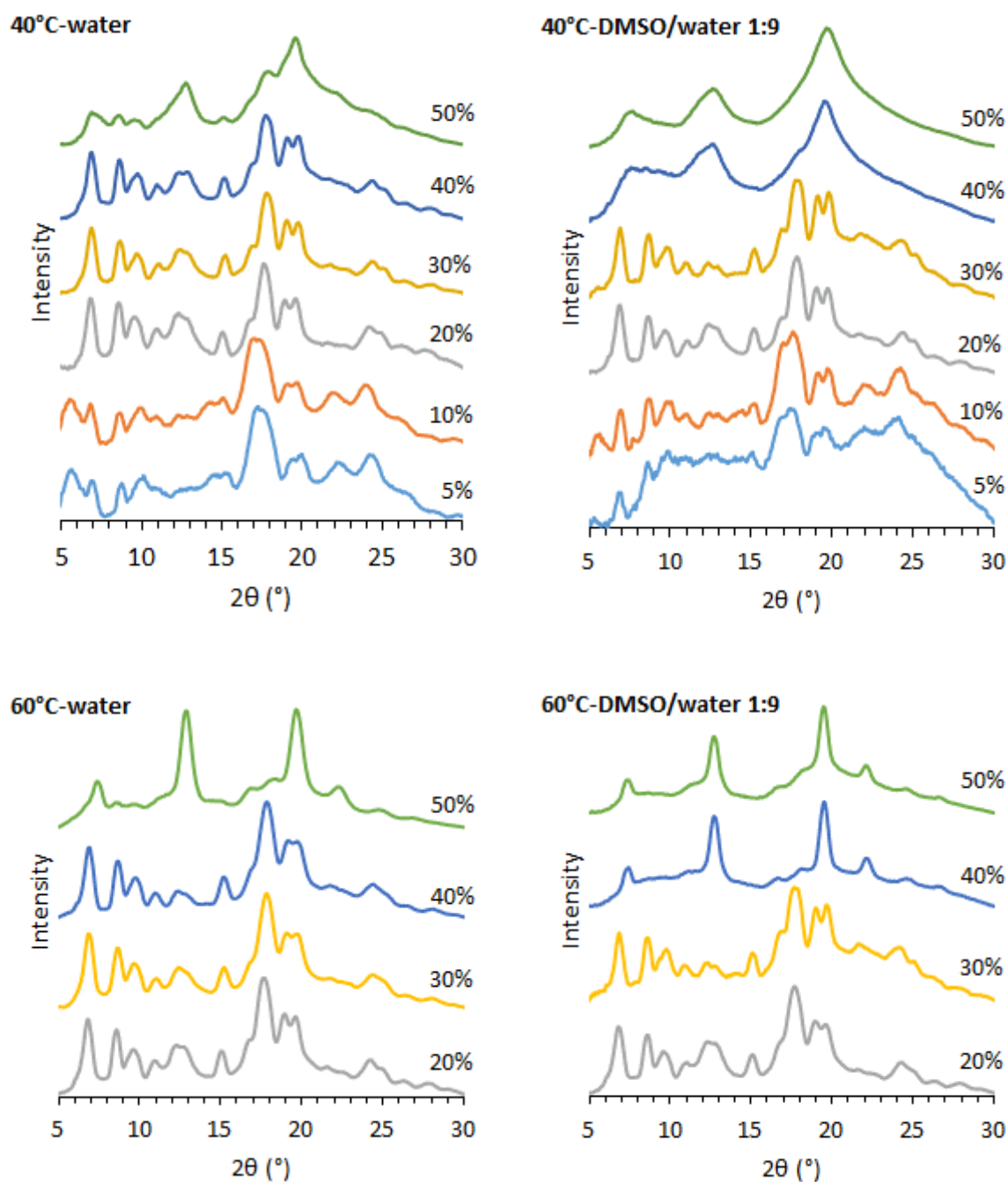


Figure S.V.4. XRD profiles of $V_{\text{butanoic acid}}$ (C4) complexes prepared with different concentrations of butanoic acid in pure water or in a 1:9 DMSO:water mixture, at 40 and 60 °C.

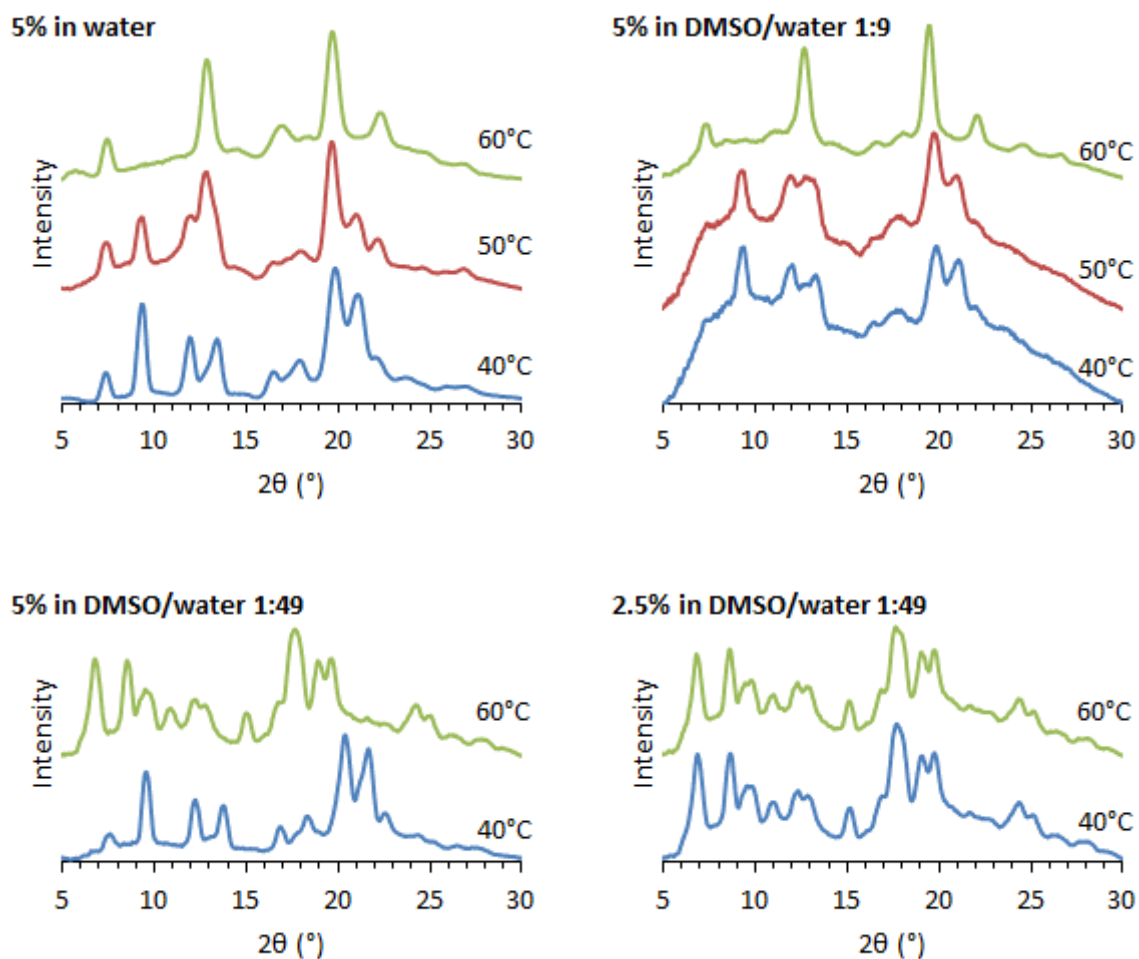


Figure S.V.5. XRD profiles of $V_{\text{pentanoic acid}}$ (C5) complexes prepared in pure water and in a 1:9 or 1:49 DMSO:water mixture at different temperatures and concentrations of pentanoic acid.

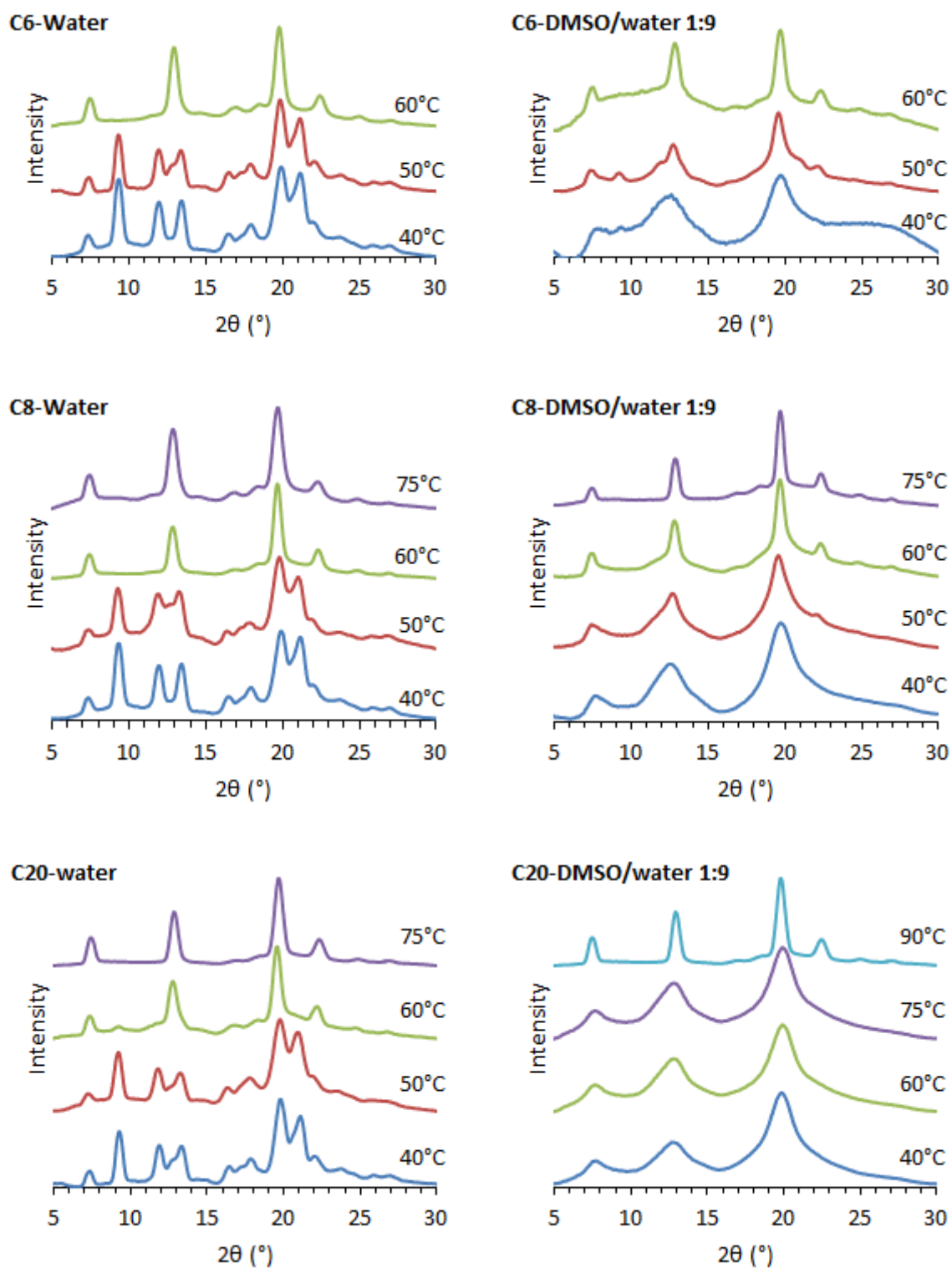


Figure S.V.6. XRD profiles of $V_{\text{hexanoic acid}}$ (C6), $V_{\text{octanoic acid}}$ (C8) and $V_{\text{icosanoic acid}}$ (C20) complexes prepared at different temperatures in pure water and in a 1:9 DMSO:water mixture.

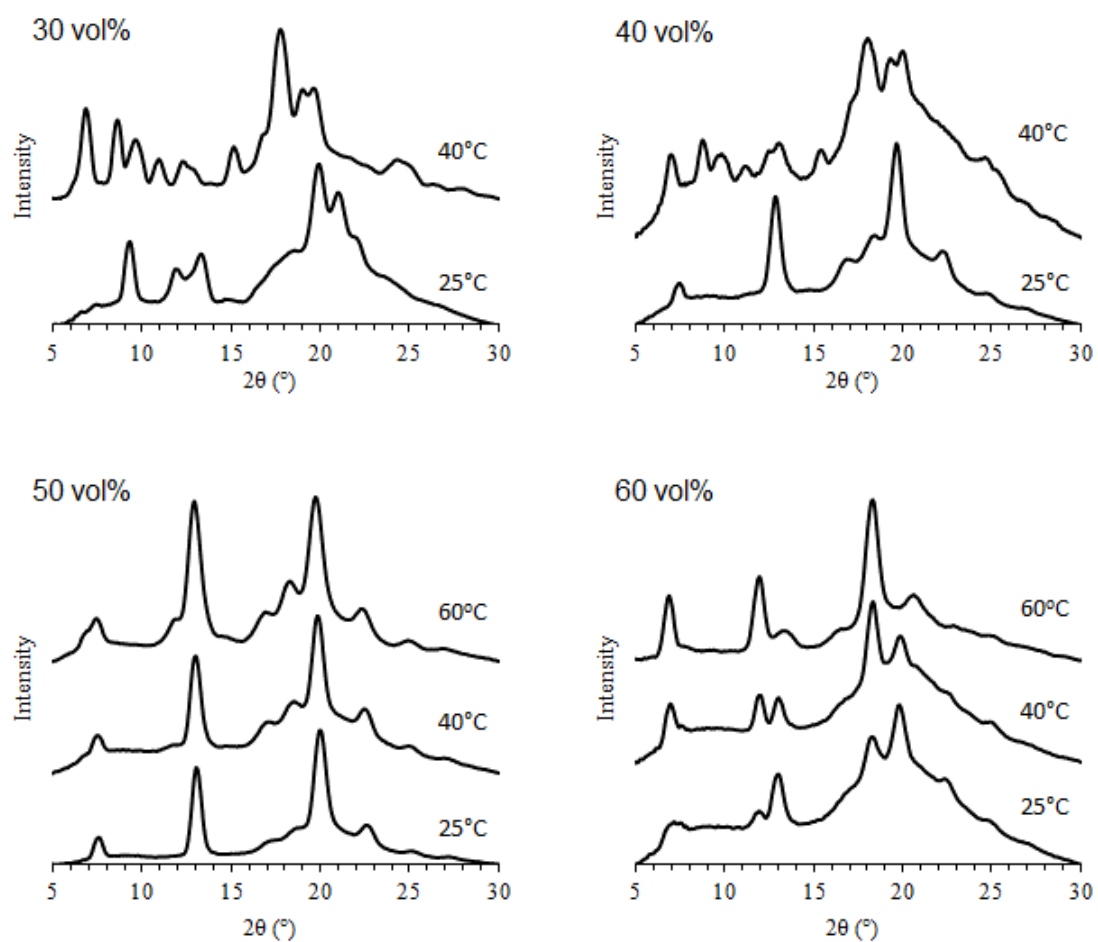


Figure S.V.7. XRD profiles of $V_{1,3}$ -butanediol prepared in the presence of different amounts of 1,3-butanediol at different temperatures.

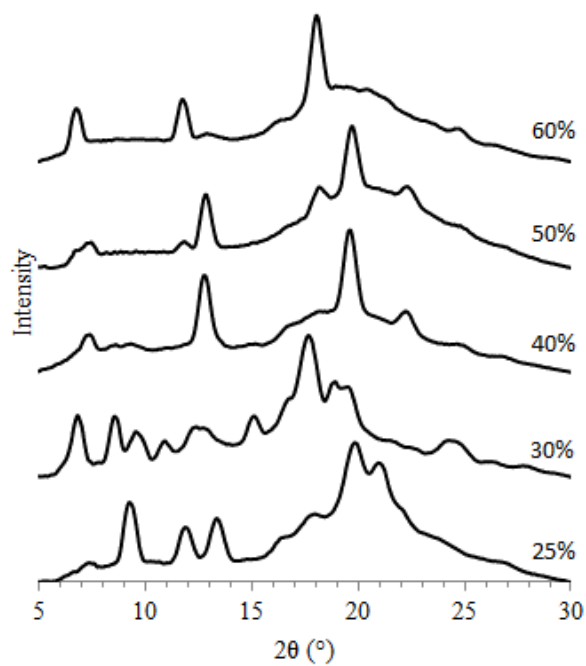


Figure S.V.8. XRD profiles of $V_{1,3}$ -butanediol prepared in the presence of different amounts of 1,3-butanediol by slow cooling to room temperature.

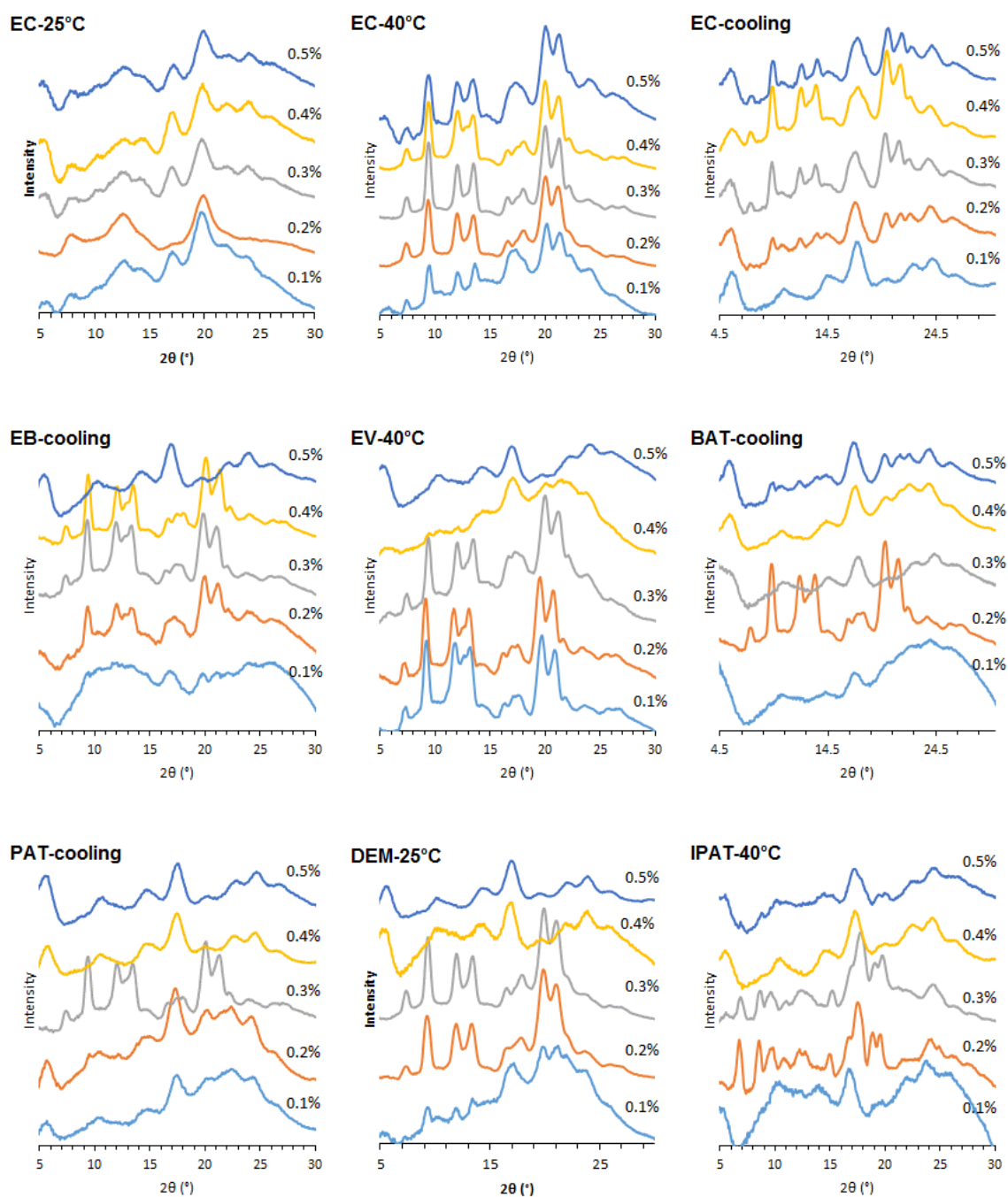


Figure S.V.9. XRD profiles of V-amylose complexed with ethyl butyrate (EB), ethyl valerate (EV), butyl acetate (BAT), pentyl acetate (PAT), diethyl malonate (DEM) and isopentyl acetate (IPAT) prepared at in different amylose concentrations (wt%) at 25 or 45 °C or cooling down in a Dewar bottle.

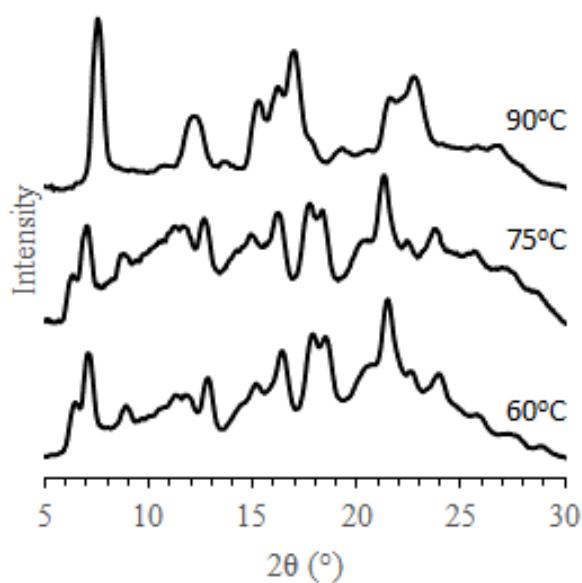


Figure S.V.10. XRD profiles of V_{1-naphthol} as a function of mixing temperature at which an excess amount of 1-naphthol was added into DP6500 amylose solution. The crystals were formed as cooling down to room temperature.

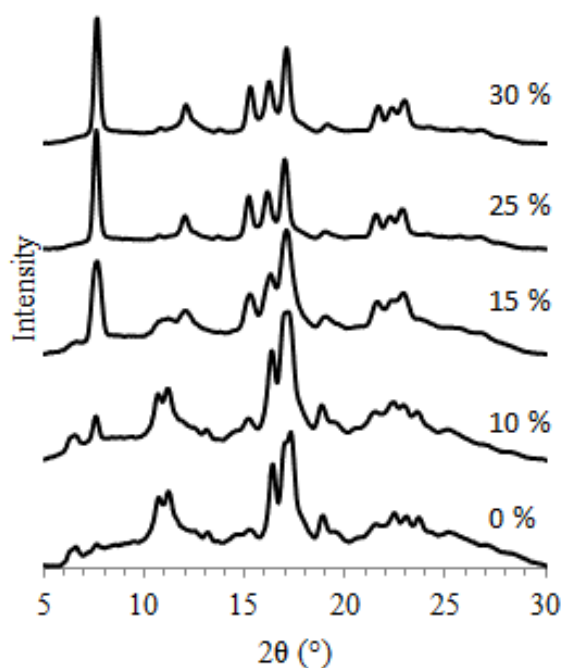


Figure S.V.11. XRD profiles of V_{quinoline} as a function of DMSO concentration. The crystallization occurred at 40 °C in 0.1 wt% DP6500 amylose solution with the presence an excess amount of quinoline.

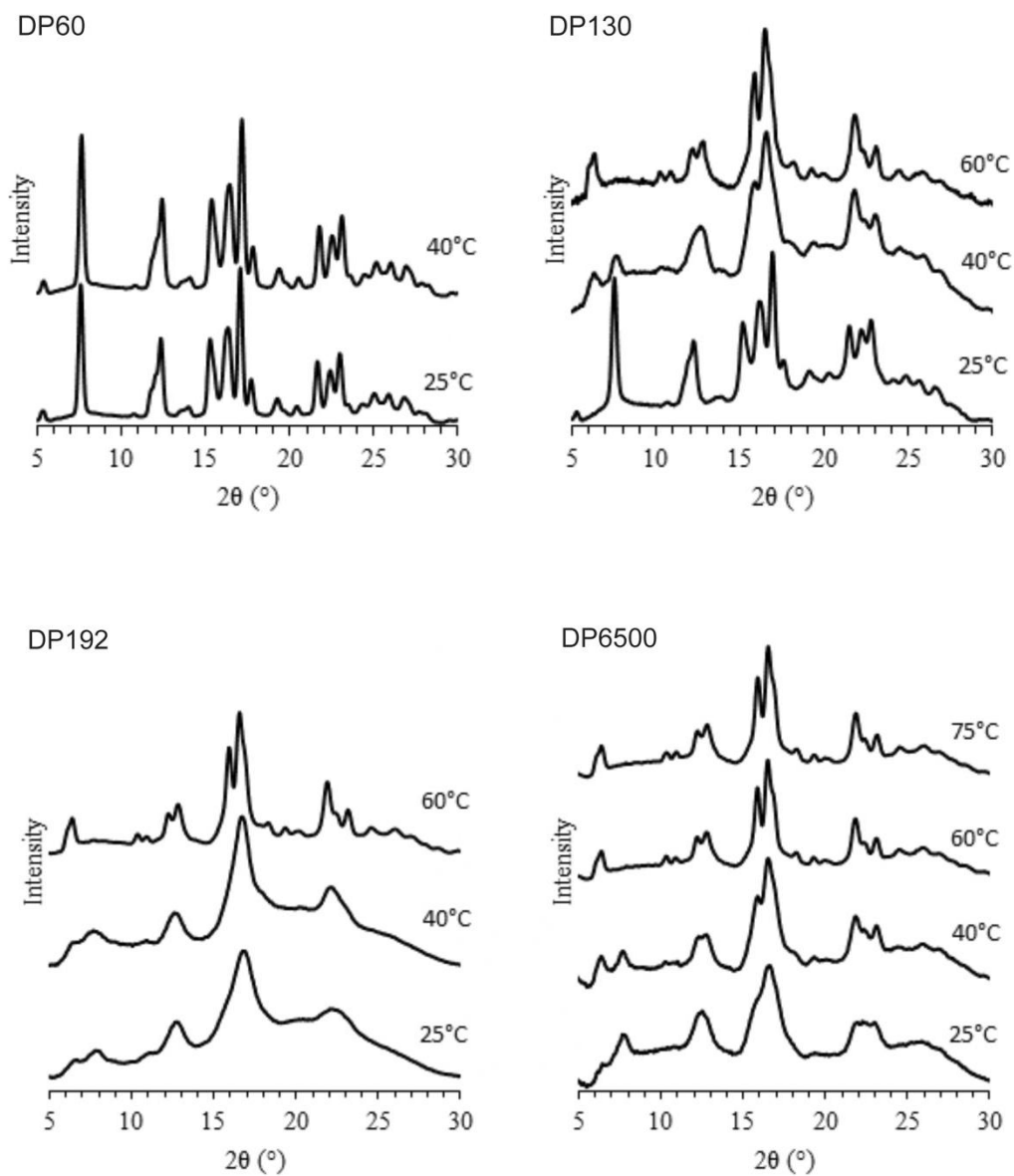


Figure S.V.12. XRD profiles of $V_{\text{salicylic acid}}$ prepared from different amylose fractions in aqueous solution at different temperatures.

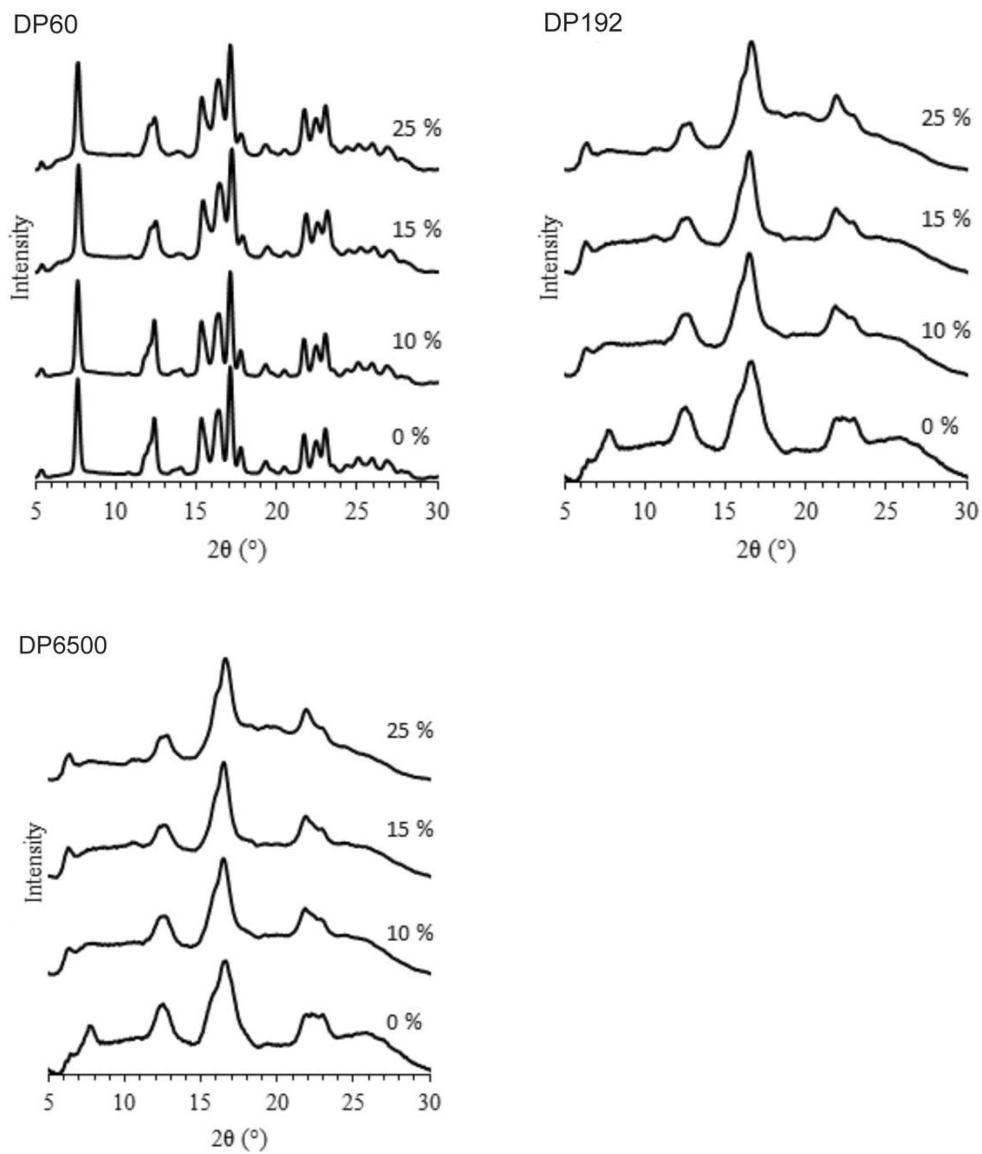


Figure S.V.13. XRD profiles of $V_{\text{salicylic acid}}$ prepared from different amylose fractions in aqueous solution in the presence of different amounts of DMSO at 25 °C.

Annex 4

Supplementary material Chapter VI

Table S.VI.1. Observed and calculated diffraction angles 2θ in XRD patterns recorded on hydrated and dry $V_{\text{ibuprofen}}$ complexes, and corresponding Miller indexes.

Hydrated complexes ^a			Dry complexes ^b		
<i>h k l</i>	2θ obs (°)	2θ cal (°)	<i>h k l</i>	2θ (°) obs	2θ (°) cal
1 1 0	4.325	4.320	0 1 0	6.93	6.89
2 0 0	6.256	6.259	1 1 0	11.95	11.94
1 2 0	6.732	6.732	0 1 1	13.07	13.13
2 1 0	6.934	6.933	1 1 1	16.46	16.37
2 2 0	8.656	8.646	1 2 0	18.27	18.29
1 3 0	9.467	9.477	1 3 0	24.99	25.01
3 1 0	9.856	9.857			
2 3 0	10.93	10.923			
3 2 0	11.110	11.132			
1 4 0	12.336	12.341			
2 0 1	12.724	12.724			
4 1 0	12.894	12.888			
3 4 0	15.208	15.210			
5 2 0	16.831	16.795			
3 5 0	17.685	17.671			
5 3 0	18.080	18.087			
6 1 0	19.056	19.090			
6 2 0	19.785	19.788			
5 5 0	21.731	21.725			
3 7 0	23.022	23.017			
4 7 0	24.485	24.500			
7 4 0	25.131	25.127			

^a indexed based on an orthorhombic unit cell with $a = 2.82(4) \pm 0.00(1)$ nm, $b = 2.96(6) \pm 0.00(1)$ nm, $c = 0.79(9) \pm 0.00(1)$ nm.

^b indexed based on a hexagonal unit cell with $a = b = 1.48(2) \pm 0.00(9)$ nm, $c = 0.79(3) \pm 0.00(5)$ nm.

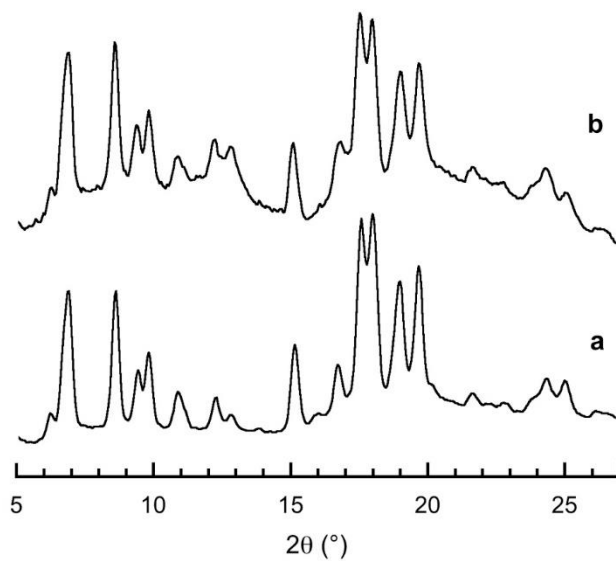


Figure S.VI.1. XRD profiles of $V_{\text{ibuprofen}}$ (a) and $V_{2\text{-propanol}}$ (b) crystalline complexes (DP6500 amylose).

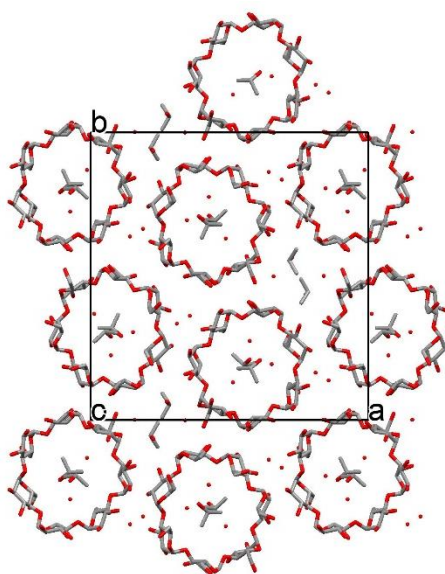


Figure S.VI.2. Axial view of the molecular model of the $V_{2\text{-propanol}}$ crystal drawn from the CIF data file provided as supplementary data by Nishiyama et al. (2010). The hydrogen atoms were omitted for clarity.